Extending Wastewater Treatment Process Models for Phosphorus Removal and Recovery

A Framework for Plant-Wide Modelling of Phosphorus, Sulfur and Iron

KIMBERLY SOLON
FACULTY OF ENGINEERING | LUND UNIVERSITY

Extending Wastewater Treatment Process Models for Phosphorus Removal and Recovery

Extending Wastewater Treatment Process Models for Phosphorus Removal and Recovery

A Framework for Plant-Wide Modelling of Phosphorus, Sulfur and Iron

by Kimberly Solon

LUND UNIVERSITY

Thesis for the degree of Doctor of Philosophy in Engineering

Thesis supervisors: Associate Professor Ulf Jeppsson
Professor Krist V. Gernaey
Dr. Xavier Flores-Alsina

Faculty opponent: Dr. Paloma Grau
University of Navarra and CEIT
San Sebastian, Spain

To be presented, with the permission of the Faculty of Engineering of Lund University, for public criticism in the M:B lecture hall, Mechanical Engineering Building, Ole Römers väg 1, Lund, on Friday the 19th of May 2017 at 10:15 a.m.

Organization	Document name
LUND UNIVERSITY Faculty of Engineering Department of Biomedical Engineering Division of Industrial Electrical Engineering and Automation	**DOCTORAL DISSERTATION** Date of disputation 2017 May 19
Author Kimberly Solon	Sponsoring organization EU SANITAS, Lund University

Title and subtitle

Extending Wastewater Treatment Process Models for Phosphorus Removal and Recovery – A Framework for Plant-Wide Modelling of Phosphorus, Sulfur and Iron

Abstract

As problems associated with shortage in resource supply arise, wastewater treatment plants turn to innovation to transform themselves into resource recovery facilities. Water groups worldwide recognize that wastewater treatment plants are no longer disposal facilities but rather sources of clean water, energy and nutrients.

One of the most important resources that can be recovered from wastewater treatment plants is phosphorus. Mathematical modelling can be utilised to analyse various operational strategies to recover phosphorus from the wastewater. However, incorporating phosphorus transformation processes in plant-wide models is complex. Firstly, the tri-valence of phosphates suggests non-ideality, which requires the use of a physico-chemical model to account for this non-ideality. Secondly, phosphorus has strong interlinks with sulfur and iron, which necessitates inclusion of their transformations in biological and physico-chemical models. Lastly, consolidating these into a plant-wide model aimed at describing phosphorus removal and/or recovery requires interfacing, modifications to the plant layout, addition of recovery unit processes and development of new control and operational strategies. The research work presented in this thesis addresses the aforementioned challenges.

A physico-chemical model is developed to take into account ion activity corrections, ion pairing effects, aqueous phase chemical equilibria, multiple mineral precipitation and gas stripping/adsorption. The model is then linked with standard approaches used in wastewater engineering, such as the Activated Sludge Model Nos. 1, 2d and 3 (ASM1, 2d, 3) and the Anaerobic Digestion Model No. 1 (ADM1). The extensions of the ASM2d and ADM1 with phosphorus, sulfur and iron-related conversions followed. And finally, the extended models and the physico-chemical model are consolidated into a plant-wide model provided by the Benchmark Simulation Model No. 2. The resulting model is used for simulation-based scenario analysis for finding ways to improve the operation of a wastewater treatment plant aimed at phosphorus removal and recovery.

Key words

Benchmark Simulation Model, Anaerobic Digestion Model, Activated Sludge Model, Physico-chemistry, Phosphorus removal, Nutrient recovery

Classification system and/or index terms (if any)

Supplementary bibliographical information	Language
	English
ISSN and key title	ISBN
	978-91-88934-79-6 (print) 978-91-88934-78-9 (pdf)
Recipient's notes	Number of pages: 238 / Price
	Security classification

I, the undersigned, being the copyright owner of the abstract of the above-mentioned dissertation, hereby grant to all reference sources permission to publish and disseminate the abstract of the above-mentioned dissertation.

Signature  Date 2017-April-12

Extending Wastewater Treatment Process Models for Phosphorus Removal and Recovery

A Framework for Plant-Wide Modelling of Phosphorus, Sulfur and Iron

by Kimberly Solon

LUND
UNIVERSITY

Cover illustration front: *Best place to grow* by Banu Örmeci

Cover illustration back: Author's portrait

© 2017 by Kimberly Solon

Division of Industrial Electrical Engineering and Automation
Department of Biomedical Engineering
Faculty of Engineering
Lund University
Box 118
SE-221 00 Lund
Sweden

ISBN: 978-91-88934-79-6 (print)
ISBN: 978-91-88934-78-9 (pdf)
CODEN: LUTEDX/(TEIE-1082/1-238/(2017)

Printed in Sweden by Media-Tryck, Lund University
Lund 2017

A straight line may be the shortest distance between two points,
but it is by no means the most interesting.

-The Doctor

Contents

Acknowledgements

This academic journey has been an overwhelming experience. Without the support and guidance of many people, this feat would not have been possible. I would like to take this opportunity to thank the people who have contributed, in one way or another, to the completion of this work.

My immense heartfelt gratitude goes to my main supervisor Associate Professor Ulf Jeppsson. I am very fortunate to be under his guidance and I could not wish for a better supervisor other than him. He has been very supportive and motivating to all my endeavours. He finds the perfect balance between giving me enough guidance with my research and giving me trust to work independently. He is one of the smartest people I know and has influenced me to be conscientious with my work (and also to abandon the Oxford comma, at least for this thesis). He has, oftentimes, gone above and beyond his duty to help me overcome my worries and anxieties and instil confidence in me. I also appreciate the countless hours he spent meticulously checking this work. Thanks will never be enough for the countless opportunities that I have had because of him.

I am also grateful to my supervisors, Professor Krist Gernaey and Dr. Xavier Flores-Alsina. Their constructive critiques nicely balanced with compliments for tasks done well have always kept me motivated. I consistently have the most fruitful and enjoyable meetings with them. I thank them for always making time for discussions and for answering even the simplest questions that I have.

During my Ph.D., I have had the chance to conduct research at Ghent University, Belgium, under the supervision of Professor Eveline Volcke. I want to thank her and her research group for a pleasant stay during my research stint. I consider her as a mentor and as the reason how I came to work on environmental modelling.

A large part of this research was made possible through collaborations with several people from various research groups. I would like to thank Professor George Ekama from the University of Cape Town, who I first met in Lund during the first few months into my Ph.D., for continuously sharing and translating his long-established practical knowledge for our model developments. I would also like to thank Professor Damien Batstone from the University of Queensland, whose inputs to the research work are invaluable. The numerous meetings and discussions with him, during his visits to Lund University and the Technical University of Denmark, have contributed in guiding the direction of my research. Professor Peter Vanrolleghem from Université Laval is also greatly acknowledged. He has spent month-long research visits in the past three years here at the Division of Industrial Electrical Engineering and Automation and I have benefited from his expert knowledge on wastewater treatment modelling,

networking/friendships and good humor. I would also like to thank Dr. Stephan Tait, Dr. Christian Kazadi Mbamba, Dr. David Ikumi, Dr. Céline Vaneeckhaute and Dr. Ernesto Barrera for the support, for the productive collaborations and for making it enjoyable working together.

I am also gratefully acknowledging Marie Skłodowska-Curie ITN SANITAS (coordinated by Associate Professor Joaquim Comas) for the funding of my Ph.D., which made all of these possible. I have met the most interesting and wonderful people because of this consortium.

I am lucky to have been surrounded by many other smart friends and I would like to thank them for their kindness and support: Celia for the wine and language lessons, Lucie for the tea-breaks and small-but-treasured chats, Laura for the friendship and nice memories during the meetings, training weeks, summer schools and conferences and Ramesh for the advices, conversations and for being the best seatmate for almost five years. I also want to thank all my colleagues at IEA for always making me feel welcome, particularly to Professor Gustaf Olsson and Dr. Magnus Arnell for the encouragements and inspirations.

My time in Lund was made enjoyable due to the friends I have made along the way. I would like to thank my Filipino friends in Sweden and in Belgium for making me feel at home abroad. I especially want to thank Mary-bell, my dear friend and housemate, for being there from the beginning and my Ate Tsiki, for being my family away from home. I would also like to thank my friends in the Philippines, who have supported me with constant communication and sending positive thoughts.

Last but not the least, I am extremely grateful to my family. My husband Koen has always believed in me and supported me to achieve this dream. The past five years has been challenging and I appreciate that he has always been there for me, patiently waiting. I would also like to thank Pa Frank and Ma Lydie for the support and words of encouragement. I am also thankful to my family for the love and confidence in me. My parents and sisters are the source of my inspiration.

List of Publications and Author's Contributions

This thesis is based on the following publications (all papers are reproduced with permission of the publisher) referred to by their Roman numerals:

I **Effects of ionic strength and ion pairing on (plant-wide) modelling of anaerobic digestion processes**

Solon, K., Flores-Alsina, X., Kazadi Mbamba, C., Volcke, E.I.P., Tait, S., Batstone, D.J., Gernaey, K.V., Jeppsson, U.

Water Research, 2015, vol. 70, pp. 235-245. (Impact factor 2015: 5.991)

II **A plant-wide aqueous phase chemistry module describing pH variations and ion speciation/pairing in wastewater treatment process models**

Flores-Alsina, X., Kazadi Mbamba, C., **Solon, K.**, Vrečko, D., Tait, S., Batstone, D.J., Jeppsson, U., Gernaey, K.V.

Water Research, 2015, vol. 85, pp. 255-265. (Impact factor 2015: 5.991)

III **Modeling the anaerobic digestion of cane-molasses vinasse: Extension of the Anaerobic Digestion Model No. 1 (ADM1) with sulfate reduction for a very high strength and sulfate rich wastewater**

Barrera, E., Spanjers, H., **Solon, K.**, Amerlinck, Y., Nopens, I., Dewulf, J.

Water Research, 2015, vol. 71, pp. 42-54. (Impact factor 2015: 5.991)

IV **Modelling phosphorus (P), sulfur (S) and iron (Fe) interactions for dynamic simulations of anaerobic digestion processes**

Flores-Alsina, X., **Solon, K.**, Kazadi Mbamba, C., Tait, S., Gernaey, K.V., Jeppsson, U., Batstone, D.J.

Water Research, 2016, vol. 95, pp. 370-382. (Impact factor 2015: 5.991)

V **Plant-wide modelling of phosphorus transformations in biological nutrient removal wastewater treatment systems: Impacts of control and operational strategies**

Solon, K., Flores-Alsina, X., Kazadi Mbamba, C., Ikumi, D.S., Volcke, E.I.P., Vaneeckhaute, C., Ekama, G.A., Vanrolleghem, P.A., Batstone, D.J., Gernaey, K.V., Jeppsson, U.

Water Research, 2017, vol. 113, pp. 97-110. (Impact factor 2015: 5.991)

Author's Contributions

Paper I: Effects of ionic strength and ion pairing on (plant-wide) modelling of anaerobic digestion processes

I performed part of the modelling work of including ion activity corrections and aqueous phase chemical equilibria on the Anaerobic Digestion Model No. 1. I was mainly responsible for writing the paper and finalisation of the model implementation for distribution.

Paper II: A plant-wide aqueous phase chemistry module describing pH variations and ion speciation/pairing in wastewater treatment process models

I performed part of the modelling work of implementing aqueous phase chemical equilibria in various Activated Sludge Models. I worked closely with Xavier Flores-Alsina and Christian Kazadi Mbamba in writing the paper. I was also responsible for the finalisation of the model implementation for distribution.

Paper III: Modeling the anaerobic digestion of cane-molasses vinasse: extension of the Anaerobic Digestion Model No. 1 (ADM1) with sulfate reduction for a very high strength and sulfate rich wastewater

I performed part of the modelling work of implementing sulfate reduction processes within the Anaerobic Digestion Model No. 1 and I assisted Ernesto Barrera in performing the model sensitivity analysis. I also worked closely with him in analysing and interpreting the results.

Paper IV: Modelling phosphorus (P), sulfur (S) and iron (Fe) interactions for dynamic simulations of anaerobic digestion processes

I performed the modelling work of implementing phosphorus, sulfur and iron-related processes within the Anaerobic Digestion Model No. 1. I worked closely with Xavier Flores-Alsina in writing the paper. I was mainly responsible for the finalisation of the model implementation for distribution.

Paper V: Plant-wide modelling of phosphorus transformations in biological nutrient removal wastewater treatment systems: Impacts of control and operational strategies

I performed the modelling work of including phosphorus, sulfur and iron-related processes in Anaerobic Digestion Model No. 1 and Activated Sludge Model No. 2d and within the Benchmark Simulation Model No. 2 platform. I was mainly responsible for writing the paper and finalisation of the model implementation for distribution.

Subsidiary Publications

Peer reviewed papers related to the subject but are not included in this thesis:

VI **A unified approach to modelling wastewater chemistry: model corrections**

Tait, S., **Solon, K.**, Volcke, E.I.P., Batstone, D.J.

3rd IWA/WEF Wastewater Treatment Modelling Seminar (WWTmod 2012), Mont-Sainte-Anne, Québec, Canada, 26-28 February 2012.

VII **Effects of influent fractionation, kinetics & stoichiometry and mass transfer on CO_2, CH_4 and H_2 production for (plant-wide) modelling of anaerobic digesters**

Solon, K., Flores-Alsina, X., Gernaey, K.V., Jeppsson, U.

13th World Congress on Anaerobic Digestion (AD13), Santiago de Compostela, Spain, 25-28 June 2013.

VIII **Effects of ion strength and ion pairing on (plant-wide) modelling of anaerobic digestion processes**

Flores-Alsina, X., Kazadi Mbamba, C., **Solon, K.**, Volcke, E.I.P., Tait, S., Batstone, D.J., Gernaey, K.V., Jeppsson, U.

IWA 9th World Water Congress and Exhibition (WWC&E2014), Lisbon, Portugal, 21-26 September 2014.

IX **Effects of influent fractionation, kinetics, stoichiometry and mass transfer on CH_4, H_2 and CO_2 production for (plant-wide) modelling of anaerobic digesters**

Solon, K., Flores-Alsina, X., Gernaey, K.V., Jeppsson, U.

Water Science and Technology, 2015, vol. 71, no. 6, pp. 42-54.

X **A plant wide aqueous phase module describing pH variations and ion speciation/pairing in wastewater treatment process models**

Flores-Alsina, X., Kazadi Mbamba, C., **Solon, K.**, Vrečko, D., Tait, S., Batstone, D.J., Jeppsson, U., Gernaey, K.V.

9th IWA Symposium on Systems Analysis and Integrated Assessment (Watermatex 2015), Gold Coast, Queensland, Australia, 14-17 June 2015.

XI **Effects of ionic strength and ion pairing on modelling of anaerobic digestion in a plant-wide perspective**

Solon, K., Flores-Alsina, X., Kazadi Mbamba, C., Volcke, E.I.P., Tait, S., Batstone, D.J., Gernaey, K.V., Jeppsson, U.

14th World Congress on Anaerobic Digestion (AD14), Viña del Mar, Chile, 15-18 November 2015.

XII **Modelling phosphorus (P), sulphur (S) and iron (Fe) interactions during the simulation of anaerobic digestion processes**

Flores-Alsina, X., **Solon, K.**, Kazadi Mbamba, C., Tait, S., Gernaey, K.V., Jeppsson, U., Batstone, D.J.

14th World Congress on Anaerobic Digestion (AD14), Viña del Mar, Chile, 15-18 November 2015.

XIII **Modelling physico-chemistry in extreme conditions**

Thompson Brewster, E., Tait, S., Vrečko, D., Flores-Alsina, X., Kazadi Mbamba, C., **Solon, K.**, Jeppsson, U., Gernaey, K.V., Batstone, D.J.

5th IWA/WEF Wastewater Treatment Modelling Seminar (WWTmod2016), Annecy, France, 2-6 April 2016.

XIV **The use of advanced aqueous phase chemistry approach with IWA biological process models in a plant-wide context**

Flores-Alsina, X., Kazadi Mbamba, C., Thompson Brewster, E., **Solon, K.**, Vrečko, D., Tait, S., Jeppsson, U., Gernaey, K.V., Batstone, D.J.

5th IWA/WEF Wastewater Treatment Modelling Seminar (WWTmod2016), Annecy, France, 2-6 April 2016.

XV **Using an extended activated sludge model for benchmarking of biological nutrient removal/recovery processes in a plant-wide perspective**

Solon, K., Flores-Alsina, X., Ekama, G.A., Ikumi, D.S., Gernaey, K.V., Jeppsson, U.

2nd IWA Conference on Holistic Sludge Management (HSM2016), Malmö, Sweden, 7-9 June 2016.

XVI **Model-based evaluation of nutrient and energy recovery control strategies in wastewater treatment systems**

Solon, K., Kazadi Mbamba, C., Flores-Alsina, X., Gernaey, K.V., Tait, S., Batstone, D.J., Jeppsson, U

12th IWA Specialized Conference on Instrumentation, Control and Automation (ICA2017), Québec, Canada, 11-14 June 2017.

Other publications related to the subject by the author:

XVII **Emerging challenges for control of the urban water system**

Paulo, L., Saagi, R., **Solon, K.**, Vallet, B.

10th IWA Leading Edge Technology Conference (LET2013), Bordeaux, France, 2-6 June 2013.

XVIII **New criteria for plant wide optimization using Benchmark Simulation Model No. 2**

Solon, K., Snip, L.

SANITAS workshop during the 2nd IWA Specialized Conference in Ecotechnologies for Sewage Treatment Plants (ecoSTP2014), Verona, Italy, 23-25 June 2014.

XIX **Extending the ADM1 with sulfur-related conversions for plant-wide modelling and benchmarking**

Solon, K., Volcke, E.I.P., Jeppsson, U.

Specialised workshop organised by COST Water2020: Conceiving Wastewater Treatment of Tomorrow – Energetic, Environmental and Economic Challenges, Le Pecq, France, 15 April 2015.

XX **Activated Sludge Model No. 3 with bioP module (ASM3 bioP) implemented within the Benchmark Simulation Model No. 1**

Solon, K.

Technical report, Division of Industrial Electrical Engineering and Automation, Lund University, Sweden, LUTEDX/(TEIE-7258)/1-75/(2015).

XXI **IWA Anaerobic Digestion Model No. 1 extended with phosphorus and sulfur – Literature review**

Solon, K.

Technical report, Division of Industrial Electrical Engineering and Automation, Lund University, Sweden, LUTEDX/(TEIE-7254)/1-16/(2015).

XXII **Reject water treatment models – Literature review**

Solon, K.

Technical report, Division of Industrial Electrical Engineering and Automation, Lund University, Sweden, LUTEDX/(TEIE-7253)/1-23/(2015).

XXIII **Physico-chemical modelling (PCM) – A literature review**

Solon, K.

Technical report, Division of Industrial Electrical Engineering and Automation, Lund University, Sweden, LUTEDX/(TEIE-7260)/1-26/(2016).

XXIV **Mathematical models for sulphate reduction processes**

Solon, K.

Technical report, Division of Industrial Electrical Engineering and Automation, Lund University, Sweden, LUTEDX/(TEIE-7262)/1-7/(2016).

Popular Summary

The objective of wastewater treatment is twofold: protecting the public health and the environment. The increase of the world's population and urbanisation has resulted to a rise in water usage and thus, wastewater production. The intensification in clean water demands, as well as depletion of other resources, have eventually led to a growing interest in resource recovery during wastewater treatment. It is recognized that valuable resources, such as clean water, nutrients and energy could be recovered from the wastewater.

Meanwhile, phosphorus is gaining considerable attention due to the alarming depletion of non-renewable phosphate rock reserves. Coincidentally, it is possible to minimize phosphorus, a eutrophying nutrient, in the effluent of wastewater treatment plants through recovery. Another relevant pollutant is sulfur which originates from certain waste streams, such as from tanneries and distilleries. In wastewater treatment plant operation, sulfur may cause problems associated with odour production, corrosion and toxicity. Highly linked to phosphorus and sulfur is iron. The latter is commonly used as a precipitant for phosphorus and has close and significant interactions with sulfur.

Mathematical modelling of wastewater treatment processes is generally used to optimise, control and gain a better understanding of the complex interactions within the plant. Although carbon and nitrogen removal processes have been widely included in plant-wide models, consideration of phosphorus, sulfur and iron has been lagging behind. In this research, the latter three are taken into account in a plant-wide model. The various key stages for the model development are stated below:

- A **physico-chemical model** was developed. This includes: *ion activity corrections* which takes into account that ions are less reactive in a non-ideal solution (such as wastewater), *aqueous phase chemical equilibria* to determine the distribution of various chemical species, *multiple mineral precipitation* to describe the transformation of various compounds from a solution to the solid phase and *gas-liquid transfer* to represent the absorption and volatilization/stripping of gas to the liquid phase and the liquid to the gas phase, respectively. This model was implemented together with standard wastewater treatment models and the results show that a physico-chemical model is important for accurate prediction of processes.

- The **biological models are extended** with processes related to phosphorus, sulfur and iron. The *Activated Sludge Model No. 2d* and *Anaerobic Digestion Model No. 1* are enhanced to include relevant transformation processes. Oxidation reactions are added for aerobic and anoxic processes while reduction reactions are added for anaerobic processes. The model extensions are tested for various case scenarios in order to analyse the interactions between phosphorus, sulfur and iron and the results show the relevance of including them in wastewater treatment process models.
- The above-mentioned model extensions are **incorporated in a plant-wide model** provided by the *Benchmark Simulation Model No. 2*. The complex interactions between phosphorus, sulfur and iron are compounded when considering the recycle of several streams (water, sludge) within a plant-wide model. Other unit processes are modified to take into account the additional state variables. A recovery unit, consisting of a gas stripper, crystallizer and dewatering units, is also modelled to describe the prospect of phosphorus recovery as struvite.

The collective model extensions are used to test various operational strategies aimed at improving the performance of a wastewater treatment plant. Using specified evaluation criteria, which likewise considers the phosphorus, sulfur and iron extensions, comparison of scenarios with different operational and control strategies is facilitated. The resulting plant-wide model is suitable for similar control strategy development aimed at improved operational cost, environmental compliance or resource recovery. Moreover, each of the enhanced models can be independently implemented and used as one sees fit for purpose.

Nomenclature

Acronyms

AD	Anaerobic digestion
ADM1	Anaerobic Digestion Model No. 1. Suffix Ox denotes model version extended with oxygen effects
AE	Algebraic equation
AER	Aerobic tank. Suffixes 1, 2 and 3 correspond to the first, second and third aerobic tank, respectively
ANAER	Anaerobic tank. Suffixes 1 and 2 correspond to the first and second anaerobic tank, respectively
ANOX	Anoxic tank. Suffixes 1 and 2 correspond to the first and second anoxic tank, respectively
AS	Activated sludge
ASM	Activated Sludge Model. Suffixes 1, 2, 2d, 3 and 3-bioP denote the model versions No. 1, 2, 2d, 3 and 3-bioP, respectively
BOD	Biological oxygen demand
BSM	Benchmark Simulation Model. Suffixes 1, 1_LT and 2 denote the model versions No. 1, 1_LT and 2, respectively
CBIM	Continuity-based interfacing method
CEIT PWM	Centro de Estudios e Investigaciones Técnicas (CEIT) plant-wide model
CFD	Computational fluid dynamics
COST	European Cooperation in Science and Technology
EBPR	Enhanced biological phosphorus removal
EQI	Effluent Quality Index
EU	European Union
HFO	Hydrous ferric oxide
HRT	Hydraulic retention time
IWA	International Water Association
OCI	Operational Cost Index
ODE	Ordinary differential equation
PAO	Phosphorus accumulating organisms
PCM	Physico-chemical model
PHA	Polyhydroxyalkanoates
PP	Polyphosphates
SRB	Sulfate-reducing bacteria
TUDP	Technical University of Delft phosphorus model
UASB	Upflow anaerobic sludge blanket
UCTPHO	University of Cape Town Activated Sludge Model
VFA	Volatile fatty acid

WFD	Water Framework Directive
WRRF	Water resource recovery facility
WWTP	Wastewater treatment plant

Chemical formulas

Al	Aluminium
C	Carbon
$CaCO_3$	Calcium carbonate
$CaHPO_4$	Dicalcium phosphate
$Ca_3(PO_4)_2$	Amorphous calcium phosphate
$Ca_4H(PO_4)_3$	Octacalcium phosphate
$Ca_5(PO_4)_3OH$	Hydroxyapatite
CO_2	Carbon dioxide
CH_4	Methane
Fe	Iron
Fe(II)	Ferrous
Fe(III)	Ferric
$FeCl_3$	Ferric chloride
$Fe(OH)_3$	Ferric hydroxide
$FePO_4$	Ferric phosphate
FeS	Ferrous sulfide
$Fe_3(PO_4)_2$	Ferrous phosphate
H, H_2	Hydrogen
H_2S	Hydrogen sulfide
HPO_4^{2-}	Hydrogen phosphate
$H_2PO_4^-$	Biphosphate
K	Potassium
$KMgPO_4$	K-struvite
$MgHPO_4$	Newberyite
$MgNH_4PO_4$	Struvite
Mg, Mg^{2+}	Magnesium
N, N_2	Nitrogen
Na^+	Sodium
NH_3	Ammonia
NH_4^+	Ammonium
O	Oxygen
P	Phosphorus
PO_4^{3-}	Phosphate
S	Sulfur

Model variables

S_A	Acetate (ASM2d)	$g.m^{-3}$
S_{aa}	Amino acids (ADM1)	$kg.m^{-3}$
S_{ac}	Total acetic acid (ADM1)	$kg.m^{-3}$
S_{ALK}	Alkalinity (ASM2d)	$kmol.m^{-3}$
S_{an}	Anions (ADM1)	$kmol.m^{-3}$
S_{bu}	Total butyric acid (ADM1)	$kg.m^{-3}$
S_{Ca+}, S_{Ca}	Calcium (ASM2d, ADM1)	$g.m^{-3}$, $kmol.m^{-3}$
S_{cat}	Cations (ADM1)	$kmol.m^{-3}$
S_{ch4}	Dissolved methane (ADM1)	$kg.m^{-3}$
S_{Cl-}, S_{Cl}	Chloride (ASM2d, ADM1)	$g.m^{-3}$, $kmol.m^{-3}$
S_F	Fermentable substrate (ASM2d)	$g.m^{-3}$
S_{fa}	Soluble fatty acids (ADM1)	$kg.m^{-3}$
S_{H+}	Proton concentration (ADM1)	$kmol.m^{-3}$
S_{h2}	Dissolved hydrogen (ADM1)	$kg.m^{-3}$
S_I	Soluble inerts (ADM1)	$kg.m^{-3}$
S_{IC}	Inorganic carbon (ADM1)	$kmol.m^{-3}$
S_{IS}	Inorganic total sulfides (ADM1)	$kg.m^{-3}$
S_{K+}, S_K	Potassium (ASM2d, ADM1)	$g.m^{-3}$, $kmol.m^{-3}$
S_{Mg2+}, S_{Mg}	Magnesium (ASM2d, ADM1)	$g.m^{-3}$, $kmol.m^{-3}$
S_{Na+}, S_{Na}	Sodium (ASM2d, ADM1)	$g.m^{-3}$, $kmol.m^{-3}$
S_{NH4}	Ammonium (ASM2d)	$g.m^{-3}$
S_{NO3}	Nitrate nitrogen (ASM2d)	$g.m^{-3}$
S_{N2}	Dinitrogen (ASM2d)	$g.m^{-3}$
S_{O2}	Dissolved oxygen (ASM2d)	$g.m^{-3}$
S_{pro}	Total propionic acid (ADM1)	$kg.m^{-3}$
S_S	Readily biodegradable COD (ASM2d)	$g.m^{-3}$
S_{SO4}	Sulfate (ASM2d, ADM1)	$g.m^{-3}$, $kmol.m^{-3}$
S_{su}	Sugars (ADM1)	$kg.m^{-3}$
S_{va}	Total valeric acid (ADM1)	$kg.m^{-3}$
X_A	Autotrophic biomass (ASM2d)	$g.m^{-3}$
X_{aa}	Amino acid degraders (ADM1)	$kg.m^{-3}$
X_{ac}	Acetate degraders (ADM1)	$kg.m^{-3}$
X_{aSRB}	Acetotrophic sulfate-reducing bacteria (ADM1)	$kg.m^{-3}$
X_{bSRB}	Butyrate-degrading sulfate-reducing bacteria (ADM1)	$kg.m^{-3}$
X_C	Composite materials (ADM1)	$kg.m^{-3}$
X_{ch}	Carbohydrates (ADM1)	$kg.m^{-3}$
X_{c4}	Valerate- and butyrate-degraders (ADM1)	$kg.m^{-3}$
X_{c4SRB}	Valerate- and butyrate-degrading sulfate-reducing bacteria (ADM1)	$kg.m^{-3}$

X_{fa}	Fatty acid-degrading acetogenic bacteria (ADM1)	$kg.m^{-3}$
X_H	Heterotrophic biomass (ASM2d)	$g.m^{-3}$
X_{HFO}	Hydrous ferric oxide (ASM2d, ADM1)	$g.m^{-3}$, $kmol.m^{-3}$
$X_{HFO,H}$	Hydrous ferric oxide with high adsorption capacity (ASM2d, ADM1)	$g.m^{-3}$, $kmol.m^{-3}$
$X_{HFO,L}$	Hydrous ferric oxide with low adsorption capacity (ASM2d, ADM1)	$g.m^{-3}$, $kmol.m^{-3}$
$X_{HFO,H,P}$	$X_{HFO,H}$ with adsorbed phosphate (ASM2d)	$g.m^{-3}$
$X_{HFO,L,P}$	$X_{HFO,L}$ with adsorbed phosphate (ASM2d)	$g.m^{-3}$
X_{hSRB}	Hydrogenotrophic sulfate-reducing bacteria (ADM1)	$kg.m^{-3}$
X_{h2}	Hydrogenotrophic methanogens (ADM1)	$kg.m^{-3}$
X_I	Inert particulates (ASM2d, ADM1)	$g.m^{-3}$, $kg.m^{-3}$
X_{li}	Lipids concentration (ADM1)	$kg.m^{-3}$
$X_{Me(OH)}$	Metal hydroxides (ASM2d)	$g.m^{-3}$
X_{MeP}	Metal phosphates (ASM2d)	$g.m^{-3}$
X_{pao}	Phosphorus accumulating organisms (ASM2d, ADM1)	$g.m^{-3}$, $kg.m^{-3}$
X_{pha}	Polyhydroxyalkanoates (ASM2d, ADM1)	$g.m^{-3}$, $kg.m^{-3}$
X_{pp}	Polyphosphates (ASM2d, ADM1)	$g.m^{-3}$, $kmol.m^{-3}$
X_{pr}	Proteins (ADM1)	$kg.m^{-3}$
X_{pro}	Propionate-degraders (ADM1)	$kg.m^{-3}$
X_{pSRB}	Propionate-degrading sulfate-reducing bacteria (ADM1)	$kg.m^{-3}$
X_S	Slowly biodegradable substrates (ASM2d)	$g.m^{-3}$
X_{S0}	Elemental sulfur (ASM2d, ADM1)	$g.m^{-3}$, $kg.m^{-3}$
X_{SRB}	Sulfate-reducing bacteria (ADM1)	$kg.m^{-3}$
X_{su}	Sugar degraders (ADM1)	$kg.m^{-3}$

Other symbols

α	Ion-specific parameter (used in ion activity correction)	-
$\alpha_{C,i}$	Mass fractions of carbon in a component *i*	-
$\alpha_{H,i}$	Mass fractions of hydrogen in a component *i*	-
$\alpha_{O,i}$	Mass fractions of oxygen in a component *i*	-
$\alpha_{N,i}$	Mass fractions of nitrogen in a component *i*	-
$\alpha_{P,i}$	Mass fractions of phosphorus in a component *i*	-
β	Ion-specific parameter (used in ion activity correction)	-
η_{NO3}	Reduction rate for nitrate oxidation	-
ρ_j	Kinetic rate	$kg.m^{-3}.d^{-1}$

γ	Activity coefficient	-
μ_{SRB}	Maximum growth rate of SRB	d^{-1}
a	Contact area between the liquid and gas phase	m^2
A	Temperature-dependent constant (used in ion activity correction)	-
AE	Aeration energy	$kWh.d^{-1}$
ASFH	Active site factor of $X_{HFO,H}$	mol^{-1}
ASFL	Active site factor of $X_{HFO,L}$	mol^{-1}
AMFe	Atomic mass of iron	$g.mol^{-1}$
AMP	Atomic mass of phosphorus	$g.mol^{-1}$
b	Disintegration rate	d^{-1}
B	Temperature-dependent constant (used in ion activity correction)	-
BM	Biomass	-
BOD_5	BOD measured after 5 days	$g\ BOD.m^{-3}$
C_i	Dissolved concentration of the gaseous component	$kg.m^{-3}$
COD	Chemical oxygen demand	$g\ COD.m^{-3}$
COD_{total}	Total COD	$g\ COD.m^{-3}$
C_{sat}	Saturation concentration	$kg.m^{-3}$
$E_{production}$	Energy production	$kWh.d^{-1}$
$f_{va,PHA}$	Yield of valerate on PHA	-
$f_{bu,PHA}$	Yield of butyrate on PHA	-
$f_{pro,PHA}$	Yield of propionate on PHA	-
$f_{ac,PHA}$	Yield of acetate on PHA	-
G_{CH4}	Methane gas production	$kg.d^{-1}$
G_{H2S}	Hydrogen sulfide gas production	$kg.d^{-1}$
I	Ionic strength	$kmol.m^{-3}$
$I_{H2S,SRB}$	Hydrogen sulfide inhibition on SRB	-
IAP	Ion activity product	-
K_A	Saturation coefficient for growth on acetate	$g.m^{-3}$
k_{cryst}	Precipitation rate constant	d^{-1}
k_{dec}	Decay rate	d^{-1}
K_{diss}	Dissolution rate constant	d^{-1}
K_{eq}	Equilibrium constant	-
K_F	Saturation coefficient for growth on readily biodegradable substrate	$g.m^{-3}$
$K_{Fe(III),Fe(II)}$	Conversion rate of Fe(III) to Fe(II)	$m^3.kmol^{-1}.d^{-1}$
$K_{H,i}$	Henry's constant	$kmol.m^{-3}.bar^{-1}$
K_{NH4}	Saturation coefficient for ammonia	$g.m^{-3}$
K_{NO3}	Saturation coefficient for nitrite	$g.m^{-3}$
K_{O2}	Saturation coefficient for oxygen	$g.m^{-3}$

K_{PO4}	Saturation coefficient for phosphate	$g.m^{-3}$
K_{SO4}	Saturation coefficient for sulfate	$g.m^{-3}$
k_L	Mass transfer rate	$m.d^{-1}$
$k_L{\cdot}a$ or k_La	Volumetric mass transfer coefficient	$m^{-3}.d^{-1}$
k_m	Maximum specific uptake rate	d^{-1}
k_{oxi}	Oxidation rate	$m^3.g^{-1}.d^{-1}$
K_P	Saturation coefficient for phosphate sorption onto HFO	$g.m^{-3}$
$K_{P,diss}$	Saturation coefficient for phosphate dissolution from HFO	$g.m^{-3}$
K_{PP}	Saturation coefficient for polyphosphate	$kg.m^{-3}$
K_{PP}	Potassium content of polyphosphate	-
$k_{red,Fe(III)}$	Reduction rate of Fe(III)	$m^3.g^{-1}.d^{-1}$
K_{SP}	Solubility product constant	-
$K_{S,SO4}$	Half saturation constant for sulfate	$kmol.m^{-3}$
M_{FeCl3}	Mass flow rate of ferric chloride	$kg\ Fe.d^{-1}$
Mg_{PP}	Magnesium content of polyphosphate	-
$M_{Mg(OH)2}$	Mass flow rate of magnesium hydroxide	$kg\ Mg.d^{-1}$
N_i	Nitrogen content of component *i*	-
$N_{Kjeldahl}$	Kjeldahl nitrogen	$g\ N.m^{-3}$
$N_{removed}$	Total nitrogen removed	$g\ N.m^{-3}$
N_{total}	Total nitrogen	$g\ N.m^{-3}$
P_i	Partial pressure	bar
P_{inorg}	Inorganic phosphorus	$g\ P.m^{-3}$
$P_{removed}$	Total phosphorus removed	$g\ P.m^{-3}$
P_{total}	Total phosphorus	$g\ P.m^{-3}$
q_{aging}	Aging rate of HFO	d^{-1}
$q_{binding}$	Sorption rate of phosphates to HFO	d^{-1}
q_{diss}	Dissolution rate of HFO	d^{-1}
$q_{coprecip-P}$	Binding rate of HFO	d^{-1}
q_{PHA}	Rate constant for storage of PHA	d^{-1}
r_i	Rate of crystallization	d^{-1}
$r_{i,G/L}$	Mass transfer rate between gas and liquid phase	d^{-1}
SI	Saturation Index	-
$S_{recovered}$	Struvite recovered	$kg\ struvite.d^{-1}$
$S_{\{i\}}$	Ion activity of ion *i*	$kmol.m^{-3}$
$S_{[i]}$	Ion concentration of ion *i*	$kmol.m^{-3}$
$SP_{disposal}$	Sludge production for disposal	$kg.d^{-1}$
TIV	Time in violation	%
TSS	Total suspended solids	$g.m^{-3}$
X_{cryst}	Concentration of the precipitate	$kg.m^{-3}$
Y_{aSRB}	Yield of aSRB	-

Y_{c4SRB}	Yield of c4SRB	-
Y_{hSRB}	Yield of hSRB	-
Y_{PO4}	Yield of biomass on phosphate	$kmol.kg^{-1}$
Y_{pSRB}	Yield of pSRB	-
Y_{SRB}	Yield of SRB	-
z_i	Charge of ion *i*	-

Chapter 1

Introduction

This chapter gives an overall view of this thesis work. In particular, it presents the motivation behind this research study and what it is expected to accomplish. Moreover, it provides the contributions of this research work to the current state of knowledge in the field and ends with a synopsis of the chapters of this thesis.

1.1. Motivation of the Research Study

The fundamental goal of treating wastewater is to protect human health. Nevertheless, protecting the environment has also become essential in the last decades, such that stringent effluent discharge limits for wastewater treatment plants have been set for eutrophying substances, organic matter, priority substances and other pollutants.

Due to the various and numerous biological, chemical and physical factors affecting wastewater treatment processes, the disturbances, dynamics and uncertainties in the influent, it is usually a challenge to control the plant. On this subject, wastewater treatment modelling is a pragmatic approach that has been widely-employed for finding ways to control and improve the performance of wastewater treatment plants as efficiently and at the lowest cost possible. Moreover, it is also effective to simply gain an understanding on the complexity of the interactions in wastewater treatment processes. The benchmark simulation models, created for objective evaluation of control strategies for wastewater treatment plants, have been used for such purposes.

Currently, there is also focus on maximizing the resource potential of wastewater. Valuable resources such as clean water, nutrients and energy could be recovered

from the wastewater while concurrently protecting the environment. Along these lines, the recovery potential of phosphorus from wastewater is gaining considerable attention since it has an adverse effect on surface waters because of its eutrophying potential all the while considering that its natural source is non-renewable and is becoming increasingly expensive. It is recognized that while phosphorus removal has been a focus of wastewater treatment plant (WWTP) design and operation, its inclusion in plant-wide models is lagging behind that of carbon and nitrogen removal. Aside from phosphorus, sulfur in wastewater is also gaining importance due to the operational problems caused by hydrogen sulfide (e.g. odour problems, corrosion, toxicity), especially when dealing with wastewater streams coming from tanneries and distilleries. Additionally, iron is also of importance as it is widely used for phosphorus removal in WWTPs and has close interlinks with sulfur.

As a consequence, current wastewater treatment models need to be updated to include processes to describe biological and chemical phosphorus removal, as well as sulfur and iron transformation processes. As there is a large interest in resource recovery, which is mostly accomplished by precipitation within the WWTP, an improved physico-chemical model is also needed. Thus, inclusion of a plant-wide pH model and extending the activated sludge and anaerobic digestion model to describe phosphorus, sulfur, iron and other relevant variables are of primary importance. The resulting model can be used for simulation-based scenario analysis aiming at finding ways to improve the operation of a WWTP designed for carbon, nitrogen and phosphorus removal.

1.2. Objectives of the Study

The main objective of this thesis is to extend wastewater treatment process models with phosphorus, iron and sulfur conversions. The extensions are required for the development of a plant-wide model platform, which allows for objective analysis and comparison of various control and operational strategies aimed at combined carbon, nitrogen and phosphorus removal from the wastewater.

To achieve the main objective, several working points are accomplished as listed below.

- Development of a physico-chemical module which includes: weak acid-base chemistry, ion activity corrections and ion pairing effects. In addition, multiple mineral precipitation as well as gas-liquid transfer processes are also included.

- Addition of iron and sulfur conversions in the Activated Sludge Model No. 2d (ASM2d).
- Addition of phosphorus, iron and sulfur conversions in the Anaerobic Digestion Model No. 1 (ADM1).
- Development of a plant-wide model comprising of these extensions using the Benchmark Simulation Model No. 2 (BSM2) platform. This phase includes, among others, developing the model interfaces, plant performance criteria and evaluation and additional processes (e.g. for struvite recovery).
- Development of control and operational strategies using the developed extended plant-wide model aimed at phosphorus removal and/or recovery.

Several limitations and assumptions are implicit in this study. The model extensions are all implemented within the framework provided by the BSM2. Greenhouse gas formation and micropollutants are not considered in the study. The influent data used in the model simulations are synthetically created but are assumed to reflect realistic wastewater influent concentrations and dynamics. Validation of the developed models, either by lab-scale experiments or full-scale tests, is not part of this work but is considered imperative. More specific and detailed limitations to each model extension are discussed in the subsequent relevant chapters.

1.3. Contributions to Research

The key contributions of this research to the state of knowledge are stated below.

- A versatile/general module which takes into account ion activity corrections and ion pairing is developed. This can be easily added to different activated sludge (AS) and anaerobic digestion (AD) models and can reliably predict pH and speciation of components under anaerobic, anoxic and aerobic conditions in AS and AD models. A solving routine is also developed that handles the systems of equations describing fast and slow reactions simultaneously.
- Phosphorus, sulfur and iron transformations under anaerobic, anoxic and aerobic conditions are added to ASM2d for plant-wide phosphorus modelling and simulation.

- An extension of ADM1 with sulfate reduction, iron reduction and phosphorus transformations is developed for plant-wide phosphorus modelling and simulation. In addition, model interfaces are developed to link the extended ASM2d and ADM1 variables.
- A platform for control strategy development, testing and evaluation for wastewater treatment plants designed for carbon, nitrogen and phosphorus removal and/or recovery is presented.
- Multi-criteria (economic/environmental) analysis of the results is provided taking into account phosphorus-related components and cost of chemicals/price of resource for effluent quality and operational cost evaluation, respectively.

This thesis is based mainly on five papers as listed in the List of Publications. This section describes the contents of these papers and the contributions of each to the research field. All of the papers are published in the journal Water Research (impact factor 2015: 5.991).

Paper I: This paper describes the implementation of the physico-chemical framework for the ADM1. It includes ion activity corrections and accounts for ion-pairing effects in order to see the effects on pH and anaerobic digestion products. Several scenarios are set up to see the physico-chemical effects from the water to the sludge line. The principles of the developed solving routine for simultaneous solution of fast and slow reactions are presented.

Paper II: This paper presents the modelling work on incorporation of the physico-chemical framework into general wastewater treatment process models, such as ASM1, ASM2d, ASM3 and ADM1. An extensive aqueous phase chemistry module is interfaced with these models, and enables depiction of speciation of different wastewater components under different conditions (e.g. aerobic, anaerobic, anoxic). The applicability of the module is also discussed. The solving routine from the previous paper is improved to include simulated annealing for optimizing initial values used in the model simulations.

Paper III: This paper presents the modelling of the anaerobic digestion of cane-molasses vinasse, a high-strength and sulfate-rich wastewater, by extending the ADM1 with sulfate reduction processes. The model is validated using experimental data and shows accurate prediction of pH, sulfides, acids, chemical oxygen demand (COD), methane and hydrogen sulfide in the gas phase. Moreover, failure of methanogenesis and sulfidogenesis at high loading rates is also predicted in the model.

Paper IV: This paper presents the extensions to the ADM1 for applications in plant-wide modelling and simulations. Because of the complex interactions between the phosphorus (P), iron (Fe) and sulfur (S) cycles, their transformations are taken into account within the anaerobic digester. Several alternatives of the extensions are simulated and the effects on the physico-chemical and biochemical transformations are analysed. The development of the model interfaces between the extended ADM1 and the plant-wide state variables is presented.

Paper V: This paper focuses on the effects of different control strategies on phosphorus transformations in wastewater treatment plants. The BSM2 platform is extended to take into account P, S and Fe transformations. This is done by extending the biological models, the interfaces, the evaluation criteria, and if need be, additional unit processes for resource recovery (i.e. stripping unit and crystallizer). Three control strategies are tested and compared using plant performance criteria, such as Effluent Quality Index (*EQI*) and Operational Cost Index (*OCI*).

The various model extensions and developments are implemented in Matlab®/Simulink®. All source code is freely distributed and presented as four model packages described below.

- The ADM1 is extended with ion activity corrections, ion pairing effects and aqueous phase equilibria. The extended ADM1 model is implemented using the BSM2. This is the supplementing model for Paper I.
- A general physico-chemical module is developed, which includes ion activity corrections, ion pairing effects and aqueous phase equilibria. This module is compatible with the biochemical models ASM1, ASM2d, ASM3 and ADM1. The ASMs are implemented using the BSM1 while the ADM1 is implemented using the BSM2. These are the supplementing models for Paper II.
- The ADM1 is extended with processes related to phosphorus, sulfur and iron. In addition, the pool of composite materials is removed and directly mapped into carbohydrates, proteins, lipids and inerts. This extended ADM1 model is implemented using the BSM2. This is the supplementing model for Paper IV.
- The ASM2d and ADM1 are both extended with processes to describe phosphorus, sulfur and iron transformations. Model interfaces, recovery unit processes and evaluation criteria are also updated to take into account the new state variables. These extensions are implemented using the BSM2. This is the supplementing model for Paper V.

1.4. Thesis Structure

This thesis presents the sequential phases of model extensions and developments related to wastewater treatment processes for plant-wide modelling of simultaneous carbon, nitrogen and phosphorus removal. Each model development is implemented and several test scenarios are evaluated and analysed. Findings for each key model development stage are also presented.

In Chapter 2, the background to the study is presented. Basic concepts are briefly discussed, focusing on the following wastewater treatment processes: activated sludge system and the Activated Sludge Models, anaerobic digestion and the Anaerobic Digestion Model No. 1, and the Benchmark Simulation Models. State-of-the-art for the aforementioned models and their current applications are discussed.

Chapter 3 starts with an overview of the physico-chemical framework and how it is relevant for this research work. The main concepts of the framework are presented as well as their implementation for coupling them with wastewater treatment process models, particularly to biological models (from Papers I and II). The chapter concludes with a scenario analysis and discussion of key findings from the relevant papers.

Mainly model developments are presented in Chapter 4. It focuses on the extensions of the biological models, ASM2d and ADM1, with processes describing phosphorus, sulfur and iron transformations (from Papers III, IV and V).

Chapter 5 combines the model developments presented in Chapters 3 and 4 into the Benchmark Simulation Model platform in order to provide a platform for control strategy development, testing and evaluation aimed at combined organics, nitrogen and phosphorus removal and/or recovery. Other relevant parts of the approach are discussed, such as: plant layout and influent characteristics, model interfaces, auxiliary models (in case of aiming for resource recovery) and extended evaluation criteria. The platform is then used for scenario analysis of different control strategies for which the findings from Paper V are discussed.

General conclusions from this research are detailed in Chapter 6, together with ideas for future work and perspectives.

Chapter 2

Background

This chapter provides an overview of the field of wastewater treatment, with principal focus on its modelling aspects. A summary of the two key biological models in this thesis: the ASM and ADM1 are presented. The chapter ends with a discussion of the BSM platform.

2.1. Wastewater Treatment

Water fulfils many functions in human society: domestic, industrial, agricultural, infrastructure, recreational, transportation use, energy use, etc. As a consequence of its usage, water becomes contaminated, which affects the water cycle and creates disturbances in natural functions (WWPA, 2016). In order to avoid this, regulations come into place and establish compulsory water quality criteria.

Early legislations related to water in the European Union (EU) focused on certain types of water uses and water areas: bathing waters (CEC, 1976), fish waters (CEC, 1978), shellfish waters (CEC, 1979) and drinking water (CEC, 1975; CEC, 1980). Experiences learned and gaps identified from former directives then led to the development of the Water Framework Directive (WFD) (CEC, 2000). It is more of a global approach for solving EU's water pollution problem aiming for good ecological and chemical quality status for all waters through involvement of all stakeholders in the development, management and implementation. Thus, it also encompasses implementation of measures from the earlier EU Directives, including the Urban Wastewater Treatment Directive (CEC, 1991) wherein the EU addresses the main source of water quality deterioration. The objective of the Urban Wastewater Treatment Directive is to protect the environment from adverse

effects of urban wastewater discharge by prescribing wastewater collection and treatment for all EU urban areas and considering different sensitivity classes of receiving waters for discharge. It sets emission limit values and in order to achieve these, wastewater should be treated up to a certain degree before disposal to receiving waters or, when applicable, before re-use.

The contaminated water, or wastewater, contains significant amounts of pollutants, which results in oxygen depletion when discharged directly to surface waters. The wastewater composition largely varies depending on the area it is collected from. It generally constitutes contaminants such as solids, biodegradable and non-biodegradable (or slowly biodegradable) compounds, nutrients, toxic substances, pathogenic organisms, etc. Each of these different types of contaminations often requires different ways of treatment (physical, chemical, biological), thus a conventional wastewater treatment plant, such as shown in Figure 2.1, also constitutes several stages wherein a certain type of pollutant is targeted to be removed in each stage. The main objective of wastewater treatment is to allow urban wastewater discharge into surface waters ensuring protection of public health and the environment (Pescod, 1992).

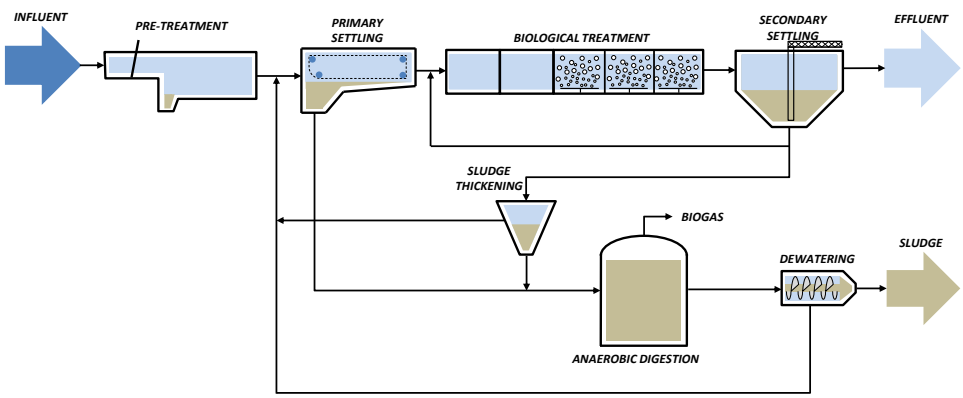

Figure 2.1. An example of a wastewater treatment plant configuration.

Typically, the influent wastewater first undergoes pre-treatment, which is aimed at removing coarse materials and particles, such as sand. These large solid materials might cause operational problems further along the treatment process, such as blocking of pumps and mains, thus their removal should be at an early stage of the treatment process. For this purpose, bar screens, sieves and grit chambers are installed. Settling of settleable undissolved particles is stimulated during the next step of primary sedimentation. Due to particle flocculation, i.e. by adding chemicals or simply by biological mechanisms, particles become larger and

settling is promoted. The next stage is biological treatment wherein microorganisms are used to consume and degrade the contaminants in the wastewater. Aeration is often provided during this stage to promote microbial growth. A secondary settling tank follows the biological treatment to separate the treated wastewater from the sludge that settles, containing the contaminant-degrading organisms. The settled sludge is fed again into the biological reactor as seen in Figure 2.1. In practice, there are different types of biological treatments employed, such as activated sludge and trickling filter. The excess sludge, which mainly contains water, is sent to a thickener/flotation unit to further remove a large part of liquid from the sludge. It is then sent to an anaerobic digester for stabilization. Here, the sludge is degraded by various types of bacteria. One of the main advantages of anaerobic digestion is the production of biogas, which can be used for heat and power generation. The residual organic matter is chemically stable and contains a reduced amount of pathogens. It then goes into a dewatering unit to reduce its volume, saving storage and making it less expensive to transport.

In WWTP operation, the main function is to effectively remove pollutants from the wastewater or convert them into less detrimental compounds, such that the effluent meets permit requirements using appropriate treatment technologies at the lowest possible cost. Reducing the cost can involve recovering resources from the process, such as nutrients, biogas and water for re-use (Verstraete et al., 2009). However, due to complex interactions of different variables relating to the operation of the wastewater treatment plant, it is time and again a challenge to control the plant operation in such a way as to treat the wastewater to levels set by legislation at the lowest possible cost. In this respect, mathematical models and simulations tools for wastewater treatment plant processes become useful in predicting their behaviour (Henze et al., 2008; Jeppsson, 1996) and in exploring different approaches to improve plant performance (Jeppsson et al., 2013). Dochain & Vanrolleghem (2001) and Gernaey et al. (2004) mention the three main application areas of models in the field of wastewater treatment, which are for: learning, design and process optimization.

The activated sludge models (Henze et al., 2000) developed by the International Water Association (IWA), especially the Activated Sludge Model No. 1 (ASM1) (Henze et al., 1987), has been the trigger for general acceptance of wastewater treatment modelling in research and also in industry (Gernaey et al., 2004). Aside from the ASM family, the Anaerobic Digestion Model No. 1 (ADM1) (Batstone et al., 2002) was later developed as a consensus model and a platform for anaerobic process modelling and simulation. All of these IWA standard models have been widely used in research resulting in thousands of publications. Moreover, they are also commonly included in proprietary wastewater treatment process simulators, such as BioWin™, GPS-X™, WEST®, STOAT™ and SIMBA®. This thesis work focuses on these two key biological models and they will be further discussed in the next subsections and chapters.

Just in the last ten years, there has been a rapid transition of WWTPs into water resource recovery facilities (WRRFs). Wastewater is now considered a resource from where nutrients, energy and water can be recovered. In line with this, plant-wide modelling of wastewater treatment processes needs to account for new processes and state variables. In this research work, emphasis is given to phosphorus removal and/or recovery. Wastewater contains significant amounts of phosphorus, which legislation requires to be reduced to legal limits before discharge onto surface waters due to the fact that it is also responsible for eutrophication. On the other hand, phosphorus is considered a limited resource and only an estimated 50-100 years is left before the known reserves of phosphate rock will be depleted (Herring & Fantel, 1993; Seyhan et al., 2012), with a more conservative estimate of up to 300 years according to Cordell & White (2011). Thus, phosphorus recovery from wastewater becomes a viable prospect to consider (Le Corre et al., 2009).

From a wastewater treatment modelling perspective, phosphorus removal and/or recovery requires an inevitable increase of model complexity in order to correctly describe phosphorus transformation processes. Since phosphorus occurs mostly as orthophosphates, such as PO_4^{3-} and HPO_4^{2-}, their valency suggests strong influence on ion pairing and ion activity, which affects pH and mineral precipitation (Tait et al., 2012). Phosphorus is also highly associated with iron as iron salts are commonly used to precipitate phosphorus (de-Bashan & Bashan, 2004; Gutierrez et al., 2010). The relationship of iron with sulfur is also significant because the former reduces phosphorus precipitation due to its preferential binding with sulfur (Kleeberg, 1997; Nürnberg, 1996) and results in release of phosphates. By itself, sulfur is also becoming important because of the adverse effects of sulfur compounds during plant operation, e.g. inhibitory effects of sulfide on some bacterial population and causing odour, corrosion and safety problems (Pol et al., 1998; Zhang et al., 2008). Thus, the development of a plant-wide model for organics, nitrogen and phosphorus removal comes in several stages: (1) the development of the aqueous phase chemical equilibria model to correctly describe and predict pH, speciation of the different compounds and precipitation reactions, (2) extension of the biological models by taking into account new state variables and (3) integration of the models into a plant-wide model with new unit processes for recovery, extended interfaces to link the different models together and new evaluation criteria (Jeppsson et al., 2013).

2.2. The Activated Sludge Models

The activated sludge models are mathematical models describing biological and chemical reactions occurring in activated sludge systems. About fifteen years prior to the publication of the Activated Sludge Model No. 1 (ASM1), several research groups had already been working on mathematical modelling of activated sludge systems. The objective of the development of the ASM1 was to create a general framework of a model with complexity as low as possible but still able to accurately predict biological processes (Henze et al., 1987). Work on ASM1 began in 1983 (Henze et al., 1987) and is the foundation for further developments of the ASMs and their extensions. They have been accepted by wastewater treatment practitioners and researchers over the last two decades. The ASMs are presented conveniently in a table form containing a stoichiometric matrix and kinetic vector (Hauduc et al., 2013; Petersen, 1965) using notations recommended by Grau et al. (1983).

The first activated sludge model, ASM1, describes biological oxidation of carbon, nitrification and denitrification and is therefore used to simulate carbon and nitrogen removal in activated sludge systems. Carbonaceous and nitrogenous compounds are subdivided into fractions based on biodegradability and solubility (Gernaey et al., 2004). The model considers four processes: (1) growth of autotrophs and heterotrophs, (2) decay of autotrophs and heterotrophs, (3) hydrolysis of particulate organics and (4) ammonification of soluble organic nitrogen. The rate of each process is expressed as a series of Monod-type switching functions, allowing it to occur only under a certain condition (e.g. whether aerobic, anoxic, anaerobic) (Seviour & Nielsen, 2010).

Due to the need to meet effluent quality standards in terms of both nitrogen and phosphorus, modelling of biological phosphorus removal became essential. This is a deficit of the ASM1, which led to the development of the Activated Sludge Model No. 2 (ASM2) (Henze et al., 1995). ASM2 is an extension of ASM1 and includes biological and chemical phosphorus removal in addition to descriptions of carbon and nitrogen removal. Three hydrolysis processes of particulate organics were distinguished based on electron acceptors. A fermentation process is also included, which necessitates distinguishing readily biodegradable substrates as either fermentable substrates or fermentation products. With respect to phosphorus-related processes, inorganic phosphorus, phosphorus accumulating organisms (PAO), polyhydroxyalkanoates (PHA) and polyphosphates (PP) are included as additional state variables. Utilizing the energy from the hydrolysis of PP, the PAO are capable of taking up fermentation products and storing them as PHA (Figure 2.2a). Furthermore, the energy obtained from respiration of PHA is used by PAO to store inorganic phosphorus as PP (Figure 2.2b). Other important

processes included in ASM2 are the precipitation of phosphate with ferric hydroxide, $Fe(OH)_3$ and the redissolution of the formed ferric phosphate, $FePO_4$.

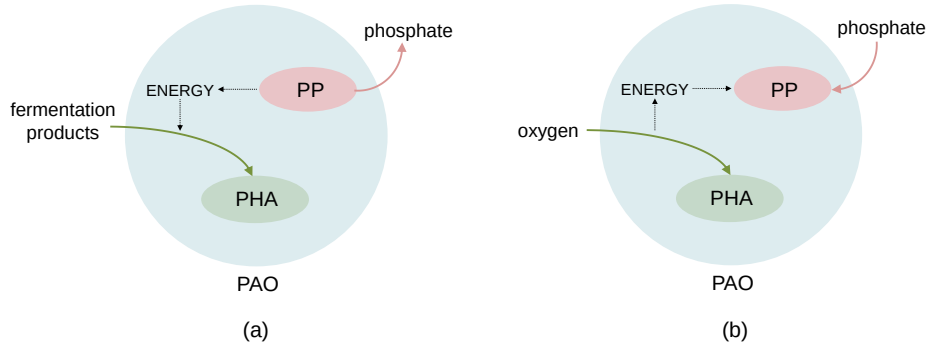

Figure 2.2. Storage mechanisms of (a) polyhydroxyalkanoates and (b) polyphosphates during anaerobic and aerobic conditions, respectively.

The ASM2 was then extended to the Activated Sludge Model No. 2d (ASM2d) (Henze et al., 1999) as understanding of the role of denitrification grew. This entails addition of two processes: (1) storage of inorganic phosphorus as PP using the energy obtained from the anoxic respiration of PHA and (2) anoxic growth of PAO. In both processes, the rate constant for storage of PP and the maximum growth rate of PAO are assumed to occur at reduced rates during anoxic conditions to account for the fact that only a fraction of the PAO has capabilities to denitrify or that denitrification occurs at a slower rate (Henze et al., 1999). This model is widely-used when accounting for enhanced biological phosphorus removal (EBPR) processes (Seviour & Nielsen, 2010).

The Activated Sludge Model No. 3 (ASM3) (Gujer et al., 1999) tackles some of the limitations of ASM1, especially dealing with issues to facilitate model calibration. An important difference between ASM1 and ASM3 is in the COD flow (Figure 2.3). In ASM1, the death-regeneration cycle of the heterotrophs and the decay of nitrifiers are strongly interrelated while for ASM3, all the conversion processes of the heterotrophs and nitrifiers are clearly separated and the decay processes are identical (Gernaey et al., 2004; Gujer et al., 1999). ASM3 also considers that substrates are first stored into cell internal storage compounds before being taken up by heterotrophic biomass. The storage of substrates, growth of heterotrophs, respiration of cell internal storage compounds and endogenous respiration of both heterotrophs and nitrifiers are assumed to occur during aerobic and anoxic conditions.

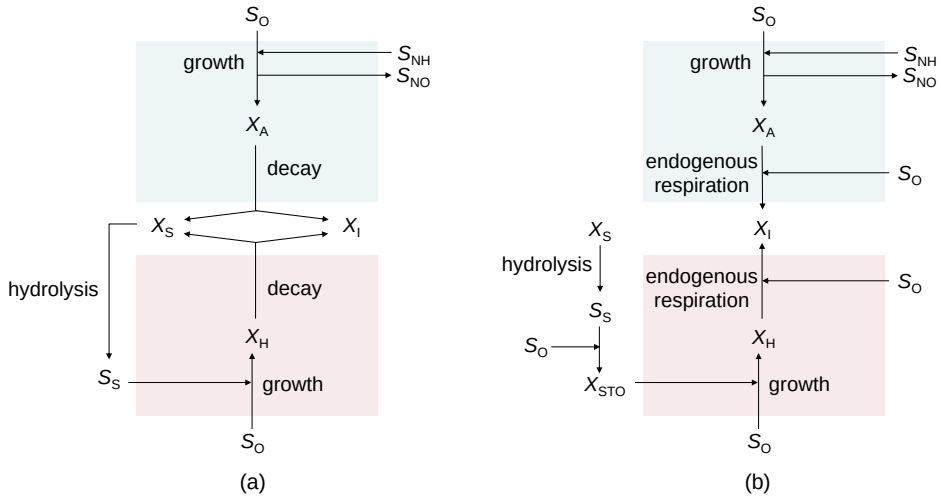

Figure 2.3. COD fluxes in (a) ASM1 and (b) ASM3 (adapted from Gernaey et al. (2004)).

Other significant extensions to the ASMs are the ASM3-bioP and TUDP models. The ASM3-bioP allows for the prediction of EBPR through inclusion of PAO-related processes adapted from ASM2d into ASM3 (Rieger et al., 2001). A metabolic phosphorus model is included in ASM2 (van Veldhuizen et al., 1999) and ASM2d (Meijer, 2004; Meijer et al., 2002) referred to as the Technical University Delft Phosphorus (TUDP) model. Both models have been applied to full-scale wastewater treatment plants. Aside from the above-discussed models, there are still a number of activated sludge models developed and used by researchers and wastewater practitioners, such as the Barker and Dold model (Barker & Dold, 1997), UCTPHO model (Wentzel et al., 1989a; Wentzel et al., 1989b; Wentzel et al., 1988) and the CEIT Plant-Wide Model (CEIT PWM) (Grau et al., 2007).

Table 2.1 presents an overview of the different processes included in the IWA published ASMs showing important features of each model. These, together with the other described models, are commonly implemented and used in numerous simulation platforms and are used to a great extent for scientific research to study biological processes in real and hypothetical systems.

Table 2.1. Overview of activated sludge models (Gernaey et al., 2004; Hauduc et al., 2013).

Model	Substrates	Nitrification	Denitrification	Heterotrophic /autotrophic decay	Hydrolysis	Bio-P	Denitrifying PAOs	Lysis of PAO/PHA	Fermentation	Chemical P removal
ASM1	CN	X	X	DR, Cst	EA					
ASM3	CN	X	X	ER, EA	Cst					
ASM2	CNP	X	X	DR, Cst	EA	X		Cst	X	X
ASM2d	CNP	X	X	DR, Cst	EA	X	X	Cst	X	X

DR = death regeneration principle; EA = electron acceptor dependent; Cst = not electron acceptor dependent; C = carbon; N = nitrogen; P = phosphorus

2.3. The Anaerobic Digestion Model No. 1

Anaerobic digestion involves the breakdown of complex molecules into simpler substances in the absence of oxygen by a population of anaerobic microorganisms, wherein, the disintegration of each type of organic compounds requires a specific type of microorganism (Lettinga & van Haandel, 1993). This established process is utilized for biological waste stabilization. During the past 25 years, anaerobic digestion has gained popularity for treatment of organic municipal waste and wastewater, of which a large percentage of the installations are located in Europe (De Baere, 2006). Compared to aerobic treatment systems, anaerobic treatment requires less energy, generates less sludge and produces valuable by-products (Chen et al., 2008; de Mes et al., 2003; Holm-Nielsen et al., 2009; Mata-Alvarez et al., 2000; Metcalf & Eddy, 2014). In addition to these, the main benefit of this process is the potential energy recovery (Appels et al., 2008; Chynoweth et al., 2001) for instance through production of methane, a strong greenhouse gas (Lashof & Ahuja, 1990).

Appels et al. (2011) mention that although the process is widely-applied, there are still further research areas to explore for further improvement and optimisation of the anaerobic digestion performance. One approach could be the use of mathematical modelling in order to gain more understanding of the complex phenomena and interactions occurring during anaerobic digestion (Yu et al., 2013), an example of which is the Anaerobic Digestion Model No. 1 (ADM1) (Batstone et al., 2002).

The ADM1 is a structured model consisting of biochemical and physico-chemical processes aimed to help in the design, operation and optimization of full-scale anaerobic digestion plants (Batstone & Keller, 2003; Batstone et al., 2002). Before

the publication of the ADM1, numerous models on anaerobic digestion were already available and have shown good performance in terms of simulation accuracy. However, it has become difficult to compare results using different models. The ADMI was proposed by the IWA Task Group for Mathematical Modelling of Anaerobic Digestion Processes not to develop a single overall model but rather to "provide a unified basis for anaerobic digestion modelling" (Batstone & Keller, 2003). Thus, ADM1 may be considered a base model, which can either be directly used or modified to adapt to more specific applications.

The biochemical processes of ADM1 are categorized into five key steps: disintegration, hydrolysis, acidogenesis, acetogenesis and methanogenesis, as shown in Figure 2.4. The disintegration stage involves the separation of the pool of composite organic materials (X_C) into carbohydrates (X_{ch}), proteins (X_{pr}) and lipids (X_{li}) as well as into inerts (X_I, S_I). This phase allows the particulate components to be readily biodegraded in the subsequent steps through lysis, non-enzymatic decay, phase separation and physical breakdown, and was mainly included to facilitate modelling of activated sludge digestion (Batstone et al., 2002; Batstone et al., 2015). During the subsequent hydrolysis, these large non-soluble polymers of carbohydrates, proteins and lipids are broken down by hydrolytic enzymes produced by hydrolytic bacteria and converted to soluble monosaccharide/sugars (S_{su}), amino acids (S_{aa}) and long chain fatty acids (S_{fa}), respectively. In most cases, hydrolysis is a relatively slow phase thus, it is the rate limiting step in the overall anaerobic digestion process (Batstone et al., 2002; Speece, 1983; van Haandel & van der Lubbe, 2012). Facultative bacteria and hydrogen-producing acidogenic bacteria (X_{su}, X_{aa}) convert the soluble organic compounds into smaller volatile fatty acids (VFAs) (S_{va}, S_{bu}, S_{pro}, S_{ac}) during the acidogenesis stage, producing hydrogen (S_{h2}) and carbon dioxide (S_{IC}) as by-products (Batstone et al., 2002). Bacteria known as acetogens (X_{fa}, X_{c4}, X_{pro}) are responsible for the formation of acetate from VFAs. Acetate is considered the most important intermediate of the anaerobic digestion process because, compared to H_2 and CO_2, it is principally the final substrate for methane production (Khanal, 2008). The last stage is the methanogenesis in which methane (S_{ch4}), carbon dioxide and water are produced from the conversion of acetate and hydrogen gas. The methanogenesis is considered to occur via two mechanisms: by acetate cleavage and through reduction of CO_2 with H_2 facilitated by aceticlastic (X_{ac}) and hydrogenotrophic methanogens (X_{h2}), respectively (Parkin & Owen, 1986).

Besides the above-mentioned biochemical conversions, non-biologically facilitated processes also take place. Acid-base processes are modelled as equilibrium processes since they are assumed to occur very fast (Batstone et al., 2002; Musvoto et al., 2000b). Only the acid-base pairs whose pKa (i.e. the negative logarithm of the acid dissociation constant) values are close to the pH of anaerobic systems are included in the ADM1. The transfer of gases, of which only

CO_2, CH_4 and H_2 gases are considered, is another physico-chemical process included in the ADM1.

ADM1 has been considered either too simple or too complex by many users. When applicable, adding relevant extensions to the model is sufficient to address its simplicity and thus enabling the model to be used for specific applications. On the other hand, model complexity can be addressed by simplification of the model (i.e. model reduction) (Batstone et al., 2006) and is often needed for control and optimization purposes (García-Diéguez et al., 2013).

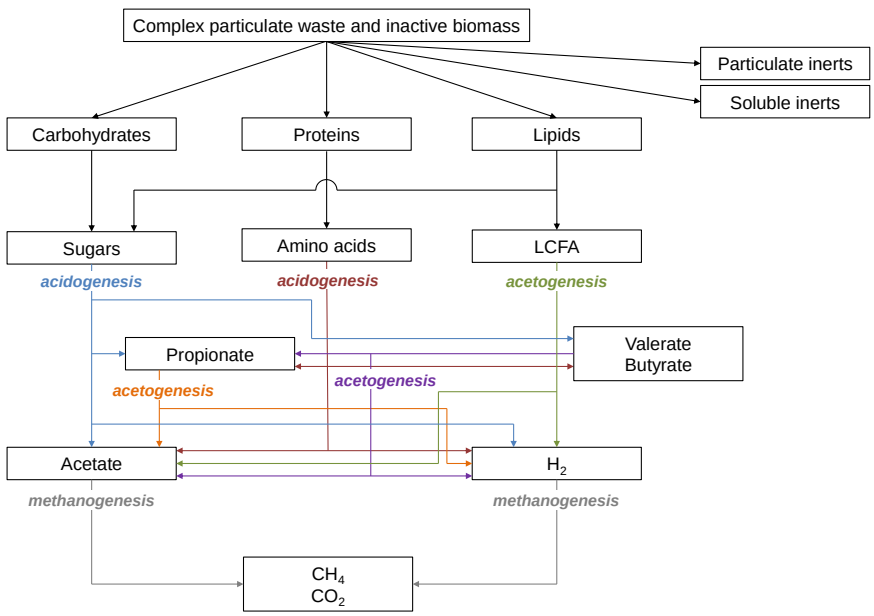

Figure 2.4. The anaerobic digestion process as described in Batstone et al. (2002).

Because of new technologies, increasing and newfound applications and the shift towards a holistic outlook on anaerobic digestion within the wastewater cycle, a growing number of extensions to the ADM1 are being requested and addressed. Batstone et al. (2006) mention that the most commonly requested extensions are on sulfate reduction, phosphorus transformations and mineral precipitation. Knobel & Lewis (2002) and Fedorovich et al. (2003) published extensions regarding sulfate reduction occurring during anaerobic digestion of sulfate-rich wastewaters. Both models consider several species of sulfate-reducing bacteria (SRB), which are able to utilize different substrates when converting sulfate to sulfide. Batstone (2006) has considered a simplified sulfate reduction model in ADM1 where only a single type of SRB is responsible for sulfate reduction, valid

for influents with S:COD of 0.1 g S.g COD^{-1}. The inclusion of phosphorus within ADM1 is important for WWTP modelling so that phosphorus transformations can be accurately tracked on a plant-wide basis (Johnson & Shang, 2006; Solon et al., 2015b). In addition, it is also linked to the sulfur cycle especially when considering EBPR processes (Wu et al., 2013), chemical phosphorus removal (de-Bashan & Bashan, 2004) and sulfide control (Gutierrez et al., 2010; Sharma et al., 2008). Initial studies on precipitation processes within ADM1 have been done by Batstone & Keller (2003) on recycling mill wastewater wherein only a single precipitate is considered (i.e. calcium carbonate, $CaCO_3$). However, in reality it is known that multiple mineral precipitations usually occur in concentrated systems, such as in anaerobic digesters (Batstone et al., 2012).

Meanwhile, the ADM1 has also been modified and/or extended for case-specific applications. For example, co-digestion is employed in order to improve biodegradability and thus increase biogas production during anaerobic digestion and numerous studies have already adapted ADM1 for co-digestion taking into account different substrates (Arnell et al., 2016; Boubaker & Ridha, 2008; Derbal et al., 2009; Esposito et al., 2008; Fezzani & Cheikh, 2008; Lübken et al., 2007; Zaher et al., 2009). Fezzani & Cheikh (2009) have added degradation processes of phenol compounds in their study on digestion of olive mill wastewater. Botheju et al. (2009) expanded the ADM1 into a model, called ADM1-Ox, which takes into account the effects of minute concentrations of oxygen in an otherwise anaerobic environment. Computational fluid dynamics (CFD) modelling is also being linked to ADM1 in order to capture the various gradients occurring in full-scale reactors (Gaden & Bibeau, 2011). Mu et al. (2008) and Tartakovsky et al. (2008) implemented ADM1 considering spatial dispersion significant in upflow anaerobic sludge bed (UASB) reactors.

For municipal wastewater treatment plant applications, Johnson & Shang (2006) mention that ADM1 is lacking the following: (1) the inclusion of phosphorus in the model which is needed for accurate tracking of struvite precipitation, (2) precipitation, (3) accurate pH prediction and (4) the fate and transport of sulfur species which is important for operation and maintenance. These issues are found to be inter-related and this thesis work consequently attempts to address and fill these gaps.

2.4. The Benchmark Simulation Models

Several early studies have presented numerous control strategies for wastewater treatment systems. Feedforward controllers were used by Davis et al. (1973) to manipulate the return sludge recycle flow rate in an activated sludge process based on the influent substrate concentration in order to minimize the effluent soluble substrate. Andrews (1974) demonstrated process control in activated sludge systems by regulating the feed points in a step-feed activated sludge system particularly targeted for poorly settling or bulking sludge, and in anaerobic digesters by studying the effect of controlling the pH through addition of base. A design manual was presented by Flanagan et al. (1977) dealing with various dissolved oxygen control systems for the activated sludge process wherein the capital and operating costs of such control systems were also compared. A simplified dynamic model was developed for the activated sludge process for automatic control purposes by Lech et al. (1978b), which they then used for testing different control strategies, such as various types of feedback and feedforward control using computer simulations (Lech et al., 1978a). Sludge recycle and wastage rates are controlled with the objective of maintaining the effluent substrate concentration below regulatory limits (Kabouris & Georgakakos, 1991). Sludge recirculation flow rate and dissolved oxygen control are the most commonly used and studied control actions for activated sludge systems (Marsili-Libelli, 1989; Olsson et al., 1985). A general overview of control as applied to wastewater treatment systems from early years until more recent times is presented by Olsson (2012) and Olsson et al. (2014).

Optimisation of wastewater treatment plant process performance could be done through any of these numerous control strategies to achieve benefits, such as process reliability, stability and even lower operational costs (Andrews, 1994; Olsson, 1992). There are several possibilities and combinations of control strategies in order to achieve the same goal. For example, improving nitrogen removal can be achieved by external carbon addition and/or by manipulating the airflow rate (Kim et al., 2004; Stare et al., 2007). These control strategies might bring about an improvement in organic carbon removal as well but might have an opposite impact on the operational cost or on the removal of another substrate, such as phosphorus. Because of the complexity, interdependency and non-linearity of the processes involved in wastewater treatment systems, it is a challenge to define control actions that will improve the plant performance (i.e. in terms of stability, substrate removal, etc.) at the lowest possible operational cost.

Mathematical models, such as those discussed in the previous subchapters, can be utilized to study the effect of different control strategies on process performance. However, it is still often difficult to evaluate and compare control strategies due to

differences in the system: variations in the influent, reactor layout, wide range of time constants, etc. (Jeppsson & Pons, 2004). In order to objectively compare different control strategies, a benchmark is necessary upon which to test them and apply standard evaluation criteria to compare them (Pons et al., 1999).

Along this line of thinking, a simulation benchmark was developed as a product of the European Cooperation in Science and Technology (COST) Actions 682 and 624 (Copp, 2002). The simulation benchmark is considered a standard simulation protocol containing guidelines for evaluating control strategies for activated sludge wastewater treatment plants. It is a simulation tool with a defined plant layout, bioprocess models, influent dynamics, sensors and actuator models and a set of evaluation criteria (Copp, 2002). The simulation benchmark was officially called the Benchmark Simulation Model No. 1 (BSM1).

The development of the BSM1 (Figure 2.5) continued within the IWA Task Group on Benchmarking of Control Strategies for Wastewater Treatment Plants. The BSM1 plant layout is composed of an activated sludge system followed by a secondary clarifier as shown in Figure 2.5, which is a common configuration for biological organic and nitrogen removal. The default activated sludge system has a Modified Ludzack-Ettinger configuration: two anoxic zones preceding three aerobic zones, and is modelled using ASM1. The secondary settler is modelled as a non-reactive unit and using the double-exponential settling velocity function by Takács et al. (1991). Influent dynamics are given for dry weather, rain weather and storm weather conditions (Gernaey et al., 2005; 2006b). Default control strategies are also provided to test the benchmark system through performance assessment. This evaluation is to test that an applied control strategy is properly implemented and to measure its effect on the plant performance. Different types of sensors and available control handles are also provided in the benchmark, together with their model descriptions. A more detailed description of the BSM1 is provided in Vrečko et al. (2014) and Gernaey et al. (2014).

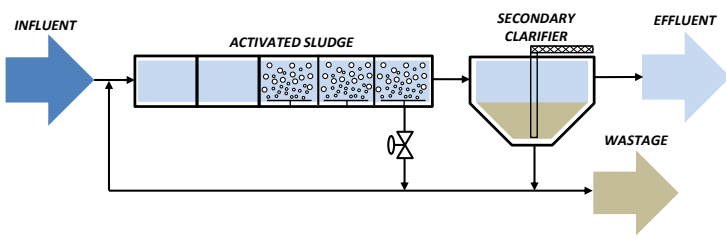

Figure 2.5. Plant layout of the Benchmark Simulation Model No. 1 (from Gernaey et al. (2014)).

BSM1 was further developed into the Long Term Benchmark Simulation Model No. 1 (BSM1_LT) (Rosén et al., 2004), wherein the evaluation period is extended from 7 to 364 days and is evidently aimed for long-term assessment of control strategies. In line with this, control actions with long-term effects are allowed, such as sludge age control. Sensor and actuator faults are also included in BSM1_LT in contrast to BSM1, wherein they are assumed ideal. With regards to fault detection and process monitoring, BSM1_LT allows monitoring of measurements in order to detect process deviations, failures and faults thus assisting in determination of what causes them (Corominas et al., 2011). It also allows comparisons of monitoring strategies of WWTPs using a new set of criteria (e.g. detection performance). In addition to all of these, temperature is taken into account, which strongly affects process parameters. A more detailed description of the BSM1_LT is provided in Gernaey et al. (2014).

The BSM1 was developed significantly into the Benchmark Simulation Model No. 2 (BSM2) for use in plant-wide control by considering both water and sludge lines. The research community has considered that the WWTP should not only be controlled on a local level but also as a whole, taking into account the interactions between the processes (Gernaey et al., 2014; Jeppsson et al., 2007; Nopens et al., 2010). Thus, in addition to the BSM1 subunits there are: a primary clarifier, thickener, anaerobic digester, dewatering unit and reject water storage tank as shown in Figure 2.6. The dynamic influent file for BSM2 is generated using an influent generator model by Gernaey et al. (2011). The primary clarifier is based on the model by Otterpohl & Freund (1992) and the anaerobic digestion process is based on the ADM1 (Batstone et al., 2002). The thickener and dewatering units are modelled as ideal continuous processes and assume 98% solids removal efficiency. Because of the difference in the set of state variables used for the biological processes, it is necessary to create model interfaces (Nopens et al., 2009) in order to couple them. The extended scope of BSM2 compared to BSM1 denotes that the number of possible control handles also substantially increases. As such, the performance evaluation criteria were modified and extended. For example, the contributions of heating energy required for the digester and the energy recovered (electricity and heat) from methane production are appropriately included in the cost index calculation; in addition, the weights assigned to ammonium and nitrate nitrogen are modified in the effluent quality index calculation. A more detailed description of the BSM2 is presented in Nopens et al. (2010) and Gernaey et al. (2014).

As mentioned frequently, the BSMs have been mainly developed as an objective multi-criteria analysis tool for comparison of control strategies in wastewater treatment systems (Flores-Alsina et al., 2008). Nevertheless, they have also been widely used as a collection of stand-alone wastewater treatment process models for use in teaching, research and process simulation.

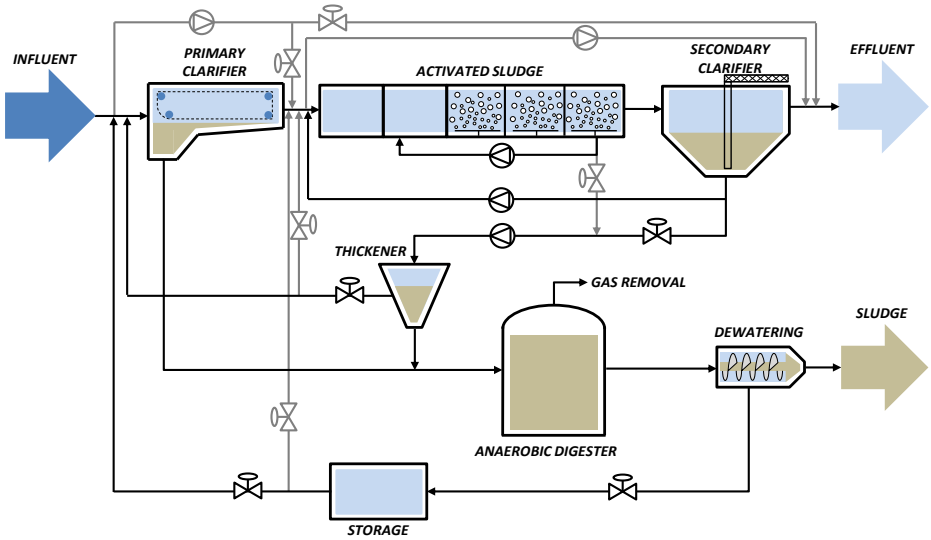

Figure 2.6. Plant layout of the Benchmark Simulation Model No. 2 (from Gernaey et al. (2014)).

After the publication of the Scientific and Technical Report of the Benchmark Simulation Models (BSM1, BSM1_LT, BSM2), it is only rational that deficiencies, challenges and new opportunities for development of the models have been recognised. Jeppsson et al. (2013) have identified several aspects as to how the models might be extended: temporal, spatial, processes within the WWTP, control strategies and evaluation tools. Some research works on these extensions have been conducted by people involved in the Task Group. For example, the BSM2 was extended to include the catchment and sewer network (Saagi et al., 2016) as well as the river (Saagi et al., 2017), the latter depicting scenarios where integrated control impacts the receiving water. Several studies have also extended the BSM to include greenhouse gas emissions from the WWTP (Arnell, 2016; Corominas et al., 2012; Flores-Alsina et al., 2011; Lindblom et al., 2016; Snip, 2015) and sewer network (Guo et al., 2012). Snip et al. (2014) and Snip (2015) have also included transformations of micropollutants in WWTPs.

One of the significant gaps in the BSMs is the phosphorus description. Plant-wide modelling of phosphorus removal and/or recovery processes is of significance due to legislation requirements and a growing interest in resource recovery. This thesis work describes in detail the development of the BSM2 extended with phosphorus removal and/or recovery processes.

Chapter 3

Physico-Chemical Framework for Wastewater Treatment Process Models

This chapter presents the motivation behind the development of a physico-chemical framework specific for wastewater treatment modelling. It also gives details about the different processes taken into consideration to account for the non-idealities and how they are modelled. The chapter ends with presenting the main results of scenario analysis performed in Papers I and II, which show the importance of including a physico-chemical framework for activated sludge modelling, anaerobic digestion modelling and plant-wide modelling.

3.1. Purpose of Physico-Chemical Modelling

Physico-chemical processes are non-biologically mediated. They are categorized as either liquid-liquid, gas-liquid or liquid-solid processes (Batstone et al., 2012). Advances in data collection and modelling related to physico-chemistry are generally established in the field of geochemistry, such that most of the available software products on water chemistry are directed for geochemical applications.

In the field of wastewater treatment modelling, the physico-chemical models (PCMs) that are used are inspired by the framework used in geochemistry. Due to the enormity of available databases and processes involved in PCMs, the number of processes and components included in wastewater treatment models is often reduced.

Due to the current needs to expand the IWA models (e.g. Activated Sludge Models, Anaerobic Digestion Model), model formulations also need to be modified and expanded. For example, anaerobic digestion systems dealing with sulfate-rich waste streams need to account for an increase in the number of state variables being considered (Fedorovich et al., 2003). Other significant components that are interacting with sulfur (S), in this case iron (Fe), also need to be taken into account (as in Paper V). In certain conditions, sulfur, in the form of sulfate, can be removed by precipitating it with Fe or aluminium (Al). Such precipitation reactions are physico-chemical processes. Modelling precipitation reactions should consider ion activities instead of the actual concentrations (Kazadi Mbamba et al., 2015a; 2015b) and this involves non-ideality corrections that are inherent to geochemical models. According to Batstone et al. (2012), systems with non-ideal conditions are modelled correctly when physico-chemical models are included.

Papers I and II focus on the development of the physico-chemical models paired with the activated sludge models and the anaerobic digestion model. This allows for dynamic calculation of pH, taking into account non-idealities. The results of these studies have shown a significant difference when compared with results obtained from the original model implementations, especially for the cases where multi-valent ions are considered. The results have strongly suggested that physico-chemical modelling is needed in order to produce accurate results.

3.2. Liquid-Liquid Processes

Acid-Base Reactions

Stumm & Morgan (1996) give the general principle of chemical equilibrium dissociation reactions:

$$HA \leftrightarrow H^+ + A^- \tag{3.1}$$

where HA is an acid dissociating into a conjugate base, A^-, and a hydrogen ion, H^+.

The chemical equilibrium can be solved either by ordinary differential equations (ODEs) or algebraic equations (AEs). The dissociation processes of acid-base reactions as well as that of ion pairing reactions can be described using ODEs with given high kinetic rate constants to show that these reactions occur more or less instantaneously (Musvoto et al., 1997, 2000b), or separately, calculated as AEs at each time step.

Ion Speciation/Pairing

In some cases, there are also non-electrostatic interactions between ions, which form ionic complexes as new chemical species. These ion pairs or ion complexes are different from the free ions (such as a hydrogen phosphate ion, HPO_4^{2-}, which is different from free orthophosphate, PO_4^{3-}) in solution. Ion complexes can increase or decrease the chemical driving force for a specific reaction to occur. Ion pairing effects on pH predictions are considered significant in systems with high total dissolved solids concentrations (Musvoto et al., 2000b), which indicates high ionic strengths, such as in high-strength anaerobic digestion liquors, sea water and concentrated industrial wastewater.

The most common ion pairs present in wastewater are set up to describe ion-pairing behaviour. This is implemented in a similar fashion as weak acid-base reactions where an algebraic procedure (Ikumi et al., 2011; Serralta et al., 2004) is used based on the assumption that ion pairs are in a state of equilibrium at all times. Total concentrations are determined by mass balances and subsequently, the ionic concentrations are calculated iteratively using a speciation sub-routine from a set of algebraic mass balances and equilibrium constant relationships (Tait et al., 2012).

Ion Activity

The effect of ionic strength, also known as ion activity ($S_{\{i\}}$), is defined as the effective concentration of any particular kind of ion in solution and is caused by electrostatic interactions between ions. It is calculated by multiplying the concentration of ion *i* ($S_{[i]}$) by a correction factor, which is called the activity coefficient (γ_i) (Stumm & Morgan, 1996):

$$S_{\{i\}} = \gamma_i \cdot S_{[i]} \tag{3.2}$$

Consider a chemical equilibrium reaction:

$$bB + cC \leftrightarrow dD \tag{3.3}$$

In infinitely dilute solutions, the ion activities can be approximated by the concentrations, as the activity coefficient approaches unity. The equilibrium constant (K_{eq}) is expressed as:

$$K_{eq} = \frac{S_{[D]}^{\ d}}{S_{[B]}^{\ b} \cdot S_{[C]}^{\ c}} \tag{3.4}$$

However, for non-ideal solutions K_{eq} is calculated as:

$$K_{eq} = \frac{S_{\{D\}}{}^{d}}{S_{\{B\}}{}^{b} \cdot S_{\{C\}}{}^{c}} = \frac{\left(\gamma_D \cdot S_{[D]}\right)^d}{\left(\gamma_B \cdot S_{[B]}\right)^b \cdot \left(\gamma_C \cdot S_{[C]}\right)^c} \quad (3.5)$$

There have been numerous studies on this topic, which have developed empirical correlations of experimental data that allow prediction of activity coefficients at various solution conditions (see Table 3.1). All of these expressions have shown that ion activity is dependent on the ionic strength (I) of the solution, which can be determined as follows:

$$I = \frac{1}{2}\sum S_{[i]} \cdot z_i^{\,2} \quad (3.6)$$

where z_i is the charge of ion i.

Table 3.1. Expressions for calculating activity coefficients and their range of applicability.

Equation name	Equation	Applicability
Debye-Hückel (Debye & Hückel, 1923)	$\log \gamma_i = -A \cdot z_i^{\,2} \cdot \sqrt{I}$	I < 0.005 mol.L^{-1}
Extended Debye-Hückel (Debye & Hückel, 1923)	$\log \gamma_i = -A \cdot z_i^{\,2} \cdot \left(\frac{\sqrt{I}}{1 + B \cdot \alpha_i \cdot \sqrt{I}}\right)$	I < 0.1 mol.L^{-1}
Güntelberg (Güntelberg, 1926)	$\log \gamma_i = -A \cdot z_i^{\,2} \cdot \left(\frac{\sqrt{I}}{1 + \sqrt{I}}\right)$	I < 0.1 mol.L^{-1}
Davies (Davies, 1938)	$\log \gamma_i = -A \cdot z_i^{\,2} \cdot \left(\frac{\sqrt{I}}{1 + \sqrt{I}} - 0.3 \cdot I\right)$	I < 0.5 mol.L^{-1}
WATEQ Debye-Hückel (Truesdell & Jones, 1973)	$\log \gamma_i = -A \cdot z_i^{\,2} \cdot \left(\frac{\sqrt{I}}{1 + B \cdot \alpha_i \cdot \sqrt{I}} + \beta_i \cdot I\right)$	I < 1 mol.L^{-1}

A and B are temperature-dependent constants, z_i is the charge of ion i, α_i and β_i are ion-specific parameters.

The calculated activity should be used in equilibrium equations as well as for weak acid-base pairing and ion complexation reactions.

The current physico-chemical models applied to wastewater treatment process modelling have used the Davies equation to describe the activity of the components. This equation is simple and does not need other constants, unlike the

extended and WATEQ Debye-Hückel equations. In addition, the Davies equation is valid for a larger range of ionic strength. The differences between the various ion activity correction equations and their relationships with ionic strength and ion types are shown in Figure 3.1, using sodium (Na^{+}) and magnesium (Mg^{2+}) as examples. It would seem best to use the WATEQ Debye-Hückel equation since it is valid for the widest range of ionic strength, however, it requires two additional parameters for each ion type considered, which are not always available in literature. Thus, the Davies equation seems to be the most fitting choice.

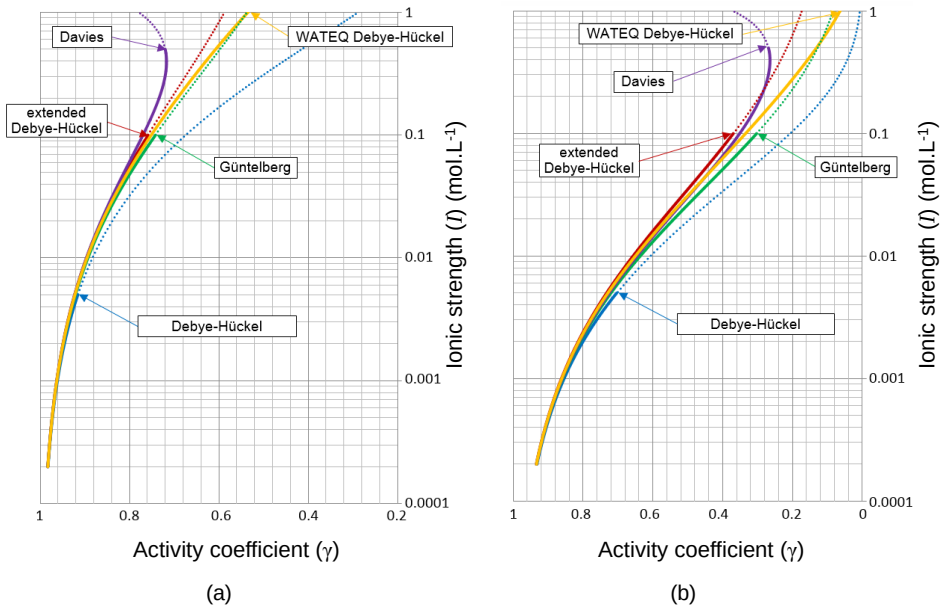

Figure 3.1. Activity coefficients of (a) sodium and (b) magnesium ions as calculated from five activity coefficient correlations (from Tait et al. (2012)).

3.3. Liquid-Solid Processes

Precipitation and Redissolution

Opposite to liquid-liquid processes, liquid-solid processes are assumed to occur slowly and take time to reach equilibrium. In order to model precipitation reactions, the possibility of precipitation is calculated first by testing if the solution is supersaturated or not. The Saturation Index (*SI*) indicates if a solution is in equilibrium, undersaturated or supersaturated with respect to a mineral (i.e.

whether mineral precipitation might occur or not) (Merkel & Planer-Friedrich, 2005; Stumm & Morgan, 1996). If $SI < 0$, the liquid phase is undersaturated, thus a mineral might dissolve into the liquid phase. If $SI = 0$, the liquid phase is saturated or at equilibrium while if $SI > 0$, the liquid phase is supersaturated and mineral precipitation might occur. It is calculated as:

$$SI = \log \frac{IAP}{K_{SP}} \tag{3.7}$$

where IAP is the ion activity product and K_{SP} is the solubility product constant of the mineral.

Considering an equilibrium reaction:

$$xM^{v+} + yA^{v-} \leftrightarrow M_xA_y \tag{3.8}$$

the IAP is calculated as:

$$IAP = \left\{M^{v+}\right\}^x \cdot \left\{A^{v-}\right\}^y \tag{3.9}$$

while K_{SP} is calculated as:

$$K_{SP} = \left\{M^{v+}\right\}_0^x \cdot \left\{A^{v-}\right\}_0^y \tag{3.10}$$

The subscript zero denotes the activities in the state of equilibrium. Note that SI only indicates what could happen thermodynamically. However, it does not indicate the rate by which the process will proceed. This means that a solution may be supersaturated for a very long time (i.e. it will take a long time for the mineral to precipitate). There are several equations available for kinetic rates describing crystallization. The general form of the crystallization rate is given by Koutsoukos et al. (1980) and first proposed by Davies & Jones (1955) as applied to silver chloride precipitation. That rate equation has been used for kinetic studies (Kazmierczak et al., 1982) as well as in modelling of precipitation reactions as applied to wastewater treatment (Barat et al., 2011; Musvoto et al., 2000a). The equation describes how the difference between the concentrations of contributing ions in a solution and their equilibrium concentrations is the thermodynamic driving force that dictates the occurrence of precipitation.

In this study, the rate of crystallization (r_i) used is presented by Kazadi Mbamba et al. (2015a), which has been adapted from the crystallization rate presented by Nielsen (1984):

$$r_i = k_{cryst} \cdot X_{cryst} \cdot \left[\left(\frac{\left\{M^{v+}\right\}^x \cdot \left\{A^{v-}\right\}^y}{K_{SP}} \right)^{\frac{1}{v}} - 1 \right]^n \quad (3.11)$$

where k_{cryst} is the precipitation rate constant, X_{cryst} is the concentration of the precipitate and n is a constant typically equal to 2.

Building the precipitation model requires identification of the possible precipitates or else there might be components not accounted for or the model will be overly complex. This is the advantage of using an external software tool because all possible precipitates can be identified. That is also the reason why it is advantageous to have prior knowledge and process understanding. In the study of Musvoto et al. (2000a), precipitates that are likely to occur in wastewater treatment plants have been identified. The types of precipitates are largely dependent on the influent composition and the metals used for chemical precipitation.

Unlike the equilibrium constants used in aqueous phase chemistry, the constants used to model precipitation reactions usually vary between databases and literature references. Because of this, one should take caution when using the solubility product constants for certain minerals. In addition, not all information can be found in one database. For example, the K_{SP} value for K-struvite and iron phosphate cannot be found in the database of MINTEQ (Gustafsson, 2010). One reason is that this database is mostly used for geochemical studies and such precipitates are not common in groundwater. One can manually add the values found elsewhere (e.g. from literature) for these minerals into the database.

Redissolution, on the other hand, can be considered as the inverse of the precipitation kinetics. In line with this, the dissolution rate equation is expressed as:

$$r_i = -k_{diss} \cdot X_{cryst} \cdot \left[\left(\frac{\left\{M^{v+}\right\}^x \cdot \left\{A^{v-}\right\}^y}{K_{SP}} \right)^{\frac{1}{v}} - 1 \right]^n \quad (3.12)$$

where k_{diss} is the dissolution rate constant.

3.4. Liquid-Gas Processes

Stripping/Volatilization and Absorption

Mass transfers between the liquid phase and gas phase are modelled to describe the dissolution of gaseous components formed during biological reactions into the aqueous phase (i.e. absorption) as well as the mass transfers of the dissolved forms of these gaseous components into the gas phase (i.e. volatilization – due to natural phenomenon or stripping – due to a mechanical device). Derived from Fick's first law (Fick, 1855), the equation below is a very common form of the kinetic rate equation for the liquid-gas transfer:

$$r_{i,G/L} = k_L \cdot a \cdot \left(K_{H,i} \cdot P_i - C_i \right) \quad (3.13)$$

where $r_{i,G/L}$ is the mass transfer rate between the gas and liquid phase, k_L is the mass transfer rate, a is the contact area between the liquid and the gas phase, $K_{H,i}$ is the Henry's constant, P_i is the partial pressure and C_i is the dissolved concentration of the gaseous component. The product of Henry's constant and the partial pressure of the gas ($K_{H,i} \cdot P_i$) gives the saturation concentration (C_{sat}). The gas transfer coefficient ($k_L \cdot a$ or $k_L a$) is dependent on temperature. ASCE (1992) gives the widely-used relationship between $k_L a$ (d^{-1}) and temperature (°C):

$$k_L a(T) = 1.024^{(T-15)} \cdot k_L a(15°C) \quad (3.14)$$

The common gaseous components, which are considered during modelling of stripping processes in wastewater treatment, are oxygen, carbon dioxide, ammonia, nitrogen, nitrous oxide, hydrogen and methane. For the study in Papers IV and V, where sulfur conversions are included, hydrogen sulfide is also considered.

3.5. Implementation Details

The aqueous phase physico-chemical processes are modelled as fast processes compared to the biological processes. For such a numerically stiff system, one solution can be to model the fast reactions as algebraic equations (AEs) while using the forward Runge-Kutta solver for the remaining slow reactions modelled as ordinary differential equations (ODEs), as was previously done for the pH and

H_2 states in the ADM1 implementation (Rosén et al., 2006). However, this method is unsuitable due to multiple interdependencies of the aqueous phase reactions. Thus, a full gradient search method (i.e. multi-variate Newton-Raphson method) was used, which requires evaluating the Jacobian. The latter involves conversion of the matrix of all algebraic equations into first order partial derivatives and then using a decomposition method for inversion of the resulting matrix. The results of this approach was verified by comparison with the results obtained using an external geochemical program (i.e. MINTEQA2).

3.6. Scenario Analysis

Activity correction based on ionic strength using the Davies equation and ion pairing of inorganic carbon, inorganic nitrogen and volatile fatty acids with several cations and anions were taken into account in the ADM1 and implemented within the BSM2 platform as presented in Paper I. This was done to show the influence of these non-idealities on the anaerobic digester performance and products as well as on the water line.

Three model variants are formulated to assess the results of the improved ADM1 model:

i. A_1 – default ADM1;

ii. A_2 – ADM1 with ionic activity correction; and,

iii. A_3 – ADM1 with ionic activity correction and ion pairing.

Each model variant is tested for different ionic strengths (I = 0.09, 0.14, 0.20, 0.25 and 0.3 mol.L^{-1}) by addition of a minor influent stream with increasing cationic loads (S_{cat} = 0, 2, 4, 6 and 8 mol-L^{-1}) representing scenarios SC1, SC2, SC3, SC4 and SC5, respectively. The pool of cations added in the different scenarios is replaced by sodium (S_{Na+}) and potassium (S_{K+}) while anions are replaced by chloride (S_{Cl-}) for model variant A_3.

The average values of the ADM1 state variables are similar for all model variants at low ionic strengths. However, the activity corrections for A_2 and A_3 affect the species distribution of the inorganic carbon species with a shift to their deprotonated forms (i.e. removal of hydrogen ions from an acid). This leads to more required reactive protons (S_{H+}) in A_2 and A_3 and they are released to maintain the charge balance. The resulting decrease in pH in A_2 and A_3 compared to A_1 causes a lower free-ammonia concentration. Thus, a lower level of free-ammonia inhibition of aceticlastic methanogenesis results in lower acetic acid

concentration, more acetate degraders and higher acetate uptake. These observations are more pronounced at higher ionic strengths, as seen in Figure 3.2b.

The increase in influent cation load to the digester unit results in a decrease of the concentration of reactive protons (S_{H+}). The corresponding increase in pH increases the free-ammonia concentration, which causes increased inhibition of acetate degraders and decreased acetate uptake. Biogas production is also decreasing at increasing cationic loads. At high ionic strengths (I = 0.3 mol.L^{-1}), ammonia inhibition is highly pronounced causing significant accumulation of acetate in the digester, which means lower biogas production as observed when comparing Figure 3.2a and Figure 3.2b.

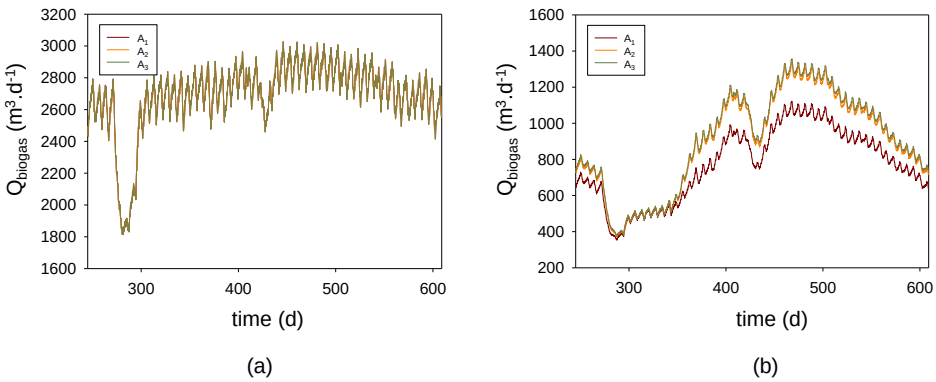

Figure 3.2. Dynamic profiles of the total biogas production in BSM2 using three model variants and two different cationic loads, (a) S_{cat} = 0 mol.L^{-1} and (b) S_{cat} = 8 mol.L^{-1} (from Paper I).

Up to an additional load of S_{cat} = 4 mol.L^{-1}, pH is higher in A_1 than in A_2 due to the release of reactive protons through ion activity of inorganic species in A_2. Above that cationic load, pH increased due to the unbalanced cationic species. This rise can no longer be buffered by the release of reactive protons, which comes from the shift of the inorganic carbon species to deprotonated forms.

For case A_3, ion-pairing would theoretically shift the inorganic species to their deprotonated forms, which would release more reactive protons and thus further decrease pH when compared to A_2. However, simulation results show that this ion-pairing effect is minimal and that the resulting pH and species distribution are very similar for A_2 and A_3. Thus, ion-pairing effects are less significant when trying to account for effects of increased salinity/pH.

The overall plant performance, represented by *EQI* and *OCI*, is similar using the three model variants for simulated scenarios with additional cationic load of S_{cat} = 0-4 mol.L^{-1} (i.e. SC1, SC2, SC3). Above that cationic load (i.e. SC4 and SC5), the

results using model variants A_2 and A_3 show significant differences from the results of A_1. For model A_1, the high ionic strength of SC4 and SC5 considerably decreases the plant performance due to ammonia inhibition. The negative effect of this ammonia inhibition on the digester results in lower biogas production (Figure 3.2) and increases the operational cost (*OCI*) (Figure 3.3b) because less energy is obtained from this biogas. The poor digester performance also leads to an increase in the total COD that is returned from the sludge line to the water line (Figure 3.4). This additional load can overload the activated sludge process and thus affects the effluent quality (Figure 3.3a). The effect of ammonia inhibition on the Effluent Quality Index (*EQI*) may be unrealistically high for model A_1 and scenario SC4 when considering the models A_2 and A_3, which take into account ionic strength and ion-pairing effects, they do not show the same significant influence on the *EQI*. Comparison of the values for model variants A_2 and A_3 for the different scenarios shows yet again that ion-pairing effects are less significant.

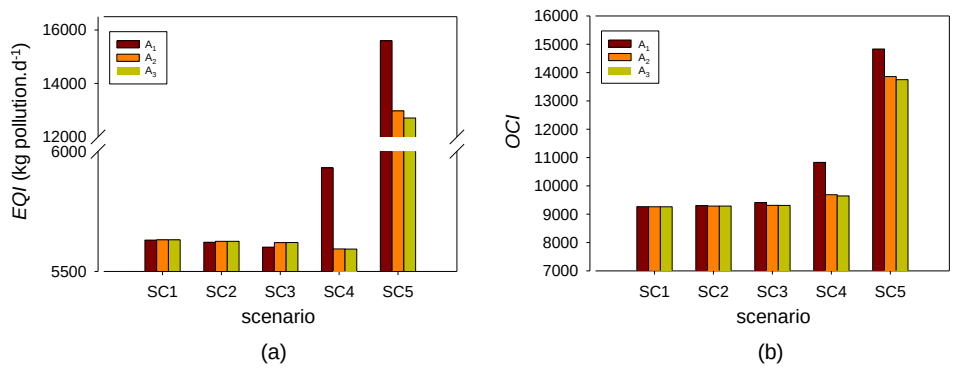

Figure 3.3. The variations in (a) *EQI* and (b) *OCI* using three model variants (A_1, A_2, A_3) and five additional cationic loads (SC1, SC2, SC3, SC4, SC5) (from Paper I).

The results show that ion activity and ion-pairing effects need not be accounted for when simulating anaerobic digestion of dilute wastewaters having ionic strength < 0.2 mol.L^{-1}. This is demonstrated by the similar *EQI*, *OCI* and biogas production values for the model variants with (A_2 and A_3) and without (A_1) corrections. Above this ionic strength, which are typical for high solids and manure digestion, ion activity corrections are required to model the effects of salinity and pH throughout the water and sludge lines of a plant-wide model. This is seen from the results on biogas production (Figure 3.2), COD load returning to the water line (Figure 3.4), *EQI* and *OCI* (Figure 3.3), wherein there are considerable differences between the results of the model without corrections (A_1) and with model corrections (A_2 and A_3).

The Davies equation is used to calculate the activity coefficients because it is valid for the range of ionic strength being tested. At higher ionic strengths (i.e. 0.5-1 mol.L^{-1}), the WATEQ Debye-Hückel equation is recommended.

It was pointed out that ion-pairing corrections are less important compared to ion activity corrections. However, it should be noted that predominantly monovalent ions were considered, whereas ion pairing of divalent and trivalent ions is known to be influential in mineral precipitation. Even though the digester pH is strongly influenced by monovalent ions, such as bicarbonate, the driving force for minerals precipitation are commonly divalent and trivalent ions. According to Tait et al. (2012), both ion activity and ion pairing are equally important when modelling digestion and precipitation of high-strength wastewaters.

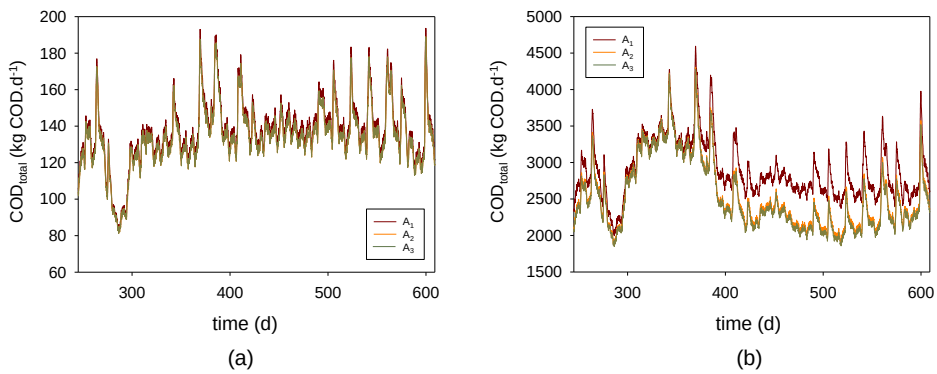

Figure 3.4. Dynamic profiles of the total COD load returning to the water line using three model variants (A_1, A_2, A_3) and two different cationic loads, (a) S_{cat} = 0 mol.L^{-1} and (b) S_{cat} = 8 mol.L^{-1} (from Paper I).

Both ion activity and ion pairing corrections are applied to the activated sludge models ASM1, ASM2d and ASM3 by implementing a plant-wide aqueous phase chemistry module in order to predict pH variations as presented in Paper II. The methodology involves consideration of 19 components and almost 120 species. The three wastewater treatment plant configurations used are (Figure 3.5):

- WWTP1 – a nitrogen removal plant consisting of five reactors in series and a secondary clarifier. The first two tanks are anoxic (ANOX1, ANOX2) and the last three tanks are aerobic (AER1, AER2, AER3), where AER3 and ANOX 1 are linked by an internal recycle. The biological reactions for the activated sludge section in WWTP1 are described using ASM1 and ASM3.

- WWTP2 – a combined nitrogen and phosphorus removal plant consisting of seven reactors in series and a secondary clarifier. Aside from two anoxic tanks and three aerobic tanks, two anaerobic tanks are added in front. The biological reactions for the activated sludge section in WWTP2 are described using ASM2d.
- WWTP3 – a full-plant model having the configuration of BSM2. It consists of the configuration of WWTP1 and further contains a primary clarifier, a sludge thickener, an anaerobic digester, a storage tank and a dewatering unit. The biological reactions for the anaerobic digester in WWTP3 are described using the original ADM1.

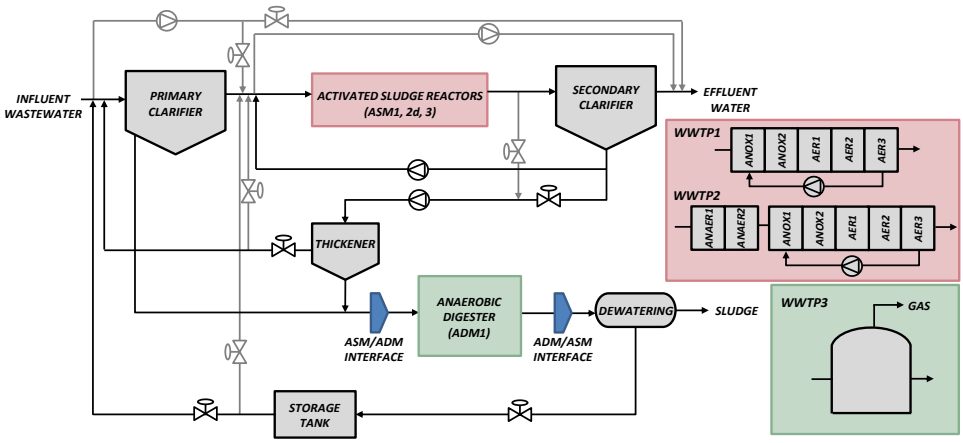

Figure 3.5. Wastewater treatment plant configuration of the wastewater treatment plants analysed (from Paper II).

The default implementation of the three activated sludge models had to be adjusted in order to include the ion pairing correction. The alkalinity state (S_{ALK}) is removed and replaced by an inorganic carbon state (S_{IC}), phosphorus is included in ASM1 and ASM3 as non-reactive, carbon dioxide stripping is included, potassium (S_{K+}) and magnesium (S_{Mg2+}) are described during modelling of formation/release of polyphosphates and chemical precipitation of metal hydroxides is omitted. The adjusted ASM models are linked to the aqueous phase module, such that the outputs of the ASM models at each integrations step are used as inputs to the aqueous phase module in order to estimate the pH. Specific cations and anions are also included, which will be used for further model extensions, such as multiple minerals precipitation or for pH adjustment.

The aqueous phase module allows not only for pH calculation but also the speciation of the wastewater composition as shown in Figure 3.6.

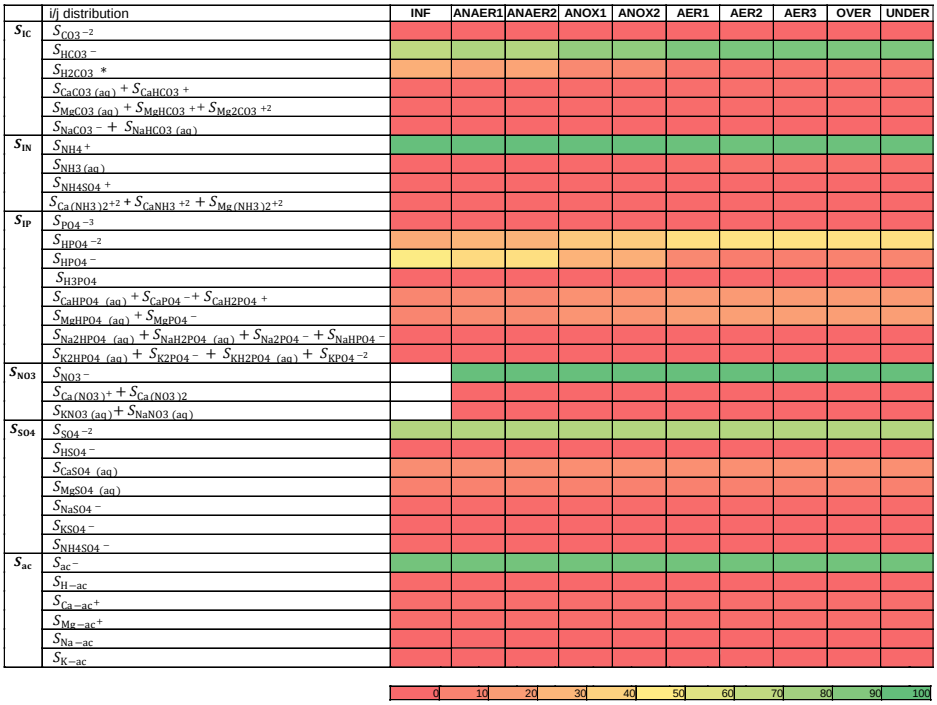

Figure 3.6. Distribution of the various C, N, P, S and acetate-related species/ion pairs in the different sections of the wastewater treatment plant (from Paper II). INF refers to the influent, OVER refers to the secondary settler overflow and UNDER refers to the secondary settler underflow. Note that there is no nitrate present in the influent.

The influent cationic loads for ASM1, ASM2d and ASM3 are identical, thus the pH prediction at the influent is the same as shown in Figure 3.7. Biological oxidation of organic substrates using nitrate as electron acceptor occurs in the anoxic zones. As nitrate is converted to nitrogen gas, a strong acid is removed thereby increasing pH. Meanwhile, oxidation of inorganic carbon and ammonium causes a decrease in pH due to production of acid. However, the carbon dioxide stripping in AER1, AER2 and AER3 causes an overall rise in pH (i.e. the CO_2 stripping might be overestimated in this case, causing a considerable pH rise). For WWTP2 with an anaerobic section as a first stage of the activated sludge unit, the pH increases in ANAER1 due to uptake of organic acids to produce polyhydroxyalkanoates. At the same time, release of inorganic phosphorus, potassium and magnesium ions from the decay of polyphosphates leads to a net decrease of pH in ANAER2. The oxidation of the organic substrates and ammonia, without air stripping, at the top of the clarifier causes a slight decrease in pH. On the other hand, the denitrification in the reactive secondary settler causes pH to increase due to the same reasons as presented for the anoxic zone. However, for

the case with biological phosphorus removal, the release of inorganic phosphorus is expected to decrease the pH in the lower part of the secondary settler.

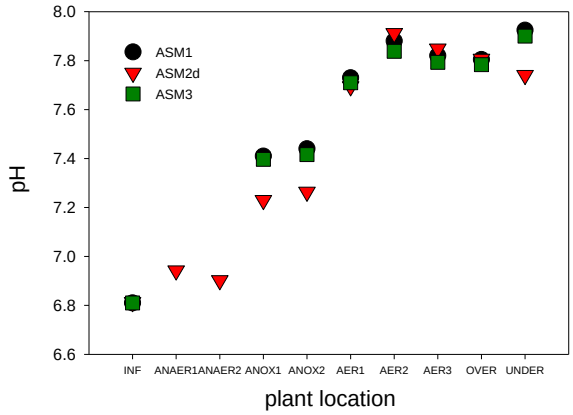

Figure 3.7. pH predictions in the different units for WWTP1 and WWTP2 using ASM1, ASM2d and ASM3 (from Paper II). INF refers to the influent, OVER refers to the secondary settler overflow and UNDER refers to the secondary settler underflow.

The WWTP3 is further set up to evaluate the impact of monovalent and divalent ion pairing on plant performance. An additional waste stream of 5 $m^3.d^{-1}$ and additional cationic influent concentrations from 0 to 2.5 $mol.L^{-1}$ are added and distributed amongst sodium and potassium (monovalent, M) or calcium and magnesium (divalent, D) to arrange a default case (Def) and five scenarios (SC1, SC2, SC3, SC4 and SC5).

Figure 3.8 shows that the highest variations in the species distribution are for the inorganic carbon and phosphorus systems depending on whether monovalent or divalent cations ions are added to the system. Calcium and magnesium have higher affinities to carbonate and phosphorus anions compared to sodium and potassium.

Carbon dioxide production is also highly affected by the addition of cationic loads. A decrease in CO_2 production is observed in the simulation results for increasing cationic loads due to the corresponding changes in the carbonate system. Furthermore, the difference between the results whether monovalent or divalent cations are added can also be observed (Figure 3.9). However, methane gas production is not affected.

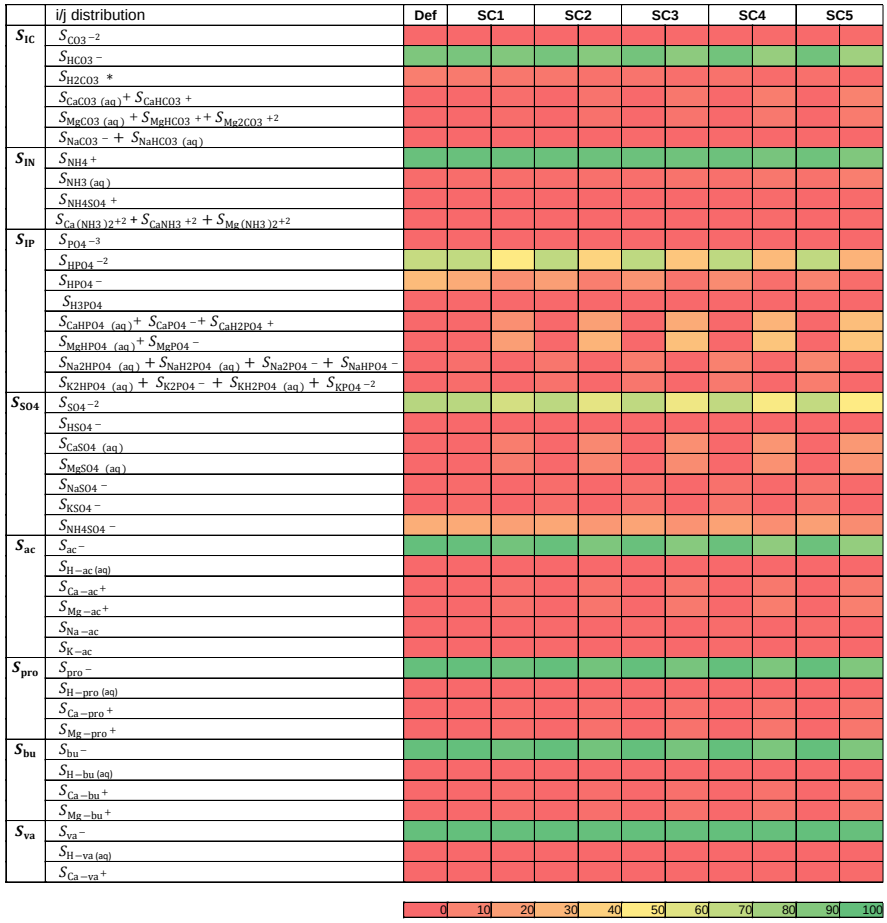

Figure 3.8. Distribution of the various C, N, P, S and VFA-related species/ion pairs for the different scenarios evaluated for WWTP3 (from Paper II).

There are limitations for this model that need to be addressed. For example, phosphorus and sulfur are not included in the ADM1. Phosphorus accumulating organisms in the anaerobic digester might cause release of phosphates and metals, which may have a significant effect on the aqueous phase chemistry of the system. Sulfate will also be reduced in the digester and therefore affect the speciation of sulfur, for which the distribution to hydrogen sulfide is important due to its inhibitive properties to methanogens. Precipitation is also not included, which means that while calcium ions are included this could over-predict the pH in the system and the carbon dioxide production. These issues are addressed in the subsequent chapter, wherein precipitation and biological reactions involving

phosphorus, sulfur and iron are included in the activated sludge models and anaerobic digestion model.

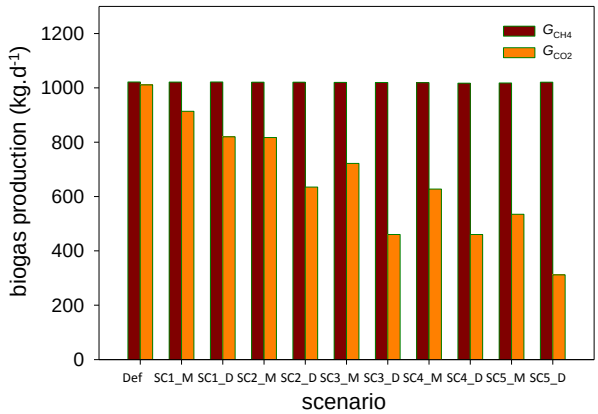

Figure 3.9. Effect of monovalent and divalent ion pairing on the biogas production for different cationic loads (from Paper II).

The approach presented in this chapter provides new prospects. For example, the pH dependency of biochemical processes can now be taken into account. Another benefit is that the distribution of the species of each component can also be used to determine free ammonia and free nitrous acid speciation, which is important for modelling high strength nitritation/nitratation processes for prediction of nitrous oxide emissions. Moreover, one of the considered significant applications of this aqueous phase module is for use when modelling mineral precipitation, wherein the kinetics is based on the saturation index (*SI*), which is calculated using activities instead of concentrations.

3.7. Summary of Key Findings

- The Anaerobic Digestion Model No. 1 is extended with correction for non-idealities: ion activity corrections and ion pairing effects, and successfully simulated within the Benchmark Simulation Model No. 2 platform. The ADM1 extended with the aqueous phase chemical equilibria model is implemented as a set of ODEs and AEs, for which a multivariate Newton-Raphson method is used to solve the algebraic interdependencies.

- Ion activity corrections have a greater influence on model results at higher ionic strengths. Thus, it is recommended that these should be applied to ADM1 at ionic strengths greater than 0.2 $mol.L^{-1}$. Monovalent ion pairing is less influential than ion activity corrections, even at higher ionic strengths, and can be excluded from ADM1, especially when minerals precipitation is not considered.

- The approach presented for implementing the aqueous phase chemistry module (i.e. ion activity corrections and ion pairing reactions) is seamlessly combined with standard wastewater treatment process models, such as ASM1, ASM2d, ASM3 and ADM1. pH and speciation of the different wastewater components under different conditions (anaerobic, anoxic, aerobic) are reliably predicted.

- It is foreseen that the aqueous phase chemistry module can improve predictions of nitrification/denitrification models by prediction of speciation of free ammonium and free nitrous acid, which have important effects on the growth of ammonia-oxidizing bacteria and nitrite-oxidizing bacteria. It could also be included together with sewer models for which ions, such as sulfur and iron transformations, are deemed important. It is also a much better starting point for the development of mineral precipitation modelling in wastewater treatment processes.

Chapter 4

Extensions to Biological Models ASM2d and ADM1

In the context of plant-wide modelling, the state of the art is that most models are still limited to the description of plant-wide carbon and nitrogen biochemical processes. In order to fill the gaps in plant-wide modelling, ASM2d is extended to include phosphorus interactions with the iron and sulfur cycles as done in Paper V. In addition phosphorus, sulfur and iron transformations are also included in the ADM1 as employed in Paper IV and partly in Paper III. Although there have been studies on the biological and chemical complexations of phosphorus during anaerobic conditions, these have not been generally considered in plant-wide interactions with the iron and sulfur cycles. The chapter ends with presenting key results from Paper IV.

4.1. Phosphorus Transformations

After the discussion of the physico-chemical framework and modelling in Chapter 3, phosphorus can now be properly accounted for in the biochemical wastewater treatment models. This subchapter describes phosphorus transformations occurring in the activated sludge process by ASM2d and anaerobic digestion by an extended ADM1.

ASM2d

ASM2d is an effort to extend ASM1 in order to describe biological phosphorus removal in activated sludge systems. It is a minor extension to ASM2 in order to take into account that phosphorus accumulating organisms use cell internal storage products for denitrification. It also includes two chemical processes to describe chemical precipitation of phosphorus. In this enhanced version of the ASM2d, these chemical precipitation reactions are omitted since a more general precipitation framework is included, which takes into account possibilities of a wider range of precipitates. In addition, new state variables related to iron and sulfur are included to ensure that the most significant interactions of these two with phosphorus are considered, especially when incorporating chemical phosphorus removal and recovery. The activated sludge configuration is modified from the Ludzack-Ettinger process to include an anaerobic section in order to promote phosphorus release under anaerobic conditions and uptake by phosphorus accumulating organisms in the subsequent anoxic and aerobic zones (Figure 4.1).

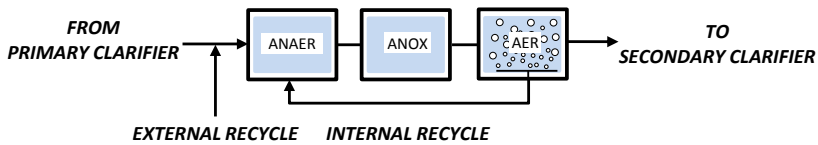

Figure 4.1. Activated sludge layout with anaerobic/anoxic/aerobic (A^2O) configuration.

An important aspect of the model is defining the phosphorus content of all soluble and particulate components in the ASM2d through elemental balances as described by Takács & Vanrolleghem (2006). It is based on the hypothesis that the mass of each component is made up of constant mass fractions of the elements C, H, O, N and P (Reichert et al., 2001). This principle can be easily extended to include other elements, such as sulfur, iron, potassium, magnesium, etc. provided that the sum of all elemental mass fractions (α) of a given component *i* equals unity (Eq. (4.1)).

$$\alpha_{C,i} + \alpha_{H,i} + \alpha_{O,i} + \alpha_{N,i} + \alpha_{P,i} = 1 \qquad (4.1)$$

One major modification relates to the accounting of the compositional analysis of polyphosphates (X_{PP}) assuming that it has a chemical formula $(K_{0.33}Mg_{0.33}PO_3)_3$. Thus, for example lysis of X_{PP} leads to release of potassium (S_{K+}) and magnesium (S_{Mg2+}).

ADM1

Modelling of phosphorus is one of the major limitations of the ADM1 (Batstone et al., 2015). Phosphorus-related processes have been addressed in commercial software packages due to engineering demands but not in academically distributed wastewater treatment models. Batstone (2006) identify that phosphorus has been requested to be included in the ADM1 in order to describe the phosphorus retention and release from the biomass and to close the phosphorus balances during plant-wide modelling.

An important aspect of phosphorus modelling is its effect on pH. In ADM1, the most important ions are tracked, except the phosphorus-related ones. It should be noted that a prerequisite to adding phosphorus and its precipitation kinetics requires taking into account physico-chemical effects, such as ion activity correction, ion pairing behaviour and relevant weak acid-base reactions. These effects are more pronounced when considering divalent and trivalent ions, such as hydrogen phosphate and phosphate, respectively.

Johnson & Shang (2006) also mention that tracking the fate of both sulfur and phosphorus in anaerobic systems are major areas that ADM1 does not currently address but are both highly important in municipal wastewater treatment systems. It has been found that the recycled stream from the dewatering of digested sludge (i.e. reject water) contains as much as 30% of the total nutrient load of the WWTP (Johnson & Shang, 2006). This high recycle load proves the importance of an accurate method of tracking phosphorus through the anaerobic digestion process.

The main concept for integrating phosphorus in ADM1 is to assume that the phosphorus-related microorganisms are still active when they reach the anaerobic digester (Ikumi et al., 2014; Wang et al., 2016). In order to handle this, some of the ASM2d processes (Henze et al., 1999), those which occur in anaerobic conditions, are included as additional processes in ADM1. The growth of phosphorus accumulating organisms (X_{PAO}) and the cell-internal storage materials, polyphosphates (X_{PP}) and polyhydroxyalkanoates (X_{PHA}), are not included as additional processes since these are known to occur only during aerobic and anoxic conditions. The phosphorus-related processes added to ADM1 are given in Table 4.1 and Table 4.2. In addition to biochemical conversions, precipitation of phosphorus with various cations is included in the extended ADM1. Precipitates considered are: amorphous calcium phosphate ($Ca_3(PO_4)_2$), hydroxyapatite ($Ca_5(PO_4)_3OH$), dicalcium phosphate ($CaHPO_4$), octacalcium phosphate ($Ca_4H(PO_4)_3$), struvite ($MgNH_4PO_4$), newberyite ($MgHPO_4$), k-struvite ($KMgPO_4$), ferrous phosphate ($Fe_3(PO_4)_2$). The precipitation kinetics are described in Section 3.3.

Table 4.1. Gujer matrix for phosphorus-related extensions to ADM1.

Component, i → / Process, j ↓	S_{va}	S_{bu}	S_{pro}	S_{ac}	S_I	X_{ch}	X_{pr}	X_{li}	X_I	X_{PHA}	X_{PP}	X_{PAO}	S_K	S_{Mg}
Storage of S_{hva} in X_{PHA}	-1									1	$-Y_{PO4}$		Y_{PO4}·K_{PP}	Y_{PO4}·Mg_{PP}
Storage of S_{hbu} in X_{PHA}		-1								1	$-Y_{PO4}$		Y_{PO4}·K_{PP}	Y_{PO4}·Mg_{PP}
Storage of S_{hpro} in X_{PHA}			-1							1	$-Y_{PO4}$		Y_{PO4}·K_{PP}	Y_{PO4}·Mg_{PP}
Storage of S_{hac} in X_{PHA}				-1						1	$-Y_{PO4}$		Y_{PO4}·K_{PP}	Y_{PO4}·Mg_{PP}
Lysis of X_{PAO}					$f_{SI,XB}$	$f_{CH,XB}$	$f_{PR,XB}$	$f_{LI,XB}$	$f_{XI,XB}$			-1		
Lysis of X_{PP}											-1		K_{PP}	Mg_{PP}
Lysis of X_{PHA}	$f_{va,PHA}$	$f_{bu,PHA}$	$f_{pro,PHA}$	$f_{ac,PHA}$						-1				

Table 4.2. Process kinetic rate equations for phosphorus-related reactions (extensions to ADM1).

Process, j ↓	Kinetics rate expressions (ρ_j, kg COD.m^{-3}.d^{-1})
Storage of S_{hva} in X_{PHA}	$q_{PHA} \cdot \frac{S_{va}}{K_A + S_{va}} \cdot \frac{X_{PP}/X_{PAO}}{K_{PP} + X_{PP}/X_{PAO}} \cdot X_{PAO} \cdot \frac{S_{va}}{S_{va} + S_{bu} + S_{pro} + S_{ac}}$
Storage of S_{hbu} in X_{PHA}	$q_{PHA} \cdot \frac{S_{bu}}{K_A + S_{bu}} \cdot \frac{X_{PP}/X_{PAO}}{K_{PP} + X_{PP}/X_{PAO}} \cdot X_{PAO} \cdot \frac{S_{bu}}{S_{va} + S_{bu} + S_{pro} + S_{ac}}$
Storage of S_{hpro} in X_{PHA}	$q_{PHA} \cdot \frac{S_{pro}}{K_A + S_{pro}} \cdot \frac{X_{PP}/X_{PAO}}{K_{PP} + X_{PP}/X_{PAO}} \cdot X_{PAO} \cdot \frac{S_{pro}}{S_{va} + S_{bu} + S_{pro} + S_{ac}}$
Storage of S_{hac} in X_{PHA}	$q_{PHA} \cdot \frac{S_{ac}}{K_A + S_{ac}} \cdot \frac{X_{PP}/X_{PAO}}{K_{PP} + X_{PP}/X_{PAO}} \cdot X_{PAO} \cdot \frac{S_{ac}}{S_{va} + S_{bu} + S_{pro} + S_{ac}}$
Lysis of X_{PAO}	$b_{PAO} \cdot X_{PAO}$
Lysis of X_{PP}	$b_{PP} \cdot X_{PP}$
Lysis of X_{PHA}	$b_{PHA} \cdot X_{PHA}$

4.2. Sulfur Transformations

Sulfate-rich waste streams are those usually coming from industries, such as petrochemical plants, leather tanning industries, ethanol production and coal-fired plants. Sulfate in the wastewater stream has been a source of operational problems, especially in the sewer system, pipelines, as well as in the anaerobic digester mainly due to its conversion to hydrogen sulfide under anaerobic conditions. A common problematic effect due to hydrogen sulfide is its odour, a distinct rotten egg-like smell at low concentrations in air (< 50 ppm), which can cause irritations at low to medium (30-100 ppm) concentrations, and is very toxic at high concentrations (> 100 ppm). Corrosion is another operational problem caused by hydrogen sulfide. It attacks several types of material that are normally used in wastewater treatment plants, such as concrete, steel, copper and iron. A further issue with hydrogen sulfide in relation to wastewater treatment plant operation, and of paramount importance, is its toxic effect on the methanogenic population, which can result in operational failure of anaerobic digesters.

Thus, including sulfur transformations in modelling of wastewater treatment processes is necessary to predict its fate and thereby, appropriate control strategies can be proposed and assessed to minimize hydrogen sulfide production.

ASM2d

The ASM2d is modified to include sulfur transformations in the biological reactor. Since the activated sludge configuration includes an anaerobic section, applicable oxidation and reduction reactions of sulfur depending on whether it is in the anaerobic zones or in the aerobic/anoxic zones, respectively, should be described.

Sulfide oxidation is described as a purely chemical reaction using either oxygen or nitrate as electron acceptors (Gutierrez et al., 2010). Sulfate reduction, on the other hand, is assumed to be biologically mediated by means of sulfate-reducing bacteria (SRB) using acetate and fermentation products as possible electron donors (Batstone, 2006; Batstone et al., 2015). The sulfur-related processes added to ASM2d are presented in Table 4.3 and Table 4.4 (Solon et al., 2016).

Hydrogen sulfide inhibition is taken into account during growth of heterotrophic organisms (X_H), phosphorus accumulating organisms (X_{PAO}), nitrifiers (X_A) and sulfate-reducing bacteria (X_{SRB}). The inhibition is due to toxicity of several bacterial groups, including the SRB themselves, to sulfide. Hydrogen sulfide stripping is also included.

ADM1

A high sulfate concentration in the digester influent can significantly affect the methanogenesis phase during anaerobic digestion. This effect is not modelled in the current version of the ADM1, but it is important in order to correctly predict the behaviour of the system under high sulfate conditions. Modelling of sulfate reduction in the ADM1 is also one of the most widely requested extensions.

Fedorovich et al. (2003) and Knobel & Lewis (2002) have developed extensions to ADM1 on sulfate reduction, which is complex, since it is intended for systems dealing with high concentrations of sulfate.

A simpler approach was developed by Batstone (2006) by assessing sulfate reduction through oxidation of available hydrogen. This model only considers a single group of microorganism, hydrogen sulfate-reducing bacteria (X_{hSRB}), which can oxidise hydrogen with sulfate as electron acceptor to produce hydrogen sulfide according to the equation:

$$X_{hSRB}: \quad 4H_2 + H_2SO_4 \rightarrow H_2S + 4H_2O \tag{4.2}$$

This group of sulfate reducers are competing with hydrogen utilisers. According to Batstone (2006), this simplified model is effective for predicting the behaviour with influent S:COD of up to 0.1 g S.g COD^{-1} (note that this value is obtained using a simplified model without considering inhibition due to sulfide and without the detailed aqueous phase chemical model). Above this level the sulfate reducers will start to oxidise the volatile fatty acids as well and the model will incorrectly predict sulfate in the effluent, and there will be underprediction of hydrogen sulfide in the gas stream.

According to the model by Fedorovich et al. (2003) and Knobel & Lewis (2002), the sulfate reduction process is carried out by four groups of microorganisms: hydrogenotrophic sulfate-reducing bacteria (X_{hSRB}), propionate-degrading sulfate-reducing bacteria (X_{pSRB}), butyrate-degrading sulfate-reducing bacteria (X_{bSRB}) and acetotrophic sulfate-reducing bacteria (X_{aSRB}). Equations (4.2), (4.3), (4.4) and (4.5) show the stoichiometric reactions describing the conversion of sulfate to hydrogen sulfide by different types of sulfate-reducing bacteria using specific kinds of substrates as electron acceptors.

$$X_{pSRB}: \quad C_2H_5COOH + 0.75H_2SO_4 \rightarrow CH_3COOH + CO_2 + H_2O + 0.75H_2S \tag{4.3}$$

$$X_{bSRB}: \quad C_3H_7COOH + 0.5H_2SO_4 \rightarrow 2CH_3COOH + 0.5H_2S \tag{4.4}$$

$$X_{aSRB}: \quad CH_3COOH + H_2SO_4 \rightarrow 2CO_2 + 2H_2O + H_2S \tag{4.5}$$

Hydrogen sulfide inhibition is taken into account in the acetogenesis and methanogenesis stages, as well as for the growth of SRB. The inhibition as described by Chen et al. (2008) is a result of competition for common substrates and also due to toxicity of several bacterial groups, including the SRB themselves, to sulfide.

Three kinds of substrate competition were described by Fedorovich et al. (2003):

i. between SRB and acidogenic bacteria for sugars and amino acids;

ii. between SRB and acetogenic bacteria for VFAs; and,

iii. between SRB and methanogens for acetate and hydrogen.

The first type is won by acidogenic bacteria therefore there is no need to modify the disintegration and hydrolysis part of the ADM1. On the other hand, SRB are found to successfully compete with acetogenic and methanogenic bacteria indicating that to describe the VFA and hydrogen removal, sulfate reduction should be included in the model.

The sulfur-related processes added to ADM1 are presented in Table 4.5 and Table 4.6 (from Paper IV). In addition to biochemical conversions, possible precipitation of sulfur with iron as ferrous sulfide (FeS) is included in the extended ADM1. The precipitation kinetics are described in Section 3.3.

Table 4.3. Gujer matrix for sulfur-related extensions to ASM2d.

Component, i → / Process, j ↓	S_{O2}	S_F	S_A	S_{NH4}	S_{N2}	S_{NO3}	X_I	X_S	S_{SO4}	S_{IS}	X_{S0}	X_{SRB}
S_{SO4} reduction on S_F		$-1/Y_{SRB}$		$-((-1/Y_{SRB})\cdot N_{SF} + N_{BM})$					$-(1-Y_{SRB})/(2\cdot Y_{SRB})$	$(1-Y_{SRB})/(2\cdot Y_{SRB})$		1
S_{SO4} reduction on S_A			$-1/Y_{SRB}$	$-N_{BM}$					$-(1-Y_{SRB})/(2\cdot Y_{SRB})$	$(1-Y_{SRB})/(2\cdot Y_{SRB})$		1
Decay of X_{SRB}				$-(f_{XI}\cdot N_{XI} + (1-f_{XI})\cdot N_{XS} - N_{Ci}$			f_{XI}	$1-f_{XI}$				-1
S_{IS} oxidation using S_{O2}	-1									-2	2	
S_{IS} oxidation using S_{NO3}					0.175	-0.175				-1	1	
X_{S0} oxidation using S_{O2}	-1.5								1		-1	
X_{S0} oxidation using S_{NO3}					0.525	-0.525			1		-1	

Table 4.4. Process kinetic rate equations for sulfur-related reactions (extensions to ASM2d).

Process, j ↓	Kinetics rate expressions (ρ_j, g COD.m^{-3}.d^{-1})
S_{SO4} reduction on S_F	$\mu_{SRB}\cdot\frac{S_F}{K_F+S_F}\cdot\frac{S_F}{S_F+S_A}\cdot\frac{S_{NH_4}}{K_{NH_4}+S_{NH_4}}\cdot\frac{S_{PO_4}}{K_{PO_4}+S_{PO_4}}\cdot\frac{S_{SO_4}}{K_{SO_4}+S_{SO_4}}\cdot\frac{K_{O_2}}{K_{O_2}+S_{O_2}}\cdot\frac{K_{NO_3}}{K_{NO_3}+S_{NO_3}}\cdot X_{SRB}\cdot I_{H_2S,SRB}$
S_{SO4} reduction on S_A	$\mu_{SRB}\cdot\frac{S_A}{K_A+S_A}\cdot\frac{S_A}{S_F+S_A}\cdot\frac{S_{NH_4}}{K_{NH_4}+S_{NH_4}}\cdot\frac{S_{PO_4}}{K_{PO_4}+S_{PO_4}}\cdot\frac{S_{SO_4}}{K_{SO_4}+S_{SO_4}}\cdot\frac{K_{O_2}}{K_{O_2}+S_{O_2}}\cdot\frac{K_{NO_3}}{K_{NO_3}+S_{NO_3}}\cdot X_{SRB}\cdot I_{H_2S,SRB}$
Decay of X_{SRB}	$k_{dec,SRB}\cdot X_{SRB}$
S_{IS} oxidation using S_{O2}	$k_{oxi,H_2S}\cdot S_{IS}\cdot S_{O_2}$
S_{IS} oxidation using S_{NO3}	$\eta_{NO_3}\cdot k_{oxi,H_2S}\cdot S_{IS}\cdot S_{NO_3}$
X_{S0} oxidation using S_{O2}	$k_{oxi,S^0}\cdot X_{S^0}\cdot S_{O_2}$
X_{S0} oxidation using S_{NO3}	$\eta_{NO_3}\cdot k_{oxi,S^0}\cdot X_{S^0}\cdot S_{NO_3}$

Table 4.5. Gujer matrix for sulfur-related extensions to ADM1.

Component, i → / Process, j ↓	S_{va}	S_{bu}	S_{pro}	S_{ac}	S_{h2}	S_I	X_{ch}	X_{pr}	X_{li}	X_I	S_{SO4}	S_{IS}	X_{hSRB}	X_{aSRB}	X_{pSRB}	X_{c4SRB}
Growth of X_{hSRB}					-1						-(1-Y_{hSRB})/64	1-Y_{hSRB}	Y_{hSRB}			
Decay of X_{hSRB}						$f_{SI,XB}$	$f_{CH,XB}$	$f_{PR,XB}$	$f_{LI,XB}$	$f_{XI,XB}$			-1			
Growth of X_{aSRB}				-1							-(1-Y_{aSRB})/64	1-Y_{aSRB}		Y_{aSRB}		
Decay of X_{aSRB}						$f_{SI,XB}$	$f_{CH,XB}$	$f_{PR,XB}$	$f_{LI,XB}$	$f_{XI,XB}$				-1		
Growth of X_{pSRB}			-1	(1-Y_{pSRB})·0.57							-(1-Y_{pSRB})·0.43/64	(1-Y_{pSRB})·0.43			Y_{pSRB}	
Decay of X_{pSRB}						$f_{SI,XB}$	$f_{CH,XB}$	$f_{PR,XB}$	$f_{LI,XB}$	$f_{XI,XB}$					-1	
Growth of X_{c4SRB} on S_{bu}		-1		(1-Y_{c4SRB})·0.8							-(1-Y_{c4SRB})·0.2/64	(1-Y_{c4SRB})·0.2				Y_{c4SRB}
Growth of X_{c4SRB} on S_{va}	-1		(1-Y_{c4SRB})·0.54	(1-Y_{c4SRB})·0.31							-(1-Y_{c4SRB})·0.15/64	(1-Y_{c4SRB})·0.15				Y_{c4SRB}
Decay of X_{c4SRB}						$f_{SI,XB}$	$f_{CH,XB}$	$f_{PR,XB}$	$f_{LI,XB}$	$f_{XI,XB}$						-1

Table 4.6. Process kinetic rate equations for sulfur-related reactions (extensions to ADM1).

Process, j ↓	Kinetics rate expressions (ρ_j, kg COD.m^{-3}.d^{-1})
Growth of X_{hSRB}	$k_{m,hSRB} \cdot \frac{S_{SO_4}}{K_{S,SO_4,hSRB} + S_{SO_4}} \cdot \frac{S_{H_2}}{K_{S,hSRB} + S_{H_2}} \cdot X_{hSRB} \cdot I_{H_2S,hSRB} \cdot I_{pH,hSRB} \cdot I_{IN,lim} \cdot I_{IP,lim}$
Decay of X_{hSRB}	$k_{dec,hSRB} \cdot X_{hSRB}$
Growth of X_{aSRB}	$k_{m,aSRB} \cdot \frac{S_{SO_4}}{K_{S,SO_4,aSRB} + S_{SO_4}} \cdot \frac{S_{ac}}{K_{S,aSRB} + S_{ac}} \cdot X_{aSRB} \cdot I_{H_2S,aSRB} \cdot I_{pH,aSRB} \cdot I_{IN,lim} \cdot I_{IP,lim}$
Decay of X_{aSRB}	$k_{dec,aSRB} \cdot X_{aSRB}$
Growth of X_{pSRB}	$k_{m,pSRB} \cdot \frac{S_{SO_4}}{K_{S,SO_4,pSRB} + S_{SO_4}} \cdot \frac{S_{pro}}{K_{S,aSRB} + S_{pro}} \cdot X_{pSRB} \cdot I_{H_2S,pSRB} \cdot I_{pH,pSRB} \cdot I_{IN,lim} \cdot I_{IP,lim}$
Decay of X_{pSRB}	$k_{dec,pSRB} \cdot X_{pSRB}$
Growth of X_{c4SRB} on S_{bu}	$k_{m,c4SRB} \cdot \frac{S_{SO_4}}{K_{S,SO_4,c4SRB} + S_{SO_4}} \cdot \frac{S_{va}}{K_{S,c4SRB} + S_{va}} \cdot \frac{S_{va}}{S_{bu} + S_{va}} \cdot X_{c4SRB} \cdot I_{H_2S,c4SRB} \cdot I_{pH,c4SRB} \cdot I_{IN,lim} \cdot I_{IP,lim}$
Growth of X_{c4SRB} on S_{va}	$k_{m,c4SRB} \cdot \frac{S_{SO_4}}{K_{S,SO_4,c4SRB} + S_{SO_4}} \cdot \frac{S_{bu}}{K_{S,c4SRB} + S_{bu}} \cdot \frac{S_{bu}}{S_{bu} + S_{va}} \cdot X_{c4SRB} \cdot I_{H_2S,c4SRB} \cdot I_{pH,c4SRB} \cdot I_{IN,lim} \cdot I_{IP,lim}$
Decay of X_{c4SRB}	$k_{dec,c4SRB} \cdot X_{c4SRB}$

4.3. Iron Transformations

Iron in the wastewater is important to model, especially when considering phosphorus removal and recovery, because of its interactions with phosphorus and sulfur, preferentially binding with the latter. Iron is often used in wastewater treatment plants for chemical precipitation in order to remove phosphorus.

ASM2d

The ASM2d is modified to include iron transformations in the biological reactor. In this model, only Fe(II) oxidation using either oxygen or nitrate as electron acceptors is included. This is assumed to be a purely chemical reaction resulting in oxidation of Fe(II) to hydrous ferric oxide, $Fe(OH)_3$ (X_{HFO}). In addition, reduction of hydrous ferric oxide to Fe(II) using inorganic sulfides and acetate are also included (Table 4.7 and Table 4.8).

The hydrous ferric oxide model (Smith et al., 2008) describes how the precipitation of X_{HFO} provides a number of adsorption sites for ions on its surface. Hauduc et al. (2015) adapted this approach focusing only on phosphates adsorption and co-precipitation. The model describes in general the precipitation and dissolution of X_{HFO}, phosphates adsorption/binding onto X_{HFO} and aging of X_{HFO}.

A simplified version of the HFO model adapted for ASM2d is shown in Figure 4.2.

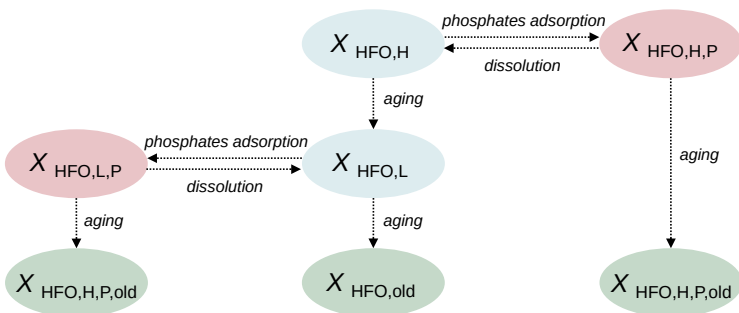

Figure 4.2. Simplified HFO model included in ASM2d and ADM1.

According to this simplified model, HFO is formed from Fe(II) oxidation. HFO initially precipitates with a high adsorption capacity ($X_{HFO,H}$), which has an open structure and easily accessible binding sites. As it ages, it loses reactivity and has a more compact structure and less accessible sites ($X_{HFO,L}$). Adsorption of phosphates onto HFO leads to production of $X_{HFO,H,P}$ and $X_{HFO,L,P}$. The kinetic rate of aging is lower for $X_{HFO,L}$ than for $X_{HFO,H}$ due to the increased probability of floc breakages (compared to aggregation) for older HFO. Similarly, HFO with bounded phosphates ($X_{HFO,H,P}$, $X_{HFO,L,P}$) also have lower kinetic rates than unbounded HFO. The adsorption kinetic rates depend on the concentration of the binding component. The complete stoichiometry and kinetic rates used are found in Table 4.11 and Table 4.12.

ADM1

The process of Fe(III) reduction is added as a process to ADM1. Fe(III), in the form of hydrous ferric oxides ($X_{HFO,L}$, $X_{HFO,H}$), is reduced to Fe(II) using hydrogen and sulfide as electron donor (Table 4.9 and Table 4.10).

In addition to biochemical conversions, precipitation of iron with sulfur and phosphate is included in the extended ADM1. Possible precipitates considered are ferrous sulfide (FeS) and ferrous phosphate ($Fe_3(PO_4)_2$). The precipitation kinetics are described in Section 3.3.

Table 4.7. Gujer matrix for iron extensions to ASM2d.

Process, j ↓ \ Component, i →	S_{O2}	S_A	S_{N2}	S_{NO3}	S_{IS}	X_{S0}	$S_{Fe(II)}$	$X_{HFO,L}$	$X_{HFO,H}$
Oxidation of $S_{Fe(II)}$ to $S_{Fe(III)}$ using S_{O2}	-0.1433						-1	0.3103	0.6897
Oxidation of $S_{Fe(II)}$ to $S_{Fe(III)}$ using S_{NO3}			0.0501	-0.0501			-1	0.3103	0.6897
Reduction of $X_{HFO,L}$ to $S_{Fe(II)}$ using S_{IS}					-0.2865	0.2865	1	-1	
Reduction of $X_{HFO,H}$ to $S_{Fe(II)}$ using S_{IS}					-0.2865	0.2865	1		-1
Reduction of $X_{HFO,L}$ to $S_{Fe(II)}$ using S_A		-0.1433					1	-1	
Reduction of $X_{HFO,H}$ to $S_{Fe(II)}$ using S_A		-0.1433					1		-1

Table 4.8. Process kinetic rate equations for iron-related reactions (extensions to ASM2d).

Process, j ↓	Kinetics rate expressions (ρ_j, g COD.m^{-3}.d^{-1})
Oxidation of $S_{Fe(II)}$ to $S_{Fe(III)}$ using S_{O2}	$k_{oxi,Fe(II)} \cdot S_{Fe(II)} \cdot S_{O_2}$
Oxidation of $S_{Fe(II)}$ to $S_{Fe(III)}$ using S_{NO3}	$\eta_{NO_3} \cdot k_{oxi,Fe(II)} \cdot S_{Fe(II)} \cdot S_{NO_3}$
Reduction of $X_{HFO,L}$ to $S_{Fe(II)}$ using S_{IS}	$k_{red,Fe(III),S_{IS}} \cdot X_{HFO,L} \cdot S_{IS} \cdot \frac{K_{O_2}}{K_{O_2}+S_{O_2}} \cdot \frac{K_{NO_3}}{K_{NO_3}+S_{NO_3}}$
Reduction of $X_{HFO,H}$ to $S_{Fe(II)}$ using S_{IS}	$k_{red,Fe(III),S_{IS}} \cdot X_{HFO,H} \cdot S_{IS} \cdot \frac{K_{O_2}}{K_{O_2}+S_{O_2}} \cdot \frac{K_{NO_3}}{K_{NO_3}+S_{NO_3}}$
Reduction of $X_{HFO,L}$ to $S_{Fe(II)}$ using S_A	$k_{red,Fe(III),S_A} \cdot X_{HFO,L} \cdot S_A \cdot \frac{K_{O_2}}{K_{O_2}+S_{O_2}} \cdot \frac{K_{NO_3}}{K_{NO_3}+S_{NO_3}}$
Reduction of $X_{HFO,H}$ to $S_{Fe(II)}$ using S_A	$k_{red,Fe(III),S_A} \cdot X_{HFO,H} \cdot S_A \cdot \frac{K_{O_2}}{K_{O_2}+S_{O_2}} \cdot \frac{K_{NO_3}}{K_{NO_3}+S_{NO_3}}$

Table 4.9. Gujer matrix for iron extensions to ADM1.

Component, i → / Process, j ↓	S_{h2}	S_{IS}	X_{S0}	$S_{Fe(II)}$	$X_{HFO,L}$	$X_{HFO,H}$
Reduction of $X_{HFO,L}$ using S_{h2}	-1			1	-0.1250	
Reduction of $X_{HFO,H}$ using S_{h2}	-1			1		-0.1250
Reduction of $X_{HFO,L}$ using S_{IS}		-1	0.7500	0.2500	-0.0313	
Reduction of $X_{HFO,H}$ using S_{IS}		-1	0.7500	0.2500		-0.0313

Table 4.10. Process kinetic rate equations for iron-related reactions (extensions to ADM1).

Process, j ↓	Kinetics rate expressions (ρ_j, kg COD.m^{-3}.d^{-1})
Reduction of $X_{HFO,L}$ using S_{h2}	$\frac{K_{Fe(III),Fe(II)} \cdot X_{HFO,L} \cdot S_{H_2}}{16}$
Reduction of $X_{HFO,H}$ using S_{h2}	$\frac{K_{Fe(III),Fe(II)} \cdot X_{HFO,H} \cdot S_{H_2}}{16}$
Reduction of $X_{HFO,L}$ using S_{IS}	$\frac{K_{Fe(III),Fe(II)} \cdot X_{HFO,L} \cdot S_{IS}}{64}$
Reduction of $X_{HFO,H}$ using S_{IS}	$\frac{K_{Fe(III),Fe(II)} \cdot X_{HFO,H} \cdot S_{IS}}{64}$

Table 4.11. Gujer matrix for HFO model included in ASM2d.

Component, i → / Process, j ↓	$X_{HFO,L}$	$X_{HFO,H}$	$X_{HFO,L,P}$	$X_{HFO,H,P}$	$X_{HFO,H,P,old}$	$X_{HFO,L,P,old}$	$X_{HFO,old}$
Aging of $X_{HFO,H}$	1	-1					
Aging of $X_{HFO,L}$	-1						1
Fast binding of P to active $X_{HFO,H}$		-1/(ASFH·(AMP/AMFe)		1/(ASFH·(AMP/AMFe)			
Slow sorption of P to active $X_{HFO,L}$	-1/(ASFL·(AMP/AMFe)		1/(ASFL·(AMP/AMFe)				
Aging of $X_{HFO,H,P}$				-1	1		
Aging of $X_{HFO,L,P}$			-1			1	
Dissolution of $X_{HFO,H,P}$ and release of P		1		-1			
Dissolution of $X_{HFO,L,P}$ and release of P	1		-1				

Table 4.12. Process kinetic rate equations for HFO reactions (extensions to ASM2d).

Process, j ↓	Kinetics rate expressions (ρ_j, g COD.m^{-3}.d^{-1})
Aging of $X_{HFO,H}$	$q_{aging,H} \cdot X_{HFO,H}$
Aging of $X_{HFO,L}$	$q_{aging,L} \cdot X_{HFO,L}$
Fast binding of P to active $X_{HFO,H}$	$q_{coprecip\text{-}P} \cdot \frac{S_{PO_4}}{K_P + S_{PO_4}} \cdot X_{HFO,H}$
Slow sorption of P to active $X_{HFO,L}$	$q_{binding\text{-}P} \cdot \frac{S_{PO_4}}{K_P + S_{PO_4}} \cdot X_{HFO,L}$
Aging of $X_{HFO,H,P}$	$q_{aging,H} \cdot X_{HFO,H,P}$
Aging of $X_{HFO,L,P}$	$q_{aging,L} \cdot X_{HFO,L,P}$
Dissolution of $X_{HFO,H,P}$ and release of P	$q_{diss,H} \cdot \frac{K_{P,diss}}{K_{P,diss} + S_{PO_4}} \cdot X_{HFO,H,P}$
Dissolution of $X_{HFO,L,P}$ and release of P	$q_{diss,L} \cdot \frac{K_{P,diss}}{K_{P,diss} + S_{PO_4}} \cdot X_{HFO,L,P}$

4.4. Modelling of Phosphorus, Sulfur and Iron Transformations in Anaerobic Digestion

The work in incorporating biochemical conversions of phosphorus and chemical transformations of sulfur and iron is done for ADM1 (Paper IV). The goal of this is to show the importance of taking into account phosphorus and its interaction with sulfur and iron during anaerobic digestion. There are anaerobic systems, which are used for the stabilization of either phosphorus-rich and/or sulfur-rich sludge, such that it becomes essential to model their interactions, which in turn could affect the whole plant-wide processes due to recycling of streams. This analysis enables evaluation of the need for model extensions in a plant-wide model.

A case study is performed by comparing four sets of model assumptions, which describes the phosphorus, sulfur and iron interactions.

i. A_0 – the BSM2 implementation of the default ADM1 with some minor changes is used. Phosphorus is modelled in the AD using a source-sink approach with a pre-defined elemental compositional for each model state variable. The composite material (X_C) is removed and directly mapped into biodegradable and inert organics. The physico-chemical framework is also included, which comprises of the weak acid-base chemistry module, ion activity corrections, ion-pairing effects and multiple mineral precipitation.

ii. A_1 – the P-related processes presented in Section 4.1 are added to the ADM1 processes in addition to the physico-chemical module.

iii. A_2 – the S-related processes presented in Section 4.2 are added to the ADM1 in addition to the P-related processes and physico-chemical module. There are two implementations of this model. One considers only a single type of SRB, which use hydrogen for sulfate reduction ($A_{2,1}$). The other considers multiple types of SRB, which utilize organic acids for sulfate reduction ($A_{2,2}$).

iv. A_3 – the Fe-related processes involves iron reduction using either hydrogen or sulfides as electron donors. These processes are added in addition to the P-related processes, S-related processes and the physico-chemical module.

A comparison of the P partitioning in the effluent for both models A_0 and A_1 results in similar distributions of P amongst soluble, organic, biomass and precipitates for the two models. Among the precipitates considered, the main compounds are struvite and calcium phosphate. Further analysis is done with

respect to mineral precipitation and biochemical P transformations at different hydraulic retention times (HRT) and different influent calcium and magnesium loads.

Increase in calcium and magnesium loads promotes precipitation. The difference between the two model variants is observed at higher cationic loads as shown in Figure 4.3. Moreover, the difference is also apparent at low HRT due to the difference in supply of P for precipitation. At high HRT, the P supply as a result of the biochemical P transformations followed by the precipitation occurs well within the corresponding process time constant. However, at low HRT, these P transformations (i.e. A_1) cause a noticeable delay in P availability resulting in a smaller quantity of precipitated P compared to the A_0.

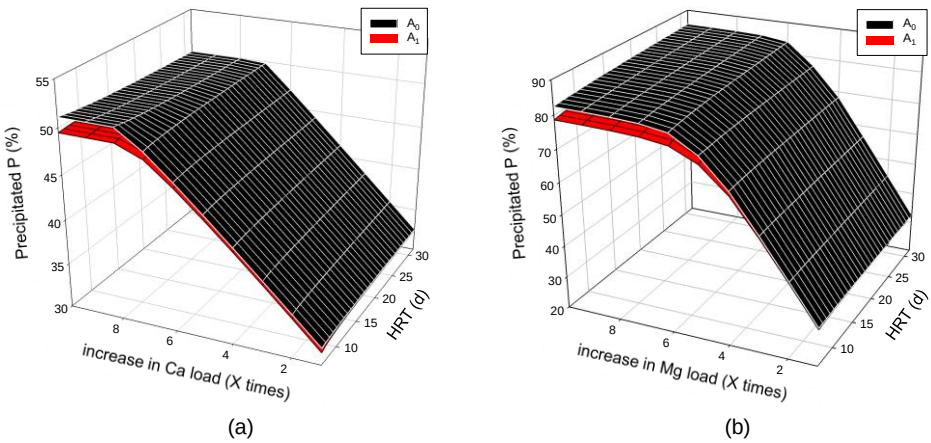

Figure 4.3. Effect of including biochemical phosphorus transformations (A_1) in the anaerobic digester at various HRT on the total precipitated P by: (a) increasing the influent calcium load and (b) increasing the influent magnesium load, as compared with the reference model A_0 (from Paper IV).

Moreover, including the biochemical P transformations in the anaerobic digestion model affects biogas production. As expected, there is higher methane production at higher HRT. Figure 4.4 shows the difference between the methane production between A_0 and A_1. There is generally a lower predicted methane gas production in A_1 because the biochemical processes involve the uptake of organic acids, which includes acetate, into PHA. Thus, there is a less available substrate for acetoclastic methanogenesis.

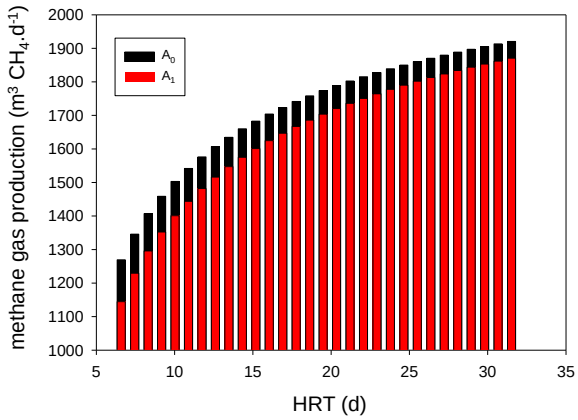

Figure 4.4. Effect of including biochemical phosphorus transformations (A_1) in the anaerobic digester at various HRT on methane gas production compared with reference model A_0 (from Paper IV).

To simulate case A_2, an influent load with S:COD ratio of 0.0025 g S.g COD^{-1} is added as sulfate. Sulfate is then transformed to hydrogen sulfide gas and dissolved sulfide, with some remaining fraction of sulfate. Both simulation results of model implementations $A_{2,1}$ and $A_{2,2}$ are similar. The reduction of sulfate to sulfide only uses hydrogen as electron donor for both models and there is no possibility to use organic acids. Figure 4.5a depicts the effect of sulfur transformations on methane production. There is a decrease in methane production at higher S:COD ratios due to higher production of sulfide, which in turn causes sulfide inhibition of the methanogens. It has also been observed that model differences between $A_{2,1}$ and $A_{2,2}$ become significant only when considering an influent with S:COD ratio greater than 0.06 g S.g COD^{-1}, such that hydrogen becomes completely depleted during reduction of sulfate to sulfide and thus other SRB use organic acids as electron source. However, such a sulfate concentration is extremely high, whereas primary and secondary sludge normally has an S:COD ratio around 0.001 g S.g COD^{-1}.

Case A_3 involves addition of Fe(III), in which it is converted into its reduced form Fe(II) under anaerobic conditions. At increasing quantities of added Fe(III), iron phosphates are formed, which decreases the quantity of struvite precipitates. This principle can be used as a control strategy to avoid undesired struvite precipitation. On the other hand, when sulfur is present the iron conversions are affected due to preferential binding of sulfur with iron. Thus, in anaerobic systems with high sulfate loads, addition of iron will result in an increase of iron sulfide precipitates. The quantity of hydrogen sulfide produced decreases (Figure 4.5b) preventing consequent methanogenesis inhibition.

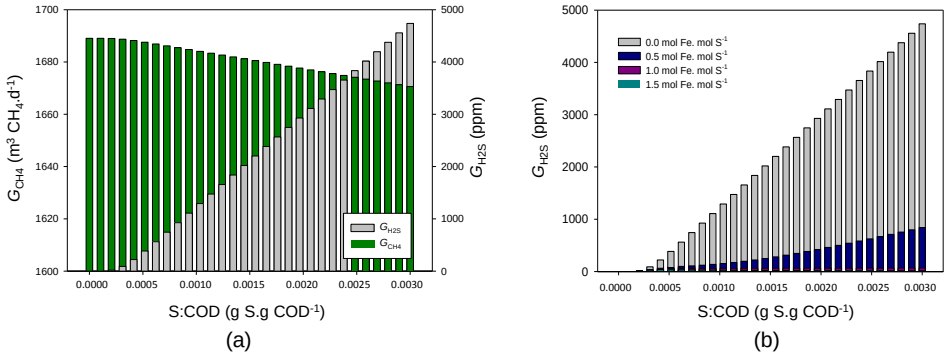

Figure 4.5. Effect of including: (a) biochemical sulfur transformations ($A_{2,1}$) on methane gas production and (b) chemical iron transformations (A_3) on hydrogen sulfide gas production in the anaerobic digester at various S:COD ratios (from Paper IV).

4.5. Modelling of Phosphorus, Sulfur and Iron Transformations in Activated Sludge Processes

The modelling and simulation study presented in the previous section is an exploratory work to show that modelling P, S and Fe transformations and their interactions in the sludge line have a significant effect on plant-wide outputs. There are several simplifications and assumptions. Firstly, iron transformations are modelled as purely chemical processes in the anaerobic digester and secondly, iron and sulfur transformations (and the precipitation reactions) were not accounted for in the activated sludge section. Nevertheless, ASM2d should be used to describe the biological reactions in the activated sludge unit, which considers phosphorus transformations. It was assumed that sulfate and iron concentrations in the influent (i.e. municipal wastewater) are not high enough to affect the phosphorus transformations in the activated sludge unit.

However, the sulfur and iron extensions to ASM2d presented in Sections 4.2 and 4.3 are to be used when: (1) chemical precipitation is employed in the activated sludge unit, (2) modelling sulfur-rich activated sludge units such as in sulfate reduction, autotrophic denitrification and nitrification integrated (SANI) processes and (3) tracking the transformations in the water line.

Chapter 5 will present the results of modelling and simulation of a wastewater treatment plant using ASM2d and ADM1 extensions for the water and sludge lines, respectively (Paper V). It will also demonstrate the practical use of the model extensions to plant-wide modelling with focus on resource recovery.

4.6. Summary of Key Findings

- The ADM1 is extended to include biochemical transformations of phosphorus and sulfur, as well as chemical iron conversions. This extension also includes implementation of the physico-chemical framework, which consists of ion activity corrections, ion-pairing effects, weak acid-base chemistry and multiple mineral precipitation reactions. The extended ADM1 model is implemented within a plant-wide framework provided by the BSM2 in order to track the P-, S- and Fe-related state variables from the sludge line and back to the water line.

- Biochemical phosphorus conversions have an effect on the prediction of amounts of precipitates and methane gas production due to the role of phosphorus accumulating organisms under anaerobic conditions. The difference between the default ADM1 implementation and the ADM1 extended with phosphorus transformations is evident at higher cationic loads and low HRT.

- Inclusion of sulfate conversions in the ADM1 also has a significant effect on biogas production prediction. At increasing S:COD ratios, methane production is decreasing due to the conversion of sulfates to sulfides during anaerobic conditions. The hydrogen sulfide produced is inhibitory to methanogens and thus affects biogas production.

- Chemical iron conversions influence precipitation reactions. At high iron concentrations, phosphates bind with iron to form precipitates resulting in less available P for struvite precipitation. In systems with the presence of sulfur, iron preferentially binds with sulfur instead of phosphates. Thus, less sulfides are produced, which then reduces inhibition of methanogenesis.

- This work assesses the influence of including P, S and Fe transformations and interactions in a plant-wide model. Inclusion of sulfur and iron extensions in the activated sludge model is presented in this chapter but not included in the case study. However, a plant-wide model with P, S and Fe conversions in the water line and sludge line is deemed important to track the fate of these compounds within the wastewater treatment plant and therefore, assist in developing control strategies for their removal and/or recovery.

Chapter 5

Plant-Wide Model Extended with Phosphorus, Sulfur and Iron

This chapter discusses the integration of the various model extensions presented in the previous chapters into a plant-wide model approach within the framework of the Benchmark Simulation Model No. 2 (BSM2). It showcases the main modifications to the BSM2 with respect to the plant layout, process models for other unit operations, model interfaces, evaluation criteria, etc. The plant-wide model allows for prediction of phosphorus fluxes from the water line to the sludge line. It also analyses the interactions with iron and sulfur on a plant-wide level. These extensions are useful for evaluating operational and control strategies aimed at energy production, resource recovery, reduction of environmental impact and decrease of the operational expenses. Key results of Paper V are presented, which is based on analysis of several scenarios depicting various operational strategies aimed at phosphorus removal and/or recovery.

5.1. Plant Layout and Influent

The models representing the wastewater treatment unit processes are implemented in a plant layout that is a modification of the BSM2 plant. It consists of: primary clarifier, activated sludge unit, secondary settler, sludge thickener, anaerobic digester, storage tank and dewatering unit. The main modification with respect to the original design of the BSM2 plant layout is on the activated sludge configuration. An anaerobic/anoxic/aerobic (A^2O) configuration (Figure 5.1) is implemented replacing the modified Ludzack-Ettinger process. An anaerobic

section is added, preceding the anoxic and aerobic sections, to promote anaerobic phosphorus release and to provide the phosphorus accumulating organisms with a competitive advantage over other bacteria. It is important to highlight that this configuration does not represent an optimal configuration for P removal, because the biological P removal is dependent on the N removal through the nitrate concentration recycled to the anaerobic reactor via the underflow recycle (i.e. nitrates overload may cause the anaerobic reactors to become anoxic). Nevertheless, it exemplifies the retrofit of many treatment plants adapting their plant layout to satisfy new and stricter effluent requirements.

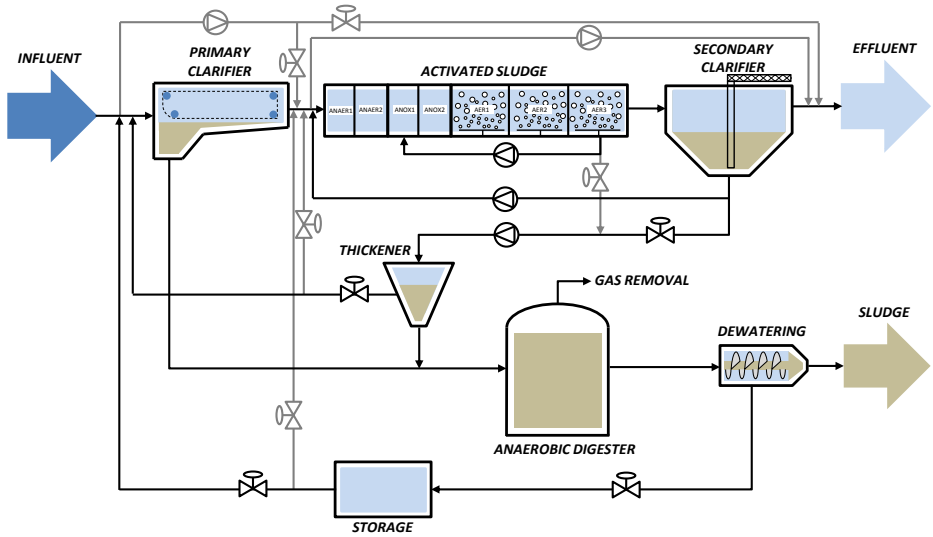

Figure 5.1. BSM2-P plant layout (from Paper V).

Model-based influent scenario generation as described in Gernaey et al. (2011) is utilized to create a dynamic wastewater influent to simulate the treatment plant performance. The model blocks for flow rate generation, chemical oxygen demand, N and P generation, temperature profile generation and sewer network and first flush effects are used to generate the influent dynamics consisting of a 12 months period of output data for the evaluation period with a 15 minutes sampling interval. The resulting daily average influent mass flow rates are presented in Table 5.1. The S influent load for this analysis is set to a high value in order to have a noticeable effect in the AD. In addition, cation and anion profiles are added so that the resulting pH is close to neutrality.

Table 5.1. Daily average influent mass flow rates.

Mass flow rates	Value	
COD	8 386	kg COD.d^{-1}
N	1 014	kg N.d^{-1}
P	197	kg P.d^{-1}
S:COD	0.003	kg S.kg COD^{-1}

5.2. Interfaces

ASM-PCM Interface

The default implementation of the ASM2d was adjusted in order to include the PCM. The main modifications are:

i. the use of inorganic carbon (S_{IC}) instead of alkalinity (S_{ALK}) as a state variable;

ii. the inclusion of mass transfer equations for CO_2, H_2S, NH_3 and N_2 (Batstone et al., 2012; Lizarralde et al., 2015);

iii. consideration of multiple cations (S_K, S_{Na}, S_{Ca}, S_{Mg}) and anions (S_{Cl}), which are tracked as soluble/reactive states; and,

iv. omission of chemical precipitation using metal hydroxides (X_{MeOH}) and metal phosphates (X_{MeP}) since the generalised kinetic precipitation model is used instead (Hauduc et al., 2015; Kazadi Mbamba et al., 2015a; 2015b).

The outputs of the ASM2d at each integration step are used as inputs for the aqueous phase module to estimate pH and ion speciation/pairing while precipitation and stripping equations are formulated as ordinary differential equations and included in the system of ODEs in the ASM2d.

ADM-PCM interface

The ADM is slightly modified to account for the updated physico-chemical model and new processes. The main modifications are:

i. the original pH solver proposed by Rosén et al. (2006) is substituted by the approach presented in Papers I and II, as detailed in Section 3.5.

ii. C, N, P, O and H fractions are updated and taken from de Gracia et al. (2006);

iii. the original ADM1 pools of undefined cations (S_{cat}) and anions (S_{an}) are substituted for specific compounds as in the ASM-PCM interface; and,

iv. the existing gas-liquid transfer equations are extended to include H_2S and NH_3.

Similar to the ASM-PCM interface, the outputs of the ADM at each integration step are used as inputs for the aqueous phase module to estimate pH and ion speciation/pairing while precipitation and stripping equations are formulated as ordinary differential equations and included in the system of ODEs in the ADM.

ASM-ADM-ASM interface

The continuity-based interfacing method (CBIM), described in Volcke et al. (2006), Zaher et al. (2007) and Nopens et al. (2009), is used for creating the interfaces between ASM-ADM-ASM to ensure elemental mass and charge conservation.

The ASM-ADM-ASM interfaces consider instantaneous processes and state variable conversions. The ASM-ADM interface instantaneous processes involve direct removal of COD demanding compounds (i.e. S_{O2} and S_{NO3}) and immediate decay of heterotrophic/autotrophic biomass. State variable conversions require the transformation of soluble fermentable organics (S_F), acetate (S_A) and biodegradable particulate organics (X_S) into amino acids (S_{aa})/sugars (S_{su})/fatty acids (S_{fa}) (soluble) and proteins (X_{pr})/lipids (X_{li})/carbohydrates (X_{ch}) (particulate), respectively. The ADM-ASM interface assumes that all compounds that can be transferred into the gas phase are stripped, and also immediate decay of the AD biomass takes place. All the biodegradable organic particulates (X_{pr}, X_{li}, X_{ch}), organic solubles (S_{aa}, S_{fa}, S_{su}) and volatile fatty acids (S_{ac}, S_{pro}, S_{bu}, S_{va}) are converted into X_S, S_F and S_A, respectively. There is no variation of Fe and S before and after the interface. A compositional analysis of each of the state variables is pre-defined and together with the corresponding stoichiometric factors the elemental compositional balance is conserved with respect to C, N, P, K, Mg, S and Fe.

5.3. Other Unit Process Models

Aside from the activated sludge unit and anaerobic digester, which are described in detail in Chapter 4, the other wastewater treatment unit processes included in the plant-wide model are listed in Table 5.2. The Otterpohl model (Otterpohl, 1995) is used to represent the primary clarification process and is able to yield sensible values of the concentrations of particulate components that are going to the activated sludge and anaerobic digestion units. The secondary clarifier is based on the double exponential velocity function proposed by Takács et al. (1991) with a 10-layer reactive configuration and using a reduction factor in the process kinetics to obtain more realistic results (Guerrero et al., 2013). The thickener and dewatering units are modelled as reactive solid separation units with biological reactions using a similar simplified approach as described by Gernaey et al. (2006a). The gas stripping unit is modelled based on Kazadi Mbamba et al. (2016) while the crystallization unit is described using the multiple mineral precipitation model as presented in Kazadi Mbamba et al. (2015b).

Table 5.2. Description of wastewater treatment unit processes included in the plant-wide model.

Variable	Description	References
primary clarifier	homogenous tank concept non-reactive	Otterpohl (1995)
secondary settler	double exponential velocity function reactive	Takács et al. (1991) Flores-Alsina et al. (2012) Guerrero et al. (2013)
activated sludge unit	ASM2d with P, S and Fe extensions	Henze et al. (1999) see Chapter 4
anaerobic digester	ADM1 with P, S and Fe extensions	Batstone et al. (2002) see Paper IV see Chapter 4
thickener	reactive	Gernaey et al. (2006a)
dewatering unit	reactive	Gernaey et al. (2006a)
storage	non-reactive	Gernaey et al. (2014)
gas stripping unit	gas stripping model	Kazadi Mbamba et al. (2016)
crystallization	multiple mineral precipitation model	Kazadi Mbamba et al. (2015b)

5.4. Extended Evaluation Criteria

To assess the performance of combined C, N and P control strategies, an updated set of evaluation criteria is necessary (Jeppsson et al., 2013; Solon & Snip, 2014). This allows for simplification of the large output dataset into a more manageable set of comparable numbers. The effluent concentrations over the evaluation period should, at all times, obey the concentration limits given in Table 5.3.

Table 5.3. Effluent quality limits.

Variable	Value
N_{total}	< 18 g N.m^{-3}
COD_{total}	< 100 g COD.m^{-3}
S_{NH}	< 4 g N.m^{-3}
TSS	< 30 g SS.m^{-3}
BOD_5	< 10 g BOD.m^{-3}
P_{total}	< 2 g P.m^{-3}

Additional consideration has been necessary to include effluent violations (frequency and magnitude) and percentiles related to P. The *percentage of time* the effluent limits are not met are reported, as well as the *number of violations*. The number of violations is defined as the number of crossings of the limit (from below to above the limit).

The Effluent Quality Index (*EQI*) reflects the amount of pollution discharged onto surface waters averaged over the period of observation based on a weighting of the effluent loads of compounds that have a major influence on the quality of the receiving water and are usually included in the legislation. The *EQI* is updated to include the additional P load, both organic and inorganic.

Another criterion is the Operational Cost Index (*OCI*). It is given as the weighted sum of costs related to sludge production, aeration, pumping, external carbon source, mixing, heating and the benefit of methane production. Because of the modifications to the plant layout and operation, additional costs are considered, such as those relating to the additional recycles (anoxic, anaerobic), aerators (CO_2 stripping) and chemicals (for chemical P precipitation and/or recovery).

5.5. Scenario Analysis

The plant-wide model is tested and used to analyse and compare several operational strategies aimed at phosphorus removal and recovery. Four dynamic scenarios are analysed:

i. A_0 – default, open loop configuration (i.e. no control);

ii. A_1 – cascade ammonium and wastage controller;

iii. A_2 – cascade ammonium and wastage controller + iron addition (i.e. chemical P precipitation) in the activate sludge section; and,

iv. A_3 – cascade ammonium and wastage controller + struvite recovery.

The default configuration without any control (A_0) represents the reference operational conditions with which the different operational/control/recovery strategies are implemented, simulated and evaluated. Dynamic profiles can be obtained using the model and some selected output variables are shown in Figure 5.2.

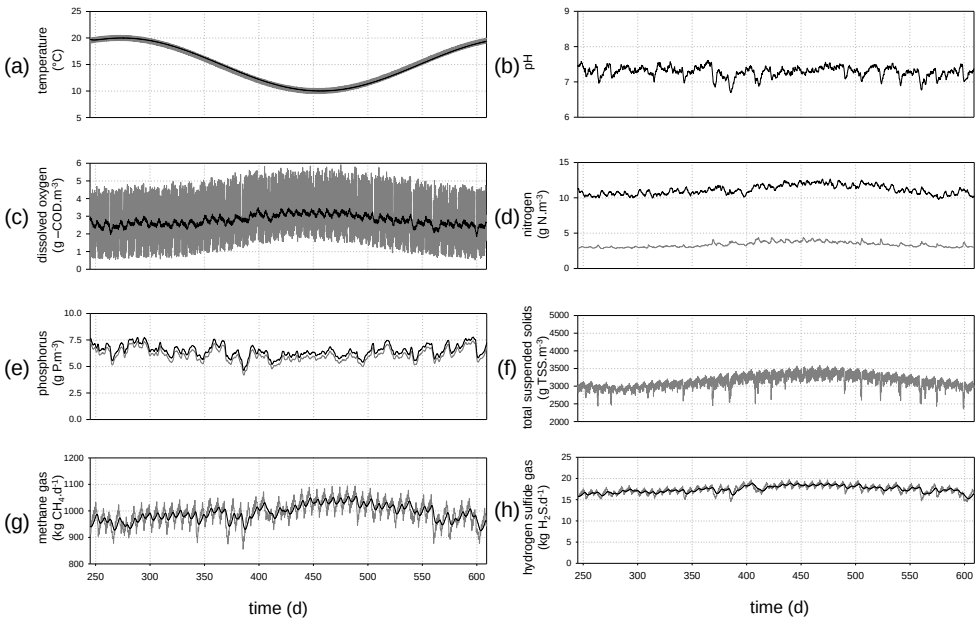

Figure 5.2. Dynamic profiles for the default open loop scenario (A_0) showing: (a) influent temperature, (b) influent pH, (c) dissolved oxygen in AER2, (d) effluent N (ammonia-N (grey) and TN (black)), (e) effluent P (inorganic phosphorus (grey) and TP (black)), (f) TSS in AER3, (g) methane gas production and (h) hydrogen sulfide gas production. An exponential smoothing filter (time constant = 3 days) is used to improve visualization of the data. Raw data is presented in grey (in (a), (b), (c), (f), (g) and (h)) (from Paper V).

The control strategy A_1 uses a cascade PI ammonium controller that manipulates the oxygen set-point in the second aerobic tank (AER2) and also the airflow in AER1 and AER3 by a factor of 2.0 and 0.5 (compared to airflow rate into AER2), respectively. The air supply rate is manipulated to control the oxygen concentration in AER2. The concentration of total suspended solids is also regulated in AER3 by manipulating the wastage flow rate. The set-point changes from 4 000 to 3 000 g TSS.m^{-3} when the temperature exceeds 15°C. This is done to ensure that the solids retention time is long enough for sufficient nitrification when temperature is low. Due to better aeration strategy in the activated sludge unit, phosphate accumulation by phosphorus accumulating organisms improves and also increases nitrification/denitrification efficiency. The operational cost, as reflected by *OCI*, is reduced compared to A_0 (see *AE* and *OCI* values in Table 5.4).

In addition to the cascade ammonium and wastage controller in scenario A_1, scenario A_2 involves the addition of iron in the form of $FeCl_3$ to the activated sludge section. The mass flow rate of $FeCl_3$ is manipulated to control the phosphate concentration in AER3. Effluent phosphorus concentrations and *EQI* are reduced but with a consequent increase in sludge production and *OCI*. Aside from the benefit of increased P removal in the water line due to chemical P precipitation, there is also an advantageous effect to the sludge line. Under anaerobic conditions, hydrous ferric oxides are reduced to Fe(II). At the same time, iron phosphates formed in the activated sludge might re-dissolve under anaerobic conditions and precipitate with sulfide as FeS. This is mainly due to the lower solubility of iron sulfide compared to iron phosphate. This scenario results in reduced problems associated with hydrogen sulfide production (i.e. inhibition, odour, corrosion) (Figure 5.3). Due to the formation of iron phosphates, less calcium phosphate and struvite are formed, which averts having their deposition in the pipes.

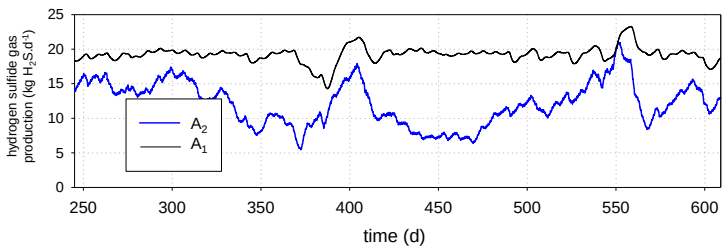

Figure 5.3. Dynamic profile of hydrogen sulfide gas production after implementing scenario A_2 (from Paper V).

Scenario A_3 has an addition of a recovery unit for struvite, which includes a stripping unit, a magnesium hydroxide dosing tank, crystallizer unit and a dewatering tank. Due to the recovery of struvite the quantities of N and P from the AD supernatant are significantly reduced. Consequently, a reduction in *EQI* is observed. Although there is chemical addition, this scenario has a lower *OCI* compared to scenario A_2 due to the lower price of magnesium hydroxide compared to iron chloride and there is also a considered benefit from selling struvite.

Scenario A_3 is further evaluated using sub-scenarios by varying the airflow rate and chemical dosing in the stripping unit. At increasing airflow rates for CO_2 stripping the pH increases, which favours struvite precipitation as shown in Figure 5.4. Similarly, increasing the magnesium dosage also drives the pH upwards. This leads to decreasing quantities of P in the digester supernatant resulting in lower *EQI* values. The *OCI* also decreases due to the consideration of the potential benefit from selling struvite. Above P/Mg stoichiometric rations, further addition of Mg is just increasing the cost without further benefit.

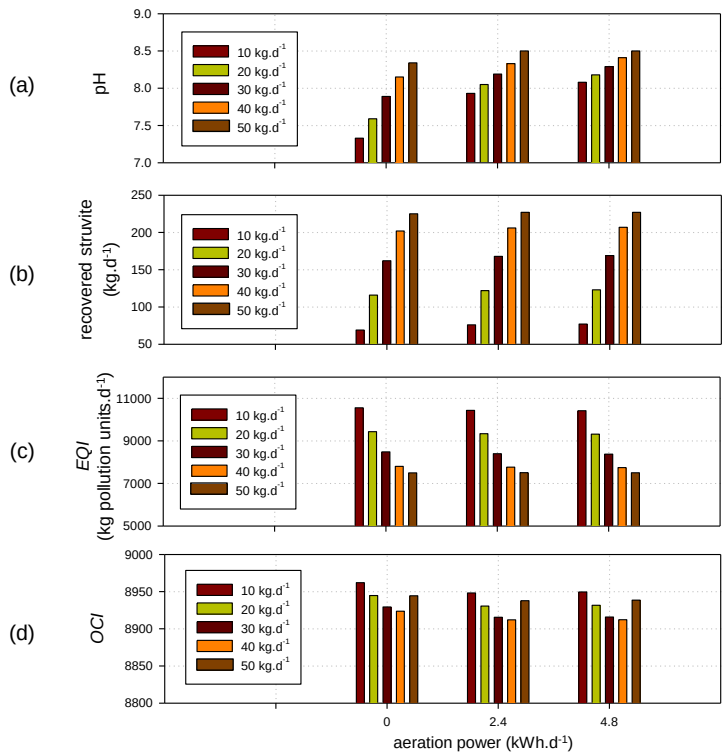

Figure 5.4. Effect of aeration power and dosage addition on (a) pH, (b) quantity of recovered struvite, (c) *EQI* and (d) *OCI* (from Paper V).

All of the proposed alternatives (A_1, A_2 and A_3) result in significant improvements compared with the open loop configuration (A_0). The implementation of controllers for a better aeration strategy and sludge wasting scheme (A_1) results in a favourable alternative. Simulation results also show that this option leads to larger N and P effluent reductions, but is also a more cost-effective way to operate the plant. Both A_2 and A_3 also substantially reduce the quantity of effluent P. However, A_3 considers a modification of the plant layout by addition of a recovery unit. Capital costs for the crystallizer, stripping unit, blowers, civil, electrical and piping works should be included in order to make a more complete techno-economic assessment. On the other hand, A_2 can be set up with an extra dosing tank. Even though the potential benefit that comes from struvite recovery is very uncertain and these results should be taken with care, the cost for each kg N and P removed is much higher for A_2 (see $N_{removed}/OCI$ and $P_{removed}/OCI$ values in Table 5.4).

Table 5.4. Evaluation criteria for the evaluated control/operational strategies (from Paper V).

Operational alternatives →	**A_0**	**A_1**	**A_2**	**A_3**	**Unit**
$N_{Kjeldahl}$	3.5	3.6	3.6	3.7	g N.m^{-3}
N_{total}	11.2	9.2	9.1	8.5	g N.m^{-3}
P_{inorg}	5.95	2.9	0.9	0.6	g P.m^{-3}
P_{total}	6.4	3.7	1.7	1.5	g P.m^{-3}
EQI	18 234	12 508	8 237	7 766	kg pollution.d^{-1}
TIV S_{NHX} (= 4 g N.m^{-3})	0.95	0.07	0.08	0.08	%
TIV N_{total} (= 14 g N.m^{-3})	0	0	0	0	%
TIV P_{total} (= 2 g N.m^{-3})	100	75	13.4	15.7	%
AE	4 000	3 146	3 218	3 194	kWh.d^{-1}
$E_{production}$	5 955	6 054	6 150	6 038	kWh.d^{-1}
$SP_{disposal}$	3 461	3 538	3 730	3 487	kg TSS.d^{-1}
M_{FeCl3}	-	-	169	-	kg Fe.d^{-1}
$M_{Mg(OH)2}$	-	-	-	40	kg Mg.d^{-1}
$S_{recovered}$	-	-	-	206	kg struvite.d^{-1}
OCI	10 201	9 495	13 770	8 912	-
G_{CH4}	992	1 009	1 025	1 006	kg CH_4.d^{-1}
G_{H2S}	17.4	19.2	12.1	19.2	kg H_2S.d^{-1}
$N_{removed}/OCI$	0.079	0.089	0.062	0.097	kg N (removed).OCI^{-1}
$P_{removed}/OCI$	0.007	0.013	0.012	0.019	kg P (removed).OCI^{-1}

The model shows the importance of linking the P with the S and Fe cycles. This is a perfect starting point for evaluating and developing control strategies for wastewater treatment plants with focus on resource recovery (Solon et al., 2017). The sub-models included can be used as modelling tools to simulate particular processes. For example, the ADM1 model can be used independently as well as the ASM2d, both of which are extended with P, S and Fe related conversions. On the other hand, the model extensions could also be applied to integrated urban water systems wherein it is important to track the chemicals added in the sewer network and how it could impact the downstream WWTP processes.

5.6. Summary of Key Findings

- The model platform Benchmark Simulation Model No. 2 is extended to include phosphorus transformations in both the water and sludge lines. The modelling of the interactions between phosphorus and the sulfur and iron cycles has been necessary.

- To evaluate the performance of the wastewater treatment plant under various operational strategies, the evaluation criteria, such as *EQI* and *OCI*, are extended to include P related compounds and additional costs for chemical addition, struvite recovery and aeration for the stripping unit.

- The simulation study involves evaluation and comparison of operational strategies using the default open loop configuration of BSM2 as the baseline. The first alternative operational strategy (A_1) implements a PI ammonia controller to manipulate the oxygen concentration in the aerobic reactors of the activated sludge unit and a wastage controller to manipulate the TSS concentration in the last aerobic tank. The second alternative operational strategy (A_2) includes the controls implemented in A_1 and an additional iron chloride addition in the activated sludge unit for phosphorus precipitation. The third alternative operational strategy (A_3) includes the controls implemented in A_1 and an additional recovery unit (with CO_2 stripping, magnesium hydroxide dosing tank and crystallizer). The three alternatives show a significant improvement in the effluent quality, especially in terms of phosphorus removal. However, the *OCI* increases significantly in A_2 due to the increase in sludge production and high cost of iron chloride. A_3 performs the best in terms of *EQI* and *OCI* but it should be noted that in the last alternative investment costs for the recovery unit are not included in the calculations and that the price of struvite should be taken with care (highly varying).

- The plant-wide model and sub-models presented in this chapter can be used as a tool to aid decision makers/wastewater engineers when upgrading/improving the sustainability and efficiency of wastewater treatment systems with respect to reducing energy consumption and increasing resource recovery. It can be utilized in the development, testing and evaluation of phosphorus control/recovery strategies.

Chapter 6

Conclusions and Future Perspectives

This chapter presents the general conclusions from this thesis and also provides perspectives for future work.

6.1. Conclusions

This thesis presents the sequential phases of developments and extensions to biological and physico-chemical wastewater treatment processes to develop a plant-wide model, which includes phosphorus, sulfur and iron conversions and interactions.

The first main work carried out was the modelling of physico-chemical effects, which included ion activity corrections, ion pairing effects and aqueous phase chemical equilibria. The physico-chemical model was implemented together and interfaced with biochemical models ASM1, ASM2d, ASM3 and ADM1. A scenario analysis was formulated and simulated to analyse and compare ADM1 results using three model variants: default ADM1, ADM1 with ion activity corrections and ADM1 with both ion activity corrections and ion pairing effects. Another scenario analysis was done for the different Activated Sludge Models paired with the physico-chemical model. The general findings of the studies are summarised below.

- Physico-chemical effects have an influence on the model results of ADM1 and are propagated throughout the entire plant model. There is a difference in the model outputs when comparing results of the default ADM1 and the ADM1 with physico-chemical corrections.

- In particular, ion activity corrections have greater influence on model results at higher ionic strengths. Pairing of ions, which have valence of one, is less influential than ion activity corrections even at higher ionic strengths and can be excluded from ADM1.

- When the physico-chemical model is implemented together with the Activated Sludge Models, the pH and speciation of the different wastewater components are reliably predicted under anaerobic, anoxic and aerobic conditions.

The subsequent work dealt with the model development by inclusion of phosphorus, sulfur and iron transformation processes in ASM2d and ADM1, on top of the physico-chemical model. The ASM2d was extended with sulfur and iron oxidation and reduction processes. In addition, hydrous ferric oxides' formation, aging, binding with phosphates and dissolution were also considered. On the other hand, the ADM1 considered biochemical phosphorus transformations and reduction of sulfate and iron. In addition, multiple mineral precipitation was also included in ADM1. Ion pairing was included since it was expected that ion pairing of multivalent ions, which are most commonly participating in precipitation reactions, would have a significant effect on the model outputs. Scenario analysis was performed to initially examine the importance of the extensions to the ADM1 in a plant-wide context. Given below are the general findings from the analysis.

- The model is able to show the transformations of phosphorus during anaerobic digestion. Consideration of biochemical phosphorus conversion describes phosphorus availability through the role of phosphorus accumulating organisms and thus affects the prediction of precipitation and biogas production.

- Similarly, the model is also able to show the effect of sulfate transformations during anaerobic conditions and how it negatively affects the anaerobic digestion process due to: competition between methanogens, acetogenic bacteria and sulfate-reducing bacteria on substrates and sulfide inhibition of methanogenesis.

- Inclusion of chemical iron conversions in the ADM1 can predict the influence on precipitation. The extended model is able to capture the interactions between phosphorus, sulfur and iron. For instance, phosphates typically precipitate with iron, however, in the presence of sulfur, iron preferentially binds with sulfur rather than with phosphates. These interactions can be used to develop operational strategies, such as mitigation of sulfide inhibition in the digester or to facilitate struvite recovery.

The final work carried out was on the integrated implementation of the developed physico-chemical module and the extended biochemical models in a plant-wide model. The Benchmark Simulation Model No. 2 was used as the starting point in order to track the fate of phosphorus, sulfur and iron in the water and sludge lines under anaerobic, anoxic and aerobic conditions. The plant-wide model was modified and extended, with respect to layout, interfaces, unit processes, evaluation criteria, etc., to take into account new state variables related to phosphorus, sulfur and iron. The plant-wide model was used to analyse and compare operational strategies aimed at phosphorus removal and/or recovery. The important conclusions from this analysis are summarised below.

- The developed plant-wide model is able to track the fate of phosphorus, sulfur and iron along the different units of the wastewater treatment plant. It can therefore be used as a tool to develop, analyse and compare operational strategies aimed at improving the plant performance designed for organics, nitrogen and phosphorus removal or aimed at enhanced phosphorus removal and/or recovery.

- The simulation study is able to capture the intricacies of wastewater treatment plant operation. For instance, certain operational strategies could improve plant performance in terms of environmental impact but could have negative consequence on the operational cost.

The plant-wide model presented in this thesis should be used as a tool to improve the performance of wastewater treatment systems with respect to environmental impact, reducing energy consumption or increasing resource recovery. Moreover, the sub-models used as building blocks for the plant-wide model can be used independently. For example, the physico-chemical model can be interfaced with other models to predict pH, speciation of components, or when modelling systems with non-ideal solutions. The ASM2d and ADM1 extensions can be used as stand-alone applications to investigate activated sludge and anaerobic systems with significant concentrations of phosphorus, sulfur or iron. Similarly, the evaluation criteria developed in the last chapter can be used to assess the sustainability of different alternatives.

The models presented in this work are all freely distributed with the aim of promoting academic research.

6.2. Future Perspectives

Some opportunities for future research topics were identified for each main phase of the research work.

The physico-chemical model presented has used the Davies equation to calculate for activity corrections, which is valid for the commonly measured ionic strengths of municipal wastewater (I < 0.5 mol.L^{-1}). Although this approach has been successfully applied to model electrochemical membrane systems (Thompson Brewster et al., 2016), results should be taken with care. When considering other high-strength waste streams, such as industrial wastewater, landfill leachate and brine from reverse osmosis, the Pitzer equation would be more valid to use. In addition, since a typical municipal wastewater influent is assumed, the most common ions found in such a wastewater are considered. One could include more ions in the physico-chemical model depending on the type of solution being studied. Another option is to use an external software tool, which is more exhaustive than the tailored model presented in this work and interface it with the biochemical models.

Future work on calibration and validation of the extended ASM2d and ADM1 models is mandatory. Because of the increase in model complexity and the associated number of state variables, model calibration and validation can be assisted by sensitivity analysis (Solon et al., 2015a). Feldman et al. (2017) used the ADM1 phosphorus and sulfur extensions to model optimization of a full-scale granular anaerobic digester while Puyol et al. (2017) used and built upon the ADM1 phosphorus and iron extensions to model and study the effect of zero valent iron on phosphorus recovery potential. In addition, similar process extensions for phosphorus, sulfur and iron, as done in ASM2d and ADM1, could be adapted and added to other biochemical models when relevant. Oxygen effects due to micro-aeration in the anaerobic digester could also be added in the ADM1 and, together with the extensions presented, could be used to model sulfide removal and control. The combination of the biochemical and physico-chemical frameworks developed in this thesis could be used for modelling high-rate and granular systems, wherein intra-granular precipitation is a common problem

There is also an opportunity for calibration and validation of the developed plant-wide model. Although a study exists regarding the validation of a plant-wide phosphorus model (Kazadi Mbamba et al., 2016), a validation with its interactions with sulfur and iron has not yet done, especially in the context of phosphorus recovery. It is nonetheless planned to use the models developed in this thesis to a study of a full-scale wastewater treatment plant in Stockholm, Sweden. Other treatment plant configurations could also be studied. Further recovery strategies can be added upon the plant-wide model. For example, enhanced biogas

production can be achieved through chemically enhanced primary treatment, wherein iron is added to the primary clarifier to increase the quantity of settled organic particles that passes to the anaerobic digester. Other control and operational strategies can be developed and tested using the plant-wide model implemented within the BSM2 platform.

Another research possibility is to combine the plant-wide model with the urban water system. The effects of adding chemicals in the sewers for control of sulfide production on the wastewater treatment plant could be explored. In addition, previous extensions to the Benchmark Simulation Models, such as greenhouse gas and micropollutant modelling could be combined with the sub-models or the plant-wide model. Increased detail in the cost calculations could also be important. Investment costs were never included in the *OCI* calculation in the BSM. However, it would be interesting to have it included especially when comparing strategies involving addition of unit processes that facilitate resource recovery.

References

American Society of Civil Engineers (ASCE) (1992). *Measurement of Oxygen Transfer in Clean Water*. New York, New York, USA: American Society of Civil Engineers.

Andrews, J.F. (1974). Dynamic models and control strategies for wastewater treatment processes. *Water Research, 8*(5), 261-289.

Andrews, J.F. (1994). Dynamic control of wastewater treatment plants. *Environmental Science & Technology, 28*(9), 434-440.

Appels, L., Baeyens, J., Degrève, J. & Dewil, R. (2008). Principles and potential of the anaerobic digestion of waste-activated sludge. *Progress in Energy and Combustion Science, 34*(6), 755-781.

Appels, L., Lauwers, J., Degrève, J., Helsen, L., Lievens, B., Willems, K., Van Impe, J. & Dewil, R. (2011). Anaerobic digestion in global bio-energy production: Potential and research challenges. *Renewable and Sustainable Energy Reviews, 15*(9), 4295-4301.

Arnell, M. (2016). *Performance Assessment of Wastewater Treatment Plants: Multi-Objective Analysis using Plant-Wide Models.* Ph.D. thesis. Lund University, Lund, Sweden.

Arnell, M., Astals, S., Åmand, L., Batstone, D.J., Jensen, P.D. & Jeppsson, U. (2016). Modelling anaerobic co-digestion in Benchmark Simulation Model No. 2: Parameter estimation, substrate characterisation and plant-wide integration. *Water Research, 98*, 138-146.

Barat, R., Montoya, T., Seco, A. & Ferrer, J. (2011). Modelling biological and chemically induced precipitation of calcium phosphate in enhanced biological phosphorus removal systems. *Water Research, 45*(12), 3744-3752.

Barker, P. & Dold, P. (1997). General model for biological nutrient removal activated-sludge systems: Model presentation. *Water Environment Research, 69*(5), 969-984.

Batstone, D.J. (2006). Mathematical modelling of anaerobic reactors treating domestic wastewater: Rational criteria for model use. *Reviews in Environmental Science and Bio/Technology*, *5*(1), 57-71.

Batstone, D.J., Amerlinck, Y., Ekama, G.A., Goel, R., Grau, P., Johnson, B., Kaya, I., Steyer, J.-P., Tait, S. & Takács, I. (2012). Towards a generalized physicochemical framework. *Water Science and Technology*, *66*(6), 1147-1161.

Batstone, D.J. & Keller, J. (2003). Industrial applications of the IWA Anaerobic Digestion Model No. 1 (ADM1). *Water Science and Technology*, *47*(12), 199-206.

Batstone, D.J., Keller, J., Angelidaki, I., Kalyuzhnyi, S.V., Pavlostathis, S.G., Rozzi, A., Sanders, W.T.M., Siegrist, H. & Vavilin, V.A. (2002). The IWA Anaerobic Digestion Model No. 1 (ADM1). *Water Science and Technology*, *45*(10), 65-73.

Batstone, D.J., Keller, J. & Steyer, J.-P. (2006). A review of ADM1 extensions, applications, and analysis: 2002-2005. *Water Science and Technology*, *54*(4), 1-10.

Batstone, D.J., Puyol, D., Flores-Alsina, X. & Rodríguez, J. (2015). Mathematical modelling of anaerobic digestion processes: Applications and future needs. *Reviews in Environmental Science and Bio/Technology*, *14*(4), 595-613.

Botheju, D., Lie, B. & Bakke, R. (2009). Oxygen effects in anaerobic digestion. *Modeling, Identification and Control*, *30*(4), 191-201.

Boubaker, F. & Ridha, B.C. (2008). Modelling of the mesophilic anaerobic co-digestion of olive mill wastewater with olive mill solid waste using Anaerobic Digestion Model No. 1 (ADM1). *Bioresource Technology*, *99*(14), 6565-6577.

Chen, Y., Cheng, J.J. & Creamer, K.S. (2008). Inhibition of anaerobic digestion process: A review. *Bioresource Technology*, *99*(10), 4044-4064.

Chynoweth, D.P., Owens, J.M. & Legrand, R. (2001). Renewable methane from anaerobic digestion of biomass. *Renewable Energy*, *22*(1), 1-8.

Copp, J.B. (Ed.) (2002). *The COST Simulation Benchmark – Description and Simulator Manual*. Luxembourg, Luxembourg: Office for Official Publications of the European Communities.

Cordell, D. & White, S. (2011). Peak phosphorus: Clarifying the key issues of a vigorous debate about long-term phosphorus security. *Sustainability*, *3*(10), 2027-2049.

Corominas, L., Flores-Alsina, X., Snip, L. & Vanrolleghem, P.A. (2012). Comparison of different modeling approaches to better evaluate greenhouse gas emissions from whole wastewater treatment plants. *Biotechnology and Bioengineering*, *109*(11), 2854-2863.

Corominas, L., Villez, K., Aguado, D., Rieger, L., Rosén, C. & Vanrolleghem, P.A. (2011). Performance evaluation of fault detection methods for wastewater treatment processes. *Biotechnology and Bioengineering*, *108*(2), 333-344.

Council of the European Communities (CEC) (1975). Directive concerning the quality of surface waters intended for the abstraction of drinking water (75/440/EEC). *Official Journal of the European Union, L 194*, 26-31.

Council of the European Communities (CEC) (1976). Directive concerning the quality of bathing waters (76/160/EEC). *Official Journal of the European Union, L 31*, 1-7.

Council of the European Communities (CEC) (1978). Directive concerning the quality of fish waters (78/659/EEC). *Official Journal of the European Union, L 222*, 1-10.

Council of the European Communities (CEC) (1979). Directive concerning the quality of shellfish waters (79/923/EEC). *Official Journal of the European Union, L 281*, 47-52.

Council of the European Communities (CEC) (1980). Directive concerning the quality of water for human consumption (80/778/EEC). *Official Journal of the European Union, L 229*, 11-29.

Council of the European Communities (CEC) (1991). Directive concerning urban waste water treatment (91/271/EEC). *Official Journal of the European Union, L 135*, 40-52.

Council of the European Communities (CEC) (2000). Directive of the European parliament and of the council establishing a framework for community action in the field of water policy (2000/60/EC). *Official Journal of the European Union, L 327*, 1-73.

Davies, C. & Jones, A. (1955). The precipitation of silver chloride from aqueous solutions: Part 2. Kinetics of growth of seed crystals. *Transactions of the Faraday Society*, *51*, 812-817.

Davies, C.W. (1938). The extent of dissociation of salts in water: Part VIII. An equation for the mean ionic activity coefficient of an electrolyte in water, and a revision of the dissociation constants of some sulphates. *Journal of the Chemical Society*, 2093-2098.

Davis, J., Kermode, R. & Brett, R. (1973). Generic feed forward control of activated sludge. *Journal of the Sanitary Engineering Division*, *99*(3), 301-314.

de-Bashan, L.E. & Bashan, Y. (2004). Recent advances in removing phosphorus from wastewater and its future use as fertilizer (1997-2003). *Water Research*, *38*(19), 4222-4246.

De Baere, L. (2006). Will anaerobic digestion of solid waste survive in the future? *Water Science and Technology*, *53*(8), 187-194.

de Gracia, M., Sancho, L., García-Heras, J.L., Vanrolleghem, P.A. & Ayesa, E. (2006). Mass and charge conservation check in dynamic models: Application to the new ADM1 model. *Water Science and Technology*, *53*(1), 225-240.

de Mes, T.Z.D., Stams, A.J.M., Reith, J.H. & Zeeman, G. (2003). Methane production by anaerobic digestion of wastewater and solid wastes. *Bio-methane & Bio-hydrogen*, 58-102.

Debye, P. & Hückel, E. (1923). De la theorie des electrolytes. I. Abaissement du point de congelation et phenomenes associes [On the theory of electrolytes. I. Freezing point depression and related phenomena]. *Physikalische Zeitschrift*, *24*(9), 185-206.

Derbal, K., Bencheikh-Lehocine, M., Cecchi, F., Meniai, A.-H. & Pavan, P. (2009). Application of the IWA ADM1 model to simulate anaerobic co-digestion of organic waste with waste activated sludge in mesophilic condition. *Bioresource Technology*, *100*(4), 1539-1543.

Dochain, D. & Vanrolleghem, P.A. (2001). *Dynamical Modelling and Estimation in Wastewater Treatment Processes*. London, UK: IWA Publishing.

Esposito, G., Frunzo, L., Panico, A. & d'Antonio, G. (2008). Mathematical modelling of disintegration-limited co-digestion of OFMSW and sewage sludge. *Water Science and Technology*, *58*(7), 1513-1519.

Fedorovich, V., Lens, P. & Kalyuzhnyi, S. (2003). Extension of Anaerobic Digestion Model No. 1 with processes of sulfate reduction. *Applied Biochemistry and Biotechnology*, *109*(1-3), 33-45.

Feldman, H., Flores-Alsina, X., Ramin, P., Kjellberg, K., Jeppsson, U., Batstone, D.J. & Gernaey, K.V. (2017). Optimizing the operational/control conditions of a full-scale industrial granular anaerobic digester. Paper presented at the 12th IWA Specialized Conference on Instrumentation, Control and Automation (ICA2017), June 11-14, Québec, Canada.

Fezzani, B. & Cheikh, R.B. (2008). Implementation of IWA Anaerobic Digestion Model No. 1 (ADM1) for simulating the thermophilic anaerobic co-digestion of olive mill wastewater with olive mill solid waste in a semi-continuous tubular digester. *Chemical Engineering Journal*, *141*(1), 75-88.

Fezzani, B. & Cheikh, R.B. (2009). Extension of the Anaerobic Digestion Model No. 1 (ADM1) to include phenolic compounds biodegradation processes for the simulation of anaerobic co-digestion of olive mill wastes at thermophilic temperature. *Journal of Hazardous Materials, 162*(2), 1563-1570.

Fick, A. (1855). Ueber diffusion [On diffusion]. *Annalen der Physik*, *170*(1), 59-86.

Flanagan, M.J., Bracken, B.D. & Roesler, J. (1977). Automatic dissolved oxygen control. *Journal of the Environmental Engineering Division*, *103*(4), 702-722.

Flores-Alsina, X., Corominas, L., Snip, L. & Vanrolleghem, P.A. (2011). Including greenhouse gas emissions during benchmarking of wastewater treatment plant control strategies. *Water Research*, *45*(16), 4700-4710.

Flores-Alsina, X., Gernaey, K.V. & Jeppsson, U. (2012). Benchmarking biological nutrient removal in wastewater treatment plants: Influence of mathematical model assumptions. *Water Science and Technology*, *65*(8), 1496-1505.

Flores-Alsina, X., Rodríguez-Roda, I., Sin, G. & Gernaey, K.V. (2008). Multi-criteria evaluation of wastewater treatment plant control strategies under uncertainty. *Water Research*, *42*(17), 4485-4497.

Gaden, D.L. & Bibeau, E.L. (2011). Modelling Anaerobic Digesters in Three Dimensions. Paper presented at the CSBE/SCGAB 2011 Annual Conference, July 10-13, Manitoba, Canada.

García-Diéguez, C., Bernard, O. & Roca, E. (2013). Reducing the Anaerobic Digestion Model No. 1 for its application to an industrial wastewater treatment plant treating winery effluent wastewater. *Bioresource Technology*, *132*, 244-253.

Gernaey, K., Jeppsson, U., Batstone, D.J. & Ingildsen, P. (2006a). Impact of reactive settler models on simulated WWTP performance. *Water Science and Technology*, *53*(1), 159-167.

Gernaey, K.V., Flores-Alsina, X., Rosén, C., Benedetti, L. & Jeppsson, U. (2011). Dynamic influent pollutant disturbance scenario generation using a phenomenological modelling approach. *Environmental Modelling & Software*, *26*(11), 1255-1267.

Gernaey, K.V., Jeppsson, U., Vanrolleghem, P.A. & Copp, J.B. (2014). *Benchmarking of Control Strategies for Wastewater Treatment Plants*. Scientific and Technical Report No. 23. London, UK: IWA Publishing.

Gernaey, K.V., Rosén, C., Benedetti, L. & Jeppsson, U. (2005). Phenomenological modeling of wastewater treatment plant influent disturbance scenarios. Paper presented at the 10th International Conference on Urban Drainage, August 21-26, Québec, Canada.

Gernaey, K.V., Rosén, C. & Jeppsson, U. (2006b). WWTP dynamic disturbance modelling – An essential module for long-term benchmarking development. *Water Science and Technology*, *53*(4-5), 225-234.

Gernaey, K.V., van Loosdrecht, M.C.M., Henze, M., Lind, M. & Jørgensen, S.B. (2004). Activated sludge wastewater treatment plant modelling and simulation: State of the art. *Environmental Modelling & Software*, *19*(9), 763-783.

Grau, P., de Gracia, M., Vanrolleghem, P.A. & Ayesa, E. (2007). A new plant-wide modelling methodology for WWTPs. *Water Research*, *41*(19), 4357-4372.

Grau, P., Sutton, P.M., Elmaleh, S., Grady, C.P.L., Jr., Gujer, W., Henze, M. & Koller, J. (1983). Recommended notation for use in the description of biological wastewater treatment processes. *Pure and Applied Chemistry*, *55*(6), 1035-1040.

Guerrero, J., Flores-Alsina, X., Guisasola, A., Baeza, J.A. & Gernaey, K.V. (2013). Effect of nitrite, limited reactive settler and plant design configuration on the predicted performance of simultaneous C/N/P removal WWTPs. *Bioresource Technology*, *136*, 680-688.

Gujer, W., Henze, M., Mino, T. & van Loosdrecht, M.C.M. (1999). Activated Sludge Model No. 3. *Water Science and Technology*, *39*(1), 183-193.

Güntelberg, E. (1926). Untersuchungen über Ioneninteraktion [Investigations on ionic interaction]. *Zeitschrift für Physikalische Chemie*, *123*, 199-247.

Guo, L., Porro, J., Sharma, K., Amerlinck, Y., Benedetti, L., Nopens, I., Shaw, A., Van Hulle, S., Yuan, Z. & Vanrolleghem, P.A. (2012). Towards a benchmarking tool for minimizing wastewater utility greenhouse gas footprints. *Water Science and Technology*, *66*(11), 2483-2495.

Gustafsson, J.P. (2010). Visual MINTEQ (Version 3.0). Retrieved from http://www2.lwr.kth.se/English/OurSoftware/vminteq/index.htm (accessed on 2014 September 1).

Gutierrez, O., Park, D., Sharma, K.R. & Yuan, Z. (2010). Iron salts dosage for sulfide control in sewers induces chemical phosphorus removal during wastewater treatment. *Water Research*, *44*(11), 3467-3475.

Hauduc, H., Rieger, L., Oehmen, A., van Loosdrecht, M.C.M., Comeau, Y., Heduit, A., Vanrolleghem, P.A. & Gillot, S. (2013). Critical review of activated sludge modeling: State of process knowledge, modeling concepts, and limitations. *Biotechnology and Bioengineering*, *110*(1), 24-46.

Hauduc, H., Takács, I., Smith, S., Szabo, A., Murthy, S., Daigger, G. & Spérandio, M. (2015). A dynamic physicochemical model for chemical phosphorus removal. *Water Research*, *73*, 157-170.

Henze, M., Grady, C.P.L., Jr., Gujer, W., Marais, G.v.R. & Matsuo, T. (1987). *Activated Sludge Model No. 1*. IWA Scientific and Technical Report No. 1. London, UK: IWA Publishing.

Henze, M., Gujer, W., Mino, T., Matsuo, T., Wentzel, M.C. & Marais, G.v.R. (1995). Wastewater and biomass characterization for the Activated Sludge Model No. 2: Biological phosphorus removal. *Water Science and Technology*, *31*(2), 13-23.

Henze, M., Gujer, W., Mino, T., Matsuo, T., Wentzel, M.C., Marais, G.v.R. & van Loosdrecht, M.C.M. (1999). Activated Sludge Model No. 2d, ASM2d. *Water Science and Technology*, *39*(1), 165-182.

Henze, M., Gujer, W., Mino, T. & van Loosdrecht, M.C.M. (2000). *Activated Sludge Models ASM1, ASM2, ASM2d and ASM3*. IWA Scientific and Technical Report No. 9. London, UK: IWA Publishing.

Henze, M., van Loosdrecht, M.C.M., Ekama, G.A. & Brdjanovic, D. (Eds.). (2008). *Biological Wastewater Treatment: Principles, Modelling and Design*. London, UK: IWA Publishing.

Herring, J.R. & Fantel, R.J. (1993). Phosphate rock demand into the next century: Impact on world food supply. *Nonrenewable Resources*, *2*(3), 226-246.

Holm-Nielsen, J.B., Al Seadi, T. & Oleskowicz-Popiel, P. (2009). The future of anaerobic digestion and biogas utilization. *Bioresource Technology*, *100*(22), 5478-5484.

Ikumi, D.S., Brouckaert, C. & Ekama, G.A. (2011). Modelling of struvite precipitation in anaerobic digestion. Paper presented at the 8th IWA Symposium on Systems Analysis and Integrated Assessment (Watermatex2011), June 20-22, San Sebastian, Spain.

Ikumi, D.S., Harding, T.H. & Ekama, G.A. (2014). Biodegradability of wastewater and activated sludge organics in anaerobic digestion. *Water Research*, *56*, 267-279.

Jeppsson, U. (1996). *Modelling Aspects of Wastewater Treatment Processes.* Ph.D. thesis. Lund University, Lund, Sweden.

Jeppsson, U., Alex, J., Batstone, D.J., Benedetti, L., Comas, J., Copp, J.B., Corominas, L., Flores-Alsina, X., Gernaey, K.V. & Nopens, I. (2013). Benchmark simulation models, quo vadis? *Water Science and Technology*, *68*(1), 1-15.

Jeppsson, U. & Pons, M.-N. (2004). The COST benchmark simulation model – Current state and future perspective. *Control Engineering Practice*, *12*(3), 299-304.

Jeppsson, U., Pons, M.-N., Nopens, I., Alex, J., Copp, J.B., Gernaey, K.V., Rosén, C., Steyer, J.-P. & Vanrolleghem, P.A. (2007). Benchmark Simulation Model No. 2: General protocol and exploratory case studies. *Water Science and Technology*, *56*(8), 67-78.

Johnson, B. & Shang, Y. (2006). Applications and limitations of ADM1 in municipal wastewater solids treatment. *Water Science and Technology*, *54*(4), 77-82.

Kabouris, J.C. & Georgakakos, A.P. (1991). Optimal real-time activated sludge regulation. Paper presented at the 1991 Georgia Water Resources Conference, March 19-20, Athens, Georgia, USA.

Kazadi Mbamba, C., Batstone, D.J., Flores-Alsina, X. & Tait, S. (2015a). A generalised chemical precipitation modelling approach in wastewater treatment applied to calcite. *Water Research*, *68*, 342-353.

Kazadi Mbamba, C., Flores-Alsina, X., Batstone, D.J. & Tait, S. (2016). Validation of a plant-wide phosphorus modelling approach with minerals precipitation in a full-scale WWTP. *Water Research*, *100*, 169-183.

Kazadi Mbamba, C., Tait, S., Flores-Alsina, X. & Batstone, D.J. (2015b). A systematic study of multiple minerals precipitation modelling in wastewater treatment. *Water Research*, *85*, 359-370.

Kazmierczak, T.F., Tomson, M.B. & Nancollas, G.H. (1982). Crystal growth of calcium carbonate. A controlled composition kinetic study. *The Journal of Physical Chemistry*, *86*(1), 103-107.

Khanal, S.K. (2008). *Anaerobic Biotechnology for Bioenergy Production: Principles and Applications*. Ames, Iowa, USA: Wiley-Blackwell.

Kim, J.-H., Chen, M., Kishida, N. & Sudo, R. (2004). Integrated real-time control strategy for nitrogen removal in swine wastewater treatment using sequencing batch reactors. *Water Research*, *38*(14), 3340-3348.

Kleeberg, A. (1997). Interactions between benthic phosphorus release and sulfur cycling in Lake Scharmützelsee (Germany). *Water, Air, & Soil Pollution*, *99*, 391-399.

Knobel, A.N. & Lewis, A.E. (2002). A mathematical model of a high sulphate wastewater anaerobic treatment system. *Water Research*, *36*(1), 257-265.

Koutsoukos, P., Amjad, Z., Tomson, M. & Nancollas, G. (1980). Crystallization of calcium phosphates: A constant composition study. *Journal of the American Chemical Society*, *102*(5), 1553-1557.

Lashof, D.A. & Ahuja, D.R. (1990). Relative contributions of greenhouse gas emissions to global warming. *Nature*, *344*, 529-531.

Le Corre, K.S., Valsami-Jones, E., Hobbs, P. & Parsons, S.A. (2009). Phosphorus recovery from wastewater by struvite crystallization: A review. *Critical Reviews in Environmental Science and Technology*, *39*(6), 433-477.

Lech, R.F., Grady, C.P.L., Jr., Lim, H.C. & Koppel, L.B. (1978a). Automatic control of the activated sludge process – II. Efficacy of control strategies. *Water Research*, *12*(2), 91-99.

Lech, R.F., Lim, H.C., Grady, C.P.L., Jr. & Koppel, L.B. (1978b). Automatic control of the activated sludge process – I. Development of a simplified dynamic model. *Water Research*, *12*(2), 81-90.

Lettinga, G. & van Haandel, A.C. (1993). *Anaerobic Digestion for Energy Production and Environmental Protection*. Washington DC, USA: Island Press.

Lindblom, E., Arnell, M., Flores-Alsina, X., Stenström, F., Gustavsson, D., Yang, J. & Jeppsson, U. (2016). Dynamic modelling of nitrous oxide emissions from three Swedish sludge liquor treatment systems. *Water Science and Technology*, *73*(4), 798-806.

Lizarralde, I., Fernández-Arévalo, T., Brouckaert, C., Vanrolleghem, P.A., Ikumi, D.S., Ekama, G.A., Ayesa, E. & Grau, P. (2015). A new general methodology for incorporating physico-chemical transformations into multi-phase wastewater treatment process models. *Water Research, 74*, 239-256.

Lübken, M., Wichern, M., Schlattmann, M., Gronauer, A. & Horn, H. (2007). Modelling the energy balance of an anaerobic digester fed with cattle manure and renewable energy crops. *Water Research, 41*(18), 4085-4096.

Marsili-Libelli, S. (1989). Modelling, Identification and Control of the Activated Sludge Process. Volume 38 in the book series: *Advances in Biochemical Engineering/Biotechnology* (pp. 89-148, A. Fiechter Ed.). Berlin, Germany: Springer.

Mata-Alvarez, J., Mace, S. & Llabres, P. (2000). Anaerobic digestion of organic solid wastes: An overview of research achievements and perspectives. *Bioresource Technology*, *74*(1), 3-16.

Meijer, S.C.F. (2004). *Theoretical and Practical Aspects of Modelling Activated Sludge Processes.* Ph.D. thesis. Delft University of Technology, Delft, Netherlands.

Meijer, S.C.F., van Loosdrecht, M.C.M. & Heijnen, J.J. (2002). Modelling the start-up of a full-scale biological phosphorous and nitrogen removing WWTP. *Water Research*, *36*(19), 4667-4682.

Merkel, B.J. & Planer-Friedrich, B. (2005). *Groundwater Geochemistry: A Practical Guide to Modeling of Natural and Contaminated Aquatic Systems* (D. K. Nordstrom Ed., 2nd ed.). Berlin, Germany: Springer.

Metcalf & Eddy (2014). *Wastewater Engineering: Treatment and Resource Recovery* (G. Tchobanoglous, H. D. Stensel, R. Tsuchihashi, & F. Burton Eds., 5th ed.). New York, New York, USA: McGraw-Hill Education.

Mu, S.J., Zeng, Y., Wu, P., Lou, S.J. & Tartakovsky, B. (2008). Anaerobic Digestion Model No. 1-based distributed parameter model of an anaerobic reactor: I. Model development. *Bioresource Technology*, *99*(9), 3665-3675.

Musvoto, E.V., Wentzel, M.C. & Ekama, G.A. (2000a). Integrated chemical-physical processes modelling – II. Simulating aeration treatment of anaerobic digester supernatants. *Water Research*, *34*(6), 1868-1880.

Musvoto, E.V., Wentzel, M.C., Loewenthal, R.E. & Ekama, G.A. (1997). Kinetic-based model for mixed weak acid/base systems. *Water SA*, *23*(4), 311-322.

Musvoto, E.V., Wentzel, M.C., Loewenthal, R.E. & Ekama, G.A. (2000b). Integrated chemical-physical processes modelling – I. Development of a kinetic-based model for mixed weak acid/base systems. *Water Research*, *34*(6), 1857-1867.

Nielsen, A.E. (1984). Electrolyte crystal growth mechanisms. *Journal of Crystal Growth*, *67*(2), 289-310.

Nopens, I., Batstone, D.J., Copp, J.B., Jeppsson, U., Volcke, E.I.P., Alex, J. & Vanrolleghem, P.A. (2009). An ASM/ADM model interface for dynamic plant-wide simulation. *Water Research*, *43*(7), 1913-1923.

Nopens, I., Benedetti, L., Jeppsson, U., Pons, M.-N., Alex, J., Copp, J.B., Gernaey, K.V., Rosén, C., Steyer, J.-P. & Vanrolleghem, P.A. (2010). Benchmark Simulation Model No 2: Finalisation of plant layout and default control strategy. *Water Science and Technology*, *62*(9), 1967-1974.

Nürnberg, G.K. (1996). Comment: Phosphorus budgets and stoichiometry during the open-water season in two unmanipulated lakes in the Experimental Lakes Area, northwestern Ontario. *Canadian Journal of Fisheries and Aquatic Sciences*, *53*(6), 1469-1471.

Olsson, G. (1992). Control of wastewater treatment systems. *ISA Transactions*, *31*(1), 87-96.

Olsson, G. (2012). ICA and me – A subjective review. *Water Research*, *46*(6), 1585-1624.

Olsson, G., Carlsson, B., Comas, J., Copp, J.B., Gernaey, K.V., Ingildsen, P., Jeppsson, U., Kim, C., Rieger, L. & Rodriguez-Roda, I. (2014). Instrumentation, control and automation in wastewater – From London 1973 to Narbonne 2013. *Water Science and Technology*, *69*(7), 1373-1385.

Olsson, G., Rundqwist, L., Eriksson, L. & Hall, L. (1985). Self-tuning control of the dissolved oxygen concentration in activated sludge systems. Paper presented at the 4th IAWPRC Workshop on Instrumentation and Control of Water and Wastewater Treatment and Transport Systems, April 27-May 4, Houston, Texas and Denver, Colorado, USA.

Otterpohl, R. (1995). *Dynamische Simulation zur Unterstützung der Planung und des Betriebes von kommunalen Kläranlagen [Dynamic Simulation to Support the Design and Operation of Municipal Wastewater Treatment Plants]*. Ph.D. thesis, Technical University of Aachen, Aachen, Germany.

Otterpohl, R. & Freund, M. (1992). Dynamic models for clarifiers of activated sludge plants with dry and wet weather flows. *Water Science and Technology*, *26*(5-6), 1391-1400.

Parkin, G.F. & Owen, W.F. (1986). Fundamentals of anaerobic digestion of wastewater sludges. *Journal of Environmental Engineering*, *112*(5), 867-920.

Pescod, M.B. (1992). *Wastewater Treatment and Use in Agriculture*. Rome, Italy: Food and Agriculture Organization of the United Nations.

Petersen, E.E. (1965). *Chemical Reaction Analysis*. Engelwood Cliffs, New Jersey, USA: Prentice-Hall.

Pol, L.W.H., Lens, P.N., Stams, A.J. & Lettinga, G. (1998). Anaerobic treatment of sulphate-rich wastewaters. *Biodegradation*, *9*(3-4), 213-224.

Pons, M.-N., Spanjers, H. & Jeppsson, U. (1999). Towards a benchmark for evaluating control strategies in wastewater treatment plants by simulation. *Computers & Chemical Engineering*, *23*, 403-406.

Puyol, D., Flores-Alsina, X., Segura, Y., Molina, R., Jerez, S., Gernaey, K.V., Melero, J.A. & Martinez, F. (2017). ZVI addition in continuous anaerobic digestion systems dramatically decreases P recovery potential: Dynamic modelling. Paper presented at the Frontiers International Conference on Wastewater Treatment (FICWTM2017), May 21-24, Palermo, Italy.

Reichert, P., Borchardt, D., Henze, M., Rauch, W., Shanahan, P., Somlyódy, L. & Vanrolleghem, P.A. (2001). River Water Quality Model No. 1 (RWQM1): II. Biochemical process equations. *Water Science and Technology*, *43*(5), 11-30.

Rieger, L., Koch, G., Kühni, M., Gujer, W. & Siegrist, H. (2001). The EAWAG Bio-P module for Activated Sludge Model No. 3. *Water Research*, *35*(16), 3887-3903.

Rosén, C., Jeppsson, U. & Vanrolleghem, P.A. (2004). Towards a common benchmark for long-term process control and monitoring performance evaluation. *Water Science and Technology*, *50*(11), 41-49.

Rosén, C., Vrečko, D., Gernaey, K.V., Pons, M.-N. & Jeppsson, U. (2006). Implementing ADM1 for plant-wide benchmark simulations in Matlab/Simulink. *Water Science and Technology*, *54*(4), 11-19.

Saagi, R., Flores-Alsina, X., Fu, G., Butler, D., Gernaey, K.V. & Jeppsson, U. (2016). Catchment & sewer network simulation model to benchmark control strategies within urban wastewater systems. *Environmental Modelling & Software*, *78*, 16-30.

Saagi, R., Flores-Alsina, X., Kroll, S., Gernaey, K.V. & Jeppsson, U. (2017). A model library for simulation and benchmarking of integrated urban wastewater systems. *Environmental Modelling & Software*, *93*, 282-295.

Serralta, J., Ferrer, J., Borrás, L. & Seco, A. (2004). An extension of ASM2d including pH calculation. *Water Research*, *38*(19), 4029-4038.

Seviour, R. & Nielsen, P.H. (2010). *Microbial Ecology of Activated Sludge*. London, UK: IWA Publishing.

Seyhan, D., Weikard, H.-P. & van Ierland, E. (2012). An economic model of long-term phosphorus extraction and recycling. *Resources, Conservation and Recycling*, *61*, 103-108.

Sharma, K., de Haas, D.W., Corrie, S., O'Halloran, K., Keller, J. & Yuan, Z. (2008). Predicting hydrogen sulfide formation in sewers: A new model. *Water*, *35*(2), 132-137.

Smith, S., Takács, I., Murthy, S., Daigger, G.T. & Szabo, A. (2008). Phosphate complexation model and its implications for chemical phosphorus removal. *Water Environment Research*, *80*(5), 428-438.

Snip, L. (2015). *Upgrading the Benchmark Simulation Model Framework with Emerging Challenges – A Study of N_2O Emissions and the Fate of Pharmaceuticals in Urban Wastewater Systems.* Ph.D. thesis, Technical University of Denmark, Kgs. Lyngby, Denmark.

Snip, L., Flores-Alsina, X., Plósz, B.G., Jeppsson, U. & Gernaey, K.V. (2014). Modelling the occurrence, transport and fate of pharmaceuticals in wastewater systems. *Environmental Modelling & Software*, *62*, 112-127.

Solon, K., Flores-Alsina, X., Ekama, G.A., Ikumi, D.S., Gernaey, K. & Jeppson, U. (2016). Using an extended activated sludge model for benchmarking of biological nutrient removal/recovery processes in a plant-wide perspective. Paper presented at the 2nd IWA Conference on Holistic Sludge Management (HSM2016), June 7-9, Malmö, Sweden.

Solon, K., Flores-Alsina, X., Gernaey, K.V. & Jeppsson, U. (2015a). Effects of influent fractionation, kinetics, stoichiometry and mass transfer on CH_4, H_2 and CO_2 production for (plant-wide) modeling of anaerobic digesters. *Water Science and Technology*, *71*(6), 870-877.

Solon, K., Kazadi Mbamba, C., Flores-Alsina, X., Gernaey, K.V., Tait, S., Batstone, D.J. & Jeppson, U. (2017). Model-based evaluation of nutrient and energy recovery control strategies in wastewater treatment systems. Paper presented at the 12th IWA Specialized Conference on Instrumentation, Control and Automation (ICA2017), June 11-14, Québec, Canada.

Solon, K. & Snip, L. (2014). New criteria for plant wide optimization using Benchmark Simulation Model No. 2. Paper presented at the SANITAS workshop during the 2nd IWA Specialized Conference in Ecotechnologies for Sewage Treatment Plants (ecoSTP2014), June 23-25, Verona, Italy.

Solon, K., Volcke, E.I.P. & Jeppson, U. (2015b). Extending the ADM1 with sulfur-related conversions for plant-wide modelling and benchmarking. Paper presented at the Specialised workshop organised by COST Water2020: Conceiving Wastewater Treatment of Tomorrow – Energetic, Environmental and Economic Challenges, April 15, Le Pecq, France.

Speece, R.E. (1983). Anaerobic biotechnology for industrial wastewater treatment. *Environmental Science & Technology*, *17*(9), 416-427.

Stare, A., Vrečko, D., Hvala, N. & Strmčnik, S. (2007). Comparison of control strategies for nitrogen removal in an activated sludge process in terms of operating costs: A simulation study. *Water Research*, *41*(9), 2004-2014.

Stumm, W. & Morgan, J.J. (1996). *Aquatic Chemistry: Chemical Equilibria and Rates in Natural Waters* (3rd ed.). New York, New York, USA: John Wiley & Sons, Inc.

Tait, S., Solon, K., Volcke, E.I.P. & Batstone, D.J. (2012). A unified approach to modelling wastewater chemistry: Model corrections. Paper presented at the 3rd IWA/WEF Wastewater Treatment Modelling Seminar (WWTmod2012), February 26-28, Québec, Canada.

Takács, I., Patry, G.G. & Nolasco, D. (1991). A dynamic model of the clarification-thickening process. *Water Research*, *25*(10), 1263-1271.

Takács, I. & Vanrolleghem, P.A. (2006). Elemental balances in activated sludge modelling. Paper presented at the IWA 5th World Water Congress and Exhibition (WWC&E2006), September 10-14, Beijing, China.

Tartakovsky, B., Mu, S.J., Zeng, Y., Lou, S.J., Guiot, S.R. & Wu, P. (2008). Anaerobic Digestion Model No. 1-based distributed parameter model of an anaerobic reactor: II. Model validation. *Bioresource Technology*, *99*(9), 3676-3684.

Thompson Brewster, E., Tait, S., Vrečko, D., Flores-Alsina, X., Kazadi Mbamba, C., Solon, K., Jeppsson, U., Gernaey, K.V. & Batstone, D.J. (2016). Modelling physico-chemistry in extreme conditions. Paper presented at the 5th IWA/WEF Wastewater Treatment Modelling Seminar (WWTmod2016), April 2-6, Annecy, France.

Truesdell, A.H. & Jones, B.F. (1973). *WATEQ, a Computer Program for Calculating Chemical Equilibria of Natural Waters*. Menlo Park, California, USA: The United States Geological Survey.

United Nations World Water Assessment Programme (WWAP) (2016). *The United Nations World Water Development Report 2016: Water and Jobs*. Paris, France: UNESCO.

van Haandel, A.C. & van der Lubbe, J.G.M. (2012). *Handbook of Biological Wastewater Treatment: Design and Optimisation of Activated Sludge Systems* (2nd ed.). London, UK: IWA Publishing.

van Veldhuizen, H., van Loosdrecht, M.C.M. & Heijnen, J.J. (1999). Modelling biological phosphorus and nitrogen removal in a full scale activated sludge process. *Water Research*, *33*(16), 3459-3468.

Verstraete, W., van de Caveye, P. & Diamantis, V. (2009). Maximum use of resources present in domestic "used water". *Bioresource Technology*, *100*(23), 5537-5545.

Volcke, E.I.P., van Loosdrecht, M.C.M. & Vanrolleghem, P.A. (2006). Continuity-based model interfacing for plant-wide simulation: A general approach. *Water Research*, *40*(15), 2817-2828.

Vrečko, D., Volcke, E.I.P., Jeppsson, U. & Gernaey, K.V. (2014). *Evaluation Criteria Description and Examples for BSM2*. Technical Report No. 13. IWA Task Group on Benchmarking of Control Strategies for Wastewater Treatment Plants. London, UK: IWA Publishing.

Wang, R., Li, Y., Chen, W., Zou, J. & Chen, Y. (2016). Phosphate release involving PAOs activity during anaerobic fermentation of EBPR sludge and the extension of ADM1. *Chemical Engineering Journal*, *287*, 436-447.

Wentzel, M.C., Dold, P.L., Ekama, G.A. & Marais, G.v.R. (1989a). Enhanced polyphosphate organism cultures in activated sludge systems. Part III: Kinetic model. *Water SA*, *15*(2), 89-102.

Wentzel, M.C., Ekama, G.A., Loewenthal, R.E., Dold, P.L. & Marais, G.v.R. (1989b). Enhanced polyphosphate organism cultures in activated sludge systems. Part II: Experimental behaviour. *Water SA*, *15*(2), 71-88.

Wentzel, M.C., Loewenthal, R.E., Ekama, G.A. & Marais, G.v.R. (1988). Enhanced polyphosphate organism cultures in activated sludge systems. Part I: Enhanced culture development. *Water SA*, *14*(2), 81-92.

Wu, D., Ekama, G.A., Lu, H., Chui, H.-K., Liu, W.-T., Brdjanovic, D., van Loosdrecht, M.C.M. & Chen, G.-H. (2013). A new biological phosphorus removal process in association with sulfur cycle. *Water Research*, *47*(9), 3057-3069.

Yu, L., Wensel, P.C., Ma, J. & Chen, S. (2013). Mathematical modeling in anaerobic digestion (AD). *Journal of Bioremediation & Biodegradation*, S4: 003.

Zaher, U., Grau, P., Benedetti, L., Ayesa, E. & Vanrolleghem, P.A. (2007). Transformers for interfacing anaerobic digestion models to pre- and post-treatment processes in a plant-wide modelling context. *Environmental Modelling & Software*, *22*(1), 40-58.

Zaher, U., Li, R., Jeppsson, U., Steyer, J.-P. & Chen, S. (2009). GISCOD: General integrated solid waste co-digestion model. *Water Research*, *43*(10), 2717-2727.

Zhang, L., de Schryver, P., de Gusseme, B., de Muynck, W., Boon, N. & Verstraete, W. (2008). Chemical and biological technologies for hydrogen sulfide emission control in sewer systems: A review. *Water Research*, *42*(1), 1-12.

Scientific Publications

Paper I

WATER RESEARCH 70 (2015) 235–245

Available online at www.sciencedirect.com

ScienceDirect

journal homepage: www.elsevier.com/locate/watres

Effects of ionic strength and ion pairing on (plant-wide) modelling of anaerobic digestion

Kimberly Solon [a], *Xavier Flores-Alsina* [b], *Christian Kazadi Mbamba* [c], *Eveline I.P. Volcke* [d], *Stephan Tait* [c], *Damien Batstone* [c], *Krist V. Gernaey* [b], *Ulf Jeppsson* [a,*]

[a] *Division of Industrial Electrical Engineering and Automation (IEA), Department of Biomedical Engineering, Lund University, Box 118, SE-221 00 Lund, Sweden*

[b] *CAPEC-PROCESS, Department of Chemical and Biochemical Engineering, Technical University of Denmark, Building 229, DK-2800 Lyngby, Denmark*

[c] *Advanced Water Management Centre (AWMC), University of Queensland, St Lucia, Brisbane, Queensland 4072, Australia*

[d] *Department of Biosystems Engineering, Ghent University, Coupure Links 653, B-9000 Gent, Belgium*

ARTICLE INFO

Article history:
Received 8 September 2014
Received in revised form
19 November 2014
Accepted 20 November 2014
Available online 12 December 2014

Keywords:
ADM1
BSM2
Non-ideality
Physico-chemical framework
Wastewater plant-wide modelling

ABSTRACT

Plant-wide models of wastewater treatment (such as the Benchmark Simulation Model No. 2 or BSM2) are gaining popularity for use in holistic virtual studies of treatment plant control and operations. The objective of this study is to show the influence of ionic strength (as activity corrections) and ion pairing on modelling of anaerobic digestion processes in such plant-wide models of wastewater treatment. Using the BSM2 as a case study with a number of model variants and cationic load scenarios, this paper presents the effects of an improved physico-chemical description on model predictions and overall plant performance indicators, namely effluent quality index (*EQI*) and operational cost index (*OCI*). The acid-base equilibria implemented in the Anaerobic Digestion Model No. 1 (ADM1) are modified to account for non-ideal aqueous-phase chemistry. The model corrects for ionic strength via the Davies approach to consider chemical activities instead of molar concentrations. A speciation sub-routine based on a multi-dimensional Newton–Raphson (NR) iteration method is developed to address algebraic interdependencies. The model also includes ion pairs that play an important role in wastewater treatment. The paper describes: 1) how the anaerobic digester performance is affected by physico-chemical corrections; 2) the effect on pH and the anaerobic digestion products (CO_2, CH_4 and H_2); and, 3) how these variations are propagated from the sludge treatment to the water line. Results at high ionic strength demonstrate that corrections to account for non-ideal conditions lead to significant differences in predicted process performance (up to 18% for effluent quality and 7% for operational cost) but that for pH prediction, activity corrections are more important than ion pairing effects. Both are likely to be required when precipitation is to be modelled.

© 2014 Elsevier Ltd. All rights reserved.

* *Corresponding author*. Tel.: +46 46 222 92 87; fax: +46 46 14 21 14.
E-mail address: ulf.jeppsson@iea.lth.se (U. Jeppsson).

http://dx.doi.org/10.1016/j.watres.2014.11.035
0043-1354/© 2014 Elsevier Ltd. All rights reserved.

Nomenclature

γ	activity coefficient
ΔH^o	enthalpy change of the reaction
A_1, A_2, A_3	physico–chemical framework 1, 2 and 3
AD	anaerobic digestion
ADM1	Anaerobic Digestion Model No. 1
a_i or a_j	activity of the species (i) or component (j)
BSM2	Benchmark Simulation Model No. 2
COD	chemical oxygen demand
CSTR	continuous stirred tank reactor
DAE	differential algebraic equation
EQI	effluent quality index (kg pollution day^{-1})
Gas_{CH_4}	methane gas production (kg day^{-1})
Gas_{CO_2}	carbon dioxide gas production (kg day^{-1})
Gas_{H_2}	hydrogen gas production (kg day^{-1})
GISCOD	general integrated solid waste co-digestion
$G(Z_i)$	vector containing the values of the set of implicit algebraic equations ($g(z_1,...,z_n)$, …, $g(z_1, …,z_n)$)
I	ionic strength (mol L^{-1})
IWA	International Water Association
J_f	analytical Jacobian of first order partial derivatives $\delta(G_1, …, G_m)/\delta(z_1, …, z_n)$
K_i	equilibrium constant
N	nitrogen
N_C	number of components
NR	Newton–Raphson
N_{sp}	number of species
OCI	operational cost index
PCM	physico–chemical model
ODE	ordinary differential equation
R	universal gas constant (bar L mol^{-1} K^{-1})
S_{ac}	acetate concentration (kmol COD m^{-3})
S_{Al}	aluminium concentration (mol L^{-1})
S_{an}	anions concentration (mol L^{-1})
S_{bu}	butyrate concentration (kmol COD m^{-3})
$S_{Ca^{+}}$	calcium concentration (mol L^{-1})
S_{cat}	cations concentration (mol L^{-1})
S_{C_i}	ith scenario
S_{Cl}	Chloride concentration (mol L^{-1})
$S_{CO_3^{-2}}$	carbonate concentration (mol L^{-1})
S_{Fe}	iron concentration (mol L^{-1})
$S_{H^{+}}$	proton concentration (mol L^{-1})
$S_{H_2CO_3^{*}}$	carbonic acid concentration (mol L^{-1})
$S_{H_2PO_4^{-}}$	dihydrogen phosphate concentration (mol L^{-1})
S_{H_2S}	hydrogen sulfide concentration (mol L^{-1})
$S_{HCO_3^{-}}$	bicarbonate concentration (mol L^{-1})
$S_{HPO_4^{-2}}$	hydrogen phosphate concentration (mol L^{-1})
S_i	species concentration (mol L^{-1})
S_{IC}	inorganic carbon (kmol m^{-3})
S_{IN}	inorganic nitrogen (kmol m^{-3})
S_j	component concentration (mol L^{-1})
S_K	potassium concentration (mol L^{-1})
$S_{Mg^{+}}$	magnesium concentration (mol L^{-1})
S_{Na}	sodium concentration (mol L^{-1})
S_{NH_3}	ammonia concentration (mol L^{-1})
$S_{NH_4^{+}}$	ammonium concentration (mol L^{-1})
$S_{PO_4^{-3}}$	phosphate concentration (mol L^{-1})
S_{pro}	propionate concentration (kmol COD m^{-3})
$S_{SO_4^{-2}}$	sulphate concentration (mol L^{-1})
S_{va}	valerate concentration (kmol COD m^{-3})
T	temperature (K)
UASB	upflow anaerobic sludge blanket
WWTP	wastewater treatment plant
z_i	of ion i
Z_i	vector of equilibrium states ($z_{1,i}$, …, $z_{n,i}$)

1. Introduction

Anaerobic digestion is a proven waste stabilization technology which is widely applied and studied because of its beneficial production of renewable biogas energy, making it a truly sustainable technology. From a systems engineering point-of-view, one of the major advances in the field of anaerobic digestion has been the development of the International Water Association (IWA) Anaerobic Digestion Model No. 1 (ADM1) (Batstone et al., 2002). The ADM1 is a general structured model consisting of biochemical and physico-chemical processes, which is useful for the design, operation and optimization of anaerobic digestion plants (Batstone et al., 2006). The adoption of the ADM1 in popular systems analysis tools, such as the plant-wide benchmark simulation model for wastewater treatment plants (BSM2), and its use as a virtual industrial system can stimulate modelling of anaerobic processes by researchers and practitioners outside the core expertise of anaerobic processes (Jeppsson et al., 2013).

Anaerobic digestion models are still being extended to include: i) improved biodegradability predictions (Astals et al., 2013); ii) inhibition factors (Wilson et al., 2012; Zonta et al., 2013); and, iii) microbial diversity (Ramirez et al., 2009). The ADM1 has been successfully implemented into multiple tank configurations: continuous stirred tank reactors (CSTRs) (Rosen et al., 2006), upflow anaerobic sludge blanket (UASB) reactors (Batstone et al., 2005; Hinken et al., 2014) and biofilm reactors described by 1D (Batstone et al., 2004) and 2D/3D models (Picioreanu et al., 2005). Important aspects about modelling frameworks and methodologies for parameter estimation and model validation in the field of anaerobic digestion processes can be found in Donoso-Bravo et al. (2011). In addition to municipal wastewater treatment, other applications of the ADM1 have been hydrogen production (Penumathsa et al., 2008), blue-algae digestion (Yuan et al., 2014) or co-digestion processes using the general integrated solid waste co-digestion (GISCOD) model interface (Zaher et al., 2009). Along this line of thinking, the ADM1 could potentially be applied to the treatment of industrial waste, animal manure, landfill leachate and brine from reverse

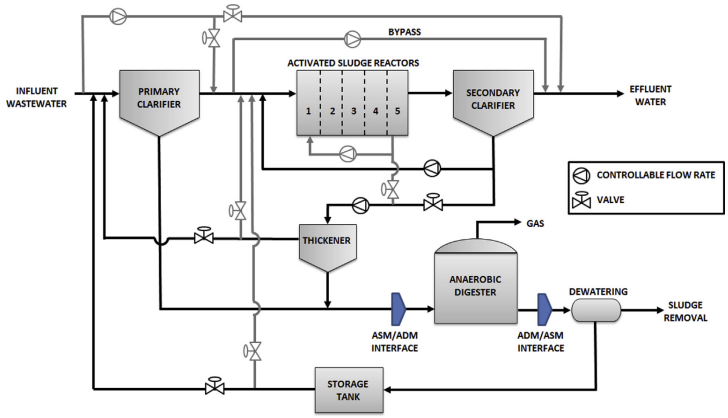

Fig. 1 – Schematic representation of the BSM2 plant (Gernaey et al., 2014).

osmosis (Batstone and Keller, 2003). Since the latter waste streams, in general, contain substantially higher salinity than domestic wastewater (ionic strengths of various waste streams can be found in Batstone et al. (2012)), it is expected that there will be significant physico-chemical effects, which may need to be accounted for in a model. It is believed that a key limitation of the ADM1, as applied to high-strength wastes, is the absence of corrections for ionic strength and ion pairing to account for non-ideal physico-chemical behaviour that occurs in such wastes (Batstone et al., 2012; Tait et al., 2012). The IWA Task Group on Generalized Physico-chemical Framework is developing a structure to better understand and represent these non-ideal behaviours in the frame of wastewater treatment modelling. By gathering complex knowledge from different disciplines and combining this in a general framework, a guideline on how to approach modelling of physico-chemical processes will be developed. The work presented here fits within the scope of work of this task group, and as such, the authors propose an extension of the ADM1 (BSM2 implementation) to include: i) ionic strength correction via the Davies equation; ii) ion pairing of inorganic carbon, inorganic nitrogen and volatile fatty acids with different cations (K^+, Na^+) and anions (Cl^-); and, iii) a new solving routine that accounts for the increased number of implicit algebraic variables without the use of an implicit differential algebraic equation (DAE) solver.

The objective of this study is to show the influence of ionic strength (as activity corrections) and ion pairing on (plant-wide) modelling of anaerobic digestion processes in wastewater treatment plants (WWTPs). The paper describes: i) how the anaerobic digester performance is affected; ii) the effect on pH and the anaerobic digestion products (CO_2, CH_4 and H_2); and, iii) how these variations are propagated from the sludge treatment to the water line.

The paper details the development of the new physico-chemical framework, the connection between the bio-kinetic and physico-chemical models, how numerical/stiffness issues have been handled and finally the differences in the predicted effluent quality (*EQI*) and operational cost (*OCI*) indices. The authors illustrate the performance of this new approach with a number of case studies. These case studies investigate the overall WWTP performance for different physico-chemical model (PCM) frameworks and cationic loads.

The main novelty of this paper relies on developing a new ADM1: i) with a physico-chemical framework implementation to describe non-ideal behaviour; ii) taking into account the interactions between biotic and non-biotic processes when mathematically describing the usefulness of control/operational strategies; and, finally iii) by integrating all the different models (physico-chemical/biochemical) in one single software.

This paper contributes to the field of wastewater engineering by filling some of the gaps which previous studies did not handle. For example model compatibility, simulation input–output transferability, ionic strength and ion pairing assessment, and WWTP and control strategy/operational procedure performance assessment. Once these models are codified, the developed platform will be an excellent tool to further analyse/evaluate the behaviour of additional compounds (phosphorus, sulphur, etc.) and for developing different chemical/recovery processes (precipitation). Indeed, the correct description of the precipitation processes in wastewater treatment system requires the consideration of non-ideal conditions (Musvoto et al., 2000; van Rensburg et al., 2003; Barat et al., 2011; Kazadi Mbamba et al., 2014).

2. Methods

2.1. *Wastewater treatment plant (WWTP) under study*

The WWTP under study is the IWA BSM2 platform proposed by Gernaey et al. (2014) (Fig. 1). The plant is treating an influent

Table 1 – Stoichiometric matrix of the species (S_i) and components (S_j).

S_i		S_j										
	Formula	S_{Na^+}	S_{K^+}	$S_{NH_4^+}$	S_{Cl^-}	$S_{CO_3^{-2}}$	S_{ac^-}	S_{pro^-}	S_{bu^-}	S_{va^-}	$\log K_i$	ΔH^o
S_{Na^+}	Na^+	1									0	0
S_{K^+}	K^+		1								0	0
$S_{NH_4^+}$	NH_4^+			1							0	0
S_{Cl^-}	Cl^-				1						0	0
$S_{CO_3^{-2}}$	CO_3^{-2}					1					0	0
$S_{H_2CO_3^*}$	$H_2CO_3^*$					1					16.68	−32
$S_{HCO_3^-}$	HCO_3^-					1					10.33	−14.6
S_{ac^-}	$C_2H_3O_2^-$						1				0	0
S_{pro^-}	$C_3H_5O_2^-$							1			0	0
S_{bu^-}	$C_4H_7O_2^-$								1		0	0
S_{va^-}	$C_5H_9O_2^-$									1	0	0
S_{NaOH}	NaOH	1									−13.90	59.81
S_{NaCl}	NaCl	1			1						−0.3	−8
$S_{NaCO_3^-}$	$NaCO_3^-$	1				1					1.27	−20.35
S_{NaHCO_3}	$NaHCO_3$	1				1					10.03	−283.3
S_{Na-ac}	$C_2H_3O_2Na$	1					1				−0.12	8
S_{KOH}	KOH		1								−13.76	55.81
S_{KCl}	KCl		1		1						−0.3	−4
S_{K-ac}	$C_2H_3O_2K$		1				1				−0.27	4
S_{NH_3}	NH_3			1							−9.25	52
S_{H-ac}	$C_2H_4O_2$						1				4.76	0.41
S_{H-pro}	$C_3H_6O_2$							1			4.87	0.75
S_{H-bu}	$C_4H_8O_2$								1		4.82	2.8
S_{H-va}	$C_5H_{10}O_2$									1	4.84	2.8

flow of 20 648 m^3 day^{-1} and a total COD and N load of 12 240 and 1140 kg day^{-1}, respectively, following the principles outlined in Gernaey et al. (2011). The activated sludge unit is a modified Ludzack–Ettinger configuration consisting of 5 tanks in series. Tanks 1 and 2 are anoxic, while tanks 3, 4 and 5 are aerobic. Tanks 1 and 5 are linked by means of an internal recycle. The ASM1 is chosen as the biological process model (Henze et al., 2000) and the double exponential settling velocity function of Takács et al. (1991) as a fair representation of the secondary settling process described by a one-dimensional model divided into ten layers. The BSM2 plant further contains a primary clarifier, a sludge thickener, an anaerobic digester, a storage tank and a dewatering unit. The ADM1 (Batstone et al., 2002) is the dynamic model implemented in this platform to describe the anaerobic digestion (AD) process. Detailed information about the plant design, operational conditions and process models of the BSM2 is reported by Gernaey et al. (2014).

2.2. Improved physico–chemical framework of the anaerobic digester

The composition of the digester aqueous phase is represented as a set of chemical entities called species S_i (mol L^{-1}) and components S_j (mol L^{-1}). As applied here, components (S_j) are selected as the fully dissociated form of the species (S_i). For example, the fully dissociated form of inorganic carbon $S_{CO_3^{-2}}$ was selected as a component (S_j), while the partially dissociated $S_{HCO_3^-}$ and undissociated $S_{H_2CO_3^*}$ forms of inorganic carbon were species (S_i) in the model. Table 1 summarizes all the considered species (rows) and how each of the species can be represented by a linear molar balance combination of the model components (columns). More details will be provided below.

2.2.1. Ionic strength corrections

In dilute wastewaters, ions in solution can be physically far apart (may not impose a chemical influence on one another), whereas when a wastewater becomes concentrated up to high-strength, the chemical interactions between ions and with the solvent become significant and have an effect. These interaction effects are commonly corrected for in a model (Stumm and Morgan, 1996) by multiplying each concentration (S_i or S_j) with an activity coefficient (γ), the product being called the chemical activity (a_i or a_j) as shown in Eq. (1):

$$a_i = \gamma_i S_i \quad (1)$$

The ionic strength (I) of the aqueous phase empirically estimates the level of interactions between ions (Hamann et al., 2007) and is commonly calculated as in Eq. (2):

$$I = \frac{1}{2}\sum_{i=1} S_i z_i^2 \quad (2)$$

where z_i is the valence of ion i. There are several correlations available that describe the relationship between activity coefficients (γ) and ionic strength for ions of different valences (Batstone et al., 2012). In the present work, the Davies approximation is used to calculate activity coefficients as shown in Eq. (3):

$$\log \gamma_i = -Az_i^2\left(\frac{\sqrt{I}}{1+\sqrt{I}} - 0.3I\right) \quad (3)$$

where A is a temperature-dependent parameter and γ_i is calculated as common activity coefficient values for monovalent, divalent and trivalent ions, respectively. The Davies approximation, which is mostly used in geochemical models, is said to be valid for ionic strengths up to 0.5 mol L^{-1} (Stumm and Morgan, 1996).

2.2.2. *Ion pairing, acid-base reactions and formulation of the equilibrium equations*

The aqueous phase reactions (weak acid-base reactions and ion pairing) are mathematically formulated by a set of non-linear algebraic equations (Stumm and Morgan, 1996; Morel and Hering, 1993) including one law of mass-action for each species (i) (Eq. (4)) and 1 M contribution balance for each component (j) (Eq. (5)) to guarantee the component conservation principle (that is, all species can be expressed as linear combinations of components). The mass action laws are commonly rearranged (Eq. (4)) with the species (i) written as the product of components (j) and the equilibrium coefficient (K_i), where $\upsilon_{i,j}$ is the stoichiometric coefficient for each respective aqueous phase reaction. This rearrangement allows substitution of the mass action laws into the molar contribution balances to eliminate the species from the equation set, which then has to be solved iteratively for the component concentrations. To illustrate, in the present study the number of species (N_{sp}) is 24, but by substitution, is reduced to 9 components to be solved implicitly (N_C).

$$a_i = K_i \prod_{j=1}^{Nc} a_j^{\upsilon_{i,j}} \quad i = 1, 2, \ldots N_{sp} \tag{4}$$

$$S_{j,tot} = S_j + \sum_{i=1}^{N_{sp}} \upsilon_{i,j}\, S_i = \frac{a_j}{\gamma} + \sum_{i=1}^{N_{sp}} \upsilon_{i,j} \frac{a_i}{\gamma} \qquad \begin{matrix} j = 1, 2, \ldots N_C \\ i = 1, 2, \ldots N_{sp} \end{matrix} \tag{5}$$

The effect of temperature on K_i is corrected for by the constant-enthalpy form of the van't Hoff equation (Stumm and Morgan, 1996). In Eq. (6), K_1 and K_2 are the equilibrium constants at temperatures T_1 and T_2 (in K), respectively, ΔH^o is the enthalpy change of the reaction and R is the universal gas constant.

$$\ln \frac{K_2}{K_1} = \frac{\Delta H^o}{R} \left(\frac{1}{T_1} - \frac{1}{T_2} \right) \tag{6}$$

Full specification of the algebraic equation set requires an additional equation, which can be resolved by the charge balance (Batstone et al., 2002), as shown in Eq. (7):

$$\sum S_{cat} - \sum S_{an} = 0 \tag{7}$$

where S_{cat} and S_{an} represent the total equivalent concentrations of cations and anions, respectively, which are the concentrations of respective ions multiplied by their valence. An alternative is the use of the proton balance (Morel and Hering, 1993), which generates the same equation set, but with a different structure.

2.2.3. *Implementation details, numerical issues and model verification*

The ADM1 implementation in the BSM2 framework is a very stiff system with some of the states reacting quickly (weak acid-base chemistry) while other states are reacting sluggishly (different biological uptake processes). Implicit numerical solvers are especially suitable to handle this type of system, and can inherently solve DAE problems such as this, but cannot be used for the BSM2 because they are intolerant to highly dynamic inputs, controller numerical characteristics, noise and step changes used in the modelling of process control scenarios. In the past, this has been resolved by solving pH and the S_{H_2} state through independent algebraic equations (Rosen et al., 2006) with the use of a forward Runge–Kutta solver for the remaining ordinary differential equations (ODEs). This approach is not applicable due to algebraic interdependencies, and was extended to a full gradient search method as follows (Eq. (8)):

$$Z_{i+1} = Z_i - J_F(Z_i)^{-1} G\left(Z_i\right) \tag{8}$$

where Z_i is the vector of equilibrium variables ($z_{1,i}$, …, $z_{n,i}$) obtained from the previous iteration step i, G (Z_i) is a vector containing the values of the set of implicit algebraic equations (g_1 (z_1, …, z_n), …, g_n (z_1, …, z_n) = [0]). The iteration is converged to a tolerance of $g_{max} < 10^{-12}$. The full analytical Jacobian (gradient) (J_F) was required for this approach, which requires symbolic manipulation of the algebraic equations in order to obtain the matrix of all first-order partial derivatives $\delta(G_1, \ldots, G_m)/\delta(z_1, \ldots, z_n)$ and the matrix inverted using the decomposition method in LinPack. The MINTEQA2 geochemical program (Allison et al., 1991) was used to verify the approach.

A global sensitivity analysis was not included in this study but could be considered in future work. Parameters related to ion pairing behaviour are found to have well-established values from literature eliminating the need for a sensitivity analysis in this regard. On the other hand, variations in ion activity-related parameters' values could have a significant effect on numerous model outputs thus, performing a global sensitivity analysis would be interesting to see the highly sensitive parameters, as well as their contributions to variations in the model outputs.

2.3. *Variants and model test cases*

The performance of the improved ADM1 model was tested with three model variants:

1. A base case (A_1) using the default ADM1 (Rosen et al., 2006) with kinetic and stoichiometric parameters at 35 °C from Gernaey et al. (2014).
2. A variant (A_2) with an ionic strength correction: iterative ionic strength and activity corrections for inorganic carbon (S_{IC}), inorganic nitrogen (S_{IN}), acetate (S_{ac^-}), propionate (S_{pro^-}), valerate (S_{va^-}), butyrate (S_{bu^-}) and free reactive protons (S_{H^+}).
3. A variant (A_3) with ionic strength correction and ion pairing: the ion activity corrections of A_2 and in addition, S_{cat} replaced by sodium (S_{Na^+}) and potassium (S_{K^+}) and S_{an} replaced by chloride (S_{Cl^-}). These monovalent ions are permitted to form soluble ion pairs (see Table 1) modelled with Eq. (4) and Eq. (5). The methanogenesis step during anaerobic digestion could be inhibited by the presence of sodium ions, and it could be expected that this inhibition

Table 2 – Average ADM1 state values with the different physico-chemical framework implementations (using BSM2 influent data).

	S_{C_1}			S_{C_2}			S_{C_3}			S_{C_4}			S_{C_5}			Units
	A_1	A_2	A_3	A_1	A_2	A_3	A_1	A_2	A_3	A_1	A_2	A_3	A_1	A_2	A_3	
pH	7.21	7.11	7.11	7.50	7.39	7.39	7.77	7.66	7.66	7.88	7.98	7.97	7.85	7.99	7.99	–
S_{H^+}	6.16E-8	9.95E-8	9.96E-8	3.16E-8	5.40E-8	5.43E-8	1.71E-8	2.92E-8	2.97E-8	1.31E-8	1.43E-8	1.46E-8	1.42E-8	1.39E-8	1.39E-8	mol L^{-1}
S_{Na^+}				0.027	0.027	0.026	0.054	0.054	0.052	0.076	0.081	0.076	0.088	0.096	0.094	mol L^{-1}
S_{K^+}				0.027	0.027	0.027	0.054	0.054	0.054	0.081	0.082	0.081	0.104	0.105	0.099	mol L^{-1}
$S_{NH_4^+}$	0.093	0.093	0.093	0.089	0.090	0.090	0.086	0.088	0.088	0.088	0.086	0.086	0.095	0.093	0.093	mol L^{-1}
S_{Cl^-}	0.005	0.005	0.005	0.005	0.005	0.005	0.006	0.006	0.006	0.006	0.006	0.006	0.007	0.007	0.007	mol L^{-1}
S_{ac^-}	0.0013	0.0010	0.0010	0.0024	0.0014	0.0014	0.0075	0.0026	0.0025	0.0768	0.0168	0.0146	0.2216	0.2009	0.1920	mol L^{-1}
S_{pro^-}	0.00016	0.00016	0.00016	0.00016	0.00016	0.00016	0.00016	0.00016	0.00016	0.00016	0.00016	0.00016	0.00017	0.00017	0.00017	mol L^{-1}
$S_{CO_3^{-2}}$	0.00008	0.00013	0.00013	0.00024	0.00043	0.00043	0.00060	0.00118	0.00115	0.00069	0.00298	0.00287	0.00023	0.00121	0.00121	mol L^{-1}
S_{bu^-}	8.71E-5	8.71E-5	8.71E-5	8.93E-5	8.93E-5	8.93E-5	8.95E-5	8.94E-5	8.94E-5	9.04E-5	8.96E-5	8.96E-5	9.24E-5	9.21E-5	9.21E-5	mol L^{-1}
S_{va^-}	5.90E-5	5.90E-5	5.90E-5	6.05E-5	6.05E-5	6.05E-5	6.06E-5	6.06E-5	6.06E-5	6.14E-5	6.07E-5	6.07E-5	6.28E-5	6.26E-5	6.26E-5	mol L^{-1}
$S_{H_2CO_3^*}$	0.00947	0.00945	0.00945	0.00762	0.00757	0.00757	0.00553	0.00538	0.00539	0.00373	0.00302	0.00304	0.00146	0.00112	0.00112	mol L^{-1}
S_{H-ac}	4.55E-6	3.37E-6	3.37E-6	4.33E-6	2.51E-6	2.50E-6	7.36E-6	2.44E-6	2.40E-6	5.78E-5	7.45E-6	6.60E-6	1.80E-4	8.56E-5	8.19E-5	mol L^{-1}
S_{H-bu}	3.66E-7	3.62E-7	3.62E-7	1.93E-7	1.89E-7	1.90E-7	1.05E-7	9.85E-8	1.00E-7	8.08E-8	4.72E-8	4.82E-8	8.92E-8	4.66E-8	4.66E-8	mol L^{-1}
$S_{HCO_3^-}$	0.0858	0.0867	0.0867	0.1344	0.1363	0.1354	0.1800	0.1861	0.1835	0.1590	0.2187	0.2154	0.0577	0.0840	0.0847	mol L^{-1}
S_{H-pro}	7.27E-7	7.18E-7	7.19E-7	3.84E-7	3.76E-7	3.79E-7	2.09E-7	1.96E-7	1.99E-7	1.61E-7	9.41E-8	9.60E-8	1.79E-7	9.35E-8	9.34E-8	mol L^{-1}
S_{H-va}	2.63E-7	2.60E-7	2.60E-7	1.38E-7	1.35E-7	1.36E-7	7.51E-8	7.07E-8	7.17E-8	5.81E-8	3.39E-8	3.46E-8	6.43E-8	3.36E-8	3.35E-8	mol L^{-1}
S_{K-ac}						1.23E-5			4.33E-5			3.61E-4			5.8E-3	mol L^{-1}
S_{KCl}						4.02E-5			8.24E-5			1.27E-4			1.6E-4	mol L^{-1}
S_{KOH}						1.82E-8			6.66E-8			2.02E-7			2.6E-7	mol L^{-1}
S_{Na-ac}				5.46E-5	1.86E-5	1.77E-5	3.40E-4	6.66E-5	6.15E-5	4.89E-3	6.17E-4	5.07E-4	1.64E-2	8.68E-3	8.2E-3	mol L^{-1}
S_{NaCl}						3.68E-5			7.46E-5			1.14E-4			1.5E-4	mol L^{-1}
$S_{NaCO_3^-}$						5.31E-5			2.60E-4			9.13E-4			4.7E-4	mol L^{-1}
S_{NaHCO_3}						8.57E-4			2.21E-3			3.72E-3			1.8E-3	mol L^{-1}
S_{NaOH}						1.34E-8			4.85E-8			1.45E-7			1.9E-7	mol L^{-1}
S_{NH_3}	0.0017	0.0011	0.0011	0.0032	0.0019	0.0019	0.0057	0.0034	0.0034	0.0075	0.0068	0.0066	0.0075	0.0076	0.0076	mol L^{-1}
I	–	0.09	0.09	–	0.14	0.14	–	0.20	0.20	0	0.25	0.25	0	0.30	0.29	mol L^{-1}
γ	1	0.78	0.78	1	0.76	0.76	1	0.74	0.74	1	0.73	0.74	1	0.73	0.73	–

will be influenced by ion activity and ion pairing. However, Omil et al. (1995) have shown that adapting the biomass to the high salinity levels could eliminate such inhibition and/or toxicity effects. It is assumed in this study that the biomass is adapted to high salinity levels and therefore, no sodium inhibition term was added to the ADM1 biokinetics.

Also, each of the model variants are tested for increases in ionic strength by adding another minor influent stream (Q_{add} = 5 m^3 day^{-1}) with different S_{cat} loads to progressively increase the ionic strength of the overall plant influent (I = 0.09–0.3 mol L^{-1}). This leads to five test scenarios, Sc_1, Sc_2, Sc_3, Sc_4 and Sc_5, with additional S_{cat} loads of 0, 2, 4, 6 and 8 mol L^{-1}, respectively. In model variant A_3, the added S_{cat} is distributed equally between S_{Na^+} and S_{K^+}. It is important to highlight that the added cations are unpaired with anions, so that a higher cation load also increases pH. This represents a scenario where a strong alkali is added (e.g. sodium hydroxide or a high alkalinity feed) to increase the alkalinity of the wastewater. All other model conditions, including influent flow rate, COD and N loads are kept identical for the three model approaches.

Simulation results are evaluated dynamically during the last 364 days of simulation in accordance with the BSM2 simulation principles, namely 200 days simulation to reach steady state followed by 609 days of dynamic influent data. The effluent quality index (*EQI*) is used to evaluate the (weighted) pollution load discharged to water bodies and the operational cost index (*OCI*) is an approximate measure of the plant's operational costs (energy, sludge production, chemicals, etc.) (Gernaey et al., 2014).

3. Results and discussion

3.1. *Influence of physico–chemical corrections on ADM1 state variables*

Table 2 shows average values of the ADM1 state variables for the three model variants (A_1, A_2 and A_3) and the five cationic load scenarios for increased ionic strengths (Sc_1, Sc_2, Sc_3, Sc_4 and Sc_5). At low ionic strengths (Sc_1) the average ADM1 state values for A_1, A_2 and A_3 seem to be similar (Table 2). However, activity corrections of A_2 and A_3 do influence the species distribution in the inorganic carbon system (S_{IC}), with deprotonated inorganic carbon ($S_{CO_3^{2-}}$, $S_{HCO_3^-}$) being up to 62% higher for A_2 and A_3 than for A_1 (Table 2). As a consequence, more reactive free protons (S_{H^+}) are required in A_2 and A_3 and are released to uphold the charge balance and thus the predicted pH is lower in A_2 and A_3 (pH 7.11) than in A_1 (pH 7.21). This release of protons is facilitated by the shift in inorganic species from protonated to deprotonated form. The lower pH in A_2 and A_3 results in a lower free ammonia (S_{NH_3}) concentration and this in turn reduces the level of free-ammonia-inhibition of aceticlastic methanogenesis (K_{I,NH_3} = 0.0018 mol L^{-1}). Consequently, free-ammonia inhibition is more pronounced for A_1 as compared to A_2 and A_3. A lower level of free-ammonia inhibition results in lower total acetic acid ($S_{H-ac} + S_{ac^-}$) concentration, more acetate degraders (X_{ac}) and

Table 3 – H_2, CO_2 and CH_4 production (gas phase) with the different physico–chemical framework implementations.

	Sc_1			Sc_2			Sc_3			Sc_4			Sc_5			Units
	A_1	A_2	A_3	A_1	A_2	A_3	A_1	A_2	A_3	A_1	A_2	A_3	A_1	A_2	A_3	
Gas_{H_2}	0.0036	0.0036	0.0036	0.0034	0.0034	0.0034	0.0031	0.0031	0.0031	0.0025	0.0027	0.0028	0.0013	0.0015	0.0015	kg day^{-1}
Gas_{CO_2}	1526.6	1523.6	1523.6	1116.0	1107.8	1108.3	725.8	710.4	711.8	376.1	350.2	353.9	77.6	70.4	71.9	kg day^{-1}
Gas_{CH_4}	1059.3	1060.0	1060.0	1054.9	1057.4	1057.4	1040.4	1053.8	1054.0	8434.0	1002.4	1008.3	442.0	518.7	527.1	kg day^{-1}

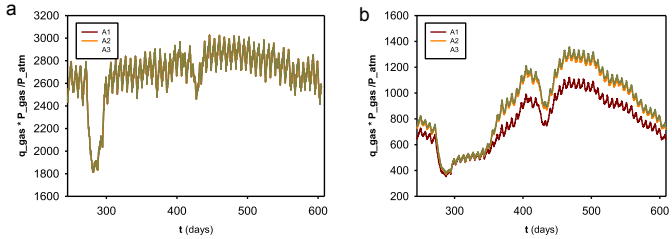

Fig. 2 – Dynamic profiles of the total biogas production in BSM2 using three different physico-chemical frameworks (A_1, A_2 and A_3) and two different cationic loads (S_{C_1}) (a) and (S_{C_5}) (b).

higher acetate uptake (Table 2). These effects are depicted in the Graphical Abstract.

Increasing influent values of S_{Na^+} and/or S_{K^+} (Table 2, comparison between S_{C_1} to S_{C_5}) values result in a reduction of S_{H^+} values (neutralized in effect), and consequently pH increases. Ionic strength (I) increases in a correlated manner (not necessarily linearly) with the applied cationic load. Higher pH values increase S_{NH_3} which then increases inhibition of acetate degraders (X_{ac}), decreases acetate uptake and consequently influences the overall hydrogen (S_{H_2})/acetate (S_{ac^-}) (electron donors) consumption. Gas production (Gas_{CH_4}, Gas_{CO_2}, Gas_{H_2}) is then also reduced (Table 3). At the high ionic strengths of scenarios S_{C_4} and S_{C_5}, free-ammonia inhibition becomes very strong, leading to very notable accumulation of acetate (S_{ac^-}) in the digester (Table 2) and a substantial decrease in overall biogas production (Table 3). Further accumulation of acetate can then decrease digester pH even further and influence many other processes, such as hydrogenotrophic methanogenesis and acetogenesis from different organics (Batstone et al., 2002). These are noted to be predominantly the effects of an overall rise in pH with increase in S_{cat} loads.

Importantly, the comparative results of A_1 and A_2 indicate the significance of ion activity corrections to account for the effects of increased salinity/pH. The results show that when cationic load is increased up to S_{C_3}, digester pH is higher with case A_1 than with case A_2. As noted above, these model differences are caused by the reactive free protons released through ion activity of inorganic carbon species in case A_2, which counteracts the alkali effect of the added cationic load and buffers the overall increase in pH. The lower pH of case A_2 causes less ammonia inhibition than in case A_1 and therefore digester performance (biogas production) is better with case A_2 than with case A_1 (more on this below).

Theoretically, ion pairing would further shift the inorganic carbon species towards their deprotonated forms, causing the release of even more free reactive protons than in case A_2. These free reactive protons would further buffer increases in pH with increasing cationic load with similar effects as noted above for ion activity. The comparative results of cases A_2 and A_3 show that the effect of ion pairing (A_3) is minor in both pH and species distributions (Table 2) and that the resulting pH and species distribution are very similar in both cases. These results thus indicate that ion pairing is less important to account for the effects of increased salinity/pH.

3.2. *Water/sludge line interactions*

In the reference scenario S_{C_1}, the simulated values of *EQI* and *OCI* are very similar for cases A_1, A_2 and A_3 (within 1%) (Fig. 4). Any differences between the results for cases A_1, A_2 and A_3 only become pronounced at the higher ionic strengths of scenarios S_{C_4} and S_{C_5}. At these high ionic strengths, free ammonia inhibition substantially decreases the anaerobic digestion performance (see previous section) and consequently the overall process performance (18% in *EQI* and 7% in *OCI* depending on whether one is using scenario A_1 or A_3 as depicted in Fig. 4).

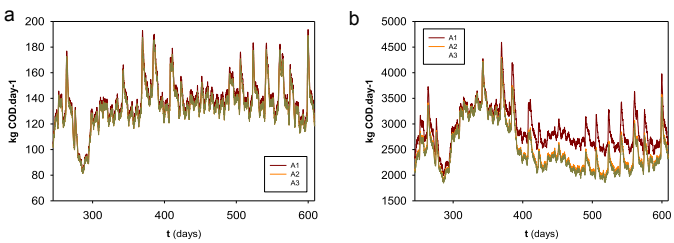

Fig. 3 – Dynamic profiles of the total COD loading returning to the water line in BSM2 using three different physico-chemical frameworks (A_1, A_2 and A_3) and two different cationic loads (S_{C_1}) (a) and (S_{C_5}) (b).

This deterioration in simulated digester performance decreases biogas recovery and especially Gas_{CH_4} (Fig. 2, also Table 3 shows a reduction of up to 50%), which in turn increases the overall operational costs (*OCI* values), because less renewable energy is being recovered from biogas.

Poor digester performance also affects the quantity/quality of the digester supernatant with a higher COD load returned from the sludge line to the water line. Fig. 3 shows the dynamic profiles of the total organic load leaving the AD unit and returning to the water line ahead of the primary clarifier.

This additional COD load can overload the activated sludge process and influence effluent quality as reflected in *EQI*. The overall result of these effects is much higher *EQI* and *OCI* values for scenario S_{C_5} as compared with scenarios S_{C_1}, S_{C_2} and S_{C_3} (Fig. 4). Interestingly, the effect of ammonia inhibition on *EQI* may be unrealistically high for case A_1 and scenario S_{C_4}, when considering that the more comprehensive model approaches of cases A_2 and A_3 do not show the same influence on *EQI* for scenario S_{C_4}. Further, it is worth noting that the differences between the *EQI* and *OCI* values of A_2 and A_3 are not so pronounced (Fig. 4), indicating that the influence of ion pairing is less important. The implications are further discussed below.

3.3. *Selection of appropriate physico–chemical framework*

Overall, the results of the present study with ADM1 in BSM2 demonstrates that ion activity or ion-pairing corrections are not required when simulating anaerobic digestion of dilute wastewaters, such as weak industrial wastewater, in a plant-wide context. This is shown by the similar plant performance indices (Fig. 4) and overall biogas production for case A_1 (no corrections) and cases A_2 and A_3 (with corrections) up to cationic load S_{C_3} ($I < 0.2$ mol L^{-1}) (Fig. 2, Table 3). In contrast, in scenarios S_{C_4} and S_{C_5} ($I > 0.2$ mol L^{-1}, which are typical for high solids digestion and manure digestion), ion activity corrections are required to correctly propagate salinity and pH effects throughout the plant-wide model. This is seen from the results for cationic load S_{C_4}, where base case A_1 (no corrections) predicts a substantial effect on the plant performance indices (Fig. 4), which is not reflected in the results from the more comprehensive case A_2 (with ion activity corrections). This is significant because, while local pH predictions in an isolated model of anaerobic digestion may be less sensitive to activity corrections (Nielsen et al., 2008; Tait et al., 2012), the present study results suggest that activity corrections are required for a plant-wide model such as BSM2 at $I > 0.2$ mol L^{-1}. In such cases the inclusion of activity corrections is fully justified and even necessary.

In the present study, the Davies approximation to ionic activity is used because it is valid for the ionic strengths that are being tested. The Davies approach is also widely used in other industry-standard aqueous equilibrium models, predominantly because it is relatively simple to implement with single respective activity coefficients for mono, di- and trivalent ions. In general with a model using the Davies approach, the equilibrium coefficients can be readily corrected directly by multiplying/dividing with activity coefficients as is relevant, and the iteration can calculate ion concentrations rather than activities. However, at higher ionic strengths of $I > 0.3$ mol L^{-1}, activity coefficients of the Davies equation unexpectedly approaches unity with further increases in ionic strength (Tait et al., 2012). Accordingly, for $0.4 < I < 1$ mol L^{-1}, the WATEQ Debye–Hückel approach (Parkhurst and Appelo, 1999) is recommended, for which activity coefficients continue to approach zero with increasing ionic strength (as expected) up to its validity limit of 1 mol L^{-1}.

The results of the present study with ADM1 in BSM2 suggest that ion pairing corrections are less important in the plant-wide context than ion activity corrections. This is seen from the near identical results (Table 2, Table 3, Figs. 2–4) for cases A_2 (without ion pairing) and A_3 (with ion pairing) for all the tested cationic load scenarios ($I = 0.09$–0.3 mol L^{-1}). It is however necessary to note that predominantly monovalent ions are considered in case A_3, whereas ion pairing with divalent and trivalent ions is known to be strong and influential in minerals precipitation (Tait et al., 2012). This is important because, while digester pH is strongly influenced by monovalent ions (such as bicarbonate), the thermodynamic driving force for minerals precipitation is determined by other participating ions, which commonly include divalent and trivalent ions. It has been suggested that ion activity and ion pairing contribute equally in high-strength wastewater, and can increase the effective saturation coefficient by an order of magnitude (Tait et al., 2009). When required for precipitation studies, an aqueous phase can be modelled with DAEs and precipitation reactions as ODEs with dedicated kinetic relationships (Batstone and Keller, 2003; Musvoto et al., 2000; van Rensburg et al., 2003; Kazadi Mbamba et al., 2014).

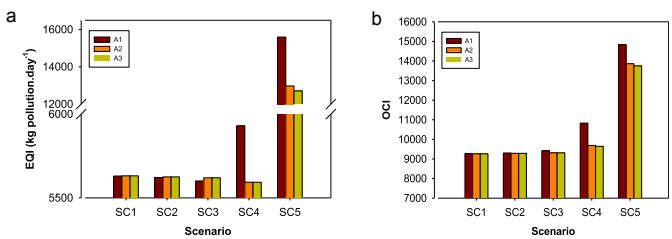

Fig. 4 – *EQI* (a) and *OCI* (b) variations in BSM2 using three different physico-chemical frameworks (A_1, A_2 and A_3) and five different scenarios with increasing cationic loads (S_{C_1}, S_{C_2}, S_{C_3}, S_{C_4} and S_{C_5}).

Current research investigates upgrading the ADM1 with phosphorus ($S_{H_2PO_4^-}/S_{HPO_4^{-2}}/S_{PO_4^{-3}}S_{PO_4^{-3}}$) and sulphur ($S_{SO_4^{-2}}/S_{H_2S}$) together with multiple metals ($S_{Ca^{+}}$, $S_{Mg^{+}}$, S_{Fe} and S_{Al}) and precipitation products (struvite, k-struvite, iron sulphide, calcium phosphate, calcium carbonate, magnesium carbonate). It is believed that the same framework as presented in Section 2 (with additional compounds and species and expanded biokinetics) can be used in such cases to correctly describe the behaviour of these new model add-ons.

4. Conclusions

The findings of this study are:

- Ion activity corrections influence salinity/pH effects in a plant-wide model such as BSM2, showing a greater influence at higher ionic strengths (I). Accordingly, it is recommended that activity corrections be applied with ADM1 at $I > 0.2$ mol L^{-1} (manure and high-solids digestion).
- Monovalent ion pairing is much less influential and much less important than ion activity corrections. Thus, ion pairing effects can be excluded from ADM1 when minerals precipitation is not under study.
- The (bio)chemical processes in ADM1 should be described mathematically as a combination of ODEs and DAEs, and a multi-dimensional Newton–Raphson method should be used to handle algebraic interdependencies.

5. Supplementary material

The MATLAB/SIMULINK code containing the implementation of the physico-chemical modelling framework in ADM1 using BSM2 as a case study is available upon request to Prof. Ulf Jeppsson (ulf.jeppsson@iea.lth.se).

Acknowledgements

Ms Solon and Dr Flores-Alsina acknowledge the Marie Curie Program of the EU 7th Framework Programme FP7/2007-2013 under REA agreement 289193 (SANITAS) and 329349 (PROTEUS) respectively. This research was also supported financially by the University of Queensland through the UQ International Scholarships (UQI) and UQ Collaboration and Industry Engagement Fund (UQCIEF). The International Water Association (IWA) is also acknowledged for their promotion of this collaboration through their sponsorship of the IWA Task Group on Generalized Physicochemical Modelling Framework (PCM). A concise version of this paper was presented at the IWA World Water Congress & Exhibition, on 21–26 September 2014, in Lisbon, Portugal.

REFERENCES

Allison, J.D., Brown, D.S., Novo-Gradac, K.J., 1991. MINTEQA2/PRODEFA2, A Geochemical Assessment Model for Environmental Systems: Version 3.0 User's Manual. Environmental Research Laboratory, Office of Research and Development, US Environmental Protection Agency, Athens, GA. EPA/600/3-91/021.

Astals, S., Esteban-Gutiérrez, M., Fernández-Arévalo, T., Aymerich, E., García-Heras, J.L., Mata-Alvarez, J., 2013. Anaerobic digestion of seven different sewage sludges: a biodegradability and modelling study. Water Res. 47 (16), 6033–6043.

Barat, R., Montoya, T., Seco, A., Ferrer, J., 2011. Modelling biological and chemically induced precipitation of calcium phosphate in enhanced biological phosphorus removal systems. Water Res. 45 (12), 3744–3752.

Batstone, D.J., Keller, J., Angelidaki, I., Kalyuzhnyi, S.V., Pavlostathis, S.G., Rozzi, A., Sanders, W.T.M., Siegrist, H., Vavilin, V.A., 2002. The IWA anaerobic digestion model No. 1 (ADM 1). Water Sci. Technol. 45 (10), 65–73.

Batstone, D.J., Keller, J., 2003. Industrial application of the IWA anaerobic digestion model No. 1 (ADM). Water Sci. Technol. 47 (12), 199–206.

Batstone, D.J., Keller, J., Blackall, L.L., 2004. The influence of substrate kinetics on the microbial community structure in granular anaerobic biomass. Water Res. 38 (6), 1390–1404.

Batstone, D.J., Hernandez, J.L.A., Schmidt, J.E., 2005. Hydraulics of laboratory and full-scale upflow anaerobic sludge blanket (UASB) reactors. Biotechnol. Bioeng. 91 (3), 387–391.

Batstone, D.J., Keller, J., Steyer, J.-P., 2006. A review of ADM1 extensions, applications, and analysis: 2002–2005. Water Sci. Technol. 54 (4), 1–10.

Batstone, D.J., Amerlinck, Y., Ekama, G., Goel, R., Grau, P., Johnson, B., Kaya, I., Steyer, J.-P., Tait, S., Takács, I., Vanrolleghem, P.A., Brouckaert, C.J., Volcke, E.I.P., 2012. Towards a generalized physicochemical framework. Water Sci. Technol. 66 (6), 1147–1161.

Donoso-Bravo, A., Mailier, J., Martin, C., Rodríguez, J., Aceves-Lara, C.A., Wouwer, A.V., 2011. Model selection, identification and validation in anaerobic digestion: a review. Water Res. 45 (17), 5347–5364.

Gernaey, K.V., Flores-Alsina, X., Rosen, C., Benedetti, L., Jeppsson, U., 2011. Dynamic influent pollutant disturbance scenario generation using a phenomenological modelling approach. Environ. Model. Softw. 26 (11), 1255–1267.

Gernaey, K.V., Jeppsson, U., Vanrolleghem, P.A., Copp, J.B., 2014. Benchmarking of Control Strategies for Wastewater Treatment Plants. IWA Scientific and Technical Report No. 23. IWA Publishing, London, UK.

Hamann, C.H., Hamnett, A., Vielstich, W., 2007. Electrochemistry. Wiley-VCH, New York, USA.

Henze, M., Gujer, W., Mino, T., van Loosdrecht, M.C.M., 2000. Activated Sludge Models ASM1, ASM2, ASM2d, and ASM3. IWA Scientific and Technical Report No. 9. IWA Publishing, London, UK.

Hinken, L., Huber, M., Weichgrebe, D., Rosenwinkel, K.-H., 2014. Modified ADM1 for modelling an UASB reactor laboratory plant treating starch wastewater and synthetic substrate load tests. Water Res. 64, 82–93.

Jeppsson, U., Alex, J., Batstone, D., Benedetti, L., Comas, J., Copp, J.B., Corominas, L., Flores-Alsina, X., Gernaey, K.V., Nopens, I., Pons, M.-N., Rodriguez-Roda, I., Rosen, C., Steyer, J.-P., Vanrolleghem, P.A., Volcke, E.I.P., Vrecko, D., 2013. Benchmark simulation models, quo vadis? Water Sci. Technol. 68 (1), 1–15.

Kazadi Mbamba, C., Flores-Alsina, X., Batstone, D., Tait, S., 2014. A Generalized Chemical Precipitation Modelling Approach in Wastewater Treatment Applied to Calcite (Submitted for publication).

Morel, F.M., Hering, J.G., 1993. Principles and Applications of Aquatic Chemistry. John Wiley and Sons, New York, USA.

Musvoto, E.V., Wentzel, M.C., Ekama, G.A., 2000. Integrated chemical–physical processes modelling – II. Simulating aeration treatment of anaerobic digester supernatants. Water Res. 34 (6), 1868–1880.
Nielsen, A.M., Spanjers, H., Volcke, E.I.P., 2008. Calculating pH in pig manure taking into account ionic strength. Water Sci. Technol. 57 (11), 1785–1790.
Omil, F., Mendez, R., Lema, J.M., 1995. Anaerobic treatment of saline wastewaters under high sulphide and ammonia content. Bioresour. Technol. 54 (3), 269–278.
Parkhurst, D.L., Appelo, C., 1999. User's Guide to PHREEQC (Version 2): a Computer Program for Speciation, Batch-reaction, One-dimensional Transport, and Inverse Geochemical Calculations. USGS, Colorado, USA.
Penumathsa, B.K., Premier, G.C., Kyazze, G., Dinsdale, R., Guwy, A.J., Esteves, S., Rodríguez, J., 2008. ADM1 can be applied to continuous bio-hydrogen production using a variable stoichiometry approach. Water Res. 42 (16), 4379–4385.
Picioreanu, C., Batstone, D.J., van Loosdrecht, M.C.M., 2005. Multidimensional modelling of anaerobic granules. Water Sci. Technol. 52 (1–2), 501–507.
Ramirez, I., Volcke, E.I.P., Rajinikanth, R., Steyer, J.-P., 2009. Modeling microbial diversity in anaerobic digestion through an extended ADM1 model. Water Res. 43 (11), 2787–2800.
Rosen, C., Vrecko, D., Gernaey, K.V., Pons, M.-N., Jeppsson, U., 2006. Implementing ADM1 for plant-wide benchmark simulations in Matlab/Simulink. Water Sci. Technol. 54 (4), 11–19.
Stumm, W., Morgan, J.J., 1996. In: Schnoor, J.L., Zehnder, A. (Eds.), Aquatic Chemistry: Chemical Equilibria and Rates in Natural Waters. John Wiley and Sons, New York, USA.
Tait, S., Clarke, W.P., Keller, J., Batstone, D.J., 2009. Removal of sulfate from high-strength wastewater by crystallisation. Water Res. 43 (3), 762–772.
Tait, S., Solon, K., Volcke, E.I.P., Batstone, D.J., 2012. A unified approach to modelling wastewater chemistry: model corrections. In: Proc. 3rd Wastewater Treatment Modelling Seminar (WWTmod2012), Mont-Sainte-Anne, Quebec, Canada, Feb. 26–28, pp. 51–62.
Takács, I., Patry, G.G., Nolasco, D., 1991. A dynamic model of the clarification thickening process. Water Res. 25 (10), 1263–1271.
van Rensburg, P., Musvoto, E.V., Wentzel, M.C., Ekama, G.A., 2003. Modelling multiple mineral precipitation in anaerobic digester liquor. Water Res. 37 (13), 3087–3097.
Wilson, C.A., Novak, J., Takacs, I., Wett, B., Murthy, S., 2012. The kinetics of process dependent ammonia inhibition of methanogenesis from acetic acid. Water Res. 46 (19), 6247–6256.
Yuan, X.Z., Shi, X.S., Yuan, C.X., Wang, Y.P., Qiu, Y.L., Guo, R.B., Wang, L.S., 2014. Modeling anaerobic digestion of blue algae: stoichiometric coefficients of amino acids acidogenesis and thermodynamics analysis. Water Res. 49, 113–123.
Zaher, U., Li, R., Jeppsson, U., Steyer, J.P., Chen, S., 2009. GISCOD: general integrated solid waste co-digestion model. Water Res. 43 (10), 2717–2727.
Zonta, Ž., Alves, M.M., Flotats, X., Palatsi, J., 2013. Modelling inhibitory effects of long chain fatty acids in the anaerobic digestion process. Water Res. 47 (3), 1369–1380.

Paper II

Water Research 85 (2015) 255–265

Contents lists available at ScienceDirect

Water Research

journal homepage: www.elsevier.com/locate/watres

A plant-wide aqueous phase chemistry module describing pH variations and ion speciation/pairing in wastewater treatment process models

Xavier Flores-Alsina [a], Christian Kazadi Mbamba [b], Kimberly Solon [c], Darko Vrecko [d], Stephan Tait [b], Damien J. Batstone [b], Ulf Jeppsson [c, *], Krist V. Gernaey [a]

[a] CAPEC-PROCESS Research Center, Department of Chemical and Biochemical Engineering, Technical University of Denmark, Building 229, DK-2800 Kgs. Lyngby, Denmark
[b] Advanced Water Management Centre (AWMC), The University of Queensland, St Lucia 4072, Brisbane, Queensland, Australia
[c] Division of Industrial Electrical Engineering and Automation (IEA), Department of Biomedical Engineering, Lund University, Box 118, SE-221 00 Lund, Sweden
[d] Department of Systems and Control, Jožef Stefan Institute, Jamova 39, SI-1000 Ljubljana, Slovenia

ARTICLE INFO

Article history:
Received 7 April 2015
Received in revised form
6 July 2015
Accepted 8 July 2015
Available online 15 July 2015

Keywords:
Activity correction
Ionic strength
Ionic behaviour
Dynamic pH prediction
Multi-dimensional Newton Raphson
Simulated annealing
Physico–chemical modelling
Water chemistry

ABSTRACT

There is a growing interest within the Wastewater Treatment Plant (WWTP) modelling community to correctly describe physico–chemical processes after many years of mainly focusing on biokinetics. Indeed, future modelling needs, such as a plant-wide phosphorus (P) description, require a major, but unavoidable, additional degree of complexity when representing cationic/anionic behaviour in Activated Sludge (AS)/Anaerobic Digestion (AD) systems. In this paper, a plant-wide aqueous phase chemistry module describing pH variations plus ion speciation/pairing is presented and interfaced with industry standard models. The module accounts for extensive consideration of non-ideality, including ion activities instead of molar concentrations and complex ion pairing. The general equilibria are formulated as a set of Differential Algebraic Equations (DAEs) instead of Ordinary Differential Equations (ODEs) in order to reduce the overall stiffness of the system, thereby enhancing simulation speed. Additionally, a multi-dimensional version of the Newton–Raphson algorithm is applied to handle the existing multiple algebraic inter-dependencies. The latter is reinforced with the Simulated Annealing method to increase the robustness of the solver making the system not so dependant of the initial conditions. Simulation results show pH predictions when describing Biological Nutrient Removal (BNR) by the activated sludge models (ASM) 1, 2d and 3 comparing the performance of a nitrogen removal (*WWTP1*) and a combined nitrogen and phosphorus removal (*WWTP2*) treatment plant configuration under different anaerobic/anoxic/aerobic conditions. The same framework is implemented in the Benchmark Simulation Model No. 2 (BSM2) version of the Anaerobic Digestion Model No. 1 (ADM1) (*WWTP3*) as well, predicting pH values at different cationic/anionic loads. In this way, the general applicability/flexibility of the proposed approach is demonstrated, by implementing the aqueous phase chemistry module in some of the most frequently used WWTP process simulation models. Finally, it is shown how traditional wastewater modelling studies can be complemented with a rigorous description of aqueous phase and ion chemistry (pH, speciation, complexation).

© 2015 Elsevier Ltd. All rights reserved.

1. Introduction

Activated Sludge Models (ASMs) have traditionally used alkalinity to determine net acid–base state of the system (Henze et al., 2000). That is, processes such as nitrification (acid producing) will decrease alkalinity, while processes such as ammonia release (base producing) will increase alkalinity. Thus, the alkalinity state provided a warning of whether pH is likely to decrease substantially away from neutrality (Batstone et al., 2012), which is simple, and effective in the specific case of nitrification. Unfortunately, the alkalinity approach has limitations for important applications since it is not possible to determine wastewater pH with the ASM

* Corresponding author.
E-mail address: ulf.jeppsson@iea.lth.se (U. Jeppsson).

http://dx.doi.org/10.1016/j.watres.2015.07.014
0043-1354/© 2015 Elsevier Ltd. All rights reserved.

Nomenclature

γ	activity coefficient
ΔH^o	enthalpy change of the reaction
AD	anaerobic digestion
ADM1	anaerobic digestion model no. 1
AER	aerobic zone
AS	activated sludge
ASM1, 2d, 3	activated sludge model no. 1, 2d, 3
ANAER	anaerobic zone
ANOX	anoxic zone
a_i or a_j	activity of the species (i) or component (j)
BSM2	benchmark simulation model no. 2
COD	chemical oxygen demand
D	divalent ion
DAE	differential algebraic equation
Gas_{CH_4}	methane gas production
Gas_{CO_2}	carbon dioxide gas production
Gas_{H_2}	hydrogen gas production
$G(Z_i)$	vector containing the values of the set of implicit algebraic equations ($g_1(z_1, \ldots, z_n)$, …, $g_n(z_1, \ldots, z_n)$)
I	ionic strength
IWA	International water association
J_f	analytical Jacobian of first order partial derivatives $\partial(G_i, \ldots, G_m)/\partial(z_i, \ldots, z_n)$
K_i	equilibrium constant
K_H	henry constant
K_La	oxygen volumetric mass transfer
$K_La_{CO_2}$	carbon dioxide volumetric transfer
M	monovalent ion
MMP	multiple mineral precipitation
N_C	number of components
NR	Newton–Raphson
N_{sp}	number of species
OCI	operational cost index
PCM	physico–chemical model
ODE	ordinary differential equation
R	universal gas constant
SA	simulated annealing
S_{ac} or S_{ac^-}	acetate concentration (total and free component)
S_{Al} or $S_{Al^{+3}}$	aluminium concentration (total and free component)
S_{an}	anion concentration
S_{bu} or S_{bu^-}	butyrate concentration (total and free component)
S_{Ca} or $S_{Ca^{+2}}$	calcium concentration (total and free component)
S_{cat}	cation concentration
S_{C_i}	ith scenario
S_{Cl} or S_{Cl^-}	chloride concentration (total and free component)
S_{IC} or $S_{CO_3^{-2}}$	inorganic carbon concentration (total and free component)
$S^*_{CO_2}$	carbon dioxide saturation concentration
SEC	secondary clarifier
S_{IN} or $S_{NH_4^+}$	inorganic nitrogen concentration (total and free component)
S_{IP} or $S_{PO_4^{+3}}$	inorganic phosphorus concentration (total and free component)
S_{Fe_2} or $S_{Fe^{+2}}$	iron (II) concentration (total and free component)
S_{Fe_3} or $S_{Fe^{+3}}$	iron (II) concentration (total and free component)
S_{H^+}	proton concentration (total and free component)
S_{H_2}	hydrogen concentration
S_{HS} or S_{HS^-}	bisulfide concentration (total and free component)
S_i	species concentration
S_j	component concentration
S_K or S_{K^+}	potassium concentrate (total and free component)ion
S_{Mg} or $S_{Mg^{+2}}$	magnesium concentration (total and free component)
S_{Na} or S_{Na^+}	sodium concentration (total and free component)
S_{NO_2} or $S_{NO_2^-}$	nitrite concentration (total and free component)
S_{NO_3} or $S_{NO_3^-}$	nitrate concentration (total and free component)
S_{pro} or S_{pro^-}	propionate concentration (total and free component)
S_{SO_4} or $S_{SO_4^{-2}}$	sulfate concentration (total and free component)
S_{va} or S_{va^-}	valerate concentration (total and free component)
T	temperature (K)
VFA	volatile fatty acids
WWTP	wastewater treatment plant
X_{MeOH}	metal hydroxides
X_{MeP}	metal phosphates
X_{PHA}	poly-hydroxy-alkanoates
X_{PP}	poly-phosphates
Z_i	vector of equilibrium states ($z_{1,i}, \ldots, z_{n,i}$)

alkalinity state, certainly not for the purposes of inorganic speciation modelling (Batstone et al., 2012).

Processes such as anaerobic digestion (Batstone et al., 2002), high strength wastewater nitrification/denitrification (Hellinga et al., 1999; Jones et al., 2007; Van Hulle et al., 2007; Ganigue et al., 2010), biological phosphorus removal (Serralta et al., 2004; Lopez-Vazquez et al., 2009) and nutrient recovery/multiple mineral precipitation (Musvoto et al., 2000; van Rensburg et al., 2003; Barat et al., 2011; Kazadi Mbamba et al., 2015a; b) require pH calculation since some of the kinetic expressions are acid–base dependent. Indeed, pH is one of the most important variables affecting stoichiometry and kinetics of biological/chemical processes occurring in wastewater treatment plants (WWTPs) (Tchobanoglous et al., 2003) and a key monitored variable due to its ease of measurement. For this reason, future modelling needs, such as plant-wide phosphorus (P) removal, will require a paradigm shift from the traditional alkalinity-based approach towards explicit calculation of pH and consequently a correct description of the aqueous phase chemistry that dictates pH.

When modelling pH, an important point to take into account is computation efficiency. It has been common to formulate pH/weak acid–base models as Ordinary Differential Equations (ODEs) (Stumm and Morgan, 1996; Musvoto et al., 2000; Hauduc et al., 2015). These equations should be tackled simultaneously with the ASM/ADM processes, where time constants differ significantly. Such systems are difficult to handle numerically unless special stiff solvers are used. Nevertheless, stiff solvers are inherently slow or unstable when input disturbances are dynamic, noise is applied or the models contain a mix of continuous and discrete elements (delay/sample and hold blocks, frequently used for example for process control applications) (Copp, 2002; Batstone et al., 2012). As a consequence, model stiffness strongly limits the (practical) application of some of the existing models. The more stochastic or random an input variable behaves, the more problematic is the simulation using a stiff solver. This is due to the structural nature of stiff solvers, which solve for future states implicitly. Stochastic inputs result in a much higher computational effort, since they disrupt both numerical stability and decrease state conformation to the implicit function used. A possible solution is to reduce model stiffness by approximating the fast ODEs as algebraic equations (AE) (Rosen et al., 2006) leaving only the slower ODEs. The obtained implicit algebraic equations can then be handled iteratively by

either a stiff or an implicit algebraic solver.

In order to be useful in a plant-wide context, an aqueous-phase chemistry module needs to predict pH in all process units across a wastewater treatment plant (WWTP, water lines/sludge lines). This is mainly because of the importance of plant-wide modelling/control has been emphasized by the chemical engineering community (Skogestad, 2000). Additionally, the module should be easily compatible with the existing ASM/ADM models and provide pH predictions without structural or mathematical manipulation of the existing models. This should be ensured, independently, by the selected model approach. Options include; 1) a common plant-wide (supermodel) approach (Fairlamb et al., 2003, Grau et al., 2007; Ekama, 2009; Barat et al., 2012; Lizaralde et al., 2015) where the whole plant is described with a common vector of aqueous-phase components; or, 2) an interface-based approach (Nopens et al., 2009; Gernaey et al., 2014) where the state variables of each models are connected by means of specific modules. The first method enables plant-wide commonality and avoids the problem of translation across interfaces, while the second method allows some simplification.

Given that for aquatic chemistry, all processes can potentially occur in all units, we propose a (general) plant-wide aqueous phase chemistry module to describe pH variation and ion speciation/pairing from the simulation outputs of wastewater treatment process models. The module works as a sub-routine and predicts cationic/anionic behaviour and identifies potential pH related problems. The proposed approach, formulated as a set of nonlinear algebraic equations, guarantees computational efficiency, does not increase model stiffness and can be handled by all types of solvers (stiff/non stiff). In addition, a multi-dimensional Newton–Raphson (NR) sub-routine specifically developed to handle algebraic interdependencies enables rapid algebraic solution of very large equation sets. Finally, the presented module is formulated so that it can be directly implemented together with most of the commonly used wastewater process models (ASM, ADM).

The main novelty of this work relies on developing a module that: (1) is generally applicable to any existing ASM/ADM model (as illustrated in this paper); (2) iteratively tracks ionic strength and calculates appropriate ion activity corrections; (3) shows the effect of the most common ion pairs playing a role within wastewater treatment works; (4) takes into account the interactions between biotic and abiotic processes; (5) complements wastewater treatment engineering studies with a rigorous description of cationic/anionic behaviour (pH, speciation, complexation); and finally, (6) integrates all the different elements (physico–chemical/biochemical model) in a single software package. The paper details the development of aqueous-phase plug-and-play module, provides implementation details and then illustrates the performance of the proposed approach with a number of simulated WWTP scenarios using the standard ASM/ADM1 models and also in the BSM2 framework. Lastly, opportunities to use the more rigorous description of the aqueous phase chemistry (as per the module) are proposed.

2. Methods

2.1. General weak-acid base chemistry model

The activated sludge/anaerobic digester aqueous phase composition is represented as a set of chemical entities called species S_i (mol.L^{-1}) and components S_j (mol.L^{-1}). A species is defined as every chemical entity to be considered for the aqueous phase. These can represent protonized/deprotonized states or paired with other ions. For the set of species, a set of components is selected which completely accounts for the molar content of the aqueous phase (that is, all species concentrations can be fully determined from an independent linear combination of component concentrations) (Stumm and Morgan, 1996). The proposed approach considers 19 components: acetate (S_{ac^-}), aluminium ($S_{Al^{+3}}$), ammonium ($S_{NH_4^+}$), butyrate (S_{bu^-}), calcium ($S_{Ca^{+2}}$), carbonate ($S_{CO3^{-2}}$), chloride (S_{Cl^-}), iron (II) ($S_{Fe^{+2}}$), iron (III) ($S_{Fe^{+3}}$), magnesium ($S_{Mg^{+2}}$), nitrate ($S_{NO_3^-}$), nitrite ($S_{NO_2^-}$), phosphate ($S_{PO_4^{-3}}$), potassium (S_{K^+}), propionate (S_{pro^-}), sodium (S_{Na^+}), sulfate ($S_{SO_4^{-2}}$), sulfide (S_{HS^-}) and valerate (S_{va^-}). Note that these component concentrations are different to the total concentrations which in turn are the output of biokinetics models. The number of species considered is almost 120 (a complete list can be found in TS1 within the Supplemental information section). In Table 1, and for exemplary purposes, a representation of the considered species (rows) and how each species can be represented by a linear molar balance combination for the inorganic carbon system (S_{IC}) is shown. A full description of the model components/species can be found in the Supplemental information section (TS2).

The equilibrium equations are formulated as a set of non-linear algebraic equations including one law of mass-action for each species (i) (Eq. (1)) and one mass balance for each component (j) (Eq. (2)) to guarantee the component conservation principle. Species (i) are expressed in a way that can be written as the product of components (j) and the equilibrium constant. In Eq. (1) and Eq. (2), a_i/S_i represents the activity/concentration of the ith species, a_j/S_j is the activity/concentration of the jth component, $\nu_{i,j}$ is the stoichiometric coefficient of the jth component in the ith species (see Table 1), γ is the activity coefficient, K_i is the equilibrium constant, N_{sp} corresponds to the number of species and N_C represents the number of components. Further information about how to include activity corrections in wastewater treatment models can be found in Solon et al. (2015).

$$a_i = K_i \prod_{j=1}^{Nc} a_j^{\nu_{i,j}} \quad i = 1, 2, \ldots, N_{sp} \tag{1}$$

$$S_{j,tot} = S_j + \sum_{i=1}^{N_{sp}} \nu_{i,j} S_i = \frac{a_j}{\gamma} + \sum_{i=1}^{N_{sp}} \nu_{i,j} \frac{a_i}{\gamma} \quad \begin{matrix} j = 1, 2, \ldots, N_C \\ i = 1, 2, \ldots, N_{sp} \end{matrix} \tag{2}$$

The effect of temperature on K_i is corrected for by the constant-enthalpy form of the van't Hoff equation (Stumm and Morgan, 1996). In Eq. (3), K_1 and K_2 are the equilibrium constants at temperatures T_1 and T_2 (in K), respectively, ΔH^o is the enthalpy change of the reaction and R is the universal gas constant.

$$\ln \frac{K_2}{K_1} = \frac{\Delta H^o}{R} \left(\frac{1}{T_1} - \frac{1}{T_2} \right) \tag{3}$$

Full specification of the algebraic equation set requires an additional equation, which can be resolved by the charge balance (Batstone et al., 2002), as shown in Eq. (4):

$$\sum S_{cat} - \sum S_{an} = 0 \tag{4}$$

where S_{cat} and S_{an} represent the total equivalent concentrations of cations and anions, respectively, which are the concentrations of respective ions multiplied by their valence. An alternative is to use a proton balance (Morel and Hering, 1993), which generates the same equation set, but with a different structure (see for example Harding et al., 2011 and Ikumi et al., 2011), and gives near identical model results (Solon et al., 2015).

Table 1
Stoichiometric matrix of the carbonate-component system (S_j) and the considered species (S_i).

I/j	Formula	$S_{CO_3^{-2}}$	$S_{Al^{+3}}$	$S_{Ca^{+2}}$	$S_{Fe^{+2}}$	$S_{Mg^{+2}}$	$S_{Na^{+}}$	log K_i	ΔH^0
$S_{CO_3^{-2}}$	CO_3^{-2}	1						0	0
$S_{Al^{+3}}$	Al^{+3}		1					0	0
$S_{Ca^{+2}}$	Ca^{+2}			1				0	0
$S_{Fe^{+2}}$	Fe^{+2}				1			0	0
$S_{Mg^{+2}}$	Mg^{+2}					1		0	0
$S_{Na^{+}}$	Na^{+}						1	0	0
$S_{Al_2(OH)_2CO_3^{+2}}$	$Al_2(OH)_2CO_3^{-2}$	1	2					4.31	0
$S_{CaCO_3(aq)}$	$CaCO_3$ (aq)	1		1				3.22	16
$S_{CaHCO_3^{+}}$	$CaHCO_3^{+}$	1		1				11.434	0
$S_{FeHCO_3^{+}}$	$FeHCO_3^{+}$	1			1			11.429	0
$S_{H_2CO_3}$	H_2CO_3	1						16.681	−32
$S_{HCO_3^{-}}$	HCO_3^{-}	1						10.329	−14.6
$S_{Mg_2CO_3^{+2}}$	$Mg_2CO_3^{+2}$	1				2		3.59	0
$S_{MgCO_3(aq)}$	$MgCO_3$ (aq)	1				1		2.92	10
$S_{MgHCO_3^{+}}$	$MgHCO_3^{+}$	1				1		11.34	−9.6
$S_{NaCO_3^{-}}$	$NaCO_3^{-}$	1					1	1.27	−20.35
$S_{NaHCO_3(aq)}$	$NaHCO_3$ (aq)	1					1	10.029	−28.33

2.2. Implementation details

The mathematical formulation of the physic-chemical model results in a mixed system of nonlinear algebraic equations (AE) and ordinary differential equations (ODEs) that have to be solved using a suitable numerical method. Such equation sets are commonly referred to as differential algebraic equations (DAEs) and this set simultaneously computes the continuum concentrations of all reacting species as a function of time. The proposed method solves the differential equations separately with an explicit ODE solver, and handles the nonlinear algebraic system using an iterative approach, in this case a multi-dimensional version of the Newton–Raphson method (Press et al., 2007).

$$Z_{i+1} = Z_i - J_F(Z_i)^{-1}\ G(Z_i) \tag{5}$$

where Z_i is the vector of equilibrium states ($z_{1,i}$,…, $z_{n,i}$) obtained from the previous iteration step i, $G(z_i)$ is a vector containing the values of the set of implicit algebraic equations ($g_1(z_i,\ldots, z_n)$ …,$g_n(z_i,\ldots, z_n)$), which has to be zero in order to satisfy the equilibrium. The full analytical Jacobian (J_F) is used for calculation of the new state values, which requires symbolic manipulation of the algebraic equations in order to obtain the matrix of all first-order partial derivatives $J=\partial(g_i,\ldots,g_n)/\partial(z_i,\ldots,z_n)$. A numerical Jacobian was found to be less convergent but is included in the code provided. The iteration is repeated as long as the elements of the error function are larger than the absolute tolerance, which in our case is set to 10^{-12}. Eq. (5) is used to solve the equilibrium set presented in Eq. (2), and the charge balance in Eq. (4) is used for calculation of ionic strength (I) and activity corrections (γ). As a result, the implementation can be easily simulated and combined with ASM/ADM while ensuring convergence and without significantly reducing simulation speed.

This method is re-enforced with the Simulated Annealing (SA) algorithm. The SA is used when the solution of the gradient (Eq (5)) is not a number or the calculated algebraic is negative. The SA is a generic probabilistic metaheuristic for the global optimization problem of locating a good approximation to the global optimum of a given function in a large search space. At each step, the SA heuristic considers some neighbouring state of the current state, and probabilistically decides between moving the system to new state or staying in at the same. These probabilities ultimately lead the system to move to states of lower energy. Typically this step is repeated until the system reaches a state that is good enough for the application, or until a given computation budget has been exhausted. (Press et al., 2007).The MINTEQ geochemical program (Allison et al., 1991) is used as a reference for verification purposes (see Supplemental information section 3).

2.3. Wastewater treatment plants under study

Three benchmark wastewater treatment plant models are considered in this study (see schematic representation in Fig. 1). Firstly, a nitrogen (N) removal plant (*WWTP1*) consisting of five reactors in series and one secondary sedimentation tank (SEC) is investigated. Tanks 1 and 2 are anoxic (ANOX1, 2) while tanks 3, 4 and 5 (AER1, 2 and 3) are aerobic. AER3 and ANOX1 are linked by means of an internal recycle (Q_{INTR}). Two cases are considered, where the behaviour of *WWTP1* is described using ASM1 and ASM3 (Henze et al., 2000), respectively. Secondly, a combined N and phosphorus (P) removal plant (*WWTP2*) is studied, where two additional anaerobic reactors (ANAER1, 2) are added ahead of *WWTP1*. The *WWTP2* plant has the same operational settings as *WWTP1*. In this case, the selected biological model is ASM2d (Henze et al., 2000). The secondary settler of both *WWTP1* and *WWTP2* is modelled using the double exponential function of Takács (Takács et al., 1991) combined with a reactive 10-layer pattern (Flores-Alsina et al., 2012). *WWTP3* has the same configuration as the Benchmark Simulation Model No. 2 (BSM2) (Gernaey et al., 2014). The activated sludge section has the same characteristics as *WWTP1*. The BSM2 plant further contains a primary clarifier, a sludge thickener, an anaerobic digester, a storage tank and a dewatering unit. The anaerobic digestion process is modelled using the Anaerobic Digestion Model No. 1 (ADM1) (Batstone et al., 2002). Additional information about the plant design, operational conditions and process models of the BSM2 platform is given in Gernaey et al. (2014).

2.4. Interfacing ASM1, 2d and 3 with the aqueous phase chemistry model

The default implementation of the three ASM models (ASM1, 2d and 3) had to be adjusted in order to include the ion speciation/pairing model. These are the main modifications:

- The ASM alkalinity state (S_{ALK}) is removed and inorganic carbon (S_{IC}) used instead. The S_{IC} is modelled as a source-sink compound to close the mass balances (inorganic carbon pool).

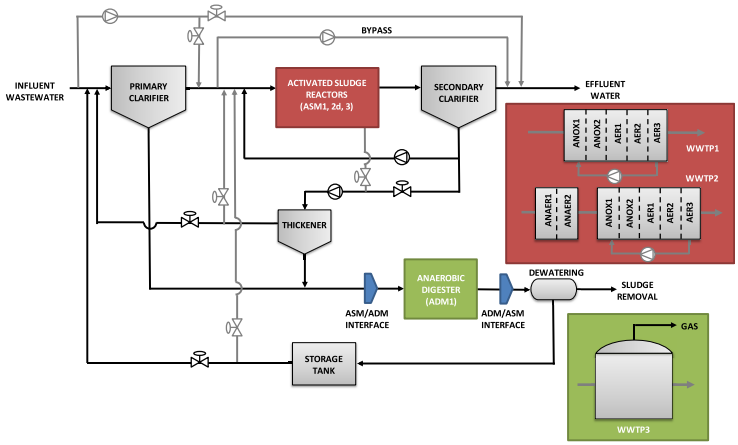

Fig. 1. Flow diagram of the wastewater treatment plants under study.

Hence, the C, N, P, O and H content of all state variables in all models is assumed known in order to calculate the mass of each element per mass of COD. Composition for the different ASMs is taken from Reichert et al. (2001).

- Phosphorus (P) is introduced in the same way in ASM1 and 3 (non-reactive).
- Carbon dioxide stripping needs to be included. Specific CO_2 volumetric mass transfer ($K_La_{CO_2}$) is calculated from the oxygen volumetric mass transfer (K_La) multiplied by the square root of the ratio between O_2 and CO_2 diffusivities. K_H (Henry coefficient) is corrected for temperature via the van't Hoff equation to correctly estimate the saturation concentration (S^*_{CO2}) (Wett and Rauch, 2003).
- The role of S_K and S_{Mg} should be explicitly described and subjected to process dynamics when modelling formation/release of poly-phosphates (X_{PP}) in the ASM2d. For stoichiometric considerations, poly-phosphates are assumed to have the composition $(K_{0.33}Mg_{0.33}PO_3)_n$ (Henze et al., 2000).
- Chemical precipitation using metal hydroxides (X_{MeOH}) and metal phosphates (X_{MeP}) is omitted since 1) kinetic expressions are alkalinity dependant (and this has been removed) and 2) those processes are not present in ASM1. Precipitation can be included by the compatible generalised kinetic precipitation model described in (Kazadi Mbamba et al., 2015a; b).

Once the three ASM models are adjusted, the outputs of the ASM models at each integration step are used as inputs for the aqueous-phase module to estimate pH from inorganic carbon (S_{IC}), inorganic nitrogen (S_{IN}), inorganic phosphorus (S_{IP}), acetate (S_{ac}), potassium (S_K), magnesium (S_{Mg}) and nitrate (S_{NO_3}). Additional cations (S_{cat}) and anions (S_{an}) are also included as tracked soluble/non-reactive states. Therefore, S_{cat} is defined as: Aluminium (S_{Al}), calcium (S_{Ca}), iron (II) ($S_{Fe2.}$), iron (III) (S_{Fe3}) and sodium (S_{Na}). S_{an} is represented by: butyrate (S_{bu}), chloride (S_{Cl}), nitrite (S_{NO_2}), propionate (S_{pro}), sulfate (S_{SO_4}), bisulfide (S_{HS}) and valerate (S_{va}). These ions will have future use for describing precipitation, other model formulations (ADM1), additional biochemical model extensions (sulphate reducing bacteria, iron reducing bacteria) or simply to adjust pH/ionic strength.

2.5. Interfacing ADM1 with the aqueous phase chemistry model

Similarly to ASM1, 2d and 3, the ADM1 is slightly modified to allow seamless interfacing. The original pH solver proposed by Rosen et al. (2006) is substituted by the approach presented in this paper. Since the ADM1 only considers organics (as COD), C, and N, P is also included using a source-sink approach similar to ASM1 and ASM3 (non-reactive). C, N, P, O and H fractions are taken from Huete et al., 2006 and De Gracia et al. (2006). The ADM state variables used for pH calculation are inorganic carbon (S_{IC}), inorganic nitrogen (S_{IN}), inorganic phosphorus (S_{IP}), acetate (S_{ac}), propionate (S_{pro}), valerate (S_{va}) and butyrate (S_{bu}). Finally the original ADM1 pools of undefined cations (S_{cat}) and anions (S_{an}) are substituted for specific compounds (see above). In this particular study, S_{cat} and S_{an} are also considered to be non-reactive. However, current research is ongoing to explicitly consider these elements by including biological P, S and Fe interactions as well as multiple mineral precipitation (MMP). This will be presented in a separate manuscript in the case of the ADM1 (Flores-Alsina et al., 2015).

3. Results

3.1. pH predictions in the influent wastewater

The pH predictions of the proposed aqueous phase chemistry model for the influent wastewater composition are illustrated in Fig. 2 (=influent cationic loads are identical for ASM1, 2d and 3 and can be found in Supplemental information section 3). Specifically, Fig. 2a shows pH dynamic values for a time span of one week using the BSM1 influent file (Copp, 2002). Simulation results in Fig. 2a (weekly) show that pH has a clear daily variation and follows the same profile as inorganic nitrogen (S_{IN}), inorganic phosphorus (S_{IP}) and acetate (S_{ac}) in the influent. These (ionic) profiles are defined according to the principles described in Gernaey et al. (2011). However, only a households (HH) contribution is assumed for inorganic carbon (S_{IC}), potassium (S_K), magnesium (S_{Mg}), calcium (S_{Ca}), sodium (S_{Na}), chloride (S_{Cl}) and sulfate (S_{SO_4}) loads.

The pH profile represents a general pollutant behaviour, namely one morning peak, one evening peak, and late night and mid-day

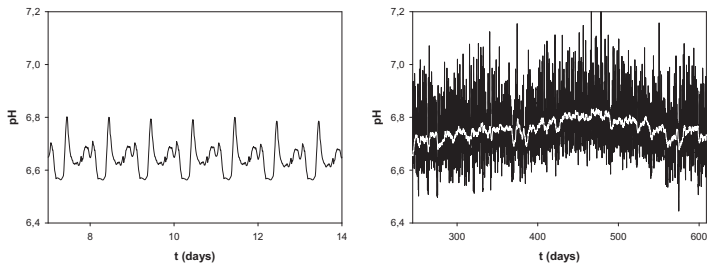

Fig. 2. Influent wastewater pH predictions using two different influent profiles: 1) a 7 days BSM1 influent file (short term) and 2) a 365 days BSM1 LT influent file (long term). An exponential smoothing filter (time constant = 3 day) is used in (b) to improve visualization of the data (in white). Influent wastewater composition is identical in the three evaluated cases (ASM1, ASM2d and ASM3).

minima. The morning and the evening peaks represent the residents going to or returning from work. The late night minimum corresponds to the sleeping hours with limited water consumption (Butler et al., 1995; Flores-Alsina et al., 2014; Martin and Vanrolleghem, 2014). The presented pattern corresponds to the pH experimental observations by Sharma et al. (2013) and Alferes 2014a, b & c.

With respect to the ionic speciation/pairing (see Fig. 3), only 2.35% of the available inorganic carbon (S_{IC}) is complexed with cations, such as Ca ($S_{CaCO_3(aq)}$, $S_{CaHCO_3^+}$), Mg ($S_{MgCO_3(aq)}$, $S_{MgHCO_3^+}$) and Na ($S_{NaCO_3^-}$, $S_{NaHCO_3(aq)}$). The dominant species (and consequently determining pH) are $S_{HCO_3^-}$ and S_{H_2CO3*} with 70.61% and 27.01%, respectively. $S_{CO_3^{-2}}$ is negligible. The same holds true for inorganic nitrogen (S_{IN}), where less than 1% is paired in the form of ammonium sulfate ($S_{NH_4SO_4^-}$) or with metallic cations ($S_{Ca(NH_3)_2^{+2}} + S_{CaNH_3^{+2}} + S_{Mg(NH_3)_2^{+2}}$). It is important to highlight that ($S_{NO_3^-}$) is not present in the influent (see white cells in Fig. 3). Inorganic phosphorus (S_{IP}) is mostly observed as $S_{HPO_4^{-2}}$ and $S_{H_2PO_4^-}$ (25.47% and 51.04%, respectively), with the remainder being distributed amongst Ca ($S_{CaHPO_4\ (aq)}$ $S_{CaPO_4^-}$), Mg ($S_{MgHPO_4\ (aq)}$, $S_{MgPO_4^-}$) and marginally with Na and K ($S_{Na_2HPO_4\ (aq)}$, $S_{Na_2PO_4^-}$, $S_{K_2HPO_4\ (aq)}$, $S_{K_2PO_4^-}$, amongst other compounds). A very small fraction remains as free phosphate ($S_{PO_4^{-3}}$). 74.51% of the sulfate is in the free-form ($S_{SO_4^{-2}}$) with the remainder 25.49% is soluble pairs with (in descending order of prominence) Ca ($S_{CaSO_4\ (aq)}$), Mg ($S_{MgSO_4\ (aq)}$), Na/K ($S_{NaSO_4^-}$, $S_{KSO_4^-}$) and ammonium ($S_{NH_4SO_4^+}$). Organic acids like acetate are mostly found in a protonated/deprotonated (S_{H-ac}/S_{ac^-}) form (95%), with the minor remainder being paired with calcium (S_{Ca-ac^+}), magnesium (S_{Mg-ac^+}) and potassium (S_{K-ac}).

Fig. 2b (yearly data) shows the effects of influent wastewater seasonal temperature on the aqueous-phase chemistry (Gernaey et al., 2014). Simulation results show a slight increase of pH

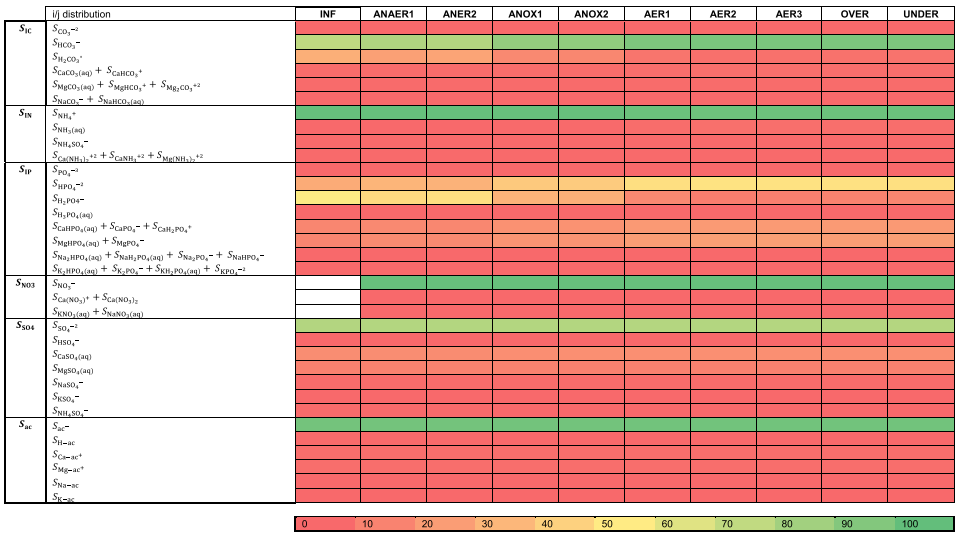

Fig. 3. Distribution of the different C, N, P, S and acetate related species/ion pairs in the different sections of *WWTP2*.

during summer time. This is mainly due to a lower concentration of free calcium ($S_{Ca^{+2}}$) and magnesium ($S_{Mg^{+2}}$) at higher temperatures and the increase of their paired forms with carbonate ($S_{CaCO_3(aq)}$, $S_{CaHCO_3^+}$, $S_{MgCO_3(aq)}$, $S_{MgHCO_3^+}$) or sulfate ($S_{CaSO_4\ (aq)}$, $S_{MgSO_4\ (aq)}$). As a result, there is a reduction in cationic charge which then requires a higher concentration of free protons (S_{H^+}) to uphold the charge balance, and overall this effect depresses pH.

The reader should be aware that some of the assumptions behind the constructed cationic profiles are quite simple (they are assumed to be constant). We are well aware that the potassium profile follows a similar profile as S_{IN} (it has basically human origin). On the other hand, we also know that in cold areas, there are sudden increases of sodium (S_{Na})/Calcium (S_{Ca}) and chloride (S_{Cl}) when salt is added as (chemical) de-icing method on roads. The latter affects conductivity, which otherwise is quite constant. Nevertheless, we did not want to focus the study on such effects (there is enough material/discussion to make a separate study). The one thing that should be noted is that the pH module presented in this paper would do exactly the same job. In other words, with more sophisticated ion profiles, the calculation method will be the same, and the resulting pH profile will be different.

3.2. pH predictions in WWTP1 & 2

The results of implementing the aqueous phase chemistry model in ASM1 and ASM3 using *WWTP1* are depicted in Fig. 4. In the anoxic zone (ANOX1 and 2) biological oxidation of organic substrates (S_{ac}) using nitrate (S_{NO_3}) as electron acceptor takes place. As a result S_{NO_3} is converted to nitrogen gas (S_{N_2}), removing an anion (i.e., strong acid), and thereby increasing pH. In the aerobic zone (AER1, 2 and 3) the organic acids (S_{ac}) and ammonium (S_{IN}) are oxidized to inorganic carbon (S_{IC}) and NO_3, respectively, both of which cause a net pH decrease (production of a weaker acid S_{IC} from the acid S_{ac} and acid S_{NO_3} from the base S_{IN}). Nevertheless, the aeration in AER1, AER2 and AER3 promotes stripping of carbon dioxide (Gas_{CO2}) which consequently causes a rise of pH. Note that aeration in AER3 is less intense compared to AER1 and 2, therefore the pH rise in that reactor is also lower. The effect of including an additional anaerobic section is also depicted in Fig. 4. Under these conditions, the uptake of organic acids (S_{ac}) produces poly-hydroxy-alkanoates (X_{PHA}). Concurrent with S_{ac} reduction, there is a release of inorganic phosphorus (S_{IP}) as well as free potassium (S_K) and magnesium (S_{Mg}) ions, which results from the decay of poly-phosphates (X_{PP}). As a consequence, there is a decrease of pH in ANAER2. A similar pattern as described for *WWTP1* also holds for the anoxic and aerobic zones in *WWTP2* (further information can be found in Supplemental information section 3). Note that the authors have defined a relatively high influent inorganic carbon (S_{IC}) to see the effects of stripping through the different activated sludge units. A lower S_{IC} would reduce these differences. In all cases (*WWTP1 & 2*) and for the three models (ASM1, 2d and 3) the oxidation of S_{ac} and S_{IN} (with no stripping), slightly decreases pH at the top of the clarifier (OVER). At the bottom of the clarifier (UNDER), in the systems without biological P removal, the extra denitrification in the reactive settler model increases pH as described above for anoxic conditions. On the other hand, when there is bio-P removal, and consequently P release, pH is predicted to decrease. Simulation results correspond well with the experimental observations of Serralta et al. (2004).

Fig. 3 shows that there are no large variations in the species distribution of *WWTP2*. It is only at the end of the aerobic section (AER3) that the pH increase (noted above) causes important changes in the ionic speciation of carbonate (S_{IC}) and phosphate (S_{IP}). Specifically, most of the inorganic carbon (92.51%) is in $S_{HCO_3^-}$ form ($S_{H_2CO_3^*}$ is stripped) near neutral pH, while the quantity of phosphate paired with metallic ions ($S_{CaHPO_4\ (aq)}$ $S_{CaPO_4^+}$, $S_{MgHPO_4\ (aq)}$, $S_{MgPO_4^+}$, $S_{Na_2HPO_4\ (aq)}$, $S_{Na_2PO_4^-}$, $S_{K_2HPO_4\ (aq)}$, $S_{K_2PO_4^-}$, ...) changes from 22.50% in the influent to 40.09% in AER3 Nitrate ($S_{NO_3^-}$) is present in the different sections of the bioreactors, but 99% is in the free form and less than 1% is paired with metallic cations. No substantial differences can be observed in the nitrogen system (S_{IN}), sulfate system (S_{SO_4}) and the distribution of organic acids (S_{H-ac}/S_{ac^-}).

3.3. pH predictions in WWTP3

The last case study shows the same model framework implemented in the BSM2 version (Gernaey et al., 2014) of the ADM1 (Batstone et al., 2002). Influent characteristics in the water line are defined in Gernaey et al. (2011). The interfaces proposed by Nopens et al. (2009) are used to convert ASM1 into ADM1 state variables. Fig. 5 shows a dynamic pH profile within the anaerobic digester using a 365 day influent file. Simulation results show that pH variation has been dramatically attenuated compared to the influent file of the water line (Fig. 2). This is mainly due to the smoothing effect that the different units of the flow diagram have on the dynamic profile (see Section 2.3). Another important point is that no seasonal variation due to temperature can be observed.

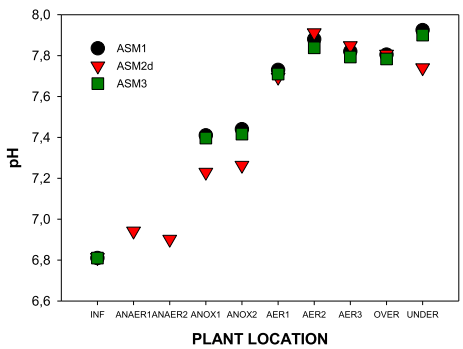

Fig. 4. pH predictions in the different units for *WWTP1* and *WWTP2* using ASM1, 2d and 3. In ASM1 and 3 an approximate 40% of readily biodegradable substrate (S_S) is assumed to be acetate S_{ac}.

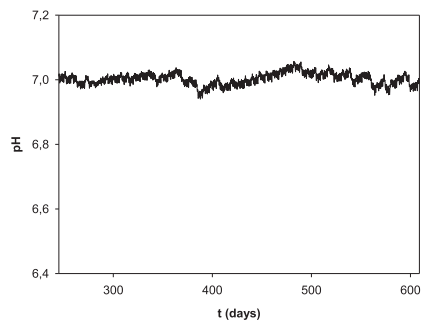

Fig. 5. pH predictions within the AD using the 365 days BSM2 influent data (after the water line).

Indeed, in this system, temperature is regulated at 35 °C and as a consequence there is no variation in the equilibrium constant (Eq. (3)). Additional information can be found in Supplemental information section 3.

The study further evaluates the behaviour of *WWTP3* when increasing the cationic load. The objective of this additional exercise is to show the impact that monovalent/divalent ion pairing can have on the predicted overall process performance. Thus, an additional waste stream with a constant flow rate of 5 $m^3.day^{-1}$ is included. The cationic influent concentrations range from 0 to 2.5 mol L^{-1}, which leads to five additional scenarios to be evaluated (SC1, SC2, SC3, SC4 and SC5). The cationic loads are (equally) distributed either into sodium (Na) and potassium (K) (monovalent) or calcium (Ca) and magnesium (Mg) (divalent). A series of simulations are re-run to see the overall effect on 1) species distribution, and 2) biogas production.

Fig. 6 illustrates the variation in the species distribution for the default case (D1) and for the five different scenarios. From the generated results, the reader may notice that the highest differences can be observed within the carbon (S_{IC}) and phosphorus (S_{IP}) systems. Fig. 6 shows substantial changes in $S_{HCO_3^-}$ depending on whether monovalent (M) (4.42%) or divalent (D) (13.58%) cations are added for the different scenarios (SC1, …, SC5) (= different ion pairs). This is mainly due to the stronger affinity of calcium and magnesium cations for carbonate ($S_{CaCO_3(aq)}$, $S_{CaHCO_3^+}$, $S_{MgCO_3(aq)}$, $S_{MgHCO_3^+}$) compared to sodium ($S_{NaCO_3^-}$, $S_{NaHCO_3(aq)}$) and potassium. The effect of ion pairing with inorganic carbon compounds also has important consequences for the different digestion products. Another important effect can be observed in the phosphorus system (S_{IP}). Again, the preferential binding of Ca and Mg ($S_{CaHPO_4(aq)}$, $S_{CaPO_4^-}$, $S_{MgHPO_4(aq)}$, $S_{MgPO_4^-}$, …) with phosphorus anions compared to Na and K ($S_{Na_2HPO_4(aq)}$, $S_{Na_2PO_4^-}$, $S_{K_2HPO_4(aq)}$, $S_{K_2PO_4^-}$, …) modifies the whole system's weak acid–base chemistry. Important differences can be observed between quantities of available (free) phosphate when monovalent or divalent cations are included with respect to the initial conditions. Hence, in the default situation 100% of P is distributed between $S_{HPO_4^{-2}}$ and $S_{H_2PO_4^-}$ acting as a pH buffer. This ratio is changed dramatically depending on whether monovalent (up to 80.82%) or divalent (up to 30.18%) cations are added.

Another important aspect that the model is considering is illustrated in Fig. 7. Results show a substantial reduction of Gas_{CO2} stripping at high divalent cationic loads (S5_D) compared to a similar scenario but with monovalent cationic loads (S5_M). This is attributed to the effect of ion pairing (Na/K versus Ca/Mg) and the resulting modifications of the $S_{HCO_3^-}/S_{H_2CO_3^*}$ ratio. Methane production (Gas_{CH4}) is not affected.

It is important to highlight that a plant wide context exposes limitations in the base ASM and ADM1 implementations (Batstone et al., 2002). Specifically, sulphur and phosphorous were not included in the ADM1. Recent investigation revealed the important role that phosphorus accumulating organisms (PAO) might have on the anaerobic digester (Ikumi et al., 2014), causing dynamic release of phosphate and metals, which as we have shown is a highly important chemical in the system. It is also well known that sulfate can potentially be reduced to sulfide (S_{H_2S}) under anaerobic conditions, and sulfide is extremely important as a pairing, buffer, and gas-active compound (Batstone et al., 2012). This extends to

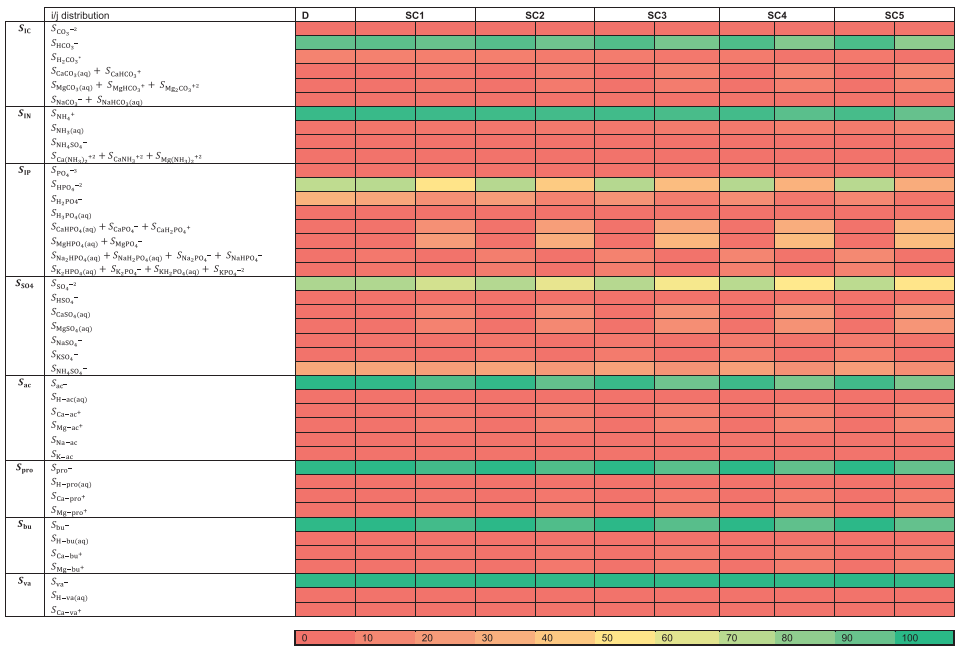

Fig. 6. Distribution of the different C, N, P, S and VFA related species/ion pairs for the different scenarios evaluated for *WWTP3*.

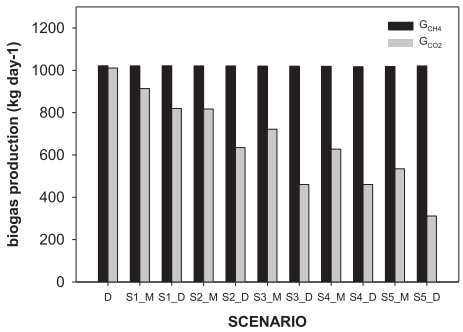

Fig. 7. Effect of (monovalent/divalent) ion pairing on the anaerobic digestion products for different cationic loads.

biology, since sulfate reducers outcompete methanogens for hydrogen (S_{H_2}). Second of all, there will be a decrease of aceticlastic and hydrogenotrophic methanogensis due to S_{H_2S} inhibition (Fedorovich et al., 2003; Barrera et al., 2014; Batstone, 2006). Finally, it must be taken into account that precipitation processes are not included (Musvoto et al., 2000; van Rensburg et al., 2003; Barat et al., 2011; Kazadi Mbamba et al., 2015a; b). Excluding the precipitation process while including the calcium ($S_{Ca^{+2}}$) ions as cations causes: (1) the model to generally over-predict pH because of ion precipitation; (2) the model to over-predict carbon dioxide gas production and the concentrations of inorganic carbon in aqueous solutions, since the latter is complexed during precipitation; and, (3) faster physico-chemical dynamics in the model in general, since the system is dynamically buffered by precipitates (e.g., $CaCO_3$, $CaPO_4$), with slow precipitation kinetics (Batstone et al., 2002). Nevertheless, the examples presented in this study, even though incomplete, are illustrative and useful to demonstrate the effect of ion pairing and consequently the capabilities of the proposed approach for implementing the aqueous phase chemistry module to describe these phenomena.

4. Discussion

4.1. General applicability of the proposed approach

The study presented in this manuscript demonstrates the general applicability of the aqueous phase chemistry module by providing guidelines on how to implement the presented approach into some of the most widespread ASM/ADM process models following a set of simple rules (Section 2.4 and 2.5). Nevertheless, it is important to highlight that the pH/speciation model described in this paper could also be implemented in combination with other models, such as the Bio-P module of the ASM3 (Rieger et al., 2001), the Technical University of Delft (TUD) extension of ASM2d (Meijer, 2004), the Barker and Dold model (Barker and Dold, 1997) and the UCTPHO model (Hu et al., 2007). In addition, predictions of nitrification-denitrification models (Hellinga et al., 1999; Ganigue et al., 2010) could be improved by the consideration of activity corrections (Batstone et al., 2012). For anaerobic digestion, the model is not just limited to ADM1. The weak acid–base model could also be linked to models presented by Siegrist et al. (2002) and Sötemann et al., 2006. Last but not the least, the model could also be included in sewer models (Sharma et al., 2013; Gernaey et al., 2011; Saagi et al., 2015) which already address the relevant sulphur and iron transformations. Since it is broadly independent of the biological processes, it is applicable to any process where active compounds are explicitly calculated.

4.2. pH dependency in ASM/ADM models

Many (bio)chemical processes are affected by pH. Nevertheless, it is only in the anaerobic digestion model that pH dependency equations have been included thus far (Batstone et al., 2002; Rosen et al., 2006). Additional equations describing how pH affects the bio-P processes could be added (Serralta et al., 2004). Another possibility is to use the speciation model to estimate free ammonia (S_{NH_3}) and free nitrous acid (S_{HNO_2}). These two species are absolutely necessary to correctly describe high strength nitritation/nitratation processes separately with ammonia-oxidising bacteria (X_{AOB}) and nitrite-oxidising bacteria (X_{NOB}). The latter has a crucial effect when one aims at describing and predicting nitrous oxide emissions correctly (Hiatt and Grady, 2008; Ni et al., 2014; Snip et al., 2014; Lindblom et al., 2014).

4.3. Precipitation model

The most immediate application of the module presented in this paper is the link with a precipitation framework. Numerous studies have stressed the need to correctly characterize ionic behaviour in order to correctly describe precipitation (Musvoto et al., 2000; van Rensburg et al., 2003; Barat et al., 2011; Hauduc et al., 2015; Kazadi Mbamba et al., 2015a; b). This is mainly due to the fact that many precipitation kinetic expressions are based on an estimated saturation index (*SI*). *SI* represents the logarithm of the ratio between the product of the different activities (a_j) and the solubility product constant (K_{sp}). The proposed aqueous-phase chemistry module provides all the necessary inputs to continuously track ionic strength and SI values for various minerals.

4.4. Model verification and experimental validation

The implementation of this general module has been verified (ring-tested) using the widely used software package MINTEQ. MINTEQ is a freeware chemical equilibrium model for the calculation of metal speciation, solubility equilibrium, sorption and other relevant chemistry in natural waters. pH values, ionic strength calculation and the composition of the selected compounds from the aqueous-phase chemistry module have been compared with MINTEQ outputs for three different cases. In all cases, differences between the proposed approach and MINTEQ are observed to be lower than 1% and are mainly due to numerical uncertainty when working with low absolute concentrations (see Supplemental information section 3). In addition, the proposed aqueous-phase chemistry module has been experimentally validated in two different studies (Kazadi Mbamba et al., 2015a; b). In these studies, the approach presented was linked to a general precipitation model and was used to predict pH variation and cationic/anionic behaviour for different types of experiments (titration, aeration) and samples (synthetic, anaerobic digestion sludge). Simulations showed that the aqueous-phase chemistry module is successfully able to reproduce those experimental results (Kazadi Mbamba et al., 2015a; b)

4.5. Solving routines and numerical issues

The present study proposes a major advance in handling complex numerical issues in wastewater treatment models. Indeed, for the first time in the wastewater field, a solver routine has been developed and implemented that is capable of handling

combinations of ODEs and DAEs with multiple interdependencies. In the original approach developed by Rosen et al. (2006), the algebraic states were solved sequentially, which did not work with interdependencies, as only the last algebraic equation to be solved would end up converging. The method developed in this study is able to evaluate the full Jacobian and use that to simultaneously make all equations converge (Section 2.2). The latter involves the use of symbolic information in order to calculate a matrix of partial derivatives, which substantially increases the complexity of the whole implementation. However, the solution is more robust and yields improved performance compared to the sequential approach or an approach based on a numerical Jacobian. In addition, the method is reinforced with the Simulated Annealing algorithm to increase the robustness of the solver and making the system not so dependant of the initial conditions. Indeed, the SA is used when the solution of the gradient (Eq (5)) is not a number or the calculated algebraic is negative. As a result, the implementation can be easily simulated and combined with ASM/ADM while ensuring convergence and without significantly reducing simulation speed.

5. Conclusions

The key outcomes can be summarized as follows:

1) The presented approach is a versatile/general module that can be easily added to different ASM/ADM models.
2) pH and ionic speciation/pairing are reliably predicted under anaerobic, anoxic and aerobic conditions in both ASM and ADM models.
3) The computing routine developed in this study (Newton Rapshon/Simulated Annealing) allows the simultaneous simulation of ODEs and DAEs with multiple algebraic inter-dependencies using different types of solvers (stiff/non stiff).
4) Wastewater modelling studies can be complemented with a rigorous description (speciation) of the inorganic species. Thus, it is possible to visualize the changes in the inorganic species when anaerobic, anoxic or aerobic conditions are modified.
5) The presented approach is a starting point upon which additional models, such as multiple mineral precipitation, can be developed.

6. Software availability

The MATLAB/SIMULINK code containing the implementation of the physico–chemical modelling framework in ASM1, 2d,3 and ADM1 implemented in the *WWTP1, 2 & 3* scenarios presented in this manuscript is available upon request. Using this code, interested readers will be able to reproduce the results summarized in this study. Please contact Prof. Ulf Jeppsson (ulf.jeppsson@iea.lth.se) at Lund University (Sweden) or Prof. Damien Batstone (damienb@awmc.uq.edu.au) at The University of Queensland (Australia).

Acknowledgements

Ms Solon and Dr Flores-Alsina acknowledge the Marie Curie Program of the EU 7th Framework Programme FP7/2007–2013 under REA agreement 289193 (SANITAS) and 329349 (PROTEUS) respectively. This research was also supported financially by the University of Queensland through the UQ International Scholarships (UQI) and UQ Collaboration and Industry Engagement Fund (UQCIEF). The International Water Association (IWA) is also acknowledged for their promotion of this collaboration through their sponsorship of the IWA Task Group on Generalized Physicochemical Modelling Framework (PCM). A concise version of this paper was submitted to be presented at the IWA 9th IWA Symposium on Systems Analysis and Integrated Assessment, 14–17 June, Gold-Coast, Australia.

Appendix A. Supplementary data

Supplementary data related to this article can be found at http://dx.doi.org/10.1016/j.watres.2015.07.014.

References

Alferes, J., Copp, J.B., Vanrolleghem, P.A., 2014a. Forecasting techniques applied to water quality time series in view of water quality assessment. In: Proceedings 11th International Conference on Hydroinformatics (HIC 2014). New York, NY, USA, August 17-21 2014.
Alferes, J., Copp, J., Weijers, S., Vanrolleghem, P.A., 2014b. Innovative water quality monitoring: automation of data collection and data assessment in practical scenarios. In: Proceedings IWA World Water Congress 2014. Lisbon, Portugal, September 21-26 2014.
Alferes, J., Lamaire-Chad, C., Chhetri, R.K., Thirsing, C., Sharma, A.K., Mikkelsen, P.S., Vanrolleghem, P.A., 2014c. Advanced monitoring of wastewater quality: data collection and data quality assurance. In: Proceedings 13th International Conference on Urban Drainage (13ICUD). Sarawak, Malaysia, September 7-12 2014.
Allison, J.D., Brown, D.S., Novo-Gradac, K.J., 1991. MINTEQA2/PRODEFA2, a Geochemical Assessment Model for Environmental Systems: Version 3.0 User's Manual. Environmental Research Laboratory, Office of Research and Development, US Environmental Protection Agency, Athens, GA. EPA/600/3–91/021.
Barat, R., Montoya, T., Seco, A., Ferrer, J., 2011. Modelling biological and chemically induced precipitation of calcium phosphate in enhanced biological phosphorus removal systems. Water Res. 45 (12), 3744–3752.
Barat, R., Serralta, J., Ruano, V., Jimenez, E., Ribes, J., Seco, A., Ferrer, J., 2012. Biological nutrient removal no 2 (BNRM2): a general model for wastewater treatment plants. Water Sci. Technol. 67 (7), 1481–1489.
Barrera, E.L., Spanjers, H., Solon, K., Amerlinck, Y., Nopens, I., Dewulf, J., 2014. Modeling the anaerobic digestion of cane-molasses vinasse: extension of the anaerobic digestion model No. 1 (ADM1) with sulfate reduction for a very high strength and sulfate rich wastewater. Water Res. 71, 42–54.
Barker, P.S., Dold, P.L., 1997. General model for biological nutrient removal activated-sludge systems: model presentation. Water Environ. Res. 69 (5), 969–984.
Batstone, D.J., Amerlinck, Y., Ekama, G., Goel, R., Grau, P., Johnson, B., Kaya, I., Steyer, J.-P., Tait, S., Takács, I., Vanrolleghem, P.A., Brouckaert, C.J., Volcke, E.I.P., 2012. Towards a generalized physicochemical framework. Water Sci. Technol. 66 (6), 1147–1161.
Batstone, D.J., 2006. Mathematical modelling of anaerobic reactors treating domestic wastewater: rational criteria for model use. Rev. Environ. Sci. Bio/Technology 5, 57–71.
Batstone, D.J., Keller, J., Angelidaki, I., Kalyuzhnyi, S.V., Pavlostathis, S.G., Rozzi, A., Sanders, W.T.M., Siegrist, H., Vavilin, V.A., 2002. The IWA anaerobic digestion model No. 1 (ADM 1). Water Sci. Technol. 45 (10), 65–73.
Butler, D., Friedler, E., Gatt, K., 1995. Characterising the quantity and quality of domestic wastewater inflows. Wat. Sci. Tech. 31 (7), 13–24.
Copp, J.B. (Ed.), 2002. The COST Simulation Benchmark – Description and Simulator Manual. Office for Official Publications of the European Communities, Luxembourg, ISBN 92-894-1658-0.
De Gracia, M., Sancho, L., García-Heras, J.L., Vanrolleghem, P., Ayesa, E., 2006. Mass and charge conservation check in dynamic models: application to the new ADM 1 model. Water Sci. Technol. 53 (1), 225–240.
Ekama, G.A., 2009. Using bioprocess stoichiometry to build a plant-wide mass balance based steady-state WWTP model. Water Res. 43 (8), 2101–2120.
Fairlamb, M., Jones, R., Takács, I., Bye, C., 2003. Formulation of a general model for simulation of pH in wastewater treatment processes. In: Proceedings of WEFTEC (Los Angeles,California).
Fedorovich, V., Lens, P., Kalyuzhnyi, S., 2003. Extension of anaerobic digestion model no. 1 with processes of sulfate reduction. Appl. Biochem. Biotechnol. 109, 33–45.
Flores-Alsina, X., Gernaey, K.V., Jeppsson, U., 2012. Benchmarking biological nutrient removal in wastewater treatment plants: influence of mathematical model assumptions. Water Sci. Technol. 65 (8), 1496–1505.
Flores-Alsina, X., Saagi, R., Lindblom, E., Thirsing, C., Thornberg, D., Gernaey, K.V., Jeppsson, U., 2014. Calibration and validation of a phenomenological influent pollutant disturbance scenario generator using full-scale data. Water Res. 51 (15), 172–185.
Flores-Alsina, X., Kazadi Mbamba, C., Solon, K., Tait, S., Gernaey, K.V., Jeppsson, U., Batstone, D.J., 2015. Modelling Phosphorus (P), Sulphur (S) and Iron (Fe) interactions during the simulation of anaerobic digestion processes (Submitted to the 14th World Congress on Anaerobic Digestion (AD14), Viña del Mar, Chile, 15–18 November 2015).
Ganigue, R., Volcke, E.I.P., Puig, S., Balaguer, M.D., Colprim, J., Sin, G., 2010. Systematic model development for partial nitrification of landfill leachate in a SBR. Water Sci. Technol. 61 (9), 2199–2210.

Gernaey, K.V., Flores-Alsina, X., Rosen, C., Benedetti, L., Jeppsson, U., 2011. Dynamic influent pollutant disturbance scenario generation using a phenomenological modelling approach. Environ. Model. Softw. 26 (11), 1255–1267.
Gernaey, K.V., Jeppsson, U., Vanrolleghem, P.A., Copp, J.B., 2014. Benchmarking of Control Strategies for Wastewater Treatment Plants. IWA Scientific and Technical Report No. 23. IWA Publishing, London, UK.
Grau, P., de Gracia, M., Vanrolleghem, P.A., Ayesa, E., 2007. A new plant-wide modelling methodology for WWTPs. Water Res. 41, 4357–4372.
Hauduc, H., Takacs, I., Smith, S., Szabo, A., Murthy, S., Daigger, G.T., Sperandio, M., 2015. A dynamic physicochemical model for chemical phosphorus removal. Water Res. 73, 157–170.
Harding, T.H., Ikumi, D.S., Ekama, G.A., 2011. Incorporating phosphorus into plant wide wastewater treatment plant modelling anaerobic digestion. In: Proc. IWA Watermatex2011, San Sebastian, Spain, 20–22 June 2011.
Hellinga, C., van Loosdrecht, M.C.M., Heijnen, J.J., 1999. Model based design of a novel process for nitrogen removal from concentrated flow. Math. Comput. Model. Dyn. Syst. 5, 351–371.
Henze, M., Gujer, W., Mino, T., van Loosdrecht, M.C.M., 2000. Activated Sludge Models ASM1, ASM2, ASM2d, and ASM3. IWA Scientific and Technical Report No. 9. IWA Publishing, London, UK.
Hiatt, W.C., Grady Jr., C.P.L., 2008. An updated process model for carbon oxidation, nitrification, and denitrification. Water Environ. Res. 80 (11), 2145–2156.
Hu, Z.R., Wentzel, M.C., Ekama, G.A., 2007. A general kinetic model for biological nutrient removal activated sludge systems: model development. Biotechnol. Bioeng. 98 (6), 1242–1258.
Huete, E., de Gracia, M., Ayesa, E., Garcia-Heras, J.L., 2006. ADM1-based methodology for the characterisation of the influent sludge in anaerobic reactors. Water Sci. Technol. 54 (4), 157–166.
Ikumi, D.S., Harding, T.H., Ekama, G.A., 2014. Biodegradability of wastewater and activated sludge organics in anaerobic digestion. Water Res. 56 (1), 267–279.
Ikumi, D., Brouckaert, C.J., Ekama, G.A., 2011. Modelling of struvite precipitation in anaerobic digestion.. In: Proc. IWA Watermatex2011, San Sebastian, Spain, 20–22 June 2011.
Jones, R.M., Dold, P., Takács, I., Chapman, K., Wett, B., Murthy, S., O'Shaughnessy, M., 2007. Simulation for operation and control of reject water treatment processes. In: Proc. WEFTEC, San Diego, 2007.
Kazadi Mbamba, C., Batstone, D., Flores-Alsina, X., Tait, S., 2015b. A systematic study of multiple minerals precipitation modelling in wastewater treatment. Water Res. 85, 359–370. http://dx.doi.org/10.1016/j.watres.2015.08.041.
Kazadi Mbamba, C., Flores-Alsina, X., Batstone, D., Tait, S., 2015a. A generalized chemical precipitation modelling approach in wastewater treatment applied to calcite. Water Res. 68 (1), 342–353.
Lindblom, E., Arnell, M., Flores-Alsina, X., Stenström, F., Gustavsson, D.J.I., Jeppsson, U., 2014. Dynamic modelling of nitrous oxide emissions from three Swedish full-scale sludge liquor treatment systems. In: IWA 9th World Water Congress and Exhibition (IWA2014), Lisbon, Portugal, 21-26 September, 2014.
Lizarralde, I., Fernandez-Arevalo, T., Brouckaert, C., Vanrolleghem, P.A., Ikumi, D., Ekama, D., Ayesa, E., Grau, P., 2015. A new general methodology for incorporating physico-chemical transformations into multiphase wastewater treatment process models. Water Res. 74, 239–256.
Lopez-Vazquez, C.M., Oehmen, A., Hooijmans, C.M., Brdjanovic, D., Gijzen, H.J., 2009. Modeling the PAO–GAO competition: effects of carbon source, pH and temperature. Water Res. 43 (2), 450–462.
Martin, C., Vanrolleghem, P.A., 2014. Analysing, completing, and generating influent data for WWTP modelling: a critical review. Environ. Model. Softw. 60, 188–201.
Meijer, S.C.F., 2004. Theoretical and Practical Aspects of Modelling Activated Sludge Processes (PhD thesis). Department of Biotechnological Engineering. Delft University of Technology, The Netherlands.
Morel, F.M., Hering, J.G., 1993. Principles and Applications of Aquatic Chemistry. John Wiley and Sons, New York, USA.
Musvoto, E.V., Wentzel, M.C., Ekama, G.A., 2000. Integrated chemical–physical processes modelling – II. Simulating aeration treatment of anaerobic digester supernatants. Water Res. 34 (6), 1868–1880.
Ni, B.J., Peng, L., Law, Y., Guo, J., Yuan, Z., 2014. Modeling of nitrous oxide production by autotrophic ammonia-oxidizing bacteria with multiple production pathways. Environ. Sci. Technol. 48 (7), 3916–3924.
Nopens, I., Batstone, D.J., Copp, J.B., Jeppsson, U., Volcke, E., Alex, J., Vanrolleghem, P.A., 2009. An ASM/ADM model interface for dynamic plant-wide simulation. Water Res. 43 (7), 1913–1923.
Press, H., Teukolsky, S.A., Vetterling, W.T., Flannery, B.P., 2007. Numerical Recipes: the Art of Scientific Computing, third ed. Cambridge University Press, New York.
Reichert, P., Borchardt, D., Henze, M., Rauch, W., Shanahan, P., Somlyódy, L., Vanrolleghem, P., 2001. River Water Quality Model No. 1. Scientific and Technical Report No. 12. IWA Publishing, London, UK.
Rieger, L., Koch, G., Kühni, M., Gujer, W., Siegrist, H., 2001. The EAWAG bio-P module for activated sludge model no.3. Water Res. 35 (16), 3887–3903.
Rosen, C., Vrecko, D., Gernaey, K.V., Pons, M.N., Jeppsson, U., 2006. Implementing ADM1 for plant-wide benchmark simulations in Matlab/Simulink. Water Sci. Technol. 54 (4), 11–19.
Saagi, R., Flores-Alsina, X., Gernaey, K.V., Jeppsson, U., 2015. System-wide benchmark simulation model for integrated analysis of urban wastewater systems. In: 9th IWA Symposium on Systems Analysis and Integrated Assessment (Watermatex2015), Gold Coast, Queensland, Australia, 14-17 June, 2015.
Serralta, J., Borras, L., Seco, A., 2004. An extension of ASM2d including pH calculation. Water Res. 38 (19), 4029–4038.
Sharma, K., Ganigue, R., Yuan, Z., 2013. pH dynamics in sewers and its modeling. Water Res. 47 (16), 6086–6096.
Siegrist, H., Vogt, D., Garcia-Heras, J.L., Gujer, W., 2002. Mathematical model for meso-and thermophilic anaerobic sewage sludge digestion. Environ. Sci. Technol. 36 (5), 1113–1123.
Skogestad, S., 2000. Plantwide control: the search for the self-optimizing control structure. J. Proc. Control 10, 487–507.
Snip, L., Boiocchi, R., Flores-Alsina, X., Jeppsson, U., Gernaey, K.V., 2014. Challenges encountered when expanding activated sludge models: a case study based on N2O production. Water Sci. Technol. 70 (7), 1251–1260.
Solon, K., Flores-Alsina, X., Kazadi Mbamba, C., Volcke, E.I.P., Tait, S., Batstone, D., Gernaey, K.V., Jeppsson, U., 2015. Effects of ionic strength and ion pairing on (plant-wide) modelling of anaerobic digestion processes. Water Res. 70, 235–245.
Sötemann, S.W., Van Rensburg, P., Ristow, N.E., Wentzel, M.C., Loewenthal, R.E., Ekama, G.A., 2006. Integrated chemical/physical and biological processes modeling Part 2-Anaerobic digestion of sewage sludges. Water sa. 31 (4), 545–568.
Stumm, W., Morgan, J.J., 1996. In: Schnoor, J.L., Zehnder, A. (Eds.), Aquatic Chemistry: Chemical Equilibria and Rates in Natural Waters. John Wiley and Sons, New York, USA.
Takács, I., Patry, G.G., Nolasco, D., 1991. A dynamic model of the clarification thickening process. Water Res. 25 (10), 1263–1271.
Tchobanoglous, G., Burton, F.L., Stensel, H.D., 2003. Wastewater Engineering: Treatment, Disposal and Reuse. McGraw-Hill, New York, New York, USA.
Van Hulle, S.W.H., Volcke, E.I.P., Lopez Teruel, J., Donckels, B., van Loosdrecht, M.C.M., Vanrolleghem, P.A., 2007. Influence of temperature and pH on the kinetics of the SHARON nitritation process. J. Chem. Technol. Biotechnol. 82, 471–480.
van Rensburg, P., Musvoto, E.V., Wentzel, M.C., Ekama, G.A., 2003. Modelling multiple mineral precipitation in anaerobic digester liquor. Water Res. 37 (13), 3087–3097.
Wett, B., Rauch, W., 2003. The role of inorganic carbon limitation in biological nitrogen removal of extremely ammonia concentrated wastewater. Water Res. 37 (5), 1100–1110.

Supplemental Information

Paper Title: A plant-wide aqueous phase chemistry module describing pH variations and ion speciation/pairing in wastewater treatment process models

Authors: Flores-Alsina, X., Kazadi Mbamba, C., Solon, K., Vrečko, D., Tait, S., Batstone, D.J., Jeppsson, U., Gernaey, K.V.

Table S1. List of considered species and their thermodynamic properties (I)

Symbol	Formula	log K_i	ΔH^0
$S_{Al-(ac)_2^+}$	Al-(Acetate)$_2^+$	4.6	41
$S_{Al(OH)_2^+}$	Al(OH)$_2^+$	-10.294	122.5
$S_{Al(OH)_3(aq)}$	Al(OH)$_{3\ (aq)}$	-16.691	176.3
$S_{Al(OH)_4^-}$	Al(OH)$_4^-$	-23	183
$S_{Al(SO_4)_2^-}$	Al(SO4)$_2^-$	5.58	11.9
$S_{Al_2(OH)_2^{+4}}$	Al$_2$(OH)$_2^{+4}$	-7.694	74.62
$S_{Al_2(OH)_2-ac^{+3}}$	Al$_2$(OH)$_2$-Acetate^{+3}	-2.414	0
$S_{Al_2(OH)_2CO_3^{+2}}$	Al$_2$(OH)$_2$CO$_3^{+2}$	4.31	0
$S_{Al_2PO_4^{+3}}$	Al$_2$PO$_4^{+3}$	18.98	0
$S_{Al_3(OH)_4^{+5}}$	Al$_3$(OH)$_4^{+5}$	-13.888	140.24
$S_{Al-ac^{+2}}$	Al-Acetate^{+2}	2.75	16
$S_{Al-bu^{+2}}$	Al-Butyrate^{+2}	2.19	0
$S_{AlCl^{+2}}$	AlCl^{+2}	-0.39	0
$S_{AlHPO_4^+}$	AlHPO$_4^+$	20.01	0
$S_{AlOH^{+2}}$	AlOH^{+2}	-4.997	47.81
$S_{AlOH-ac^+}$	AlOH-Acetate$^+$	-0.147	0
$S_{Al-pro^{+2}}$	Al-Propionate^{+2}	2.3	12
$S_{AlSO_4^+}$	AlSO$_4^+$	3.84	9
$S_{Ca(NH_3)_2^{+2}}$	Ca(NH$_3$)$_2^{+2}$	-18.59	0
$S_{Ca(NO_3)_2}$	Ca(NO$_3$)$_2$	-4.5	0
S_{Ca-ac^+}	Ca-Acetate$^+$	1.18	4
S_{Ca-bu^+}	Ca-Butyrate$^+$	0.94	33.472
S_{CaCl^+}	CaCl$^+$	0.4	4
$S_{CaCO_3(aq)}$	CaCO$_{3\ (aq)}$	3.22	16
$S_{CaH_2PO_4^+}$	CaH$_2$PO$_4^+$	20.923	-6
$S_{CaHCO_3^+}$	CaHCO$_3^+$	11.434	0
$S_{CaHPO_4(aq)}$	CaHPO$_{4\ (aq)}$	15.035	-3
$S_{CaNH_3^{+2}}$	CaNH$_3^{+2}$	-9.04	0
$S_{CaNO_3^+}$	CaNO$_3^+$	0.5	-5.4
S_{CaOH^+}	CaOH$^+$	-12.697	64.11
$S_{CaPO_4^-}$	CaPO$_4^-$	6.46	129.704
S_{Ca-pro}	Ca-Propionate$^+$	0.93	33.472
$S_{CaSO_4(aq)}$	CaSO4 $_{(aq)}$	2.36	7.1
S_{Ca-va^+}	Ca-Valerate$^+$	0.3	0
$S_{Fe-(ac)_2^+}$	Fe-(Acetate)$_2^+$	7.57	0
$S_{Fe-(ac)_3(aq)}$	Fe-(Acetate)$_{3\ (aq)}$	95.867	0
$S_{Fe(NH_3)_2^{+2}}$	Fe(NH$_3$)$_2^{+2}$	-16.24	89
$S_{Fe(NH_3)_3^{+2}}$	Fe(NH$_3$)$_3^{+2}$	-25.05	133
$S_{Fe(NH_3)_4^{+2}}$	Fe(NH$_3$)$_4^{+2}$	-34.23	177
$S_{Fe(NO_2)^{+2}}$	Fe(NO$_2$)$^{2+}$	4.72	0
$S_{Fe(NO_2)_3(aq)}$	Fe(NO$_2$)$_{3\ (aq)}$	6.78	0
$S_{Fe(OH)_2(aq)}$	Fe(OH)$_{2\ (aq)}$	-20.494	119.62
$S_{Fe(OH)_2^+}$	Fe(OH)$_2^+$	-5.75	37.7
$S_{Fe(OH)_3^-}$	Fe(OH)$_3^-$	-30.991	126.43
$S_{Fe(OH)_3(aq)}$	Fe(OH)$_{3\ (aq)}$	-15	75.3
$S_{Fe(OH)_4^-}$	Fe(OH)$_4^-$	-22.7	154.8
$S_{Fe(SO4)_2^-}$	Fe(SO$_4$)$_2^-$	5.38	19.2
$S_{Fe_2(OH)_2^{+4}}$	Fe$_2$(OH)$_2^{+4}$	-2.894	56.42
$S_{Fe_3(OH)_4^{+5}}$	Fe$_3$(OH)$_4^{+5}$	-6.288	65.24

Table S1. List of considered species and their thermodynamic properties (II)

Symbol	Formula	log K_i	ΔH^0
S_{Fe-ac^+}	Fe-Acetate$^+$	1.4	0
$S_{Fe-ac^{+2}}$	Fe-Acetate^{+2}	4.24	25
$S_{Fe-bu^{+2}}$	Fe-Butyrate^{+2}	3.41	11
S_{FeCl^+}	$FeCl^+$	-0.2	0
$S_{FeCl^{+2}}$	$FeCl^{+2}$	1.48	23
$S_{FeH_2PO_4^+}$	$FeH_2PO_4^+$	22.273	0
$S_{FeH_2PO_4^{+2}}$	$FeH_2PO_4^{+2}$	23.85	0
$S_{FeHCO_3^+}$	$FeHCO_3^+$	11.429	0
$S_{FeHPO_4(aq)}$	$FeHPO_{4\ (aq)}$	15.975	0
$S_{FeHPO_4^+}$	$FeHPO_4^+$	22.285	-305.432
S_{FeHS^+}	$FeHS^+$	5.62	0
$S_{FeNH_3^{+2}}$	$FeNH_3^{+2}$	-7.84	44.1
$S_{FeNO_2^{+2}}$	$FeNO_2^{+2}$	3.2	0
S_{FeOH^+}	$FeOH^+$	-9.397	55.81
$S_{FeOH^{+2}}$	$FeOH^{+2}$	-2.02	25.1
$S_{Fe-pro^{+2}}$	Fe-Propionate^{+2}	3.71	21
$S_{FeSO_4(aq)}$	$FeSO_{4\ (aq)}$	2.39	8
$S_{FeSO_4^+}$	$FeSO_4^+$	4.25	25
$S_{Fe-va^{+2}}$	Fe-Valerate^{+2}	3.51	13
$S_{H_2CO_3^*(aq)}$	H_2CO_3* $_{(aq)}$	16.681	-32
$S_{H_2PO_4^-}$	$H_2PO_4^-$	19.573	-18
$S_{H_2S(aq)}$	$H_2S_{\ (aq)}$	7.02	-22
$S_{H_3PO_4(aq)}$	H_3PO_4	21.721	-10.5
$S_{H-ac(aq)}$	H-Acetate $_{(aq)}$	4.757	0.41
$S_{H-bu(aq)}$	H-Butyrate $_{(aq)}$	4.818	2.8
$S_{HCO_3^-}$	HCO_3^-	10.329	-14.6
$S_{HNO_2(aq)}$	$HNO_{2\ (aq)}$	3.15	0
$S_{HPO_4^{-2}}$	$HPO4^{-2}$	12.375	-15
$S_{H-pro(aq)}$	H-Propionate $_{(aq)}$	4.874	0.75
$S_{HSO_4^-}$	HSO_4^-	1.99	22
$S_{H-va(aq)}$	H-Valerate $_{(aq)}$	4.843	2.8
$S_{K_2HPO_4(aq)}$	$K_2HPO_{4\ (aq)}$	13.5	0
$S_{K_2PO_4^-}$	K_2PO4^-	2.26	0
$S_{K-ac(aq)}$	K-Acetate $_{(aq)}$	-0.27	4
$S_{KCl(aq)}$	$KCl_{\ (aq)}$	-0.3	-4
$S_{KH_2PO_4(aq)}$	$KH_2PO4_{\ (aq)}$	19.873	0
$S_{KHPO_4^-}$	$KHPO4^-$	13.255	0
$S_{KNO_3(aq)}$	$KNO_{3\ (aq)}$	-0.19	-12
$S_{KOH(aq)}$	$KOH_{\ (aq)}$	-13.757	55.81
$S_{KPO_4^{-2}}$	KPO_4^{-2}	1.43	15
$S_{KSO_4^-}$	KSO_4^-	0.85	4.1
$S_{Mg(NH_3)_2^{+2}}$	$Mg(NH_3)_2^{+2}$	-18.29	99
$S_{Mg_2CO_3^{+2}}$	$Mg_2CO_3^{+2}$	3.59	0
S_{Mg-ac^+}	Mg-Acetate$^+$	1.26	0
S_{Mg-bu^+}	Mg-Butyrate$^+$	0.96	0
S_{MgCl^+}	$MgCl^+$	0.6	4
$S_{MgCO_3(aq)}$	$MgCO_{3\ (aq)}$	2.92	10
$S_{MgHCO_3^+}$	$MgHCO_3^+$	11.34	-9.6
$S_{MgHPO_4(aq)}$	$MgHPO_{4\ (aq)}$	0.97	42.677

Table S1. List of considered species and their thermodynamic properties (III)

Symbol	Formula	log K_i	ΔH^0
S_{MgOH^+}	$MgOH^+$	-11.417	67.81
$S_{MgPO_4^-}$	$MgPO_4^-$	4.654	129.704
S_{Mg-pro^+}	Mg-Propionate$^+$	0.97	42.677
$S_{MgSO_4(aq)}$	$MgSO_{4\ (aq)}$	2.26	5.8
$S_{Na_2HPO_4(aq)}$	$Na_2HPO_{4\ (aq)}$	13.32	0
$S_{Na_2PO_4^-}$	$Na_2PO_4^-$	2.59	0
$S_{Na-ac(aq)}$	Na-Acetate $_{(aq)}$	-0.12	8
$S_{NaCl(aq)}$	$NaCl_{\ (aq)}$	-0.3	-8
$S_{NaCO_3^-}$	$NaCO_3^-$	1.27	-20.35
$S_{NaH_2PO_4(aq)}$	$NaH_2PO_{4\ (aq)}$	19.873	0
$S_{NaHCO_3(aq)}$	$NaHCO_{3\ (aq)}$	10.029	-283.301
$S_{NaHPO_4^-}$	$NaHPO_4^-$	13.445	0
$S_{NaNO_3(aq)}$	$NaNO_{3\ (aq)}$	-0.55	0
$S_{NaOH(aq)}$	$NaOH_{\ (aq)}$	-13.897	59.81
$S_{Na_2PO_4^{-2}}$	$Na_2PO_4^{-2}$	1.43	8
$S_{NaSO_4^-}$	$NaSO_4^-$	0.74	1
$S_{NH_3(aq)}$	$NH_{3\ (aq)}$	-9.244	52
$S_{NH_4SO_4^-}$	$NH_4SO_4^-$	1.03	0
S_{OH^-}	OH^-	-13.997	55.81
$S_{S^{-2}}$	S^{-2}	-17.4	49.4

Table S2. Stoichiometric matrix of the species (S_i) and components (S_j) (I)

	S_{ac^-}	$S_{Al^{+3}}$	S_{bu^-}	$S_{CO3^{-2}}$	$S_{Ca^{+2}}$	S_{Cl^-}	$S_{Fe^{+2}}$	$S_{Fe^{+3}}$	S_{HS^-}	S_{K^+}	$S_{Mg^{+2}}$	$S_{NH_4^+}$	$S_{NO_2^-}$	$S_{NO_3^-}$	S_{Na^+}	$S_{PO_4^{-3}}$	S_{pro^-}	$S_{SO_4^{-2}}$	S_{va^-}
S_{ac^-}	1																		
$S_{Al^{+3}}$		1																	
S_{bu^-}			1																
$S_{CO_3^{-2}}$				1															
$S_{Ca^{+2}}$					1														
S_{Cl^-}						1													
$S_{Fe^{+2}}$							1												
$S_{Fe^{+3}}$								1											
S_{HS^-}									1										
S_{K^+}										1									
$S_{Mg^{+2}}$											1								
$S_{NH_4^+}$												1							
$S_{NO_2^-}$													1						
$S_{NO_3^-}$														1					
S_{Na^+}															1				
$S_{PO_4^{-3}}$																1			
S_{pro^-}																	1		
$S_{SO4^{-2}}$																		1	
S_{va^-}																			1
$S_{Al-(ac)2^+}$	2	1																	
$S_{Al(OH)_2^+}$		1																	
$S_{Al(OH)_3(aq)}$		1																	
$S_{Al(OH)_4^-}$		1																	
$S_{Al(SO_4)_2^-}$		1																2	
$S_{Al_2(OH)_2^{+4}}$		2																	
$S_{Al_2(OH)_2-ac^{+3}}$	1	2																	
$S_{Al_2(OH)_2CO_3^{+2}}$		2		1															
$S_{Al_2PO_4^{+3}}$		2														1			
$S_{Al_3(OH)_4^{+5}}$		3																	
$S_{Al-ac^{+2}}$	1	1																	
$S_{Al-bu^{+2}}$		1	1																
$S_{AlCl^{+2}}$		1				1													
$S_{AlHPO_4^+}$		1														1			
$S_{AlOH^{+2}}$		1																	
$S_{AlOH-ac^+}$	1	1																	

Table S2. Stoichiometric matrix of the species (S_i) and components (S_j) (II)

	S_{ac^-}	$S_{Al^{+3}}$	S_{bu^-}	$S_{CO3^{-2}}$	$S_{Ca^{+2}}$	S_{Cl^-}	$S_{Fe^{+2}}$	$S_{Fe^{+3}}$	S_{HS^-}	S_{K^+}	$S_{Mg^{+2}}$	$S_{NH_4^+}$	$S_{NO_2^-}$	$S_{NO_3^-}$	S_{Na^+}	$S_{PO_4^{-3}}$	S_{pro^-}	$S_{SO_4^{-2}}$	S_{va^-}
$S_{Al-pro^{+2}}$		1															1		
$S_{AlSO_4^+}$		1																1	
$S_{Ca(NH_3)_2^{+2}}$					1							2							
$S_{Ca(NO_3)_2}$					1									2					
S_{Ca-ac^+}	1				1														
S_{Ca-bu^+}			1		1														
S_{CaCl^+}					1	1													
$S_{CaCO_3(aq)}$				1	1														
$S_{CaH_2PO_4^+}$					1											1			
$S_{CaHCO_3^+}$				1	1														
$S_{CaHPO_4(aq)}$					1											1			
$S_{CaNH_3^{+2}}$					1							1							
$S_{CaNO_3^+}$					1									1					
S_{CaOH^+}					1														
$S_{CaPO_4^-}$					1											1			
S_{Ca-pro}					1												1		
$S_{CaSO_4(aq)}$					1													1	
S_{Ca-va^+}					1														1
$S_{Fe-(ac)_2^+}$	2							1											
$S_{Fe-(ac)_3(aq)}$	3							1											
$S_{Fe(NH_3)_2^{+2}}$							1					2							
$S_{Fe(NH_3)_3^{+2}}$							1					3							
$S_{Fe(NH_3)_4^{+2}}$							1					4							
$S_{Fe(NO_2)^{+2}}$								1					2						
$S_{Fe(NO_2)_3(aq)}$								1					3						
$S_{Fe(OH)_2(aq)}$							1												
$S_{Fe(OH)_2^+}$								1											
$S_{Fe(OH)_3^-}$							1												
$S_{Fe(OH)_3(aq)}$								1											
$S_{Fe(OH)_4^-}$								1											
$S_{Fe(SO4)_2^-}$								1										2	
$S_{Fe_2(OH)_2^{+4}}$								2											
$S_{Fe_3(OH)_4^{+5}}$								3											
S_{Fe-ac^+}	1						1												
$S_{Fe-ac^{+2}}$	1							1											

Table S2. Stoichiometric matrix of the species (S_i) and components (S_j) (III)

	S_{ac^-}	$S_{Al^{+3}}$	S_{bu^-}	$S_{CO3^{-2}}$	$S_{Ca^{+2}}$	S_{Cl^-}	$S_{Fe^{+2}}$	$S_{Fe^{+3}}$	S_{HS^-}	S_{K^+}	$S_{Mg^{+2}}$	$S_{NH_4^+}$	$S_{NO_2^-}$	$S_{NO_3^-}$	S_{Na^+}	$S_{PO_4^{-3}}$	S_{pro^-}	$S_{SO_4^{-2}}$	S_{va^-}
$S_{Fe-bu^{+2}}$			1					1											
S_{FeCl^+}						1	1												
$S_{FeCl^{+2}}$						1		1											
$S_{FeH_2PO_4^+}$							1									1			
$S_{FeH_2PO_4^{+2}}$								1								1			
$S_{FeHCO_3^+}$				1			1												
$S_{FeHPO_4(aq)}$							1									1			
$S_{FeHPO_4^+}$								1								1			
S_{FeHS^+}							1		1										
$S_{FeNH_3^{+2}}$							1					1							
$S_{FeNO_2^{+2}}$								1					1						
S_{FeOH^+}							1												
$S_{FeOH^{+2}}$								1											
$S_{Fe-pro^{+2}}$								1									1		
$S_{FeSO_4(aq)}$							1											1	
$S_{FeSO_4^+}$								1										1	
$S_{Fe-va^{+2}}$								1											1
$S_{H_2CO_3^*(aq)}$				1															
$S_{H_2PO_4^-}$																1			
$S_{H_2S(aq)}$									1										
$S_{H_3PO_4(aq)}$																1			
$S_{H-ac(aq)}$	1																		
$S_{H-bu(aq)}$			1																
$S_{HCO_3^-}$				1															
$S_{HNO_2(aq)}$													1						
$S_{HPO_4^{-2}}$																1			
$S_{H-pro(aq)}$																	1		
$S_{HSO_4^-}$																		1	
$S_{H-va(aq)}$																			1
$S_{K_2HPO_4(aq)}$										2						1			
$S_{K_2PO_4^-}$										2						1			
$S_{K-ac(aq)}$	1									1									
$S_{KCl(aq)}$						1				1									
$S_{KH_2PO_4(aq)}$										1						1			
$S_{KHPO_4^-}$										1						1			

Table S2. Stoichiometric matrix of the species (S_i) and components (S_j) (IV)

	S_{ac^-}	$S_{Al^{+3}}$	S_{bu^-}	$S_{CO3^{-2}}$	$S_{Ca^{+2}}$	S_{Cl^-}	$S_{Fe^{+2}}$	$S_{Fe^{+3}}$	S_{HS^-}	S_{K^+}	$S_{Mg^{+2}}$	$S_{NH_4^+}$	$S_{NO_2^-}$	$S_{NO_3^-}$	S_{Na^+}	$S_{PO_4^{-3}}$	S_{pro^-}	$S_{SO_4^{-2}}$	S_{va^-}
$S_{KNO_3(aq)}$										1				1					
$S_{KOH(aq)}$										1									
$S_{KPO_4^{-2}}$										1						1			
$S_{KSO_4^-}$										1								1	
$S_{Mg(NH_3)_2^{+2}}$											1	2							
$S_{Mg_2CO_3^{+2}}$				1							2								
S_{Mg-ac^+}	1										1								
S_{Mg-bu^+}			1								1								
S_{MgCl^+}						1					1								
$S_{MgCO_3(aq)}$				1							1								
$S_{MgHCO_3^+}$				1							1								
$S_{MgHPO_4(aq)}$											1					1			
S_{MgOH^+}											1								
$S_{MgPO_4^-}$											1					1			
S_{Mg-pro^+}											1						1		
$S_{MgSO_4(aq)}$											1							1	
$S_{Na_2HPO_4(aq)}$															2	1			
$S_{Na_2PO_4^-}$															2	1			
$S_{Na-ac(aq)}$	1														1				
$S_{NaCl(aq)}$						1									1				
$S_{NaCO_3^-}$				1											1				
$S_{NaH_2PO_4(aq)}$															1	1			
$S_{NaHCO_3(aq)}$				1											1				
$S_{NaHPO_4^-}$															1	1			
$S_{NaNO_3(aq)}$														1	1				
$S_{NaOH(aq)}$															1				
$S_{Na_2PO_4^{-2}}$															1	1			
$S_{NaSO_4^-}$															1			1	
$S_{NH_3(aq)}$												1							
$S_{NH_4SO_4^-}$												1						1	
S_{OH^-}																			
$S_{S^{-2}}$									1										

Table S3-1. ASM Influent conditions and model verification

Symbol (totals)		*Units*	Symbol (component)	This study	Minteq	
S_{ac}	27.8	g COD. m^{-3}	S_{ac^-}	0.0004	0.0004	mol.L^{-1}
S_{Al}		g Al. m^{-3}	$S_{Al^{+3}}$			mol.L^{-1}
S_{bu}		g COD. m^{-3}	S_{bu^-}			mol.L^{-1}
S_{Ca}	120.0	g Ca. m^{-3}	$S_{Ca^{+2}}$	0.0027	0.0027	mol.L^{-1}
S_{IC}	150.0	g C. m^{-3}	$S_{CO_3^{-2}}$	3.38E-06	2.97E-06	mol.L^{-1}
S_{Cl}	225.0	g Cl. m^{-3}	S_{Cl^-}	0.0063	0.0063	mol.L^{-1}
S_{Fe2}		g Fe. m^{-3}	$S_{Fe^{+2}}$			mol.L^{-1}
S_{Fe3}		g Fe. m^{-3}	$S_{Fe^{+3}}$			mol.L^{-1}
S_{HS}		g COD. m^{-3}	S_{HS^-}			mol.L^{-1}
S_{K}	60.0	g K. m^{-3}	S_{K^+}	0.0015	0.0015	mol.L^{-1}
S_{Mg}	60.0	g Mg. m^{-3}	$S_{Mg^{+2}}$	0.0022	0.0022	mol.L^{-1}
S_{IN}	31.5	g N. m^{-3}	$S_{NH_4^+}$	0.0022	0.0022	mol.L^{-1}
S_{NO2}		g N. m^{-3}	$S_{NO_2^-}$			mol.L^{-1}
S_{NO3}		g N. m^{-3}	$S_{NO_3^-}$			mol.L^{-1}
S_{Na}	80.0	g Na. m^{-3}	S_{Na^+}			mol.L^{-1}
S_{IP}	9.0	g P. m^{-3}	$S_{PO_4^{-3}}$	3.86E-10	3.25E-10	mol.L^{-1}
S_{pro}		g COD. m^{-3}	S_{pro^-}			mol.L^{-1}
S_{SO4}	30.0	g S. m^{-3}	$S_{SO_4^{-2}}$	0.0007	0.0007	mol.L^{-1}
S_{va}		g COD. m^{-3}	S_{va^-}			mol.L^{-1}
			S_{H^+}	**1.77E-07**	**1.93e-07**	**mol.L^{-1}**
			pH	**6.69**	**6.65**	
			I	**0.0230**	**0.0230**	**mol.L^{-1}**
			γ	**0.87**	**0.87**	

Table S3-2. AER3 effluent conditions (ASM2d) and model verification

Symbol (totals)		*Units*	Symbol (component)	This study	Minteq	
S_{ac}	0,0055	g COD. m^{-3}	S_{ac^-}	8.17E-08	8.16E-08	mol.L^{-1}
S_{Al}		g Al. m^{-3}	$S_{Al^{+3}}$			mol.L^{-1}
S_{bu}		g COD. m^{-3}	S_{bu^-}			mol.L^{-1}
S_{Ca}	120.0	g Ca. m^{-3}	$S_{Ca^{+2}}$	0.0027	0.0027	mol.L^{-1}
S_{IC}		g C. m^{-3}	$S_{CO_3^{-2}}$	2.84E-05	2.14e-5	mol.L^{-1}
S_{Cl}	225.0	g Cl. m^{-3}	S_{Cl^-}	0.0063	0.0063	mol.L^{-1}
S_{Fe2}		g Fe. m^{-3}	$S_{Fe^{+2}}$			mol.L^{-1}
S_{Fe3}		g Fe. m^{-3}	$S_{Fe^{+3}}$			mol.L^{-1}
S_{HS}		g COD. m^{-3}	S_{HS^-}			mol.L^{-1}
S_{K}	56,1	g K. m^{-3}	S_{K^+}	0.0014	0.0014	mol.L^{-1}
S_{Mg}	57,6	g Mg. m^{-3}	$S_{Mg^{+2}}$	0.0022	0.0022	mol.L^{-1}
S_{IN}	1,1	g N. m^{-3}	$S_{NH_4^+}$	7.63E-05	7.65E-05	mol.L^{-1}
S_{NO2}		g N. m^{-3}	$S_{NO_2^-}$			mol.L^{-1}
S_{NO3}	7,4	g N. m^{-3}	$S_{NO_3^-}$	0.005	0.005	mol.L^{-1}
S_{Na}	80.0	g Na. m^{-3}	S_{Na^+}			mol.L^{-1}
S_{IP}	0.0061	g P. m^{-3}	$S_{PO_4^{-3}}$	5.04E-11	3.75E-11	mol.L^{-1}
S_{pro}		g COD. m^{-3}	S_{pro^-}			mol.L^{-1}
S_{SO4}	30.0	g S. m^{-3}	$S_{SO_4^{-2}}$	0.0007	0.0007	mol.L^{-1}
S_{va}		g COD. m^{-3}	S_{va^-}			mol.L^{-1}
			S_{H^+}	**1.55E-08**	**1.95E-08**	**mol.L^{-1}**
			pH	**7.81**	**7.76**	
			I	**0.0205**	**0.0205**	**mol.L^{-1}**
			γ	**0.87**	**0.87**	

Table S3-3. AD effluent conditions (ADM1) and model verification

Symbol (total)		*Units*	Symbol (component)	This study	Minteq	
S_{ac}	0.0662	kg COD. m^{-3}	S_{ac^-}	0.0010	0.0010	$mol.L^{-1}$
S_{Al}		kmol Al. m^{-3}	$S_{Al^{+3}}$			$mol.L^{-1}$
S_{bu}	0.0138	kg COD. m^{-3}	S_{bu^-}	0.0001	0.0001	$mol.L^{-1}$
S_{Ca}	0.0048	kmol Ca. m^{-3}	$S_{Ca^{+2}}$	0.0025	0.0026	$mol.L^{-1}$
S_{IC}	0.0913	kmol C. m^{-3}	$S_{CO_3^{-2}}$	1,45E-04	1.62E-04	$mol.L^{-1}$
S_{Cl}	0.0096	kmol Cl. m^{-3}	S_{Cl^-}	0.0095	0.0095	$mol.L^{-1}$
S_{Fe2}		kmol Fe. m^{-3}	$S_{Fe^{+2}}$			$mol.L^{-1}$
S_{Fe3}		kmol Fe. m^{-3}	$S_{Fe^{+3}}$			$mol.L^{-1}$
S_{HS}		kg COD. m^{-3}	S_{HS^-}			$mol.L^{-1}$
S_{K}	0.0025	kmol K. m^{-3}	S_{K^+}	0.0024	0.0024	$mol.L^{-1}$
S_{Mg}	0.0049	kmol Mg. m^{-3}	$S_{Mg^{+2}}$	0.0026	0.0027	$mol.L^{-1}$
S_{IN}	0.0934	kmol N. m^{-3}	$S_{NH_4^+}$	0.0903	0.0908	$mol.L^{-1}$
S_{NO2}		kmol N. m^{-3}	$S_{NO_2^-}$			$mol.L^{-1}$
S_{NO3}		kmol N. m^{-3}	$S_{NO_3^-}$			$mol.L^{-1}$
S_{Na}	0.0051	kmol Na. m^{-3}	S_{Na^+}	0.0047	0.0048	$mol.L^{-1}$
S_{IP}	0.0065	kmol P. m^{-3}	$S_{PO_4^{-3}}$	8.56E-08	1.04E-07	$mol.L^{-1}$
S_{pro}	0.0173	kg COD. m^{-3}	S_{pro^-}	0.0002	0.0002	$mol.L^{-1}$
S_{SO4}	0.0061	kmol S. m^{-3}	$S_{SO_4^{-2}}$	0.0040	0.0041	$mol.L^{-1}$
S_{va}	0.0121	kg COD. m^{-3}	S_{va^-}	6.56E-05	5.81E-05	$mol.L^{-1}$
			S_{H^+}	**8.04E-08**	**8.02E-08**	**$mol.L^{-1}$**
			pH	**6.97**	**6.97**	
			I	**0.122**	**0.123**	**$mol.L^{-1}$**
			γ	**0.76**	**0.76**	

Paper III

WATER RESEARCH 71 (2015) 42–54

Available online at www.sciencedirect.com

ScienceDirect

journal homepage: www.elsevier.com/locate/watres

Modeling the anaerobic digestion of cane-molasses vinasse: Extension of the Anaerobic Digestion Model No. 1 (ADM1) with sulfate reduction for a very high strength and sulfate rich wastewater

Ernesto L. Barrera [a,e,*], *Henri Spanjers* [b], *Kimberly Solon* [c], *Youri Amerlinck* [d], *Ingmar Nopens* [d], *Jo Dewulf* [e]

[a] *Study Center of Energy and Industrial Processes, Sancti Spiritus University, Ave de los Martires 360, 60100 Sancti Spiritus, Cuba*

[b] *Faculty of Civil Engineering and Geosciences, Department of Water Management, Section Sanitary Engineering, Delft University of Technology, Stevinweg 1, 2628 CN Delft, The Netherlands*

[c] *Division of Industrial Electrical Engineering and Automation (IEA), Department of Biomedical Engineering (BME), Lund University, Box 118, SE-221 00 Lund, Sweden*

[d] *BIOMATH, Department of Mathematical Modeling, Statistics and Bioinformatics, Ghent University, Coupure Links 653, 9000 Gent, Belgium*

[e] *Research Group ENVOC, Faculty of Bioscience Engineering, Ghent University, Coupure Links 653, 9000 Ghent, Belgium*

ARTICLE INFO

Article history:
Received 7 July 2014
Received in revised form
22 October 2014
Accepted 15 December 2014
Available online 24 December 2014

Keywords:
ADM1
Mathematical modeling
Simulation

ABSTRACT

This research presents the modeling of the anaerobic digestion of cane-molasses vinasse, hereby extending the Anaerobic Digestion Model No. 1 with sulfate reduction for a very high strength and sulfate rich wastewater. Based on a sensitivity analysis, four parameters of the original ADM1 and all sulfate reduction parameters were calibrated. Although some deviations were observed between model predictions and experimental values, it was shown that sulfates, total aqueous sulfide, free sulfides, methane, carbon dioxide and sulfide in the gas phase, gas flow, propionic and acetic acids, chemical oxygen demand (COD), and pH were accurately predicted during model validation. The model showed high (±10%) to medium (10%–30%) accuracy predictions with a mean absolute relative error ranging from 1% to 26%, and was able to predict failure of methanogenesis and sulfidogenesis when the sulfate loading rate increased. Therefore, the kinetic parameters and the

Abbreviations: ADM1, Anaerobic Digestion Model No. 1; aSRB, Acetate sulfate reducing bacteria; COD, Chemical oxygen demand; CI, Confidence interval; COV, Covariance matrix; FIM, Fisher information matrix; hMA, Hydrogenotrophic methanogenic archea; hSRB, Hydrogenotrophic sulfate reducing bacteria; LCFA, Long chain fatty acids; ODE, Ordinary differential equation; OLR, Organic loading rate; pSRB, Propionate sulfate reducing bacteria; SCOD, Soluble COD concentration; SLR, Sulfate loading rate; SRB, Sulfate reducing bacteria; UASB, Upflow anaerobic sludge bed; XCOD, Particulate COD concentration.

* *Corresponding author*. Study Center of Energy and Industrial Processes, Sancti Spiritus University, Ave de los Martires 360, 60100 Sancti Spiritus, Cuba. Tel.: +53 41336118, +32 92645948 (Belgium).

E-mail addresses: ernestol@uniss.edu.cu, ErnestoLuis.BarreraCardoso@UGent.be (E.L. Barrera), h.l.f.m.Spanjers@tudelft.nl (H. Spanjers), kimberly.solon@iea.lth.se (K. Solon), Youri.Amerlinck@UGent.be (Y. Amerlinck), ingmar.nopens@UGent.be (I. Nopens), Jo.Dewulf@UGent.be (J. Dewulf).

http://dx.doi.org/10.1016/j.watres.2014.12.026

0043-1354/© 2014 Elsevier Ltd. All rights reserved.

Sulfate reduction
Vinasse

model structure proposed in this work can be considered as valid for the sulfate reduction process in the anaerobic digestion of cane-molasses vinasse when sulfate and organic loading rates range from 0.36 to 1.57 kg SO_4^{2-} m^{-3} d^{-1} and from 7.66 to 12 kg COD m^{-3} d^{-1}, respectively.

© 2014 Elsevier Ltd. All rights reserved.

Nomenclature

C_i	Carbon content of the component i kmol C kg COD^{-1}
eff_COD	Effluent COD concentration kg COD m^{-3}
I_{1-4}	Inhibition functions –
$I_{h2s,j}$	Sulfide inhibition function for process j –
$I_{pH,j}$	pH inhibition function for process j –
$K_{A/B,i}$	Acid-base kinetic parameter for component i m^3 $kmol^{-1}$ d^{-1}
$K_{a,i}$	Acid-base equilibrium coefficient for component i kmol m^{-3}
$k_{dec,j}$	First order decay rate for process j d^{-1}
$K_{H,i}$	Henri's law coefficient for component i kmol m^{-3} bar^{-1}
$K_{I,h2s,j}$	50% inhibitory concentration of free H_2S on the process j kmol m^{-3}
k_La	Gas–liquid transfer coefficient d^{-1}
$k_{m,j}$	Monod maximum specific uptake rate for process j kg COD_S_i kg $COD\_X_i^{-1}$ d^{-1}
$K_{S,j}$	Half saturation coefficient of component i on process j (for SO_4^{2-} units are in kmol m^{-3}) kg COD m^{-3}
N_i	Nitrogen content of the component i kmol N kg COD^{-1}
$P_{gas,i}$	Pressure of gas component i bar
Q_{gas}	Gas flow rate m^3 d^{-1}
S_i	Concentration of the soluble components i (for hydrogen ions, sulfates, sulfides and its ionized forms units are in kmol m^{-3}) kg COD_S_i m^{-3}
$S_{gas,i}$	Gas phase concentration of the component i (for H_2S units are in kmol m^{-3}) Fraction
TCOD	Total COD concentration kg COD m^{-3}
$t_{\alpha,df}$	t-values obtained from the Student-t distribution –
X_i	Concentration of the particulate component i kg COD m^{-3}
Y_i	Yield of biomass on substrate kg COD_X_i kg $COD\_S_i^{-1}$

Greek letter

$\Gamma_{n,m}$	Sensitivity value of the nth process variable (y) with respect to the mth model parameter (θ) –
$\nu_{i,j}$	Biochemical rate (or liquid phase yield) coefficient for component i on process j –
ρ_j	Kinetic rate of process j (for acid-base and gas–liquid equations units are in kmol m^{-3} d^{-1}) kg COD_S_i m^{-3} d^{-1}
δ	Perturbation factor Fraction
σ	Standard deviations Vary with θ
α	Significance level %

Subscript

bac	Pertaining to bacteria –
dec	Pertaining to decay processes –
df	Degree of freedom
free	Undissociated form of the species –
gas	Pertaining to the gas phase –
i	Pertaining to soluble or particulate component –
j	Pertaining to processes –
I	Pertaining to the inert fraction –

1. Introduction

Many industrial processes, especially in food and fermentation industries, generate wastewaters with high levels of chemical oxygen demand (COD) and sulfate (Zub et al., 2008). Vinasse obtained from ethanol distillation in the sugar cane industry (cane-molasses vinasse) is a typical example of very high strength and sulfate rich liquid substrate (Barrera et al., 2013). Hence, the anaerobic digestion of vinasse promotes the activity of sulfate reducing bacteria (SRB) producing sulfide. The latter is distributed among aqueous sulfide (H_2S free, HS^- and S^{2-}), hydrogen sulfide in the biogas and insoluble metallic sulfides.

Modeling has proven to be an important tool for understanding, design and control of the sulfate reduction process (Batstone, 2006). A simple approach to model sulfate reduction is by considering the oxidation (by SRB) of the available hydrogen only (Batstone, 2006). However, in systems with high sulfate concentrations volatile fatty acids (butyric, propionic and acetic) have, to be included as electron donors in the sulfate degradation reactions in addition to hydrogen (Batstone, 2006). Barrera et al. (2014) provided a characterization of the sulfate reduction process in the anaerobic digestion of a very high strength and sulfate rich vinasse. The authors demonstrated that propionate sulfate reducing bacteria considerably contribute to propionic acid degradation at SO_4^{2-}/COD ratios $\leq$0.10 as a result of hydrogen limitation. This suggests that reactions involving volatile fatty acids need to be included to properly model sulfate reduction in the anaerobic digestion of such vinasses. The Anaerobic Digestion Model No. 1 (ADM1), developed by the IWA Task Group for Mathematical Modeling of Anaerobic Digestion Processes, is one of the most sophisticated and complex anaerobic digestion models, involving 19 biochemical processes and two types of

physiochemical processes (Batstone et al., 2002). The simple approach of Batstone (2006) to model sulfate reduction as an extension of ADM1 has been used to model the anaerobic digestion of vinasse under dynamic conditions without success, exhibiting under prediction of H_2S and over prediction of volatile fatty acids (Hinken et al., 2013). In order to extend ADM1, Fedorovich et al. (2003) included the sulfate reduction process starting from previously reported work (Kalyuzhnyi et al., 1998; Kalyuzhnyi and Fedorovich, 1998; Knobel and Lewis, 2002; Ristow et al., 2002). The approach of Fedorovich et al. (2003) can be considered as complex because of the inclusion of valerate/butyrate, propionate, acetate and hydrogen in the sulfate degradation reactions (Batstone, 2006). This model (Fedorovich et al., 2003) was calibrated for organic deficient (SO_4^{2-}/COD ratios $\geq$ 1.5) synthetic wastewaters (Omil et al., 1996, 1997), hereby focusing on volatile fatty acids, sulfates and methane gas phase concentrations. Furthermore, the agreement between model and experimental values for the concentrations of total aqueous sulfide (S_{h2s}), free sulfides ($S_{h2s,free}$) and gas phase sulfides ($S_{gas,h2s}$) was not reported. Likely because of these limitations, the extension of Fedorovich et al. (2003) is not commonly used (Lauwers et al., 2013).

Consequently, an extension of ADM1 with sulfate reduction to model the anaerobic digestion of a very high strength and sulfate rich vinasse may overcome the current limitation of models by (1) describing the sulfate reduction process in the anaerobic digestion of vinasse, (2) predicting the sulfur compounds in both the gas and liquid phases, (3) increasing applicability of ADM1 to specific industrial wastewaters (vinasse), and (4) simplifying the existing approach to reduce complexity and to support further implementations.

Therefore, the work presented here attempts to model the anaerobic digestion of real cane-molasses vinasse by extending ADM1 with sulfate reduction for a very high strength and sulfate-rich complex wastewater, including volatile fatty acids (propionic and acetic acids) in the sulfate degradation reactions, hereby including an accurate prediction of S_{h2s}, $S_{h2s,free}$ and $S_{gas,h2s}$.

2. Materials and methods

2.1. Experimental data

Experimental observations from a characterization study of the sulfate reduction process in the anaerobic digestion of a very high strength and sulfate-rich vinasse (Barrera et al., 2014) were used for model calibration and validation. During these experiments a 3.5 L UASB reactor was operated under dynamic conditions for a period of 75 days (following a 55 day start-up period). The experimental set-up, analytical methods and operating conditions are described in detail in Barrera et al. (2014). They can be briefly described as follows, where the E-codes indicate successive experiments conducted under different operating conditions:

- E–1 to E–3: the concentration of influent COD and SO_4^{2-} was gradually increased while keeping the SO_4^{2-}/COD ratio at 0.05.
- E–3 to E–4: the influent SO_4^{2-} was increased whereas the influent COD concentration was decreased to increase the SO_4^{2-}/COD ratio to 0.1.
- E–4 to E–6: the concentration of influent COD and SO_4^{2-} was increased while keeping the SO_4^{2-}/COD ratio at 0.1.
- E–7: the concentration of influent COD and SO_4^{2-} was reduced to control toxicity, keeping the SO_4^{2-}/COD ratio at 0.1.
- E–8 and E–9: the influent SO_4^{2-} was increased while keeping a constant influent COD concentration to increase the SO_4^{2-}/COD ratio to 0.15 and 0.20, respectively.

Operating conditions were grouped in data set D1 (operating conditions E–1, E–2, E–3 and E–4 in Barrera et al. (2014)) for calibration and direct validation, and data set D2 (operating conditions E–5, E–6, E–7, E–8 and E–9 in Barrera et al. (2014)) for cross validation.

2.2. Model description and implementation

The original ADM1 is described in a scientific and technical report prepared by an IWA Task Group (Batstone et al., 2002). This model takes into account seven bacterial groups. The biological degradation processes are described using Monod kinetics, while the extracellular processes (disintegration and hydrolysis) and the biomass decay are described using first-order kinetics.

The ADM1 extension with sulfate reduction for high strength and sulfate rich wastewater was implemented in MatLab/Simulink 2008b following the original ADM1 (Batstone et al., 2002) and the approaches discussed by Barrera et al. (2013). The model was implemented as a set of ordinary differential equations using the ODE 15s as numerical solver.

Based on experimental observations previously discussed in Barrera et al. (2014), butyric acid was neglected as organic matter for SRB in the model structure ($\leq$5% of the total volatile fatty acids concentration), whereas propionic (considered incompletely oxidized by propionate SRB) and acetic acids, as well as hydrogen, were considered as the electron donors for the sulfate reduction processes following the biochemical degradation reactions (1), (2) and (3) below:

$$C_2H_5COOH + 0.75H_2SO_4 \rightarrow CH_3COOH + CO_2 + H_2O + 0.75H_2S \quad (1)$$

$$CH_3COOH + H_2SO_4 \rightarrow 2CO_2 + 2H_2O + H_2S \quad (2)$$

$$4H_2 + H_2SO_4 \rightarrow H_2S + 4H_2O \quad (3)$$

Consequently, three SRB groups were considered to be active inside the reactor; i.e. propionate sulfate reducing bacteria (pSRB), acetate sulfate reducing bacteria (aSRB) and hydrogenotrophic sulfate reducing bacteria (hSRB). A dual term Monod type kinetics was used to describe the uptake rate of these substrates (Fedorovich et al., 2003). The biochemical rate coefficients ($v_{i,j}$) and kinetic rate equation (ρ_j) for soluble and particulate components are listed in Table 1. Similar to decay of other microbial species, first order kinetics was used to describe the decay of SRB. Additionally, rate coefficients and kinetic rate equations for acid-base reactions for sulfides and sulfates (in the form recommended by Rosen and

Table 1 – Biochemical rate coefficients ($\nu_{i,j}$) and kinetic rate equation (ρ_j) for soluble and particulate components added to ADM1 to model the sulfate reduction process in the anaerobic digestion of cane-molasses vinasse.

	Component i →	6	7	8	8a	9a	10	11	13	21a	22a	23a	Rate (ρ, kg COD m^{-3} d^{-1})
j	Process ↓	S_{pro}	S_{ac}	S_{h2}	S_{so4}	S_{h2s}	S_{IC}	S_{IN}	X_c	X_{pSRB}	X_{aSRB}	X_{hSRB}	
10a	Uptake of Propionate by pSRB	−1	$(1-Y_{pSRB})0.57$		$-(1-Y_{pSRB})$ 0.43/64	$(1-Y_{pSRB})$ 0.43/64	$-\sum_{i=1-9a;\ i=11-24} C_i\nu_{i,10a}$	$-Y_{pSRB}\cdot N_{bac}$		Y_{pSRB}			$k_{m,pSRB}\cdot\frac{S_{pro}}{K_{S,pro}+S_{pro}}\cdot\frac{S_{so4}}{K_{S,so4,pSRB}+S_{so4}}\cdot X_{pSRB}\cdot I_4$
11a	Uptake of Acetate by aSRB		−1		$-(1-Y_{aSRB})/64$	$(1-Y_{aSRB})/64$	$-\sum_{i=1-9a;\ i=11-24} C_i\nu_{i,11a}$	$-Y_{aSRB}\cdot N_{bac}$			Y_{aSRB}		$k_{m,aSRB}\cdot\frac{S_{ac}}{K_{S,ac}+S_{ac}}\cdot\frac{S_{so4}}{K_{S,so4,aSRB}+S_{so4}}\cdot X_{aSRB}\cdot I_4$
12a	Uptake of Hydrogen by hSRB			−1	$-(1-Y_{hSRB})/64$	$(1-Y_{hSRB})/64$	$-\sum_{i=1-9a;\ i=11-24} C_i\nu_{i,12a}$	$-Y_{hSRB}\cdot N_{bac}$				Y_{hSRB}	$k_{m,hSRB}\cdot\frac{S_{h2}}{K_{S,h2}+S_{h2}}\cdot\frac{S_{so4}}{K_{S,so4,hSRB}+S_{so4}}\cdot X_{hSRB}\cdot I_4$
17a	Decay of X_{pSRB}						$-C_{bac}+C_{xc}$	$-N_{bac}+N_{xc}$	1	−1			$k_{dec,XpSRB}\cdot X_{pSRB}$
18a	Decay of X_{aSRB}						$-C_{bac}+C_{xc}$	$-N_{bac}+N_{xc}$	1		−1		$k_{dec,XaSRB}\cdot X_{aSRB}$
19a	Decay of X_{hSRB}						$-C_{bac}+C_{xc}$	$-N_{bac}+N_{xc}$	1			−1	$k_{dec,XhSRB}\cdot X_{hSRB}$
		Total propionate (kg COD m^{-3})	Total acetate (kg COD m^{-3})	Total hydrogen gas (kg COD m^{-3})	Total sulfates (kmol m^{-3})	Hydrogen sulfide (kmol m^{-3})	Inorganic carbon (kmol m^{-3})	Inorganic nitrogen (kmol m^{-3})	Composites (kg COD m^{-3})1	Propionate SRB (kg COD m^{-3})	Acetate SRB (kg COD m^{-3})	Hydrogeno-trophic SRB (kg COD m^{-3})	Inhibition term for X_{c4} & X_{pro} (See I_2 in Batstone et al. (2002)) $I_2\cdot I_{h2s,8-10}$ Inhibition term for X_{ac} (See I_3 in Batstone et al. (2002)) $I_3\cdot I_{h2s,11}$ Inhibition term for X_{h2} (See I_1 in Batstone et al. (2002)) $I_1\cdot I_{h2s,12}$ Inhibition term for pSRB, aSRB & hSRB $I_4 = I_{pH}\cdot I_{h2s,(10a,\ 11a,12a)}$

Table 2 – Rate coefficients ($v_{i,j}$) and kinetic rate equation (ρ_j) for acid-base reactions in the differential equation implementation added to ADM1 to model the sulfate reduction process in the anaerobic digestion of cane-molasses vinasse.

	Component i →	8a.1	8a.2	9a.1	9a.2	Rate (ρ_j, kmol m^{-3} d^{-1})
j	Process ↓	S_{hso4-}	$S_{so4}2-$	$S_{h2s,free}$	S_{hs-}	
A12	Sulfide acid–base			1	−1	$K_{A/B,h2s} \cdot (S_{hs-} \cdot (S_{H+} + K_{a,h2s}) - K_{a,h2s} \cdot S_{h2s,total})$
A13	Sulfate acid–base	1	−1			$K_{A/B,so4} \cdot (S_{so4,total} \cdot S_{H+} - (K_{a,so4} + S_{H+}))$

Jeppsson (2006)) were considered (Table 2). Un-dissociated sulfuric acid (H_2SO_4) and sulfide ions (S^{2-}) were considered negligible and were not included in the acid-base reactions. As sulfuric acid is a strong acid (pKa < −2), it can be considered completely dissociated, whereas sulfide ions S^{2-} exist in small amounts (pKa ≈ 14) in the liquid phase of anaerobic reactors in which a pH between 6.5 and 8 is required. The dissociation Eqs (4) and (5) were included in the model.

$$HSO_4^- \rightleftarrows H^+ + SO_4^{2-} \quad pK_a = 1.99 \tag{4}$$

$$H_2S \rightleftarrows H^+ + HS^- \quad pK_a = 7.01 \tag{5}$$

To model the stripping of H_2S, the liquid phase yield coefficient ($v_{i,j}$) and the rate equations (ρ_j) for liquid–gas transfer process were also included (Table 3). Nomenclature in Tables 1–3 was adopted from ADM1 (Batstone et al., 2002).

Despite the fact that S_{h2s} has been found to inhibit anaerobic digestion (Visser et al., 1996), $S_{h2s,free}$ was assumed to be inhibitory for modeling purposes (Kalyuzhnyi et al., 1998; Kalyuzhnyi and Fedorovich, 1998; Knobel and Lewis, 2002; Ristow et al., 2002). A non-competitive inhibition function for sulfides ($I_{h2s,j}$) was considered in all cases (Knobel and Lewis, 2002). The inhibition terms I_1 and I_2 were adopted from the original ADM1 for the uptake of sugars, amino acids and long chain fatty acids (processes not shown in Table 1). However, the inhibition term for valerate, butyrate and propionate degraders (I_2 in Batstone et al. (2002)) as well as the inhibition term for acetotrophic methanogens (I_3 in Batstone et al. (2002)) and the inhibition term for hydrogenotrophic methanogens (I_1 in Batstone et al. (2002)) was multiplied by $I_{h2s,j}$ in order to include the free sulfide inhibition in this model extension. The inhibition term I_4 was added to account for pH inhibition ($I_{pH,j}$) and $I_{h2s,j}$ of pSRB, aSRB and hSRB (see inhibition terms in Table 1). All pH inhibitions were based on the Hill function as suggested in Rosen and Jeppsson (2006).

Table 3 – Liquid phase yield coefficient ($v_{i,j}$) and rate equations (ρ_j) for the liquid–gas transfer process added to ADM1 to model the sulfate reduction process in the anaerobic digestion of cane-molasses vinasse.

	Component i →	9a	Rate (ρ_j, kmol m^{-3} d^{-1})
j	Process ↓	$S_{h2s,free}$	
T9a	H_2S Transfer	−1	$k_La \cdot (S_{h2s,free} - K_{H,h2s} \cdot P_{gas,h2s})$

2.3. Model inputs and initial conditions

The influent characterization of cane-molasses vinasse is shown in Table 4. Sugar, protein and lipid contents were experimentally determined in the filtered and unfiltered vinasse and used to calculate the soluble sugars (S_{su}) and particulate carbohydrates (X_{ch}), the soluble amino acids (S_{aa}) and particulate proteins (X_{pr}) as well as the long chain fatty acids (S_{fa}) and particulate lipids (X_{li}), respectively. The total cation concentration was determined as the sum of Na^+, K^+, Ca^{2+}, Mg^{2+}, Mn^{2+}, and Zn^{2+} species concentrations whereas NO_2^-, NO_3^-, PO_4^{3-}, and Cl^- concentrations were used to determine the total anion concentration of vinasse.

The difference between the soluble COD (SCOD) and the total COD of S_{su}, S_{aa}, S_{fa} and S_{ac} was assumed to be the soluble inert concentration of vinasse (S_I). Similarly, the difference between the COD concentration of the particulate matter (XCOD) and the total COD of X_{ch}, X_{pr} and X_{li} was assumed to be the particulate inert concentration of vinasse (X_I) (See Table 4). The concentrations of these known input variables (S_{su}, S_{aa}, S_{fa}, S_{ac}, S_I, X_{ch}, X_{pr}, X_{li}, and X_I) under specific operating conditions (E−1 to E−9) were calculated from the total COD (TCOD) of the diluted vinasse at these operating conditions and the compositions of raw vinasse as given in Table 4. This is illustrated for sugars in Eq. (6).

$$S_{su\_operating\ conditions(E-1\ to\ E-9)} = \frac{TCOD\_diluted\_vinasse\_operating\ conditions(E-1\ to\ E-9)}{TCOD\_raw\_vinasse\_Table\ 4} \cdot S_{su\_raw\ vinasse\_Table\ 4} \tag{6}$$

ADM1 requires a large number of input variables. Reasonable assumptions were made for the concentration of the unknown input variables S_{h2}, S_{ch4}, X_{su}, X_{aa}, X_{fa}, X_{c4}, X_{pro}, X_{ac}, X_{h2}, X_{pSRB}, X_{aSRB} and X_{hSRB}. Their default concentrations in ADM1 were set for the operating condition E−1, whereas concentrations for the cases E−2 to E−9 were calculated similar to Eq. (6).

The initial conditions for the dynamic simulation were estimated as recommended by Rieger et al. (2012). Steady state simulations were run and the values of the state variables at the end of this simulation period were used as initial conditions for the dynamic simulation. Since this procedure assumes that the reactor is operated in a typical way for an extended period prior to the dynamic simulation (similar to the experiments used for calibration and validation), this was

Table 4 – Model based influent characterization of cane-molasses vinasse.

Components	Names	Units	Values
Solubles			
S_{su}	Sugar concentration	kg COD m^{-3}	33.73
S_{aa}	Amino acid concentration	kg COD m^{-3}	5.82
S_{fa}	LCFA concentration	kg COD m^{-3}	0.09
S_{ac}	Acetic acid concentration	kg COD m^{-3}	1.36
S_{SI}	Inert concentration	kg COD m^{-3}	16.97
SCOD	Soluble COD concentration	kg COD m^{-3}	57.97
Particulates			
X_{ch}	Carbohydrate concentration	kg COD m^{-3}	6.91
X_{pr}	Protein concentration	kg COD m^{-3}	0.09
X_{li}	Lipid concentration	kg COD m^{-3}	0.14
X_I	Inert concentration	kg COD m^{-3}	0.00
X_c	Composite concentration	kg COD m^{-3}	0.00
XCOD	Particulate COD concentration	kg COD m^{-3}	7.15
TCOD	Total COD	kg COD m^{-3}	65.12
Total cation	Total cation concentration	kmol m^{-3}	0.315
Total anion	Total anion concentration	kmol m^{-3}	0.073

considered sufficient to establish the initial conditions for this work (Rieger et al., 2012).

2.4. *Sensitivity analysis*

Despite the fact that all parameters affect the model output, the output sensitivity differs from one parameter to another. Sensitivity analysis has been widely applied to reduce model complexity, to determine the significance of model parameters and to identify dominant parameters (Dereli et al., 2010; Silva et al., 2009; Tartakovsky et al., 2008).

The local relative sensitivity analysis method (Dochain and Vanrolleghem, 2001) is employed here in order to calculate sensitivity functions for the dynamic simulations.

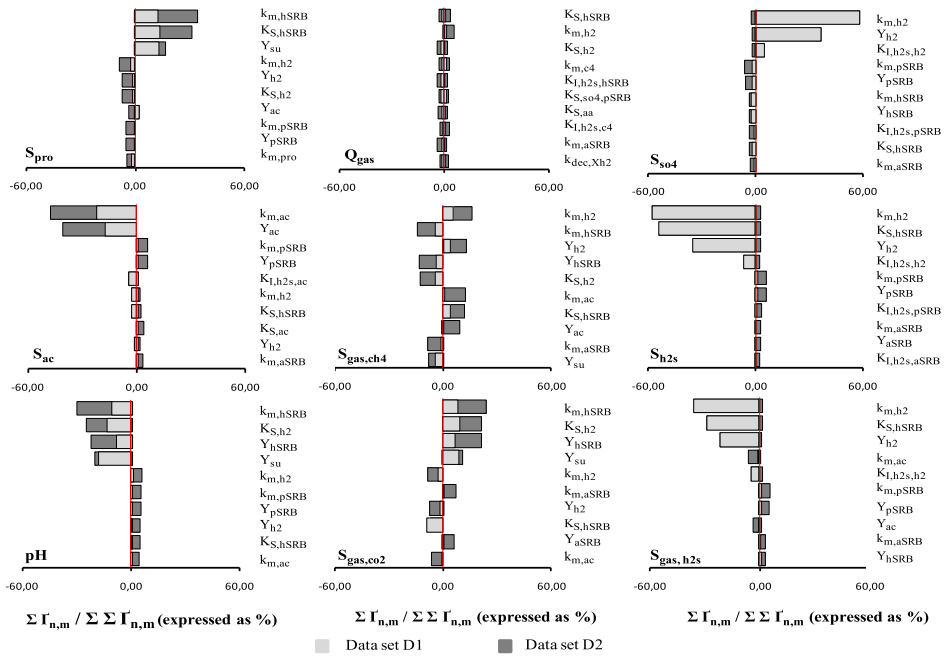

Fig. 1 – Most sensitive model parameters arranged in descending order, for the process variables S_{pro}, S_{ac}, pH, Q_{gas}, $S_{gas,ch4}$, $S_{gas,co2}$, S_{so4}, S_{h2s}, and $S_{gas,h2s}$.

The numerical calculation of sensitivity functions uses the finite difference approximation (Dochain and Vanrolleghem, 2001). The sensitivities are quantified in terms of the variation of measurable process variables under the perturbation of model parameters in their neighborhood domain (Eq. (7)). The value of the perturbation factor δ was chosen such that the differences between the resulting sensitivity values of different parameters can be detected.

$$r'_{n,m}(t) = \frac{\partial y_n(t)/y_n(t)}{\partial\theta_m/\theta_m} = \frac{(y_n(t,\theta_m+\delta\cdot\theta_m) - y_n(t,\theta_m))/y_n(t,\theta_m)}{\delta\cdot\theta_m/\theta_m} \quad (7)$$

where $r'_{n,m}$ is the dimensionless sensitivity value of the nth process variable with respect to the mth model parameter; y_n (n = 1, … 9) denotes the nth process variable (i.e. S_{pro}, S_{ac}, pH, Q_{gas} (gas flow), $S_{gas,ch4}$, $S_{gas,co2}$, S_{so4}, S_{h2s}, and $S_{gas,h2s}$); θ_m is the mth model parameter, m = 1, … 40 (see parameters in Appendix A); and $\theta_m+\delta\cdot\theta_m$ is the perturbated parameter value. The sensitivity values for each process variable to each model parameter for data set D1 (days 0–36) and data set D2 (days 37–75), were computed as $\sum r'_{n,m}(t)$ (expressed as % in respect to the total $\sum\sum r'_{n,m}(t)$) and arranged in descending order.

2.5. Model calibration, parameter uncertainties and validation procedure

Calibration of the more sensitive model parameters is now required. Model calibration was performed on an expert –basis by a trial and error approach, driven by knowledge from the sensitivity analysis and using the parameter ranges reported in the literature as constraints. The iterative procedure reported by Dereli et al. (2010) was applied.

In order to provide information about the uncertainty of the calibrated parameters, confidence intervals (CI) for the resulting set of parameters were calculated based on the Fisher information matrix (FIM) (Eq. (8)) (Dochain and Vanrolleghem, 2001).

$$FIM = \sum_{i=1}^{t}\left(\frac{\partial y_n}{\partial\theta_m}(t)\right)^T \sum^{-1}\cdot\left(\frac{\partial y_n}{\partial\theta_m}(t)\right) \quad (8)$$

where, $\partial y_n/\partial\theta_m(t)$ are the absolute sensitivity values and $\sum^{-1}$ is calculated as the inverse of the covariance matrix of the measurement error (Dochain and Vanrolleghem, 2001). Subsequently, the covariance matrix (COV) can be approximated by the inverse of the FIM matrix ($COV = FIM^{-1}$) and the standard deviations (σ) for the parameters (θ_m) can be obtained by using Eq. (9) (Dochain and Vanrolleghem, 2001).

$$\sigma(\theta_m) = \sqrt{COV_{m,m}} \quad (9)$$

Confidence intervals for the parameters (Eq. (10)) were calculated for a confidence level of 95% ($\alpha = 0.05$) and the t-value was obtained from the Student-t distribution.

$$\theta_m \pm t_{\alpha,df}\cdot\sigma(\theta_m) \quad (10)$$

Once a set of estimated parameters has been obtained, it is necessary to question the predictive quality of the resulting model through validation (Donoso-Bravo et al., 2011). Direct and cross validation are usually considered as steps of the model validation procedure (Donoso-Bravo et al., 2011). Therefore, the data was divided into two subsets as recommended by Donoso-Bravo et al. (2011): (1) data used during model calibration (data set D1) for direct validation, and (2) unseen data (data set D2) for cross validation. The accuracy of the predictions for direct and cross validation were determined by using the mean absolute relative error and they were classified as high (±10%) or medium (10%–30%) accurate quantitative prediction (Batstone and Keller, 2003).

3. Results and discussion

3.1. Sensitivity analysis

Steady state simulations using the ADM1 benchmark parameter values (Rosen and Jeppsson, 2006) and values given by Fedorovich et al. (2003) for sulfate reduction showed discrepancies greater than 50% between the experimental results and the model predictions.

To further improve the dynamic predictions, a sensitivity analysis was performed under dynamic conditions in order to determine the most important parameters to be used in the dynamic calibration. The resulting local sensitivity values ($\sum r'_{n,m}/\sum\sum r'_{n,m}$, expressed as %) for each process variable (S_{pro}, S_{ac}, pH, Q_{gas}, $S_{gas,ch4}$, $S_{gas,co2}$, S_{so4}, S_{h2s}, and $S_{gas,h2s}$) are shown in Fig. 1. The perturbation factor δ was set as 1% for all the calculations as in Tartakovsky et al. (2008). It is noteworthy that negative values indicated a decrease of the process variable when the parameter was perturbed.

Fig. 1 allows the identification of the most sensitive model parameters for each process variable. For example, the process variable S_{pro} is highly sensitive to parameters $k_{m,hSRB}$, $K_{S,hSRB}$ and Y_{su} (see nomenclature of the parameters in Appendix A), whereas S_{ac} is highly sensitive to $k_{m,ac}$ and Y_{ac}. The fact that some model parameters affected several process variables at the same time (e.g. the model parameter Y_{su} affected the process variables S_{pro}, pH, $S_{gas,ch4}$ and $S_{gas,co2}$) was also useful for model calibration. Additionally, it was observed from the sensitivity analysis that the effect of the model parameters from days 0 to 36 (data set D1) varied in comparison to those from days 37 to 75 (data set D2) (Fig. 1). In that sense, an increased sensitivity towards $k_{m,hSRB}$ on S_{pro} was observed near the end of the experiments (data set D2) because of the increase of influent sulfates (see experimental conditions in Barrera et al. (2014)), which made the sulfate reduction process predominant leading to a higher sensitivity (with respect to data set D1).

Therefore, the sensitivity analysis enabled ranking the effect of the model parameters on each process variable, which yields information useful for model calibration.

3.2. Model calibration

The model was calibrated using 36 days of dynamic data (data set D1). During these days, the organic loading rate (OLR) of the upflow anaerobic sludge bed (UASB) reactor was gradually increased from 7.66 to 12.00 kg COD m^{-3} d^{-1} and later reduced to 7.9 kg COD m^{-3} d^{-1}. At the same time, the sulfate loading rate (SLR) was increased from 0.36 to 0.76 kg SO_4^{2-} m^{-3} d^{-1} at a constant hydraulic retention time of 4.86 days, resulting in an increase of the SO_4^{2-}/COD ratio from 0.05 to 0.10 (Barrera et al., 2014).

Initial values of the model state variables were taken from steady state simulations at the operating conditions of E–1 and the dynamic input variables were calculated from the influent characterization of cane-molasses vinasse (Table 4), as illustrated in Eq. (6).

An iterative method (Dereli et al., 2010) was applied for the calibration of the most sensitive parameters by fitting the model to the experimental results for the process variables S_{so4}, S_{h2s}, $S_{h2s,free}$, $S_{gas,h2s}$, Q_{gas}, $S_{gas,ch4}$, $S_{gas,co2}$, S_{pro}, S_{ac}, eff_COD (effluent COD) and pH. Although a larger number of ADM1 parameters were sensitive to the process variables (Fig. 1), only $k_{m,pro}$, $k_{m,ac}$, $k_{m,h2}$, and Y_{h2} were used for calibration, as the sensitivity analysis revealed them to be among the most sensitive model parameters (Fig. 1). In this way, the number of calibrated ADM1 parameters was kept to a strict minimum. In addition, all sulfate reduction parameters (70% among the most sensitive parameters of Fig. 1) were calibrated. The estimated parameter values providing the best fit (based on the mean absolute relative error) between model predictions and experimental results are reported in column 7 (Calibration this work) of Appendix A. All other parameters were adopted from Rosen and Jeppsson (2006).

During calibration, the values obtained for $k_{m,pro}$, $k_{m,ac}$, and $k_{m,h2}$ were in agreement with values used to calibrate the anaerobic digestion of cane-molasses (Romli et al., 1995) (Column 5, Appendix A). The fact that parameter values used for calibration in Romli et al. (1995) were used for calibration in this work, was likely because of the similar characteristics of both substrates (cane-molasses and cane-molasses vinasse, respectively), which favored the uptake rate of propionate, acetate and hydrogen leading to required modification (in respect to ADM1 parameter values) of $k_{m,pro}$, $k_{m,ac}$, and $k_{m,h2}$ during the calibration in this work (Appendix A).

Concerning the calibration of the sulfate reduction parameters, the yield coefficients, the Monod maximum specific uptake rates and the half saturation coefficients were found in the range of values found in the literature (Barrera et al., 2013). However, the 50% inhibitory concentrations of free H_2S (Appendix A) were lower than the values used to calibrate the sulfate reduction processes (Barrera et al., 2013), but similar to experimental values reported as inhibitory (150 mg S L^{-1} (0.0047 kmol m^{-3})) for methanogens and SRB (except for propionate degraders, which is 70 mg S L^{-1} (0.0022 kmol m^{-3})) (Rinzema and Lettinga, 1988). These values agreed well with the experimental observations used for calibration in this work (Barrera et al., 2014) and therefore they can be considered a better approximation for the real phenomena.

In contrast, fitting of $K_{S,so4,pSRB}$, $K_{S,so4,aSRB}$, and $K_{S,so4,hSRB}$ was required to predict S_{so4} as these parameters solely impact this process variable (results not shown). Values up to 10 times higher than those from the literature (Barrera et al., 2013) were retrieved for $K_{S,so4,pSRB}$, $K_{S,so4,aSRB}$, and $K_{S,so4,hSRB}$. This observation was attributed to the use (by previous modelers) of experimental observations based on organic deficient substrates (SO_4^{2-}/COD ratios $\geq$ 1.5) (Alphenaar et al., 1993; Omil et al., 1996, 1997) to fit models (Fedorovich et al., 2003; Kalyuzhnyi et al., 1998), by increasing the maximum specific uptake rate and decreasing the half saturation coefficient of SRB. The half saturation coefficient for hSRB ($K_{S,hSRB}$) agreed well with values reported (Batstone et al., 2006) and was 86% of the half saturation coefficient of hydrogenotrophic methanogenic archea (hMA), showing that hSRB can outcompete hMA for hydrogen (Omil et al., 1997; Rinzema and Lettinga, 1988).

3.3. Parameter uncertainty estimation

The confidence intervals (CI) for the calibrated parameters are shown in Appendix A. They were found to be below 20% in all cases which yields a satisfactory confidence in the determined set of parameters (confidence level 95%). The correlation between the calibrated parameters was also calculated based on the covariance matrix (COV), rendering the following results:

- Strong correlation ($\geq$0.7) between the parameter pairs [$k_{m,aSRB}$, Y_{aSRB}]; [$k_{m,pro}$, $K_{I,h2s,pro}$]; and [$k_{m,ac}$, $K_{I,h2s,ac}$].
- Moderate correlation (0.4–0.7) between the parameter pairs [Y_{h2}, Y_{hSRB}]; [$k_{m,pSRB}$, Y_{pSRB}]; [$k_{m,hSRB}$, $K_{S,hSRB}$]; [$K_{S,so4,aSRB}$, $K_{S,so4,hSRB}$]; [$K_{S,so4,hSRB}$, $K_{I,h2s,h2}$]; [$K_{S,so4,pSRB}$, $K_{I,h2s,aSRB}$]; [$K_{S,so4,pSRB}$, $K_{I,h2s,hSRB}$]; and [$k_{m,hSRB}$, $K_{I,h2s,hSRB}$].

3.4. Direct validation

The deviation between model predictions and experimental observations was used for direct validation. The results are shown in Fig. 2. It can be seen that the process variables (except for S_{pro}) were predicted quite well after the model calibration (Fig. 2A–H), exhibiting a mean absolute relative error below 10% (1%–9.7%), which is considered as a high accuracy quantitative prediction (Batstone and Keller, 2003). However, deviations between model predictions and experimental values for S_{pro} (Fig. 2G) led to a mean absolute relative error higher than 30%, which can be considered as a qualitative prediction that can demonstrate the overall qualitative response of the system (Batstone and Keller, 2003).

The increase of the OLR and the influent COD concentration in a UASB reactor fed with vinasse caused an increase of the propionic acid concentration (Harada et al., 1996). However, in the experimental values used for calibration in this work, S_{pro} remained constant (see experimental values in Fig. 2G) when the OLR was increased on day 8 (Barrera et al., 2014). This was likely because sludge in the UASB reactor assimilated the increase of the OLR by degrading the excess propionate. Despite the fact that the model could not predict

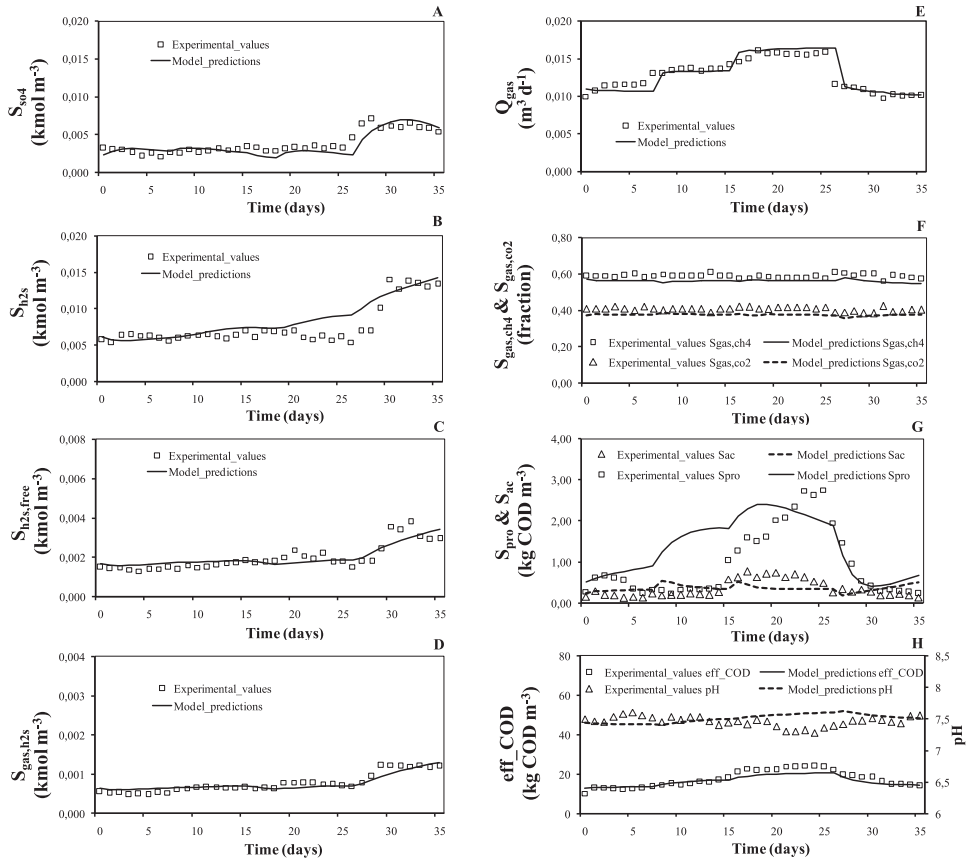

Fig. 2 – Comparison between experimental values and model predictions after the model calibration: (A) S_{so4}, (B) S_{h2s}, (C) $S_{h2s,free}$, (D) $S_{gas,h2s}$, (E) Q_{gas}, (F) $S_{gas,ch4}$ & $S_{gas,co2}$, (G) S_{pro} & S_{ac}, and (H) eff_COD & pH.

this observation (Fig. 2G), the over prediction observed for S_{pro} during days 8–15 when the OLR increased was in agreement with the phenomenon described by Harada et al. (1996). Moreover, the under prediction of S_{pro} during days 23–25 can be attributed to the slight under prediction of $S_{h2s,free}$ (constant at the concentration of 0.0018 kmol m^{-3}) that reduces the inhibitory effect of sulfide on propionate degrading bacteria during the simulation (Fig. 2C).

Additionally, the over prediction of S_{h2s} during days 21–27 (Fig. 2B) can be attributed to hydrogen sulfide loss during the experiments used for calibration as the sulfur recovery in the reactor outlet streams decreases from 100% to 90% (Barrera et al., 2014).

3.5. *Cross validation*

A cross validation study was performed to assess the quality and applicability of the calibrated model. The model outputs were compared with data set D2 (days 37–75) under the operating conditions E–5, E–6, E–7, E–8 and E–9 (Barrera et al., 2014) without changing the previously optimized parameter set. During these periods, the OLR and SLR of the UASB reactor were in the range of 7.72–10.69 kg COD m^{-3} d^{-1} and 0.76–1.57 kg SO_4^{2-} m^{-3} d^{-1}, respectively (Barrera et al., 2014). SO_4^{2-}/COD ratios of 0.10, 0.15 and 0.20 were applied in the periods covering the validation study unlike the periods used for the calibration study.

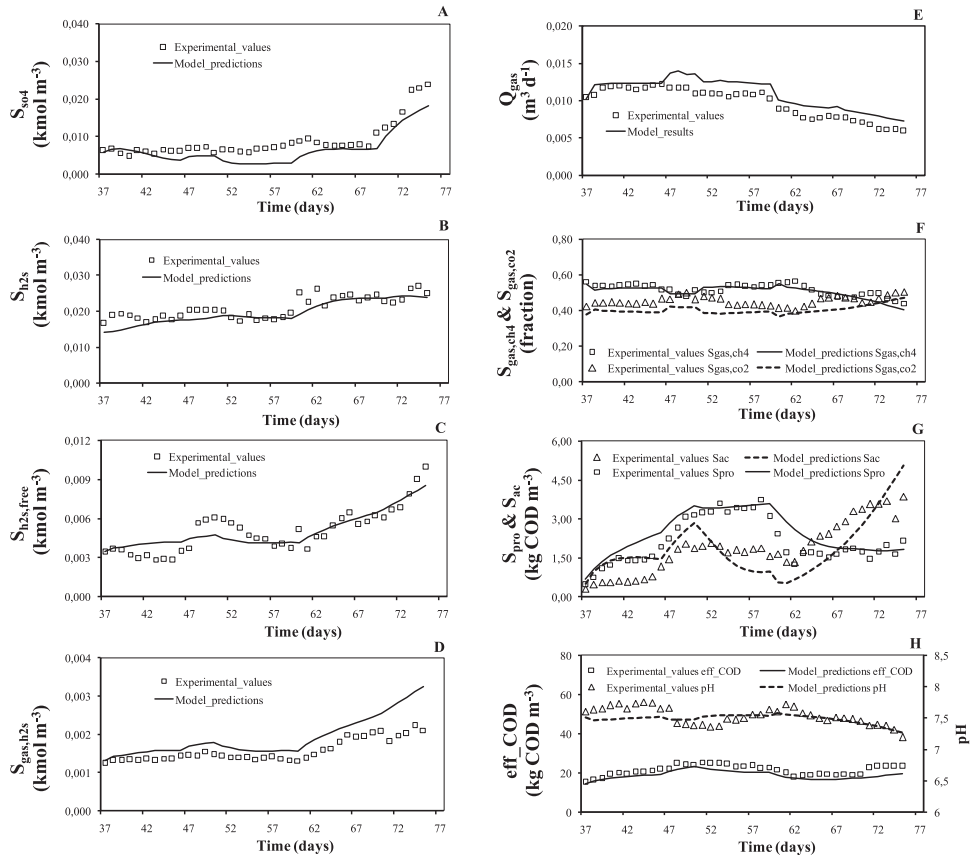

Fig. 3 – Validation of model predictions with experimental values: (A) S_{so4}, (B) S_{h2s}, (C) $S_{h2s,free}$, (D) $S_{gas,h2s}$, (E) Q_{gas}, (F) $S_{gas,ch4}$ & $S_{gas,co2}$, (G) S_{pro} & S_{ac}, and (H) eff_COD & pH.

Fig. 3 (B, C, F, G & H) presents the comparison of model predictions and experimental values for the process variables during the validation study. As can be seen, S_{h2s}, $S_{h2s,free}$, $S_{gas,ch4}$, $S_{gas,co2}$, S_{ac}, and pH were well predicted by the model showing a mean absolute relative error below 10% (1%–10%), which is considered as a highly accurate quantitative prediction (±10%) (Batstone and Keller, 2003). A medium accurate quantitative prediction (10%–30%) was achieved for S_{pro}, S_{so4}, $S_{gas,h2s}$, Q_{gas}, and eff_COD (Fig. 3 A, E, G & H), as the mean absolute relative error ranged from 12% to 26% (Batstone and Keller, 2003).

The underestimation observed for S_{so4} during days 51–62 and 73 to 75 (Fig. 3A), was in agreement with the lower $S_{h2s,free}$ predicted during these days (Fig. 3C), which reduced the inhibitory effect of $S_{h2s,free}$ on SRB during the simulation. The excess consumption of sulfate was accumulated in the gas phase since higher $S_{gas,h2s}$ and Q_{gas} were predicted during these periods (Fig. 3D and E). This was likely due to the assumption of a constant gas–liquid transfer coefficient (200 d^{-1}) for H_2S even when the biogas production rate, and consequently its stripping effect, decreased after day 60 in the model predictions (Fig. 3E). The over and under predictions of $S_{h2s,free}$ from days 40 to 45 and 48 to 55, respectively (Fig. 3C), were attributed to slight deviations (±3.1%) in the pH prediction (Fig. 3H).

During the validation period the model was also able to predict the reactor failure (for methanogenesis and sulfidogenesis) from days 70 to 75. Methanogenesis failure in the model predictions was evidenced by a pH decrease due to S_{ac} increase, which led to a decrease of Q_{gas} and $S_{gas,ch4}$ (Fig. 3E, F, G & H). At the same time, sulfidogenesis failure in the model prediction was evidenced by the increase of S_{so4} while S_{h2s} remained constant, showing that the increase in

the SLR resulted in accumulation of sulfates in the effluent rather than conversion to hydrogen sulfide (Fig. 3A and B). In addition, the model predicted an $S_{h2s,free}$ increase as a result of a pH decrease showing a severe sulfide inhibition during these days (Fig. 3C and H). A discussion on the effect of the high sulfate concentrations on the methane production rates as well as on the inhibition effects of H_2S to the anaerobic consortia (methanogens and sulfate reducing bacteria) can be found in Barrera et al. (2014).

4. Conclusions

An extension of ADM1 with sulfate reduction was proposed, calibrated and validated for the description of the anaerobic digestion of cane-molasses vinasse (high strength and sulfate rich wastewater). Based on the results of a sensitivity analysis, only four parameters of the original ADM1 ($k_{m,pro}$, $k_{m,ac}$, $k_{m,h2}$ and Y_{h2}) and all the sulfate reduction parameters were fitted during calibration. Despite the fact that some deviations were observed between model predictions and experimental values, it was shown that the process variables S_{so4}, S_{h2s}, $S_{h2s,free}$, $S_{gas,h2s}$, Q_{gas}, $S_{gas,ch4}$, $S_{gas,co2}$, S_{pro}, S_{ac}, eff_COD, and pH were predicted reasonably well during model validation. The model showed high (±10%) to medium (10%–30%) accurate quantitative predictions with a mean absolute relative error ranging from 1 to 26%. Moreover, the model was able to predict failure of methanogenesis and sulfidogenesis when the sulfate loading rate increased. Therefore, the kinetic parameters and the model structure proposed in this work can be considered as valuable to describe the sulfate reduction process in the anaerobic digestion of cane-molasses vinasse, by predicting the sulfur compounds in the gas and liquid phases, increasing the applicability of ADM1 to specific industrial wastewaters (vinasse).

Acknowledgments

The authors wish to express their gratitude to Dr. Jeppsson Ulf (Department of Industrial Electrical Engineering and Automation, Lund University, Sweden) for kindly providing the codes and documents related to ADM1. This work has been supported financially by the VLIR Program, Project ZEIN2009PR362 (Biogas production from waste from local food, wood and sugar cane industries for increasing self-sufficiency of energy in Sancti Spiritus, Cuba).

Appendix A. Stoichiometric and kinetic parameters selected for sensitivity analysis. Values reported in literature and calibrated for this work.

Parameter	Names	Units	Benchmark values[a]	Cane-molasses[b]	Sulfate reduction[c]	Calibration this work	CI (95%)
Y_{su}	Yield of sugar degraders (X_{su})	kg COD_X_{su} kg COD_S_{su}^{-1}	0.100			0.100	
Y_{aa}	Yield of amino acids degraders (X_{aa})	kg COD_X_{aa} kg COD_S_{aa}^{-1}	0.080			0.080	
Y_{fa}	Yield of LCFA degraders (X_{fa})	kg COD_X_{fa} kg COD_S_{fa}^{-1}	0.060			0.060	
Y_{c4}	Yield of valerate and butyrate degraders (X_{c4})	kg COD_X_{c4} kg COD_$S_{va\ \&\ bu}^{-1}$	0.060			0.060	
Y_{pro}	Yield of propionate degraders (X_{pro})	kg COD_X_{pro} kg COD_S_{pro}^{-1}	0.040			0.040	
Y_{ac}	Yield of acetate degraders (X_{ac})	kg COD_X_{ac} kg COD_S_{ac}^{-1}	0.050			0.050	
Y_{h2}	Yield of hydrogen degraders (X_{h2})	kg COD_X_{h2} kg COD_S_{h2}^{-1}	0.060			0.070	±0.0042
Y_{pSRB}	Yield of pSRB (X_{pSRB})	kg COD_X_{pSRB} kg COD_S_{pro}^{-1}	0.0329[d]		0.027–0.035	0.035	±0.0040
Y_{aSRB}	Yield of aSRB (X_{aSRB})	kg COD_X_{aSRB} kg COD_S_{ac}^{-1}	0.0342[d]		0.033–0.041	0.041	±0.0060
Y_{hSRB}	Yield of hSRB (X_{hSRB})	kg COD_X_{hSRB} kg COD_S_{h2}^{-1}	0.0366[d]		0.037–0.077	0.051	±0.0047
$k_{m,su}$	Monod maximum specific uptake rate of sugars by X_{su}	kg COD_S_{su} kg COD_X_{su}^{-1} d^{-1}	30			30	
$k_{m,fa}$	Monod maximum specific uptake rate of LCFA by X_{fa}	kg COD_S_{fa} kg COD_X_{fa}^{-1} d^{-1}	6			6	
$k_{m,c4}$	Monod maximum specific uptake rate of HVa & HBu by X_{c4}	kg COD_$S_{va\ \&\ bu}$ kg COD_X_{c4}^{-1} d^{-1}	20			20	
$k_{m,pro}$	Monod maximum specific uptake rate of HPr by X_{pro}	kg COD_S_{pro} kg COD_X_{pro}^{-1} d^{-1}	13	15		16	±1.21
$k_{m,ac}$	Monod maximum specific uptake rate of HAc by X_{ac}	kg COD_S_{ac} kg COD_X_{ac}^{-1} d^{-1}	8	9.4		12	±0.73
$k_{m,h2}$	Monod maximum specific uptake rate of H_2 by X_{h2}	kg COD_S_{h2} kg COD_X_{h2}^{-1} d^{-1}	35	43		43	±4.26
$k_{m,pSRB}$	Monod maximum specific uptake rate of HPr by pSRB	kg COD_S_{pro} kg COD_X_{pSRB}^{-1} d^{-1}	12.6[d]		9.60–23.1	23	±2.35

– (*continued*)

Parameter	Names	Units	Benchmark values[a]	Cane-molasses[b]	Sulfate reduction[c]	Calibration this work	CI (95%)
$k_{m,aSRB}$	Monod maximum specific uptake rate of HAc by aSRB	kg COD_S_{ac} kg COD_X_{aSRB}^{-1} d^{-1}	7.1[d]		4.19–18.5	18.5	±2.32
$k_{m,hSRB}$	Monod maximum specific uptake rate of H_2 by hSRB	kg COD_S_{h2} kg COD_X_{hSRB}^{-1} d^{-1}	26.7[d]		26.7–64.9	63	±7.81
$k_{dec,Xac}$	First order decay rate for X_{ac}	d^{-1}	0.020			0.020	
$k_{dec,Xh2}$	First order decay rate for X_{h2}	d^{-1}	0.020			0.020	
$K_{S,su}$	Half saturation coefficient for the uptake of sugars by X_{su}	kg COD_S_{su} m^{-3}	0.500			0.500	
$K_{S,aa}$	Half saturation coefficient for the uptake of amino acids by X_{aa}	kg COD_S_{aa} m^{-3}	0.300			0.300	
$K_{S,c4}$	Half saturation coefficient for the uptake of HVa & HBu by X_{c4}	kg COD_$S_{va\ \&\ bu}$ m^{-3}	0.200			0.200	
$K_{S,pro}$	Half saturation coefficient for the uptake of HPr by X_{pro}	kg COD_S_{pro} m^{-3}	0.100			0.100	
$K_{S,ac}$	Half saturation coefficient for the uptake of HAc by X_{ac}	kg COD_S_{ac} m^{-3}	0.150			0.150	
$K_{S,h2}$	Half saturation coefficient for the uptake of H_2 by X_{h2}	kg COD_S_{h2} m^{-3}	7.0e-6			7.0e-6	
$K_{S,pSRB}$	Half saturation coefficient for the uptake of HPr by pSRB	kg COD_S_{pro} m^{-3}	0.110[d]		0.015–0.295	0.110	±0.010
$K_{S,aSRB}$	Half saturation coefficient for the uptake of HAc by aSRB	kg COD_S_{ac} m^{-3}	0.220[d]		0.024–0.220	0.120	±0.015
$K_{S,hSRB}$	Half saturation coefficient for the uptake of H_2 by hSRB	kg COD_S_{h2} m^{-3}	0.000100[d]		4.0e-6[e] – 1.0e-4	6e-06	±6.2e-7
$K_{S,so4,pSRB}$	Half saturation coefficient for the uptake of SO_4^{2-} by pSRB	kmol m^{-3}	0.000200[d]		7.7e-5 – 2.0e-4	0.00200	±0.00039
$K_{S,so4,aSRB}$	Half saturation coefficient for the uptake of SO_4^{2-} by aSRB	kmol m^{-3}	0.000100[d]		1.0e-4 – 2.9e-4	0.00100	±0.00023
$K_{S,so4,hSRB}$	Half saturation coefficient for the uptake of SO_4^{2-} by hSRB	kmol m^{-3}	0.000104[d]		9.0e-6 – 1.0e-4	0.00105	±0.00017
$K_{I,h2s,c4}$	50% inhibitory concentration of free H_2S for X_{c4}	kmol m^{-3}	0.00750[d]		0.0075[d]	0.00440	±0.00065
$K_{I,h2s,pro}$	50% inhibitory concentration of free H_2S for X_{pro}	kmol m^{-3}	0.00750[d]		0.0075[d]	0.00280	±0.00048
$K_{I,h2s,ac}$	50% inhibitory concentration of free H_2S for X_{ac}	kmol m^{-3}	0.00720[d]		0.0072[d]	0.00440	±0.00053
$K_{I,h2s,h2}$	50% inhibitory concentration of free H_2S for X_{h2}	kmol m^{-3}	0.00630[d]		0.0063[d]	0.00440	±0.00075
$K_{I,h2s,pSRB}$	50% inhibitory concentration of free H_2S for pSRB	kmol m^{-3}	0.00813[d]		0.0058–0.0089	0.00480	±0.00086
$K_{I,h2s,aSRB}$	50% inhibitory concentration of free H_2S for aSRB	kmol m^{-3}	0.00780[d]		0.0051–0.018	0.00470	±0.00028
$K_{I,h2s,hSRB}$	50% inhibitory concentration of free H_2S for hSRB	kmol m^{-3}	0.00780[d]		0.0078–0.017	0.00470	±0.00083

CI: confidence interval.
[a] Rosen and Jeppsson (2006).
[b] Romli et al. (1995).
[c] Barrera et al. (2013).
[d] Fedorovich et al. (2003).
[e] Batstone et al. (2006).

REFERENCES

Alphenaar, P., Visser, A., Lettinga, G., 1993. The effect of liquid upward velocity and hydraulic retention time on granulation in UASB reactors treating wastewater with a high sulphate content. Bioresour. Technol. 43 (3), 249–258.

Barrera, E.L., Spanjers, H., Dewulf, J., Romero, O., Rosa, E., 2013. The sulfur chain in biogas production from sulfate-rich liquid substrates: a review on dynamic modeling with vinasse as model substrate. J. Chem. Technol. Biotechnol. 88, 1405–1420.

Barrera, E.L., Spanjers, H., Romero, O., Rosa, E., Dewulf, J., 2014. Characterization of the sulfate reduction process in the anaerobic digestion of a very high strength and sulfate rich vinasse. Chem. Eng. J. 248, 383–393.

Batstone, D., 2006. Mathematical modelling of anaerobic reactors treating domestic wastewater: rational criteria for model use. Rev. Environ. Sci. Biotechnol. 5 (1), 57–71.

Batstone, D.J., Keller, J., 2003. Industrial applications of the IWA anaerobic digestion model no. 1 (ADM1). Water Sci. Technol. 47 (12), 199–206.

Batstone, D.J., Keller, J., Angelidaki, I., Kalyuzhnyi, S.V., Pavlostathis, S.G., Rozzi, A., Sanders, W.T.M., Siegrist, H., Vavilin, V.A., 2002. The IWA Anaerobic Digestion Model No 1. Scientific and Technical Report No. 13. IWA Publishing, London.

Batstone, D.J., Keller, J., Steyer, J.P., 2006. A review of ADM1 extensions, applications, and analysis: 2002–2005. Water Sci. Technol. 54 (4), 1–10.

Dereli, R.K., Ersahin, M.E., Ozgun, H., Ozturk, I., Aydin, A.F., 2010. Applicability of anaerobic digestion model no. 1 (ADM1) for a specific industrial wastewater: opium alkaloid effluents. Chem. Eng. J. 165 (1), 89–94.

Dochain, D., Vanrolleghem, P.A., 2001. Dynamical Modelling and Estimation in Wastewater Treatment Processes. IWA Publishing, London, UK.

Donoso-Bravo, A., Mailier, J., Martin, C., Rodríguez, J., Aceves-Lara, C.A., Wouwer, A.V., 2011. Model selection, identification and validation in anaerobic digestion: a review. Water Res. 45 (17), 5347–5364.

Fedorovich, V., Lens, P., Kalyuzhnyi, S., 2003. Extension of anaerobic digestion model no. 1 with processes of sulfate reduction. Appl. Biochem. Biotechnol. 109, 33–45.

Harada, H., Uemura, S., Chen, A.-C., Jayadevan, J., 1996. Anaerobic treatment of a recalcitrant distillery wastewater by a thermophilic UASB reactor. Bioresour. Technol. 55 (3), 215–221.

Hinken, L., Patón Gassó, M., Weichgrebe, D., Rosenwinkel, K.H., 2013. Implementation of Sulphate Reduction and Sulphide Inhibition in ADM1 for Modelling of a Pilot Plant Treating Bioethanol Wastewater. Santiago de Compostela. Spain.

Kalyuzhnyi, S., Fedorovich, V., Lens, P., Hulshoff Pol, L., Lettinga, G., 1998. Mathematical modelling as a tool to study population dynamics between sulfate reducing and methanogenic bacteria. Biodegradation 9 (3), 187–199.

Kalyuzhnyi, S.V., Fedorovich, V.V., 1998. Mathematical modelling of competition between sulphate reduction and methanogenesis in anaerobic reactors. Bioresour. Technol. 65 (3), 227–242.

Knobel, A.N., Lewis, A.E., 2002. A mathematical model of a high sulphate wastewater anaerobic treatment system. Water Res. 36 (1), 257–265.

Lauwers, J., Appels, L., Thompson, I.P., Degrève, J., Impe, J.F.V., Dewil, R., 2013. Mathematical modelling of anaerobic digestion of biomass and waste: power and limitations. Prog. Energy Combust. Sci. 39, 383–402.

Omil, F., Lens, P., Hulshoff Pol, L.W., Lettinga, G., 1996. Effect of upward velocity and sulphide concentration on volatile fatty acid degradation in a sulphidogenic granular sludge reactor. Process Biochem. 31, 699–710.

Omil, F., Lens, P., Hulshoff Pol, L.W., Lettinga, G., 1997. Characterization of biomass from a sulfidogenic, volatile fatty acid-degrading granular sludge reactor. Enzyme Microb. Technol. 20, 229–236.

Rieger, L., Gillot, S., Langergraber, G., Shaw, A., 2012. Good Modelling Practice: Guidelines for Use of Activated Sludge Models. IWA Publishing.

Rinzema, A., Lettinga, G., 1988. Anaerobic treatment of sulfate-containing waste water. In: Wise, D.L. (Ed.), Biotreatment Systems, vol. III. CRC Press Inc, Boca Raton, USA, pp. 65–109.

Ristow, N.E., Whittington-Jones, K., Corbett, C., Rose, P., Hansford, G.S., 2002. Modelling of a recycling sludge bed reactor using AQUASIM. Water S.A 28 (1), 111–120.

Romli, M., Keller, J., Lee, P.J., Greenfield, P.F., 1995. Model prediction and verification of a two stage high-rate anaerobic wastewater treatment system subject to shock loads. Process Saf. Environ. Prot. 73, 151–154.

Rosen, C., Jeppsson, U., 2006. Aspects on ADM1 Implementation within the BSM2 Framework. Department of Industrial Electrical Engineering and Automation (IEA). Lund University, Lund, Sweden.

Silva, F., Nadais, H., Prates, A., Arroja, L., Capela, I., 2009. Modelling of anaerobic treatment of evaporator condensate (EC) from a sulphite pulp mill using the IWA anaerobic digestion model no. 1 (ADM1). Chem. Eng. J. 148, 319–326.

Tartakovsky, B., Mu, S.J., Zeng, Y., Lou, S.J., Guiot, S.R., Wu, P., 2008. Anaerobic digestion model no. 1-based distributed parameter model of an anaerobic reactor: II. model validation. Bioresour. Technol. 99 (9), 3676–3684.

Visser, A., Hulshoff Pol, L.W., Lettinga, G., 1996. Competition of methanogenic and sulfidogenic bacteria. Water Sci. Technol. 33 (3), 99–110.

Zub, S., Kurissoo, T., Menert, A., Blonskaja, V., 2008. Combined biological treatment of high-sulphate wastewater from yeast production. Water Environ. J. 22 (4), 274–286.

Paper IV

Water Research 95 (2016) 370–382

Contents lists available at ScienceDirect

Water Research

journal homepage: www.elsevier.com/locate/watres

Modelling phosphorus (P), sulfur (S) and iron (Fe) interactions for dynamic simulations of anaerobic digestion processes

Xavier Flores-Alsina [a, *], Kimberly Solon [b], Christian Kazadi Mbamba [c], Stephan Tait [c], Krist V. Gernaey [a], Ulf Jeppsson [b], Damien J. Batstone [c]

[a] CAPEC-PROCESS Research Center, Department of Chemical and Biochemical Engineering, Technical University of Denmark, Building 229, DK-2800 Kgs. Lyngby, Denmark
[b] Division of Industrial Electrical Engineering and Automation, Department of Biomedical Engineering, Lund University, Box 118, SE-221 00 Lund, Sweden
[c] Advanced Water Management Centre, The University of Queensland, St Lucia, Brisbane, Queensland 4072, Australia

ARTICLE INFO

Article history:
Received 18 December 2015
Received in revised form
29 February 2016
Accepted 5 March 2016
Available online 10 March 2016

Keywords:
ADM1 extensions
Aqueous phase chemistry model
Multiple mineral precipitation
Phosphorus recovery
Physico-chemical modelling
Simulation
Water resource recovery facilities

ABSTRACT

This paper proposes a series of extensions to functionally upgrade the IWA Anaerobic Digestion Model No. 1 (ADM1) to allow for plant-wide phosphorus (P) simulation. The close interplay between the P, sulfur (S) and iron (Fe) cycles requires a substantial (and unavoidable) increase in model complexity due to the involved three-phase physico-chemical and biological transformations. The ADM1 version, implemented in the plant-wide context provided by the Benchmark Simulation Model No. 2 (BSM2), is used as the basic platform (A_0). Three different model extensions (A_1, A_2, A_3) are implemented, simulated and evaluated. The first extension (A_1) considers P transformations by accounting for the kinetic decay of polyphosphates (X_{PP}) and potential uptake of volatile fatty acids (VFA) to produce polyhydroxyalkanoates (X_{PHA}) by phosphorus accumulating organisms (X_{PAO}). Two variant extensions ($A_{2,1}$/$A_{2,2}$) describe biological production of sulfides (S_{IS}) by means of sulfate reducing bacteria (X_{SRB}) utilising hydrogen only (autolithotrophically) or hydrogen plus organic acids (heterorganotrophically) as electron sources, respectively. These two approaches also consider a potential hydrogen sulfide (Z_{H_2S}) inhibition effect and stripping to the gas phase (G_{H_2S}). The third extension (A_3) accounts for chemical iron (III) ($S_{Fe^{3+}}$) reduction to iron (II) ($S_{Fe^{2+}}$) using hydrogen (S_{H_2}) and sulfides (S_{IS}) as electron donors. A set of pre/post interfaces between the Activated Sludge Model No. 2d (ASM2d) and ADM1 are furthermore proposed in order to allow for plant-wide (model-based) analysis and study of the interactions between the water and sludge lines. Simulation ($A_1 - A_3$) results show that the ratio between soluble/particulate P compounds strongly depends on the pH and cationic load, which determines the capacity to form (or not) precipitation products. Implementations A_1 and $A_{2,1}$/$A_{2,2}$ lead to a reduction in the predicted methane/biogas production (and potential energy recovery) compared to reference ADM1 predictions (A_0). This reduction is attributed to two factors: (1) loss of electron equivalents due to sulfate (S_{SO_4}) reduction by X_{SRB} and storage of X_{PHA} by X_{PAO}; and, (2) decrease of acetoclastic and hydrogenotrophic methanogenesis due to Z_{H_2S} inhibition. Model A_3 shows the potential for iron to remove free S_{IS} (and consequently inhibition) and instead promote iron sulfide (X_{FeS}) precipitation. It also reduces the quantities of struvite ($X_{MgNH_4PO_4}$) and calcium phosphate ($X_{Ca_3(PO_4)_2}$) that are formed due to its higher affinity for phosphate anions. This study provides a detailed analysis of the different model assumptions, the effect that operational/design conditions have on the model predictions and the practical implications of the proposed model extensions in view of plant-wide modelling/development of resource recovery strategies.

© 2016 Elsevier Ltd. All rights reserved.

1. Introduction

The International Water Association (IWA) Anaerobic Digestion Model No. 1 (ADM1) (Batstone et al., 2002) describes activated sludge stabilization processes and has been effectively applied (in both industry and academia) to model a large number of

* Corresponding author. Department of Chemical and Biochemical Engineering, Technical University of Denmark (DTU), Søltofts Plads, Building 227 (postal address: Building 229), DK-2800 Kgs. Lyngby, Denmark.
E-mail address: xfa@kt.dtu.dk (X. Flores-Alsina).
URL: http://www.kt.dtu.dk

http://dx.doi.org/10.1016/j.watres.2016.03.012
0043-1354/© 2016 Elsevier Ltd. All rights reserved.

Nomenclature

A	Alternative model formulation
AD	Anaerobic digestion
ADM1	Anaerobic Digestion Model No. 1
AER	Aerobic section
ANOX	Anoxic section
ASM	Activated Sludge Model
ASM2d	Activated Sludge Model No. 2d
BSM2	Benchmark Simulation Model No. 2
CBIM	Continuity-based interfacing method
$CONV_{AD-AS}$	Conversion ADM1 – ASM2d interface
$CONV_{AS-AM}$	Conversion ASM2d – ADM1 interface
Fe	Iron
G_{CH_4}	Methane production rate (gas) (ADM1) (kg day^{-1})
G_{CO_2}	Carbon dioxide production rate (gas) (ADM1) (kg day^{-1})
G_{H_2}	Hydrogen production rate (gas) (ADM1) (kg day^{-1})
G_{H_2S}	Hydrogen sulfide production rate (gas) (ADM1) (kg day^{-1})
IWA	International Water Association
MMP	Multiple mineral precipitates
P	Phosphorus
PAO	Phosphorus accumulating organisms
PRIM	Primary clarifier
$PROCESS_{AD-AS}$	Process ADM1– ASM2d interface
$PROCESS_{AS-AD}$	Process ASM2d – ADM1 interface
Q_{intr}	Internal recycle flow (between AER and ANOX) (m^3 day^{-1})
S	Sulfur
SEC2	Secondary clarifier
SI	Saturation index
SRB	Sulfate reducing bacteria
S_A	Total acetic acid (ASM2d) (g COD m^{-3})
S_{aa}	Amino acids (ADM1) (kg COD m^{-3})
S_{ac}	Total acetic acid (ADM1) (kg COD m^{-3})
S_{an}	Anions (ADM1) (kmol m^{-3})
S_{bu}	Total butyric acid (ADM1) (kg COD m^{-3})
S_{Ca}	Calcium (ASM2d – ADM1) (g m^{-3}) (kmol m^{-3})
S_{cat}	Soluble cations (ADM1) (kmol m^{-3})
S_{Cl}	Chloride (ASM2d – ADM1) (g m^{-3}) (kmol m^{-3})
S_F	Fermentable substrate (ASM2d) (g COD m^{-3})
S_{fa}	Fatty acids (ADM1) (kg COD m^{-3})
$S_{Fe^{2+}}$	Iron (II) (ASM2d – ADM1) (g m^{-3}) (kmol m^{-3})
$S_{Fe^{3+}}$	Iron (III) (ASM2d – ADM1) (g m^{-3}) (kmol m^{-3})
S_{H_2}	Hydrogen (ADM1) (kg COD m^{-3})
S_{IS}	Inorganic total sulfides (ADM1) (kg COD m^{-3})
S_{IC}	Inorganic carbon (ADM1) (kmol m^{-3})
S_{IN}	Inorganic nitrogen (ADM1) (kmol m^{-3})
S_{IP}	Inorganic phosphorus (ADM1) (kmol m^{-3})
S_K	Potassium (ASM2d – ADM1) (g m^{-3}) (kmol m^{-3})
S_{Mg}	Magnesium (ASM2d – ADM1) (g m^{-3}) (kmol m^{-3})
S_{Na}	Sodium (ASM2d – ADM1) (g m^{-3}) (kmol m^{-3})
S_{NH_x}	Total ammonia nitrogen (ASM2d) (g m^{-3})
S_{pro}	Total propionic acid (ADM1) (kg COD m^{-3})
S_{PO_4}	Phosphate (ASM2d) (g m^{-3})
S_{su}	Sugars (ADM1) (kg COD m^{-3})
S_{S_0}	Elemental sulfur (ADM1) (kmol m^{-3})
S_{SO_4}	Sulfate (ASM2d – ADM1) (g m^{-3}) (kmol m^{-3})
S_{va}	Total valeric acid (ADM1) (kg COD m^{-3})
THK	Thickener
VFA	Volatile fatty acids
WRRF	Water resource recovery facility
WWTP	Wastewater treatment plant
X_A	Autotrophic biomass (ASM2d) (g COD m^{-3})
X_{ac}	Acetate degraders (ADM1) (kg COD m^{-3})
X_{AlPO_4}	Aluminum phosphate (ASM2d – ADM1) (g m^{-3}) (kmol m^{-3})
$X_{BIOMASS}$	Total biomass (ADM1) (kg COD m^{-3})
X_c	Composite material (ADM1) (kg COD m^{-3})
X_{C4}	Butyrate and valerate degraders (ADM1) (kg COD m^{-3})
X_{CaCO_3}	Calcite (ASM2d – ADM1) (g m^{-3}) (kmol m^{-3})
$X_{CaCO_{3a}}$	Aragonite (ASM2d – ADM1) (g m^{-3}) (kmol m^{-3})
$X_{Ca_3(PO_4)_2}$	Amorphous calcium phosphate (ASM2d – ADM1) (g m^{-3}) (kmol m^{-3})
$X_{Ca_5(PO_4)_3(OH)}$	Hydroxylapatite (ASM2d – ADM1) (g m^{-3}) (kmol m^{-3})
$X_{Ca_8H_2(PO_4)_6}$	Octacalcium phosphate (ASM2d – ADM1) (g m^{-3}) (kmol m^{-3})
X_{ch}	Carbohydrates (ADM1) (kg COD m^{-3})
X_{FePO_4}	Iron (III) phosphate (ASM2d – ADM1) (g m^{-3}) (kmol m^{-3})
$X_{Fe_3(PO_4)_2}$	Iron (II) phosphate (ASM2d – ADM1) (mol L^{-1}) (kmol m^{-3})
X_{FeS}	Iron sulfide (ASM2d – ADM1) (mol L^{-1}) (kmol m^{-3})
X_H	Heterotrophic biomass (ASM2d) (g COD m^{-3})
X_i	Inert particulate organics (ASM2d – ADM1) (g COD m^{-3}) (kg COD m^{-3})
X_{KMgPO_4}	K-struvite (ASM2d – ADM1) (g m^{-3}) (kmol m^{-3})
X_{li}	Lipids (ADM1) (kg COD.m^{-3}) (g m^{-3}) (kmol m^{-3})
X_{MgCO_3}	Magnesite (ASM2d – ADM1) (g m^{-3}) (kmol m^{-3})
X_{MgHPO_4}	Newberyte (ASM2d – ADM1) (g m^{-3}) (kmol m^{-3})
$X_{MgNH_4PO_4}$	Struvite (ASM2d – ADM1) (g m^{-3}) (kmol m^{-3})
X_{PAO}	Phosphorus accumulating organisms (ASM2d – ADM1) (g COD m^{-3}) (kg COD m^{-3})
X_{PHA}	Polyhydroxyalkanoates (ASM2d – ADM1) (g COD m^{-3}) (kg COD m^{-3})
X_{PP}	Polyphosphates (ASM2d – ADM1) (g m^{-3}) (kmol m^{-3})
X_{pr}	Proteins (ADM1) (kg COD m^{-3})
X_{pro}	Propionate degraders (ADM1) (kg COD m^{-3})
X_{SRB}	Sulfate reducing bacteria (ADM1) (kg COD m^{-3})
Z_i	Chemical species concentration of species i (algebraic variable of the physico-chemical module) (kmol m^{-3})

wastewater treatment plants (WWTPs) (Donoso-Bravo et al., 2011). The implementation of the ADM1 within the Benchmark Simulation Model No. 2 (Gernaey et al., 2014) and the need to evaluate plant-wide control strategies, in a relatively short period of time enabled intensive research on computationally-efficient versions of the model (Rosen et al., 2006). As a result, it is possible to simulate the ADM1 with several verified/ring-tested implementations and it is included in the standard model libraries in most software packages developed for simulation of WWTPs (MatLab, GPS-X, Mike-WEST, Simba, FORTRAN) (Jeppsson et al., 2013). In spite of the success of the ADM1, the model still omits important processes taking place during anaerobic digestion (Batstone et al., 2015). Indeed, the ADM1 only describes organic/inorganic carbon (C) and nitrogen (N) transformations and does not take into account phosphorus (P) transformations and its close link with the sulfur (S) and iron (Fe) cycles. This is an important issue for existing model application, and becomes a larger problem as wastewater treatment plants are transformed to water resource recovery facilities

(WRRFs), which will change the requirements for model-based analysis significantly (Vanrolleghem et al., 2014).

Plant-wide descriptions of P (and thus of S and Fe, because of strong interlinks) require a major but unavoidable model upgrade to a greater degree of complexity with many additional biochemical transformations and three-phase physico-chemical processes (gas-liquid-solid). For example, sulfate is reduced to sulfides in the sewer and primary treatment, with the sulfide binding with Fe (II/III) and releasing phosphorus. Once in the activated sludge plant, the sulfide is biologically reoxidised into sulfur and sulfate and iron is reoxidised into Fe (III). This releases iron to bind with phosphorus (as iron phosphate precipitate), with simultaneous biological assimilation and polyphosphate (PP) accumulation. Further details about P, S and Fe links in the water line can be found in Batstone et al. (2015).

In the anaerobic digester, experimental observations have revealed that phosphorus accumulating organisms (PAO) can play a role while they are still alive, with release of PP resulting in volatile fatty acid (VFA) accumulation under anaerobic conditions (Ikumi et al., 2011; Harding et al., 2011; Wang et al., 2016). In addition, phosphorus is a highly influential component affecting AD physico-chemistry (van Rensburg et al., 2003; Ikumi et al., 2014), with formation of multiple buffers and precipitates with key metals such as calcium, magnesium, aluminum and iron. Hence, there is a need for a proper aqueous phase model that continuously tracks ionic strength, describes weak acid-base chemistry and accounts for potential ion pairing taking place (Solon et al., 2015; Lizarralde et al., 2015; Flores-Alsina et al., 2015). Several research studies have already demonstrated the importance of a proper aqueous phase chemical model when predicting phosphorus (or any other compound) precipitation (Musvoto et al., 2000; van Rensburg et al., 2003; Barat et al., 2011; Kazadi Mbamba et al., 2015a,b).

The behaviour of sulfur (S) is closely related with phosphorus. Anaerobic S cycling includes sulfate reduction to sulfides. The classical key process in the sulfur cycle is the biological sulfate reduction performed by sulfate reducing bacteria (SRB) (Hao et al., 2014). SRB can anaerobically reduce the sulfate both autolithotrophically (using hydrogen as electron donor and carbon dioxide as carbon source) and hetero-organotrophically (using organic compounds as electron donor and carbon source). Sulfate reduction was not originally incorporated in the ADM1 but has been implemented as side or main processes (Fedorovich et al., 2003; Batstone, 2006; Barrera et al., 2015; Liu et al., 2015a,b). The main principle relies on that SRB generally outcompete acetogens and methanogens for electron equivalents (such as hydrogen or organic acids) (Kalyuzhnyi and Fedorovich, 1998). The produced sulfide is inhibitory and causes odour and corrosion (Utgikar et al., 2002).

The iron (Fe) oxidation/reduction processes are also relevant, and should be accounted for due to a strong link with both phosphorus and sulfur cycles (Rodriguez-Freire et al., 2014; Poulton et al., 2004). Under anaerobic conditions Fe (III) is chemically reduced to Fe (II) using a range of electron donors (H_2, VFAs, H_2S or NO_3^-) (Stumm and Morgan, 1996). This reaction can also be biologically mediated (Stucki et al., 2007; Zhang et al., 2013). Fe (II) can remove sulfide by precipitation as ferrous sulfide (Nielsen et al., 2005; Xiao et al., 2013) or can precipitate as Fe (II/III) phosphates (Mamais et al., 1994). Finally, iron phosphates formed in the activated sludge process water line might re-dissolve under anaerobic conditions in the digesters to precipitate with sulfide. This results because of a much lower solubility of iron sulfide as compared to iron phosphate (Ge et al., 2013). This process can be used as a control method because it can reduce undesirable inhibition/odour/corrosion problems (Zhang et al., 2013) or produce struvite in the digesters rather than in subsequent sludge pipelines (van Rensburg et al., 2003). Iron reduction is required in a model both to balance electron equivalents in the AD process, as well as to account for the different stoichiometry and thermodynamics of Fe (II) precipitation versus Fe (III) precipitation.

The main objective of this paper is to develop an extended anaerobic digestion model that: (1) mechanistically describes all the main biochemical and physico-chemical processes required for the P, S and Fe cycles; (2) analyzes the interactions between P, S and Fe and the impact on anaerobic digestion products (biogas, precipitates); and (3) provides a set of interfaces to facilitate the connection with state of the art Activated Sludge Models (ASM1, 2d & 3) and thereby allowing for plant-wide analysis/evaluation. The paper details the development of a new extended anaerobic digestion model by sequentially implementing systematic additions, showing their impact for a broad range of design/operational conditions using different simulation scenarios. This study responds to new challenges/needs that wastewater engineers will face when considering future WRRF operations, aiming for maximum energy and nutrient resource recovery. Lastly, opportunities that arise by the availability of the new model are discussed in the manuscript.

2. Methods

2.1. Influent characteristics

The influent characteristics follow the same principles as outlined in Gernaey et al. (2011). The water line of the WWTP under study is adapted from the BSM2 (Gernaey et al., 2014), and is made up of a primary clarifier (PRIM), an activated sludge unit (ASU) (A_2O configuration) (Tchobanoglous et al., 2003) and a secondary clarifier (SEC2). The proposed primary clarifier (PRIM) is modelled according to the principles stated in Otterpohl and Freund (1992). The ASU is comprised of seven continuously stirred tank reactors (CSTRs) in series. Tanks 1 and 2 are anaerobic (ANAER1, 2), tanks 3 and 4 are anoxic (ANOX1, 2) while tanks 5, 6 and 7 are aerobic (AER1, 2 and 3). AER3 and ANOX1 are linked by means of an internal recycle (Q_{intr}). In this case, the selected biological model is ASM2d (Henze et al., 2000) modified according to Flores-Alsina et al. (2015). The SEC2 is modelled using the double exponential function of Takács (Takács et al., 1991) implemented in a 10-layer reactive pattern (Flores-Alsina et al., 2012). Sludge wasted from SEC2 passes through an ideal thickener unit (THK) with a fixed TSS concentration in the underflow (7%) and constant removal efficiency (98%) (Jeppsson et al., 2007). The combined sludge from the PRIM and the THK has the following characteristics: 8386 kg COD d^{-1}, 478 kg N.d^{-1} and 177 kg P.d^{-1}. The resulting AD influent flow rate is 190 m^3 day^{-1}. In order to ensure a pH close to neutrality in the influent, the concentrations of cations (S_{cat}): potassium (S_K), sodium (S_{Na}), calcium (S_{Ca}), magnesium (S_{Mg}), iron ($S_{Fe^{3+}}$ / $S_{Fe^{2+}}$) and anions (S_{an}): chloride (S_{Cl}) sulfate (S_{SO_4}) and sulfides (S_{IS}) are adjusted accordingly (= constant loads, but time varying concentrations). Additional details about influent conditions can be found in Table 1.1 in the Supplemental Information Section 1.

2.2. ADM1 extensions

In this case study, four sets of model assumptions describing P/S/Fe-related processes within the ADM1 framework are compared.

- In the reference case (A_0), the BSM2 implementation of ADM1 (Rosen et al., 2006) describes the anaerobic digestion process with the following changes; P is modelled using a source-sink approach assuming a predefined elemental (C, H, N, P, O) composition (de Gracia et al., 2006). The original composite material variable (X_c) is removed and decay products are

directly mapped into biodegradable (X_{pr}, X_{li} and X_{ch}) and inert (X_i) organics (Batstone et al., 2015). Phosphorus limitation is included in all the uptake rates as a secondary substrate/nutrient limitation. The ADM1 is also upgraded with an improved physico-chemical description. This framework is comprised of: (1) a speciation/complexation aqueous-phase chemistry model (Solon et al., 2015; Flores-Alsina et al., 2015); and, (2) a multiple mineral precipitation model (MMP) (Kazadi Mbamba et al., 2015a,b). The first quantifies pH and describes ionic behaviour by consideration of non-ideality, including ion complexation/pairing and ion activities instead of molar ion concentrations. The aqueous-phase chemistry model resolves, via a set of non-linear algebraic equations, the concentrations of specific chemical species that participate in physico-chemical processes such as gas exchange and mineral precipitation. The species concentrations are expressed by a unique nomenclature (Z_i) reflecting the solution of an algebraic equation set. In the MMP model, precipitation is described as a reversible process using the saturation index (*SI*) as the chemical driving force. *SI* represents the logarithm of the ratio between the product of the respective activities of reactants that are each raised to the power of their respective stoichiometric coefficients, and the solubility product constant (K_{sp}). The precipitation equation depends on the reaction rate, the concentration of the mineral solid phase and the order of the reaction. The proposed MMP model includes the minerals: calcite (X_{CaCO_3}), aragonite ($X_{CaCO_{3a}}$), amorphous calcium phosphate ($X_{Ca_3(PO_4)_2}$), hydroxylapatite ($X_{Ca_5(PO_4)_3(OH)}$), octacalcium phosphate ($X_{Ca_8H_2(PO_4)_6}$), struvite ($X_{MgNH_4PO_4}$), newberyte (X_{MgHPO_4}), magnesite (X_{MgCO_3}), k-struvite (X_{KMgPO4}), iron sulfide (X_{FeS}), iron phosphates ($X_{FePO_4}/X_{Fe_3(PO_4)_2}$) and aluminum phosphate (X_{AlPO_4}). Note that water molecules from hydration are excluded from the calculations of solid states for these minerals. Kinetic parameters were selected with reference to Kazadi Mbamba et al. (2015 a,b). Finally, interfaces between ASM2d and ADM1 follow the same principles as stated in Volcke et al. (2006), Zaher et al. (2007) and Nopens et al. (2009). This implementation assumes instantaneous decay of phosphorus accumulating organism (X_{PAO}) and immediate lysis of polyhydroxyalkanoates (X_{PHA}) and polyphosphates (X_{PP}). Additional information about the interfaces can be found in Section 2.3. The selected kinetic and stoichiometric parameters correspond to 35 °C (Batstone et al., 2002). The model matrix formulation and parameter values can be found in the Supplemental Information Sections 2 (Tables 1.1a, 1.1b, 5.1 and 5.2) and 4.

- The second extension (A_1) enables P release consistent with the Activated Sludge Model No. 2d (ASM2d) (Henze et al., 2000). Consequently phosphorus accumulating organisms (X_{PAO}), polyhydroxyalkanoates (X_{PHA}) and polyphosphates (X_{PP}) are included as state variables, which implies inclusion of seven new processes: (1–4) uptake of valerate (S_{va}), butyrate (S_{bu}), propionate (S_{pro}) and acetate (S_{ac}) to form X_{PHA} as well as the (5–7) decay of phosphorus accumulating organisms (X_{PAO}) and lysis of polyhydroxyalkanoates (X_{PHA}) and polyphosphates (X_{PP}). The kinetic expressions for processes 1–4 contain competitive uptake inhibition terms for the different substrates (Batstone et al., 2002). Growth of phosphorus accumulating organisms (X_{PAO}) and storage of polyphosphates (X_{PP}) are not included as there are no aerobic/anoxic conditions in the digester. Kinetic parameters reported in Henze et al. (2000), Ikumi et al. (2011), Harding et al. (2011) and Ikumi et al. (2014) are used in this study. Matrix formulation and parameter values can be found in the Supplemental Information Sections 2 (Table 2.1) and 4.
- In the third model extension (A_2), sulfate (S_{SO_4}) re-transformations are described by means of two different approaches. Firstly ($A_{2,1}$), sulfate (S_{SO_4}) is reduced to sulfide (S_{IS}) by means of one single group of sulfate reducing bacteria ($X_{SRB\_H_2}$, autolithotrophs) using hydrogen (S_{H_2}) as electron donor (Batstone, 2006). In the second approach ($A_{2,2}$), sulfate (S_{SO_4}) is also reduced to sulfide (S_{IS}), but this time with multiple electron donors (X_{SRB_ac}, X_{SRB_pro}, X_{SRB_c4}). Therefore, besides using hydrogen (X_{SRB_H2}) as electron donor, $A_{2,2}$ accounts for the potential use of organic acids (valerate (S_{va}), butyrate (S_{bu}), propionate (S_{pro}), acetate (S_{ac})) by diverse SRBs (heterorganotrophs) (Fedorovich et al., 2003; Batstone, 2006; Barrera et al., 2015; Liu et al., 2015a,b). This adds a substantial degree of complexity to the model. Hydrogen sulfide (Z_{H_2S}) is calculated from total sulfide (S_{IS}) using the aqueous-phase model (Flores-Alsina et al., 2015). A high sulfide concentration (Z_{H_2S}) inhibits the metabolism of traditional degraders of hydrogen (X_{H_2}), acetate (X_{ac}), propionate (X_{pro}) and butyrate/valerate (X_{c4}) and X_{SRB} (Fedorovich et al., 2003; Barrera et al., 2015). pH, N, P and hydrogen inhibitions for SRB are based on the same mathematical structure as defined in Batstone et al. (2002) and Barrera et al. (2015). The model also includes mass transfer equations for changes in total dissolved sulfide (S_{IS}) by gas transfer of hydrogen sulfide (Z_{H_2S}) from the liquid phase to G_{H_2S} in the gas phase (Rosen et al., 2006). The latter has an effect on the total biogas production. In this case study, S_{IS} is modelled in COD units to facilitate closing the mass balances (see Supplemental Information Section 4). Kinetic values for SRB are selected to out-compete traditional microorganisms as is done by Batstone (2006) and Barrera et al. (2015). Matrix formulation and parameter values can be found in the Supplemental Information Sections 2 (Tables 3.1 and 5.1) and 4.
- In the last evaluated model formulation (A_3), iron (III) ($S_{Fe^{3+}}$) is converted to iron (II) ($S_{Fe^{2+}}$) utilising hydrogen (S_{H_2}) and/or sulfides (S_{IS}) as electron donors. The produced iron (II) ($S_{Fe^{2+}}$) can subsequently precipitate and produce iron sulfide (X_{FeS}) and iron phosphates ($X_{FePO_4}/X_{Fe_3(PO_4)_2}$). The pH (and consequently S_{H^+}) is adjusted automatically to accommodate the decrease in $S_{Fe^{3+}}$ and the increase in $S_{Fe^{2+}}$ (Solon et al., 2015; Flores-Alsina et al., 2015). A second-order reaction rate is used to describe the chemical reduction kinetics of $S_{Fe^{3+}}$ to $S_{Fe^{2+}}$ and kinetic parameters are adjusted to ensure fast conversion rates. Literature data reports that the chemical reduction of $S_{Fe^{3+}}$ to $S_{Fe^{2+}}$ takes place within a few hours (Mamais et al., 1994; Nielsen et al., 2005; Zhang et al., 2008). Matrix formulation and parameter values can be found in the Supplemental Information Sections 2 (Tables 4.1 and 5.1) and 4.

2.3. ASM2d – ADM1 interface

The interface between ASM2d and the modified ADM1 is based on the methodology described in Zaher et al. (2007) and Nopens et al. (2009). The approach is further expanded with the continuity-based interfacing method (CBIM) (Volcke et al., 2006) ensuring elemental conservation principles. Thus, the first ASM2d-ADM1 prototype considers: (1) (instantaneous) processes ($PROCESS_{AS\text{-}AD}$ *1*, *2*, *3*, *4* and *5*) are included in the ASM2d-ADM1 interface (A_0). In $PROCESS_{AS\text{-}AD}$ *1* and *2* all negative COD compounds (i.e. S_{O_2} and S_{NO_3}) are removed utilising acetate (S_A) or any other biodegradable substrate

in a predefined order (Nopens et al., 2009), with an associated growth of biomass (X_H). In $PROCESS_{AS\text{-}AD}$ *3*, the existing biomass (X_H, X_A, X_{PAO}) decays and is directly converted into the ADM1 states of proteins (X_{pr}), lipids (X_{li}), carbohydrates (X_{ch}) and inerts (X_I) at the interface. $PROCESS_{AS\text{-}AD}$ *4* and 5 represent the lysis of polyhydroxyalkanoates (X_{PHA}) and polyphosphates (X_{PP}). This first process ($PROCESS_{AS\text{-}AD}$ *4*) increases the quantity of organic acids: acetate (S_{ac}) (40%), propionate (S_{pro}) (40%), butyrate (S_{bu}) (10%) and valerate (S_{va}) (10%). The second process ($PROCESS_{AS\text{-}AD}$ *5*) considers (X_{PP}) solubilisation into phosphates (S_{PO_4}), potassium (S_K) and magnesium (S_{Mg}). In this study polyphosphates (X_{PP}) are assumed to have the composition of $((K_{0.33}Mg_{0.33}PO_3)_n$ (Henze et al., 2000). In implementation A_1 the role of X_{PAO} may also be modelled as a state in the ADM1 and hence $PROCESS_{AS\text{-}AD}$ *3*, *4* and *5* will be omitted (X_{PAO}, X_{PHA} and X_{PP} will be considered as state variables within the ADM1 model structure). In all cases, elemental changes (C, N, P, S, K, Mg, Fe, etc.) are accounted for by assuming a predefined composition analysis (Reichert et al., 2001) and by using suitable stoichiometric factors (Henze et al., 2000; Batstone et al., 2002; de Gracia et al., 2006).

The final adjustment between ASM2d and ADM1 implies five different conversions ($CONV_{AS\text{-}AD}$ *1, 2, 3, 4* and 5). $CONV_{AS\text{-}AD}$ *1* and *2* involve the transformation of soluble fermentable organics (S_F) and biodegradable particulate organics (X_S) into amino acids (S_{aa})/sugars (S_{su})/fatty acids (S_{fa}) (soluble) and $X_{pr}/X_{li}/X_{ch}$ (particulate), respectively. First, the quantities of S_F going to S_{aa} and X_S going to X_{pr} are calculated from the quantity of available soluble and particulate nitrogen in the organic matter. The remaining S_F is mapped into S_{su} since the sugars do not contain any nitrogen. The remaining organic biodegradable particulates (X_S) not allocated into X_{pr} are distributed into 70% of lipids (X_{li}) and 30% of carbohydrates (X_{ch}) (Siegrist et al., 2002; Nopens et al., 2009). State variables S_{IC}, S_{IN} and S_{IP} are used as source-sink to adjust the composition between ASM2d-ADM1 state variables during $PROCESS_{AS\text{-}AD}$ and $CONV_{AS\text{-}AD}$. The last conversions ($CONV_{AS\text{-}AD}$ *3*, *4* and *5*) involve the adjustment between ASM2d and the modified ADM1 S_A, S_I and X_I. For simplification purposes, the same elemental composition is assumed, and therefore conversion is immediate. No further modification is assumed for the remaining cations and anions.

2.4. ADM1-ASM2d interfaces

A similar approach is followed to link the outputs of the modified ADM1 with ASM2d state variables (Volcke et al., 2006; Zaher et al., 2007; Nopens et al., 2009). This second interface also distinguishes between: (1) (instantaneous) processes ($PROCESS_{AD\text{-}AS}$); and, (2) conversions ($CONV_{AD\text{-}AS}$). In comparison with the ASM2d-ADM1 interface, the number of $PROCESS_{AD\text{-}AS}$ and $CONV_{AD\text{-}AS}$ is the same independent of which modelling approach (A_0 to A_3) is being used (see Section 2.2).

Two different processes are included in the ADM1 – ASM2d interface. $PROCESS_{AD\text{-}AS}$ *1* converts all the biomass (X_{C4}, X_{pro}, X_{ac}, X_{H2}, $X_{SRB\_H_2}$, X_{SRB_ac}, X_{SRB_pro}, X_{SRB_c4}) into biodegradable (X_S) and non-biodegradable (X_I) organic particulates (Henze et al., 2000). $PROCESS_{AD\text{-}AS}$ *2* strips some compounds that can be transferred into the gas phase, such as hydrogen (S_{H_2}) and methane (S_{CH_4}). Through conversions, $CONV_{AD\text{-}AS}$ *1* turns all the particulate material (X_{pr}, X_{li}, X_{ch}) into biodegradable organics X_S. A similar conversion is performed by $CONV_{AD\text{-}AS}$ *2* and *3*. $CONV_{AD\text{-}AS}$ *2* transforms amino acids (S_{aa}), fatty acids (S_{fa}) and sugars (S_{su}) into fermentable compounds (S_F). $CONV_{AD\text{-}AS}$ *3* converts organic acids (S_{ac}, S_{pro}, S_{bu}, S_{va}) into acetate (S_A). The same principle as in the ASM2d-modified ADM1 interface applies for S_I and X_I in $CONV_{AD\text{-}AS}$ *4* & *5*, respectively. Similarly, state variables S_{IC}, S_{IN} and S_{IP} are used as source-sink to adjust the composition between ADM1-ASM2D state variables. No modifications are applied for the rest of the cations and anions, and elemental balances (C, N, P, S, K, Mg, Fe, etc.) are conserved using a pre-defined composition analysis and corresponding stoichiometric factors (Reichert et al., 2001; Henze et al., 2000; Batstone et al., 2002; de Gracia et al., 2006).

3. Results

3.1. Interfaces

3.1.1. ASM2d-ADM1 interface

Table 1 presents a summary of the inputs and outputs (I/O) for this interface for both scenarios A_0 and A_1 at steady state. The main differences between A_0 and A_1 are largely because A_1 preserves Bio-P related states across the interface for subsequent reaction in the anaerobic digester. Key states affected are: (1) X_{PAO} decay ($PROCESS_{AS\text{-}AD}$ *3*) resulting in increased proteins (X_{pr}), lipids (X_{li}), carbohydrates (X_{ch}) and inerts (X_I) (compared to A_1); (2) X_{PHA} hydrolysis ($PROCESS_{AS\text{-}AD}$ *4*) resulting in increased VFAs – acetate (S_{ac}), propionate (S_{pro}), butyrate (S_{bu}) and valerate (S_{va}) (compared to A_1); and, (3) X_{PP} hydrolysis ($PROCESS_{AS\text{-}AD}$ *5*) with subsequent increase

Table 1
ASM2d to ADM1 interface: ADM1 state variables after the interface for scenarios A_0 and A_1. Default units are used in each model (ASM2d/ADM1).

ASM2d			ADM1	A_0	A_1	
S_{O2}	0.0	g-COD m^{-3}				
S_F	26.4	g COD m^{-3}	$S_{su} + S_{aa}$	0.026	0.026	kg COD m^{-3}
S_A	17.7	g COD m^{-3}	$S_{va} + S_{bu} + S_{pro} + S_{ac}$	0.042	0.018	kg COD m^{-3}
S_I	27.2	g COD m^{-3}	S_I	0.027	0.027	kg COD m^{-3}
S_{NH_x}	18.6	g N m^{-3}	S_{IN}	0.050	0.036	Kmol N m^{-3}
S_{N_2}	5.1	g N m^{-3}				
S_{NOx}	0.02	g N m^{-3}				
S_{PO_4}	4.7	g P m^{-3}	S_{IP}	0.023	0.006	kmol P m^{-3}
S_{IC}	79.0	g C m^{-3}	S_{IC}	0.032	0.021	kmol C m^{-3}
X_I	10,964.4	g COD m^{-3}	X_I	12.332	11.946	kg COD m^{-3}
X_S	19,084.8	g COD m^{-3}	$X_{ch} + X_{pr} + X_{li}$	31.393	27.917	kg COD m^{-3}
X_H	9479.4	g COD m^{-3}				
X_{PAO}	3862.2	g COD m^{-3}	X_{PAO}		3.862	kg COD m^{-3}
X_{PP}	450.9	g P m^{-3}	X_{PP}		0.015	kmol P m^{-3}
X_{PHA}	24.6	g COD m^{-3}	X_{PHA}		0.025	kg COD m^{-3}
X_A	333.8	g COD m^{-3}				
S_{Na}	70.0	g Na m^{-3}	S_{Na}	0.003	0.003	kmol Na m^{-3}
S_K	19.8	g K m^{-3}	S_K	0.005	0.001	kmol K m^{-3}
S_{Cl}	1035	g Cl m^{-3}	S_{Cl}	0.029	0.029	kmol Cl m^{-3}
S_{Ca}	300.0	g Ca m^{-3}	S_{Ca}	0.007	0.007	kmol Ca m^{-3}
S_{Mg}	189.9	g Mg m^{-3}	S_{Mg}	0.013	0.008	kmol Mg m^{-3}

Table 2
ADM1 to ASM2d interface: ADM1 and ASM2d state variables before and after the interface for scenario A_1. Default units are used in each model (ASM2d/ADM1).

ADM1	A_1		ASM2d		
			S_{O2}		g-COD m^{-3}
$S_{su} + S_{aa} + S_{fa}$	0.134	kg COD m^{-3}	S_F	134.5	g COD m^{-3}
$S_{va} + S_{bu} + S_{pro} + S_{ac}$	0.101	kg COD m^{-3}	S_A	353.9	g COD m^{-3}
S_I	0.027	kg COD m^{-3}	S_I	27.2	g COD m^{-3}
S_{IN}	0.080	kmol N m^{-3}	S_{NH_x}	1291.7	g N m^{-3}
			S_{N_2}		g N m^{-3}
			S_{NOx}		g N m^{-3}
S_{IP}	0.008	kmol P m^{-3}	S_{PO_4}	298.1	g P m^{-3}
S_{IC}	0.059	kmol C m^{-3}	S_{IC}	885.3	g C m^{-3}
X_I	12.345	kg COD m^{-3}	X_I	12,704.9	g COD m^{-3}
$X_{ch} + X_{pr} + X_{li}$	4.979	kg COD m^{-3}	X_S	8218.9	g COD m^{-3}
			X_H		g COD m^{-3}
			X_{PAO}		g COD m^{-3}
X_{PP}	8.05E-06	kmol P m^{-3}	X_{PP}		g P m^{-3}
X_{PHA}	0.252	kg COD m^{-3}	X_{PHA}		g COD m^{-3}
			X_A		g COD m^{-3}
$X_{BIOMASS}$	3.600	kg COD m^{-3}			
S_{SO_4}		kmol S m^{-3}	S_{SO_4}		g S m^{-3}
S_{Na}	0.003	kmol Na m^{-3}	S_{Na}	70	g Na m^{-3}
S_K	0.005	kmol K m^{-3}	S_K	208.8	g K m^{-3}
S_{Cl}	0.029	kmol Cl m^{-3}	S_{Cl}	1035	g Cl m^{-3}
S_{Ca}	0.001	kmol Ca m^{-3}	S_{Ca}	20.5	g Ca m^{-3}
S_{Mg}	0.001	kmol Mg m^{-3}	S_{Mg}	28.3	g Mg m^{-3}
$X_{Ca_3(PO_4)_3}$	0.002	kmol m^{-3}	$X_{Ca_3(PO_4)_2}$	722.5	g m^{-3}
$X_{MgNH_4PO_4}$	0.011	kmol m^{-3}	$X_{MgNH_4PO_4}$	1578.6	g m^{-3}
S_{H_2}	2.65E-07	kg COD m^{-3}			
S_{CH4}	0.052	kg COD m^{-3}			
G_{H_2}	0.004	Kg H_2 d^{-1}			
G_{CH_4}	1069.1	Kg CH_4 d^{-1}			
G_{CO_2}	1880.5	Kg CO_2 d^{-1}			

of ions: phosphorus (S_{IP}), potassium (S_K) and magnesium (S_{Mg}) (compared to A_1). The reactive processes also have an impact on inorganic carbon (S_{IC}) and nitrogen (S_{IN}). The total elemental loads are identical in all three cases (before and after the interface for both models), but the COD content and elemental distribution (C, N, P, K, Mg, etc.) for the individual state variables are different (for details, see mass balances for the influent before and after the interface for the different model formulations in the Supplemental Information Section 1 (Tables 1.1, 1.2 and 1.3).

3.1.2. ADM1-ASM2d interface

Table 2 summarises the steady state I/O results for this interface. AD biomass decays in the interface, and it is converted into biodegradable (X_S) and non-biodegradable (X_I) organic particulates ($PROCESS_{AD\text{-}AS}$ *1*). As stated in the methods, gases are lost ($PROCESS_{AD\text{-}AS}$ *2*) and degradable compounds are mapped into X_S ($CONV_{AD\text{-}AS}$ *1*), S_F ($CONV_{AD\text{-}AS}$ *2*) and S_A ($CONV_{AD\text{-}AS}$ *3*), respectively. Differences between the cationic loads in Tables 1 and 2 are attributed to precipitation (see reductions in calcium (S_{Ca}) and magnesium (S_{Mg})) A more detailed description of the mass balances between anaerobic digestion influent before and after the interface can be found in the Supplemental Information Section 1 (Tables 1.4 and 1.5). As mentioned above, elements are preserved, but redistributed amongst the states.

3.2. Modelling (bio)chemical phosphorus transformations in anaerobic digesters

Figure 1a illustrates the effect of P transformations within ADM1 (A_0, A_1) under steady state conditions. Before entering the AD, most of the P remains in particulate form and it is allocated (decreasing order) into polyphosphates (X_{PP}) (>49%), biomass (X_H, X_A, X_{PAO}) (32%) and other organics (X_I, X_S) (19%). Comparatively, the soluble fraction (S_{PO_4}, S_I) is very low (<1%). Precipitation is currently not active in the activated sludge section. Influent pH is 7.2 and the N/P ratio (soluble) is around 4. Fig. 1 also shows that in spite of the type of interface (A_0 and A_1), predictions of P partitioning in the effluent converge to the same point. In both cases, 27% of the P is solubilized (S_{IP}) and the rest remains as particulate (X_{li}, biomass and precipitates). The latter substantially modifies the (soluble) N/P ratio (4.5) and decreases the pH (6.9). Specific values can be found in the Supplemental Information Section 1 (Table 1.4). With respect to precipitates the predominant compound is $X_{MgNH_4PO_4}$ and $X_{Ca_3(PO_4)_2}$. This was also observed by Kazadi-Mbamba et al. (2015b) in digestate analysis. In general, the quantity and type of precipitates as well as the ratio between soluble/particulate P strongly depends on digester pH and anionic and cationic influent composition (Musvoto et al., 2000; van Rensburg et al., 2003).

Fig. 2 further explores the effects of mineral precipitation and biochemical P transformations. This effect is investigated at: (1) a number of hydraulic retention times (HRT); and, (2) for different Ca and Mg loads. As expected, an increase in cationic load generally increases P precipitation (artificially promoted) (Fig. 2a and b). The differences between immediate (A_0) and delayed (A_1) P availability on P precipitation only become apparent at higher cationic loads and low HRT, which is due to differences in P supply for precipitation. At high HRT P precipitation is rapid compared to the corresponding process time constants and is thus in general at quasi-equilibrium. This observation agrees with findings of Kazadi-Mbamba et al. (2015b). When the concentration of $S_{Mg^{2+}}$ is increased, the quantity of precipitated P in the form of $X_{MgNH_4PO_4}$ is higher. In contrast, when the $S_{Ca^{2+}}$ concentration increases there is an increase in P precipitation (as $X_{Ca_3(PO_4)_2}$), but less pronounced due to competition with inorganic carbon and precipitation of X_{CaCO_3}. Again, this behaviour agrees with the experimental observations of Kazadi-Mbamba et al. (2015b).

Fig. 2c illustrates the effects of including biochemical phosphorus transformations (A_0, A_1) on biogas production. At low HRT

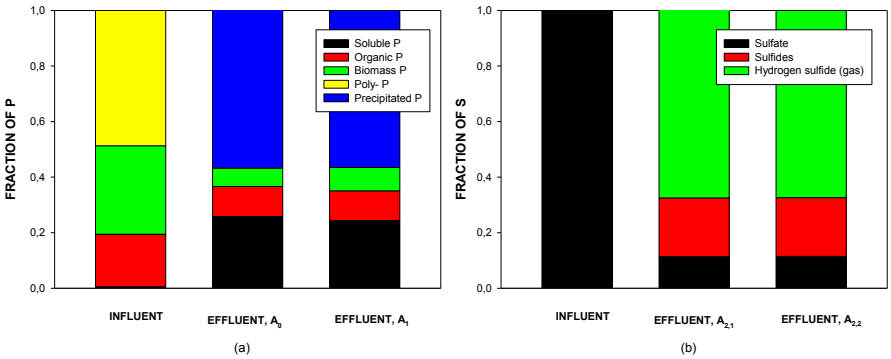

Fig. 1. Representation of P and S partitioning, for the inflow (INFLUENT) and outflow (EFFLUENT) of the AD section. The total quantity of P in both influent and effluent is 178 kg P day^{-1}. The total quantity of S in both INFLUENT and EFFLUENT is 21 kg S day^{-1} (S:COD ratio in the influent is 0.0025 kg S kg COD^{-1}).

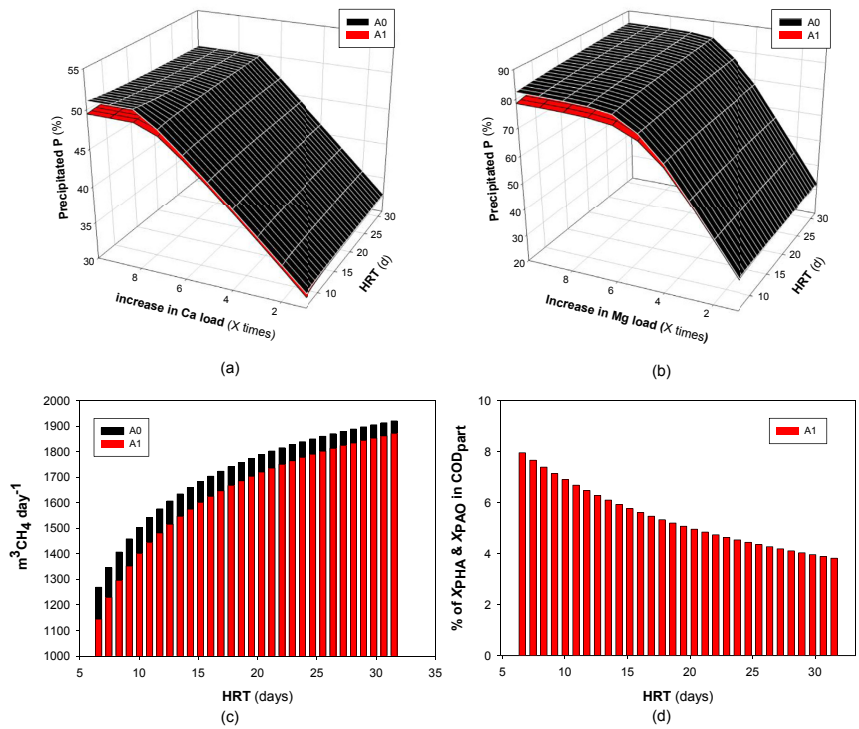

Fig. 2. Using A_0 as the reference simulation, investigation of the effect of including biochemical phosphorus transformations (A_1) at different HRT on: (a) the total precipitated P by increasing the influent calcium; (b) the total precipitated P by increasing the influent magnesium; (c) the methane (G_{CH_4}) formation; and, (d) the fraction of X_{PAO} and X_{PHA} in the particulate COD. The default HRT is 20 days and the ratio between the AD liquid (V_{LIQ}) and gas (V_{GAS}) volumes is 0.088.

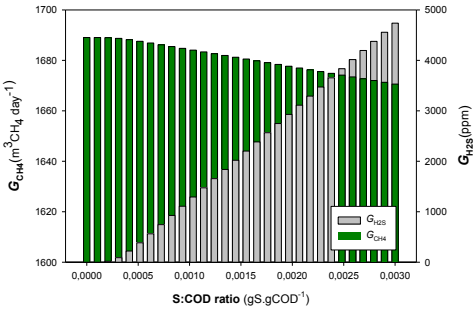

Fig. 3. Effect on biogas production of biochemical autolithotrophic S transformations ($A_{2,1}$). Influent COD is 8386 kg day^{-1}.

(<10 days), phosphorus accumulating organisms (X_{PAO}) can release S_{IP}, $S_K$and S_{Mg} from X_{PP}, and can use the associated energy to store organic acids (S_{va}, S_{bu}, S_{pro} and S_{ac}) in the form of X_{PHA} (see the reduced contribution of X_{PHA} and X_{PAO} with increasing HRT in Fig. 2d). As a result, there is a decrease in methane production by up to 11% (G_{CH_4}, Fig. 2c) due to a loss in the available substrate for acetotrophic methanogens (X_{ac}). For scenario A_1, there is also a corresponding reduction in the carbon dioxide production (G_{CO_2}) (by up to 11%), which is simply correlated with G_{CH_4} due to decreased acetoclastic methanogenesis. The difference between G_{CH_4} and G_{CO_2} is less pronounced at longer HRTs (>30 d) because at longer HRTs: (1) X_{PAO} is completely decayed due to inactivity; and, (2) the resulting X_{PHA} is more fully hydrolysed (see reduced contribution of X_{PHA} and X_{PAO} in Fig. 2d). The variations in the content of organic acids (S_{va}, S_{bu}, S_{pro} and S_{ac}), inorganic carbon (S_{IC}), nitrogen (S_{IN}) and phosphorus (S_{IP}) cause minute changes in the weak acid-base chemistry of the system (pH differences can be up to 1%) (results not shown). Some of these findings were also reported by Wang et al. (2016).

3.3. Modelling biochemical sulfate transformations in anaerobic digesters

The baseline simulations for the default case are illustrated in Fig. 1b. A S:COD ratio of 0.0025 kg S kg COD^{-1} is assumed (=110 g S m^{-3}). S arrives to the AD as sulfate ($S_{Na_2SO_4}$) and is transformed to hydrogen sulfide gas (G_{H_2S}) (68% = 3865 ppm) and dissolved sulfides (S_{IS}) (21%) (23 g S m^{-3}). There is also a remaining (not converted) fraction of sulfate (S_{SO_4}) (11%). The digester operating pH is 6.9. The same AD behaviour is obtained for the two evaluated model implementations ($A_{2,1}$ and $A_{2,2}$). In both models, electrons are coming from S_{H_2} i.e. there is no possibility for SRB to use organic acids to reduce sulfate (see Supplemental Information Section 1).

The effects of sulfur transformations on methane productivity and hydrogen sulphide partial pressure are shown in Fig. 3. At high S:COD ratio (with addition of $X_{Na_2SO_4}$), there is a decrease in G_{CH_4} production, attributed to: (1) sulfide inhibition of acetoclastic and hydrogenotrophic methanogenesis; and, (2) competition between SRB and X_{H_2}, X_{ac}, X_{pro} and X_{c4} for electron equivalents (S_{H_2}). These result in a higher allocation of influent COD to S_{H_2S} instead of S_{CH_4} and a reduction in overall energy recovery. Similar effects have been observed by Barrera et al. (2015) and Liu et al. (2015a,b).

Additional simulation results show that both models provide very similar results for the evaluated S:COD ratios (see Supplemental Information Section 3, Fig. 1). Nevertheless, model discrepancies between $A_{2,1}$ (chemotrophic – only H_2 as electron donor) and $A_{2,2}$ (heterotrophic – H_2 and VFA as electron donors) can be observed specifically when the S:COD ratio is higher than 0.06 g S.g COD^{-1} (see Supplemental Information Section 3, Fig. 1). Indeed, model $A_{2,1}$ (where X_{SRB_H2} is the only considered SRB) is a valid prediction model until S_{H_2} is depleted (or totally inhibited by Z_{H_2S}). In these situations, other (heterorganotrophic) SRB (X_{SRB_ac}, X_{SRB_pro}, X_{SRB_c4}) are also capable of obtaining electrons from organic acids (S_{va}, S_{bu}, S_{pro}, S_{ac}) to further reduce S_{SO_4} to S_{IS}. Only in these situations, it seems justifiable to increase model complexity (and consequently calibration efforts) by considering additional SRB with multiple metabolisms. This supports the more limited analysis made by Batstone (2006). The reader should be aware that a S:COD ratio higher than 0.06 g S.g COD^{-1} is extremely high, particularly for activated sludge digestion where this ratio is closer to 0.001 g S.g COD^{-1} under most circumstances.

3.4. Modelling chemical iron transformations in anaerobic digesters

When $S_{Fe^{3+}}$ is externally added (as X_{FeCl_3}) and enters the AD it will rapidly be converted into $S_{Fe^{2+}}$ (Mamais et al., 1994; Batstone et al., 2015). This produces phosphorus hydroxides (X_{FePO_4} and $X_{Fe_3(PO_4)_2}$) and reduces the quantity of struvite ($X_{MgNH_4PO_4}$) as illustrated in Fig. 4a. The principle could be used as

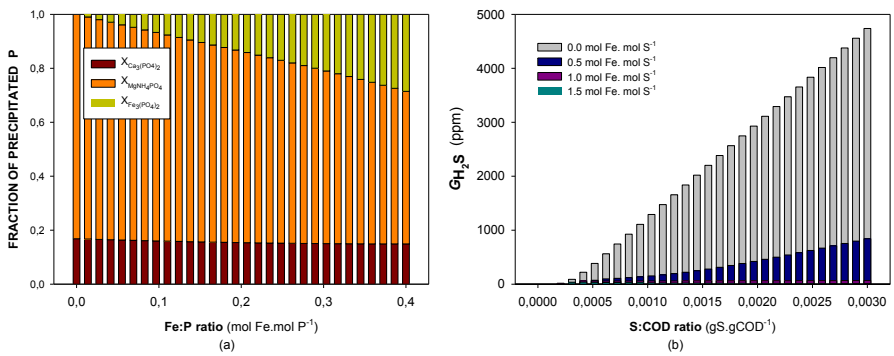

Fig. 4. Effect of X_{FeCl_3} addition on the digestion products: (a) precipitates; and, (b) G_{H_2S}. A_3 (S conversions are autolithotrophic) is used to run the simulations. Influent COD is 8386 kg day^{-1}.

		A_1	$A_{2,1}$ S:COD (kg S.kg COD^{-1})					A_3 Fe:S (mol Fe.mol S^{-1})				
			0.0006	0.0012	0.0018	0.0024	0.003	1	1	1	1	1
S_{SO4}	$Z_{SO_4^{2-}}$		73.09	73.06	73.03	72.99	72.96	72.61	72.15	71.82	71.48	71.15
	$Z_{HSO_4^-}$		0.00	0.00	0.00	0.00	0.00	0.00	0.00	0.00	0.00	0.00
	$Z_{CaSO_4(aq)}$		0.80	0.78	0.75	0.73	0.72	0.84	0.86	0.87	0.89	0.90
	$Z_{MgSO_4(aq)}$		1.43	1.38	1.33	1.28	1.24	1.55	1.62	1.67	1.73	1.78
	$Z_{NaSO_4^-} + S_{KSO_4^-}$		1.73	1.96	2.18	2.40	2.62	1.71	1.92	2.13	2.33	2.53
	$Z_{NH_4(SO_4)^-}$		22.96	22.83	22.71	22.59	22.47	22.77	22.46	22.24	22.01	21.79
	$Z_{Fe(SO_4)_2^-} + S_{FeSO_4(aq)}$							0.51	0.99	1.27	1.55	1.84
S_{IS}	Z_{HS^-}		50.78	51.47	52.24	53.00	53.73	3.22	1.69	1.31	1.07	0.89
	Z_{H_2S}		49.22	48.53	47.76	47.00	46.27	3.18	1.66	1.29	1.05	0.88
	Z_{S_2}		0.00	0.00	0.00	0.00	0.00	0.00	0.00	0.00	0.00	0.00
	Z_{FeHS^+}							93.60	96.65	97.40	97.88	98.23

0 10 20 30 40 50 60 70 80 90 100

Fig. 5. Distribution of the S species/ion pairs for the different model implementations (A_1, $A_{2,1}$ and A_3), and for a range of S:COD and Fe:S ratios. The 0–100 distributions are calculated from the total quantity of total compound (S_{SO_4}, S_{IS}).

a control strategy to avoid undesired/spontaneous struvite precipitation and it is in agreement with conclusions of Mamais et al. (1994). In presence of S, Fe conversions have important physico-chemical implications, because when Fe is not present, inorganic sulfur is observed as Z_{HS^-} and Z_{H_2S}, whereas once iron is added, ion pairs such as Z_{FeHS^-} become more abundant. This is illustrated in Fig. 5, which presents a summary of the relative abundance of various sulfur chemical species in the aqueous phase (as a fraction of total S) for different S:COD ratios. As a direct result of these changes, there is an increase of the iron precipitates (X_{FeS}) and a reduction of the G_{H_2S} production. Fig. 4b presents the modelled hydrogen sulphide partial pressure at different S:COD ratios. When the molar ratio Fe:S is higher than 1, almost all sulfide is precipitated, which causes a drop in the hydrogen sulfide partial pressure. Other studies show similar G_{H_2S} and X_{FeS} behaviour when $S_{Fe^{3+}}$ is added (Zhang et al., 2013; Xiao et al., 2013; Liu et al., 2015a,b).

3.5. Dynamic results

Fig. 6 shows the simulation results of: (1) the dynamic influent generated according to the principles outlined by Gernaey et al. (2011); and, (2) using the wastewater treatment units described in Sections 2.1 and 3 for three different modelling approaches (A_0, A_1 and $A_{2,1}$). HRT is set to the default BSM2 value (= 19 days, V_{LIQ} = 3400 m^3 and V_{GAS} = 300 m^3). The dynamic profiles depicted in Fig. 6a and b lead us to the same conclusions as reported in Section 3.3. The potential uptake of organic acids (S_{ac}, S_{pro}, S_{bu}, S_{va}) by X_{PAO} reduces the quantity of methane produced (G_{CH_4}). This is mainly due to the (temporal) storage of these substrates as X_{PHA}. Similar results could be observed when the influent S_{SO_4} load increased. SRB (X_{SRB_H2}) outcompete methanogens (X_{H2}, X_{ac}) and therefore higher S:COD (L1 = 0.001, L2 = 0.002 and L3 = 0.003) ratios increase the allocation of COD to S_{H_2S} instead of S_{CH_4}. As a result the relative amount of S_{H_2S} in the total biogas production increases. In addition, S_{H_2S} causes odour problems, increases the risk of corrosion and inhibits the growth of AD bacteria. Fig. 7 depicts again the effect of adding X_{FeCl_3} at different stoichiometric ratios (mol Fe mol S^{-1}) and for the same S:COD ratio (0.002 g S.g COD^{-1}). As was shown in Section 3.4, $S_{Fe^{3+}}$ reduction to $S_{Fe^{2+}}$ and subsequent X_{FeS} precipitation decreases G_{H_2S}. Hence, when iron addition is higher the relative amount of S_{H_2S} in the total biogas production is reduced (see additional simulations in the Supplemental Information Section 3, Fig. 2). The same effect on S physico-chemistry and S_{SO_4} and S_{IS} speciation is observed as described in Fig. 5.

4. Discussion

The model results presented in this paper demonstrate the links between the physico-chemical and biochemical transformations of P, S, and Fe. The observations noted above also suggest the effects

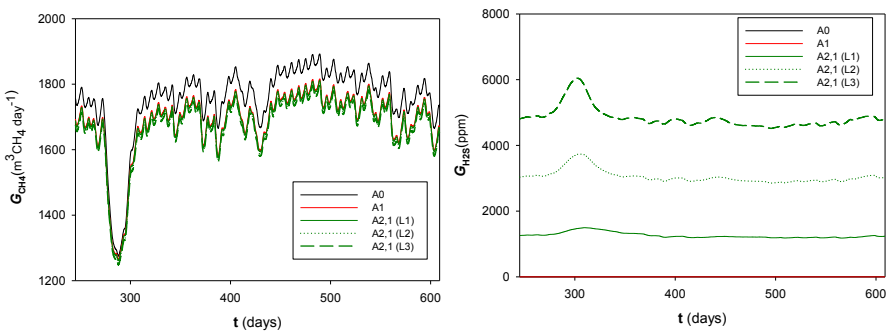

Fig. 6. Effect of including biochemical P and S transformations on the AD products: (a) G_{CH_4}; and, (b) G_{H_2S} for different S:COD ratios. L1 = 0.001 g S g COD^{-1}, L2 = 0.002 g S g COD^{-1} and L3 = 0.003 g S g COD^{-1}. The reduced methane production around days 275–300 corresponds to the lower load arriving to the plant due to the holiday period (August). A 3-day exponential moving average filter is used to improve the readability of the results.

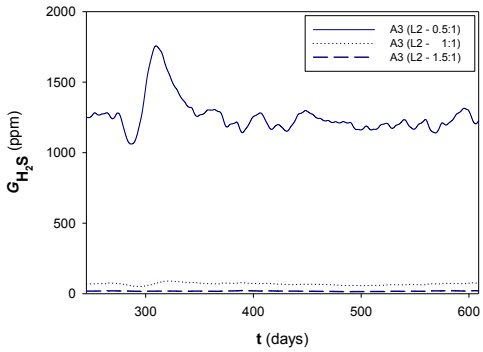

Fig. 7. Effect of X_{FeCl_3} addition on the G_{H_2S} production in the biogas. The S:Fe ratio goes from 0.5 to 1.5. The S:COD ratio is L2 = 0.001 g S g COD^{-1}. Simulated time is 1 year. A 3-day exponential moving average filter is used to improve the readability of the results.

that X_{PAO}, X_{SRB} and X_{FeCl_3} might have on AD products (CO_2, H_2, CH_4, H_2S, precipitates), thus highlighting the predictive capability of the model beyond simple descriptions of process states. Furthermore, a set of interfaces easily links the ADM with standard ASM models (Henze et al., 2000) to allow for plant-wide evaluations (Jeppsson et al., 2007). This also enables modelling of future phosphorus control/recovery strategies in the context of a WRRF (Jeppsson et al., 2013). In the following section, we discuss the applicability of model assumptions used to describe P, S and Fe interactions, suitability of the number of considered processes, and some practical implications for plant-wide modelling/development of resource recovery strategies.

4.1. Implementation details

Modelling P, S and Fe together with multiple mineral precipitation is not straightforward (Musvoto et al., 2000; van Rensburg et al., 2003; Barat et al., 2011) but is necessary to properly present phosphorus transformations in the ADM1. The potential interactions of P with other compounds (Ca, Mg, Fe) and the complex chemistry (trivalence gives a strong non-ideal behaviour) require a substantial investment in model development and testing (Solon et al., 2015; Kazadi Mbamba et al., 2015a,b). Special attention has to be paid to numerics (Lizarralde et al., 2015; Flores-Alsina et al., 2015). In this particular case the equations of the weak acid-base chemistry module are solved by combining a gradient method with the simulated annealing algorithm (stochastic method) (Flores-Alsina et al., 2015). The combination of both increases the robustness of the approach and makes the system of equations less dependent on the initial conditions (a common problem with all Newton-Raphson methods). The physico-chemical model is verified using the geochemical software MINTEQ (Allison et al., 1991). The continuity of the biochemical model is checked with the methodology proposed by Hauduc et al. (2010) (see mass balances in the Supplemental Information Sections 2 and 4 for COD, C, N, P and other elements). Model stiffness has been further reduced by including hydrogen (S_{H2}) as an algebraic instead of a differential equation, as suggested by Rosen et al. (2006). Nevertheless the combination of the modified ADM1 with the ASM2d introduces additional stiffness again, and this is further complicated by the implementation of controllers with stochastic/time delay issues.

4.2. Model adaptation, verification & experimental validation

The set of models presented in this study offers a fair representation of a typical process scenario with the expanded model analysis taking place in the sludge line of a WRRF. For instance, the original ADM1 (biochemical) implementation (A_0) has been previously tested by other research groups and validated in many facilities (Donoso-Bravo et al., 2011). Influent characterization is a key issue for successful model predictions (Jimenez et al., 2014, 2015). The P module used in the present study is extracted from literature, and has also been previously calibrated and validated (Ikumi et al., 2011; Harding et al., 2011; Wang et al., 2016). The same applies for the S module (Fedorovich et al. 2003; Batstone, 2006; Barrera et al., 2015; Liu et al., 2015a,b) and the Fe module (Nielsen et al., 2005; Liu et al., 2015a). The physico-chemical framework has been implemented and validated in several studies (Kazadi Mbamba et al., 2015a,b; Thompson-Brewster et al., 2015). Finally, the original interfaces (Nopens et al., 2009), which have been mathematically improved via the CBIM approach (Volcke et al., 2006), have also been previously validated (Zaher et al., 2007, 2009; Nopens et al., 2009). The latter allows for plant-wide model descriptions that only require locally relevant (unit-specific) state variables (for example methanogens need not be considered in the activated sludge section). The combined system (ASM2d +ADM1+interfaces) is calibrated and validated in a large plant-wide modelling project in Queensland, Australia (Kazdi-Mbama et al., 2016). Default parameter values can be used to develop control/benchmark plant-wide control strategies involving the three (P, S and Fe) elements (Gernaey et al., 2014).

While there are large amounts of data generally available on operation of laboratory scale digesters, there is very limited combined pH, soluble phosphorus, cation and sulfur data for full-scale digesters and even less information within the context of WWTPs. The modelled N:P ratio (= 4) and modelled pH (= 6.9) observed in the present study lie within general expectations of mixed sludge digestion, but a broader validation using detailed sampling programmes is considered highly justified. Higher in-digester pH values may result from higher influent hardness and could cause lower soluble phosphorus levels and larger amounts of calcium and magnesium partitioned to the sludge line. However, these effects require further mechanistic analysis with modelling of precipitation in the activated sludge process, and this is beyond the scope of the present study (although the approaches outlined are transferable).

4.3. Number of considered (bio)chemical processes

Even though the presented extended version of the anaerobic digestion model has substantially increased the number of considered processes, it is not exhaustive. For example, an important decision is modelling $S_{Fe^{3+}}$ as a pure chemical process, when there are several processes that describe iron transformation processes biologically (iron reducing bacteria) (Liu et al., 2015a). This simplification avoids over-parameterization while still offering a reasonably descriptive level. Possibly more important is consideration of X_{FePO4} re-dissolution (and formation in the activated sludge). The $S_{Fe^{3+}}$ ions that are bound to $S_{PO_4^{3-}}$ will likely be released in AD conditions, where they will precipitate with sulfide that has formed in the digester, attributable to the low solubility of X_{FeS} in comparison with X_{FePO4} (Pikaar et al., 2014; Ge et al., 2013). This requires full extension of the activated sludge line models as well. A wide range of other precipitates can be included, for example $CaSO_4$ (Tait et al., 2009), Fe_2S_3 (Atlas and Büyükgüngör, 2008) and $FeCO_3$ (Mamais et al., 1994). A comprehensive review of ADM1 potential research avenues can be found in Batstone et al. (2015). The

approach is compatible with extended applications of the phosphorus:sulfur cycle, including potentially saline wastewater treatment (Wang et al., 2009), and phosphorus and sulfur recovery (Le Corre et al., 2009).

4.4. Extension to plant-wide modelling

The present paper, in proposing an interface system, a combined physico-chemical approach (including use of a common precipitation approach) and a state implementation framework for Fe, S, and P addresses many of the major challenges in plant-wide phosphorus and sulfur modelling (Vanrolleghem et al., 2014), and indeed, extension of ASM/ADM models to high sulfur activated sludge units such as the SANI process (Wang et al., 2009). The key challenges remaining for plant-wide modelling include modelling the phosphorus and sulfur cycles within the activated sludge system (ASM). This requires inclusion of sulfide (S_{IS}) oxidation to sulfate (S_{SO_4}) and iron oxidation (to $S_{Fe^{3+}}$) in addition to the already implemented polyphosphate uptake and release mechanisms represented in the ASM2d (X_{PP}). This is beyond the scope of this paper, but is relatively straightforward, with oxygen (S_{O2}) and nitrate (S_{NO3}) as potential electron sinks. This would allow a mechanistic description of key phenomena – such as plant-wide Fe cycling and prediction of odour formation potential in major unit operations – even outside the plant boundaries (e.g. in the sewer system) (Saagi et al., 2016).

4.5. Practical implication and development of (recovery) strategies in WRRF

The platform and the set of models presented herein will substantially increase the potential control strategies that can be evaluated for a future WRRF. Indeed, the mathematical description of the interactions between the P and S system, will allow obtaining reliable predictions of: (1) potential nutrients that can be recovered (via precipitation); and, (2) the total quantity of energy (electrical/thermal) that can be obtained from methane production (via co-generation).

The results reported in Sections 3.2 and 4 demonstrate the role that X_{PAO} might play in terms of the AD performance at low SRT. For this reason, special attention must be paid when modelling a two-phase anaerobic digestion system (acid–methane digestion). Indeed, the potential uptake of organic acids by X_{PAO} is an important process to consider in that type of system where the SRT ranges from 1 to 2 days. The latter might affect the predictions of the quantity of produced acids and therefore the total methane production in the subsequent stage. The results presented in Figs. 1 and 3 would in that case be even more pronounced.

The results in this study lead to conclude that P precipitation can be used as a control mechanism to reduce N- and P-rich loads in digester supernatant. Additional plant layout modifications, for example the addition of a stripping unit for pH control and the construction of a crystallizer, can be assessed in this model (Lizarralde et al., 2015). The latter will allow future users to evaluate the cost of aeration (to increase pH) versus the addition of metal salts to promote struvite precipitation.

Another important aspect is energy recovery. The set of models presented in this study take into account the effect that S compounds, particularly sulfide, might have on the methanogens. Indeed, SRB outcompete traditional AD bacteria for substrate (hydrogen, organic acids) and they are less sensitive to H_2S inhibition. This information could be used to develop odour/corrosion risk indices on the basis of the simulation results (see for example Comas et al. (2008)) that can also be used for the purpose of establishing control strategies to reduce some of these undesired phenomena, similar to the work presented by Flores-Alsina et al. (2009) on using the risk of occurrence of settling problems as additional information to improve control strategies. Reliable methane quantification combined with additional turbine/energy models will allow the estimation of the number of kWh/day that can be obtained from biogas. Users can use the developed models to evaluate the cost of metal addition, versus the gain in digester performance (sludge stabilization) and the electrical/thermal benefit of the use of biogas.

5. Conclusions

This paper has addressed some of the existing ADM1 structural limitations by proposing special modules dealing with P/S/Fe simultaneously. All these elements are described with the aid of a new physico-chemical framework (aqueous phase chemistry model + multiple mineral precipitation models). The key findings of the presented research, based on the first prototype, are summarized in the following points:

- The proportioning of soluble and particulate P in the digester outlet depends on the cationic load, which is linked to pH and minerals precipitation.
- Potential uptake of organics by X_{PAO} to form X_{PHA} could have an important effect on overall biogas production.
- The model describes the role that SRB play in treating sludge with high S content leading to H_2S formation and potentially reduction of methane formation due to inhibition and loss of electrons.
- Influent iron has a profound impact on sulfide ions because of iron sulfide precipitation (X_{FeS}). As a result, hydrogen sulfide gas production (G_{H_2S}) is reduced, sulfide inhibition is less and methane/energy recovery is increased.
- The presented model can be easily linked with standard activated sludge models through the outlined interfaces that would allow the development, testing and evaluation of recovery strategies at a plant-wide level. We particularly note application of the model to the next generation of water resource recovery facilities (WRRF), which are critically dependent on a mechanistic phosphorus modelling approach.

6. Software availability

The MATLAB/SIMULINK code presented in this paper is available upon request, including the implementation of the physico-chemical modelling framework in ADM1 with P, S and Fe extensions. Using this code, interested readers will be able to reproduce the results summarized in this study. To express interest, please contact Dr. Ulf Jeppsson (ulf.jeppsson@iea.lth.se) at Lund University (Sweden), Prof. Krist V. Gernaey (kvg@kt.dtu.dk) or Dr. Xavier Flores-Alsina (xfa@kt.dtu.dk) at the Technical University of Denmark (Denmark) or Dr. Damien Batstone (damienb@awmc.uq.edu.au) at The University of Queensland (Australia).

Acknowledgements

Dr Flores-Alsina is grateful to the financial support from the REWARD project , funded by the Innovation Fund Denmark (project 1308-0027B) and the collaborative international consortium WATERJPI2015 WATINTECH of the Water Challenges for a Changing World Joint Programming Initiative (Water JPI) 2015 call. Ms Solon and Dr Flores-Alsina acknowledge the Marie Curie Program of the EU 7th Framework Programme FP7/2007-2013 under REA agreement 289193 (SANITAS) and 329349 (PROTEUS), respectively. Ms

Solon also acknowledges EU COST action Water_2020 (contract no. ES1202) and the Swedish Water & Wastewater Association (contract no. 12-123). Prof. Eveline Volcke is acknowledged for the supervision of Ms Solon during her research stay at Ghent University (Belgium). The authors gratefully acknowledge the feedback provided by Professor Peter A. Vanrolleghem, Canada Research Chair in Water Quality Modelling, Université Laval, Quebec, Canada. The research was also supported financially by the University of Queensland through the UQ International Scholarships (UQI). The International Water Association (IWA) is acknowledged for their promotion of this collaboration through their sponsorship of the IWA Task Group on Generalized Physicochemical Modelling Framework (PCM). A concise version of this paper was presented at the 14th IWA World Congress on Anaerobic Digestion (Viña de Mar, Chile, 15-18 Nov., 2015).

Appendix A. Supplementary data

Supplementary data related to this article can be found at http://dx.doi.org/10.1016/j.watres.2016.03.012.

References

Allison, J.D., Brown, D.S., Novo-Gradac, K.J., 1991. MINTEQA2/PRODEFA2, a Geochemical Assessment Model for Environmental Systems: Version 3.0 User's Manual. Environmental Research Laboratory, Office of Research and Development. US Environmental Protection Agency, Athens, GA, USA. EPA/600/3–91/021.

Atlas, L., Büyükgüngör, H., 2008. Sulfide removal in petroleum refinery wastewater by chemical precipitation. J. Hazard. Mater. 153 (1–2), 462–469.

Barat, R., Montoya, T., Seco, A., Ferrer, J., 2011. Modelling biological and chemically induced precipitation of calcium phosphate in enhanced biological phosphorus removal systems. Water Res. 45 (12), 3744–3752.

Barrera, E.L., Spanjers, H., Solon, K., Amerlinck, Y., Nopens, I., Dewulf, J., 2015. Modeling the anaerobic digestion of cane-molasses vinasse: extension of the Anaerobic Digestion Model No. 1 (ADM1) with sulfate reduction for a very high strength and sulfate rich wastewater. Water Res. 71, 42–54.

Batstone, D.J., 2006. Mathematical modelling of anaerobic reactors treating domestic wastewater: rational criteria for model use. Rev. Environ. Sci. Biotechnol. 5, 57–71.

Batstone, D.J., Keller, J., Angelidaki, I., Kalyuzhnyi, S.V., Pavlostathis, S.G., Rozzi, A., Sanders, W.T.M., Siegrist, H., Vavilin, V.A., 2002. Anaerobic Digestion Model No. 1. IWA Scientific and Technical Report No. 13. IWA Publishing, London, UK.

Batstone, D.J., Puyol, D., Flores-Alsina, X., Rodriguez, J., 2015. Mathematical modelling of anaerobic digestion processes: applications and future needs. Rev. Environ. Sci. Biotechnol. 14 (4), 595–613.

Comas, J., Rodríguez-Roda, I., Gernaey, K.V., Rosen, C., Jeppsson, U., Poch, M., 2008. Risk assessment modelling of microbiology-related solids separation problems in activated sludge systems. Environ. Model. Softw. 23 (10–11), 1250–1261.

de Gracia, M., Sancho, L., García-Heras, J.L., Vanrolleghem, P., Ayesa, E., 2006. Mass and charge conservation check in dynamic models: application to the new ADM1 model. Water Sci. Technol. 53 (1), 225–240.

Donoso-Bravo, A., Mailier, J., Martin, C., Rodríguez, J., Aceves-Lara, C.A., Wouwer, A.V., 2011. Model selection, identification and validation in anaerobic digestion: a review. Water Res. 45 (17), 5347–5364.

Fedorovich, V., Lens, P., Kalyuzhnyi, S., 2003. Extension of Anaerobic Digestion Model No. 1 with processes of sulfate reduction. Appl. Biochem. Biotechnol. 109, 33–45.

Flores-Alsina, X., Comas, J., Rodriguez-Roda, I., Gernaey, K.V., Rosen, C., 2009. Including the effects of filamentous bulking sludge during the simulation of WWTP using a risk assessment model. Water Res. 43 (18), 4527–4538.

Flores-Alsina, X., Gernaey, K.V., Jeppsson, U., 2012. Benchmarking biological nutrient removal in wastewater treatment plants: influence of mathematical model assumptions. Water Sci. Technol. 65 (8), 1496–1505.

Flores-Alsina, X., Kazadi Mbamba, C., Solon, K., Vrecko, D., Tait, S., Batstone, D., Jeppsson, U., Gernaey, K.V., 2015. A plant-wide aqueous phase chemistry module describing pH variations and ion speciation/pairing in wastewater treatment models. Water Res. 85, 255–265.

Ge, H., Zhang, L., Batstone, D.J., Keller, J., Yuan, Z., 2013. Impact of iron salt dosage to sewers on downstream anaerobic sludge digesters: sulfide control and methane production. J. Environ. Eng. 139, 594–601.

Gernaey, K.V., Flores-Alsina, X., Rosen, C., Benedetti, L., Jeppsson, U., 2011. Dynamic influent pollutant disturbance scenario generation using a phenomenological modelling approach. Environ. Model. Softw. 26 (11), 1255–1267.

Gernaey, K.V., Jeppsson, U., Vanrolleghem, P.A., Copp, J.B., 2014. Benchmarking of Control Strategies for Wastewater Treatment Plants. IWA Scientific and Technical Report No. 23. IWA Publishing, London, UK.

Hao, T.W., Xiang, P.Y., Mackey, H.R., Chi, K., Lu, H., Chui, H.K., van Loosdrecht, M.C.M., Chen, G.H., 2014. A review of biological sulfate conversions in wastewater treatment. Water Res. 65, 1–21.

Harding, T.H., Ikumi, D.S., Ekama, G.A., 2011. Incorporating phosphorus into plant wide wastewater treatment plant modelling anaerobic digestion. In: Proc. IWA Watermatex2011, San Sebastian, Spain, 20–22 June 2011.

Hauduc, H., Rieger, L., Takacs, I., Heduit, A., Vanrolleghem, P.A., Gillot, S., 2010. A systematic approach for model verification: application on seven published activated sludge models. Water Sci. Technol. 61 (4), 825–839.

Henze, M., Gujer, W., Mino, T., van Loosdrecht, M.C.M., 2000. Activated Sludge Models ASM1, ASM2, ASM2d, and ASM3. IWA Scientific and Technical Report No. 9. IWA Publishing, London, UK.

Ikumi, D.S., Brouckaert, C.J., Ekama, G.A., 2011. Modelling of struvite precipitation in anaerobic digestion. In: Proc. IWA Watermatex2011, San Sebastian, Spain, 20–22 June 2011.

Ikumi, D.S., Harding, T.H., Ekama, G.A., 2014. Biodegradability of wastewater and activated sludge organics in anaerobic digestion. Water Res. 56 (1), 267–279.

Jeppsson, U., Alex, J., Batstone, D., Benedetti, L., Comas, J., Copp, J.B., Corominas, L., Flores-Alsina, X., Gernaey, K.V., Nopens, I., Pons, M.-N., Rodriguez-Roda, I., Rosen, C., Steyer, J.-P., Vanrolleghem, P.A., Volcke, E.I.P., Vrecko, D., 2013. Benchmark simulation models, quo vadis? Water Sci. Technol. 68 (1), 1–15.

Jeppsson, U., Pons, M.N., Nopens, I., Alex, J., Copp, J.B., Gernaey, K.V., Rosen, C., Steyer, J.P., Vanrolleghem, P.A., 2007. Benchmark Simulation Model No 2 – general protocol and exploratory case studies. Water Sci. Technol. 56 (8), 287–295.

Jimenez, J., Gonidec, E., Cacho Rivero, J.A., Latrille, E., Vedrenne, F., Steyer, J.-P., 2014. Prediction of anaerobic biodegradability and bioaccessibility of municipal sludge by coupling sequential extractions with fluorescence spectroscopy: towards ADM1 variables characterization. Water Res. 50, 359–372.

Jimenez, J., Aemig, Q., Doussiet, N., Steyer, J.-P., Houot, S., Patureau, D., 2015. A new organic matter fractionation methodology for organic wastes: bioaccessibility and complexity characterization for treatment optimization. Bioresour. Technol. 19, 344–353.

Kalyuzhnyi, S.V., Fedorovich, V.V., 1998. Mathematical modelling of competition between sulphate reduction and methanogenesis in anaerobic reactors. Bioresour. Technol. 65, 227–242.

Kazadi-Mbamba, C., Flores-Alsina, X., Batstone, D., Tait, S., 2015a. A generalized chemical precipitation modelling approach in wastewater treatment applied to calcite. Water Res. 68 (1), 342–353.

Kazadi-Mbamba, C., Batstone, D., Flores-Alsina, X., Tait, S., 2015b. Generalised approach to dynamic modelling of multiple and competing chemical precipitation reactions in wastewater. Water Res. 85, 359–370.

Kazdi-Mbama, C., Flores-Alsina, X., Batstone, D., Tait, S., 2016. Validation of a plant-wide modelling approach with minerals precipitation in a full-scale WWTP. Water Res. (submitted manuscript).

Le Corre, K.S., Valsami-Jones, E., Hobbs, P., Parsons, S.A., 2009. Phosphorus recovery from wastewater by struvite crystallization: a review. Crit. Rev. Environ. Sci. Technol. 39 (6), 433–477.

Liu, Y., Zhang, Y., Ni, B.J., 2015a. Evaluating enhanced sulfate reduction and optimized volatile fatty acids (VFA) composition in anaerobic reactor by Fe (III) addition. Environ. Sci. Technol. 49 (4), 2123–2321.

Liu, Y., Zhang, Y., Ni, B.J., 2015b. Zero valent iron simultaneously enhances methane production and sulfate reduction in anaerobic granular sludge reactors. Water Res. 75, 292–300.

Lizarralde, I., Fernandez-Arevalo, T., Brouckaert, C., Vanrolleghem, P.A., Ikumi, D., Ekama, D., Ayesa, E., Grau, P., 2015. A new general methodology for incorporating physico-chemical transformations into multiphase wastewater treatment process models. Water Res. 74, 239–256.

Mamais, D., Pitt, P.A., Cheng, Y.W., Loiacono, J., Jenkins, D., 1994. Determination of ferric chloride dose to control struvite precipitation in anaerobic sludge digesters. Water Environ. Res. 66 (7), 912–918.

Musvoto, E.V., Wentzel, M.C., Ekama, G.A., 2000. Integrated chemical-physical processes modelling - II. Simulating aeration treatment of anaerobic digester supernatants. Water Res. 34 (6), 1868–1880.

Nielsen, A.H., Lens, P., Vollertsen, J., Hvitved-Jacobsen, T., 2005. Sulfide-iron interactions in domestic wastewater from a gravity sewer. Water Res. 39 (12), 2747–2755.

Nopens, I., Batstone, D.J., Copp, J.B., Jeppsson, U., Volcke, E., Alex, J., Vanrolleghem, P.A., 2009. An ASM/ADM model interface for dynamic plant-wide simulation. Water Res. 43 (7), 1913–1923.

Otterpohl, R., Freund, M., 1992. Dynamic models for clarifiers of activated sludge plants with dry and wet weather flows. Water Sci. Technol. 26 (5–6), 1391–1400.

Pikaar, I., Sharma, K.R., Hu, S., Gernjak, W., Keller, J., Yuan, Z., 2014. Reducing sewer corrosion through integrated urban water management. Science 345, 812–814.

Poulton, S.W., Krom, M.D., Raiswell, R., 2004. A revised scheme for the reactivity of iron (oxyhydr)oxide minerals towards dissolved sulfide. Geochim. Cosmochim. Acta 68 (18), 3703–3715.

Reichert, P., Borchardt, D., Henze, M., Rauch, W., Shanahan, P., Somlyody, L., Vanrolleghem, P.A., 2001. River Water Quality Model No.1. IWA Scientific and Technical Report No. 12. IWA Publishing, London, UK.

Rodriguez-Freire, L., Sierra-Alvarez, R., Root, R., Chorover, J., Field, J.A., 2014. Biomineralization of arsenate to arsenic sulfides is greatly enhanced at mildly acidic conditions. Water Res. 66, 242–253.

Rosen, C., Vrecko, D., Gernaey, K.V., Pons, M.-N., Jeppsson, U., 2006. Implementing ADM1 for plant-wide benchmark simulations in Matlab/Simulink. Water Sci.

Technol. 54 (4), 11–19.
Saagi, R., Flores-Alsina, X., Fu, G., Gernaey, K.V., Jeppsson, U., Butler, D., 2016. Catchment and sewer network simulation model to benchmark control strategies within urban wastewater systems. Environ. Model. Softw. 78, 16–30.
Siegrist, H., Vogt, D., Garcia-Heras, J., Gujer, W., 2002. Mathematical model for meso and thermophilic anaerobic sewage sludge digestion. Environ. Sci. Technol. 36, 1113–1123.
Solon, K., Flores-Alsina, X., Kazadi Mbamba, C., Volcke, E.I.P., Tait, S., Batstone, D., Gernaey, K.V., Jeppsson, U., 2015. Effects of ionic strength and ion pairing on (plant-wide) modelling of anaerobic digestion processes. Water Res. 70, 235–245.
Stucki, J.W., Lee, K., Goodman, B.A., Kostka, J.E., 2007. Effects of in situ biostimulation on iron mineral speciation in a sub-surface soil. Geochim. Cosmochim. Acta 71, 835–843.
Stumm, W., Morgan, J.J., 1996. In: Schnoor, J.L., Zehnder, A.J.B. (Eds.), Aquatic Chemistry: Chemical Equilibria and Rates in Natural Waters. John Wiley and Sons, New York, USA.
Tait, S., Clarke, W.P., Keller, J., Batstone, D.J., 2009. Removal of sulfate from high-strength wastewater by crystallisation. Water Res. 43 (3), 762–772.
Takács, I., Patry, G.G., Nolasco, D., 1991. A dynamic model of the clarification thickening process. Water Res. 25 (10), 1263–1271.
Tchobanoglous, G., Burton, F.L., Stensel, H.D., 2003. Wastewater Engineering: Treatment, Disposal and Reuse. McGraw-Hill, New York, USA.
Thompson Brewster, E., Mehta, C.M., Radjenovic, J., Batstone, D.J., 2015. A mechanistic model for electrochemical nutrient recovery systems. Water Res. 94, 176–186.
Utgikar, V.P., Harmon, S.M., Chaudhary, N., Tabak, H.H., Govind, R., Haines, J.R., 2002. Inhibition of sulfate-reducing bacteria by metal sulfide formation in bioremediation of acid mine drainage. Environ. Toxicol. 17, 40–48.
van Rensburg, P., Musvoto, E.V., Wentzel, M.C., Ekama, G.A., 2003. Modelling multiple mineral precipitation in anaerobic digester liquor. Water Res. 37 (13), 3087–3097.
Vanrolleghem, P., Flores-Alsina, X., Guo, L., Solon, K., Ikumi, D., Batstone, D.J., Brouckaert, C., Takacs, I., Grau, P., Ekama, G.A., Jeppsson, U., Gernaey, K.V., 2014. Towards BSM2-GPS-X: a plant-wide benchmark simulation model not only for carbon and nitrogen, but also for greenhouse gases (G), phosphorus (P), sulphur (S) and micropollutants (X), all within the fence of WWTPs/WRRFs. In: Proc. 4th IWA/WEF Wastewater Treatment Modelling Seminar, Spa, Belgium, 30 March-2 April 2014.
Volcke, E.I.P., van Loosdrecht, M.C.M., Vanrolleghem, P.A., 2006. Continuity-based model interfacing for plant-wide simulation: a general approach. Water Res. 40 (15), 2817–2828.
Wang, J., Lua, H., Chen, G.H., Ngai Laua, G., Tsang, W.L., van Loosdrecht, M.C.M., 2009. A novel sulfate reduction, autotrophic denitrification, nitrification integrated (SANI) process for saline wastewater treatment. Water Res. 43 (9), 2363–2372.
Wang, R., Yongmei, L., Chen, W., Zou, J., Chen, Y., 2016. Phosphate release involving PAOs activity during anaerobic fermentation of EBPR sludge and the extension of ADM1. Chem. Eng. J. 297 (1), 436–447.
Xiao, X., Sheng, G.-P., Mu, Y., Yu, H.-Q., 2013. A modeling approach to describe ZVI-based anaerobic system. Water Res. 47 (16), 6007–6013.
Zaher, U., Grau, P., Benedetti, L., Ayesa, E., Vanrolleghem, P.A., 2007. Transformers for interfacing anaerobic digestion models to pre- and post-treatment processes in a plant-wide modelling context. Environ. Model. Softw. 22 (1), 40–58.
Zaher, U., Rongping, L., Jeppsson, U., Steyer, J.-P., Chen, S., 2009. GISCOD: general integrated solid waste co-digestion model. Water Res. 43 (10), 2717–2727.
Zhang, J., Zhang, Y., Chang, J., Quan, X., Li, Q., 2013. Biological sulfate reduction in the acidogenic phase of anaerobic digestion under dissimilatory Fe (III)-reducing conditions. Water Res. 47 (6), 2033–2040.
Zhang, L., De Schryver, P., De Gusseme, B., De Muynck, W., Boon, N., Verstraete, W., 2008. Chemical and biological technologies for hydrogen sulfide emission control in sewer systems: a review. Water Res. 42 (1–2), 1–12.

Supplemental Information

Paper Title: Modelling phosphorus (P), sulfur (S) and iron (Fe) interactions for dynamic simulations of anaerobic digestion processes

Authors: Flores-Alsina, X., Solon, K., Kazadi Mbamba, C., Tait, S., Gernaey, K.V., Jeppsson, U., Batstone, D.J.

Table 1.1 Mass balance for the ASM2d state variables before the interface. *X* refers to (dissolved) cations/anions Na, Cl, Ca, S and Fe

COD	β_C	β_N	β_P	β_K	β_{Mg}	β_X	symbol	g.m^{-3}	COD	C	N	P	K	Mg	Na	Cl	Ca	S	Fe
	g C.gstoich^{-1}	g N.gstoich^{-1}	g P.gstoich^{-1}	g K.gstoich^{-1}	g Mg.gstoich^{-1}	g X.gstoich^{-1}			kg COD.day^{-1}	kg C.day^{-1}	kg N.day^{-1}	kg P.day^{-1}	kg K.day^{-1}	kg Mg.day^{-1}	kg Na.day^{-1}	kg Cl.day^{-1}	kg Ca.day^{-1}	kg S.day^{-1}	kg Fe.day^{-1}
-1							S_{O2}	**0,00**	0.00										
1							S_F	**26,44**	5.06	1.61	0.17	0.03							
1	0.3184	0.0335	0.0056				S_A	**17,66**	3.38	1.27									
1	0.3750						S_I	**27,23**	5.21	1.89	0.31	0.03							
	0.3618	0.0600	0.0065				S_{NH_4}	**18,58**			3.56								
-1.7143		1					S_{N_2}	**5,07**	-1.67		0.97								
-4.5714		1					S_{NO_x}	**0,02**	-0.02		0.00								
		1					S_{PO_4}	**4,69**				0.90							
			1				S_{IC}	**78,99**		15.12		0.00							
1	1						X_I	**10964,41**	2,098.66	759.25	125.97	13.62							
1	0.3618	0.0600	0.0065				X_S	**19084,76**	3,652.95	1,163.20	122.44	20.41							
1	0.3184	0.0335	0.0056	1			X_H	**9479,39**	1,814.42	664.29	156.30	39.08							
1	0.3661	0.0861	0.0215	1			X_{PAO}	**3862,20**	739.25	270.65	63.68	15.92							
	0.3661	0.0861	0.0215	0.42043	0.2614		X_{PP}	**450,87**				86.30	36.28	22.56					
1	0	0	1				X_{PHA}	**24,64**	4.72	1.42									
1	0.300						X_A	**333,79**	63.89	23.39	5.50	1.38							
	0.3661	0.0861	0.0215	1			S_K	**19,79**					3.79						
					1		S_{Mg}	**189,87**						36.34					
						1	S_{Na}	**70**							13.40				
						1	S_{Cl}	**1035**								198.11			
						1	S_{Ca}	**300**									57.42		
						1	S_{SO_4}	**0**											

total loading (kg.day^{-1})	**8,385.87**	**2,902.08**	**478.92**	**177.66**	**40.07**	**58.90**	**13.40**	**198.11**	**57.42**

total loading (kmol.day^{-1})		**241.88**	**34.21**	**5.73**	**1.02**	**2.42**	**0.58**	**5.58**	**1.44**

Table 1.2 Mass balance for a subset of the ADM1 state variables after the interface (model A_0). X_{PAO}decay and X_{PP} and X_{PHA} hydrolyse in the interface. *X* refers to (dissolved) cations/anions Na. Cl. Ca. S and Fe

COD	β_C	β_N	β_P	β_K	β_{Mg}	β_X	symbol	kg COD.m^{-3}	COD	C	N	P	K	Mg	Na	Cl	Ca	S	Fe
	kmol C. kg stoich^{-1}	kmol N. kg stoich^{-1}	kmol P. kg stoich^{-1}	kmol K. kg stoich^{-1}.	kmol Mg. kg stoich^{-1}	kmol X. kg stoich^{-1}			kg COD.day^{-1}	kmol C. day^{-1}	kmol N. day^{-1}	kmol P. day^{-1}	kmol K. day^{-1}	kmol Mg. day^{-1}	kmol Na. day^{-1}	kmol Cl. day^{-1}	kmol Ca. day^{-1}	kmol S. day^{-1}	kmol Fe. day^{-1}
1	0.0313						S_{su}	**0.018**	3.53	0.11									
1	0.0307						S_{aa}	**0.008**	1.53	0.05	0.01								
1	0.0214						S_{fa}												
1	0.0240						S_{va}	**0.002**	0.47	0.01									
1	0.0250						S_{bu}	**0.002**	0.47	0.01									
1	0.0268						S_{pro}	**0.010**	1.89	0.05									
1	0.0313						S_{ac}	**0.027**	5.24	0.16									
	1						S_{IC}	**0.032***		6.09									
		1					S_{IN}	**0.050***			9.50								
1	0.0301	0.0043	0.0002				S_I	**0.027**	5.21	0.16	0.02	0.00							
1	0.0313						X_{ch}	**9.082**	1.738.34	54.32	0.00	0.00							
1	0.0258	0.0071					X_{pr}	**9.543**	1.826.53	56.15	14.44	0.00							
1	0.0219		0.0003				X_{li}	**12.768**	2.443.91	53.58	0.00	0.84							
1	0.0301	0.0043	0.0002				X_I	**12.332**	2.360.42	71.16	10.12	0.49							
			1.0000				S_{IP}	**0.023***	0.00	0.00	0.00	4.40							
1	0.0301						X_{PHA}												
			1	0.3333	0.3333		X_{PP}												
1	0.0305	0.0062	0.0007				X_{PAO}												
						1	S_{SO_4}												
						1	S_{Na}	**0.003***							0.58				
				1			S_K	**0.005***					1.03						
						1	S_{Cl}	**0.029***								5.58			
						1	S_{Ca}	**0.007***									1.44		
					1		S_{Mg}	**0.013***						2.42					
-1.7143		1					S_{N_2}	**0.0004*****	-1.67		0.07								

total loading (kmol.day^{-1})	**241.88**	**34.21**	**5.73**	**1.02**	**2.42**	**0.58**	**5.58**	**1.44**	
total loading (kg.day^{-1})	**8,385.87**	**2,902.08**	**478.92**	**177.66**	**40.07**	**58.90**	**13.40**	**198.11**	**57.42**

*units are kmol.m^{-3}

**not used as state variable in ADM1 but necessary to close the COD and N mass balances

Table 1.3 Mass balance for a subset of the ADM1 state variables after the interface (model A_1). X_{PAO}. X_{PP} and X_{PHA} are considered as state variables. *X* refers to (dissolved) cations/anions Na. Cl. Ca. S and Fe

COD	β_C	β_N	β_P	β_K	β_{Mg}	β_X	symbol	kg COD.m^{-3}	COD	C	N	P	K	Mg	Na	Cl	Ca	S	Fe
	kmol C. kg stoich^{-1}	kmol N. kg stoich^{-1}	kmol P. kg stoich^{-1}	kmol K. kg stoich^{-1}.	kmol Mg. kg stoich^{-1}	kmol X. kg stoich^{-1}			kg COD.day^{-1}	kmol C. day^{-1}	kmol N. day^{-1}	kmol P. day^{-1}	kmol K. day^{-1}	kmol Mg. day^{-1}	kmol Na. day^{-1}	kmol Cl. day^{-1}	kmol Ca. day^{-1}	kmol S. day^{-1}	kmol Fe. day^{-1}
1	0.0313						S_{au}	**0.018**	3.53	0.11									
1	0.0307						S_{aa}	**0.008**	1.53	0.05	0.01								
1	0.0214						S_{fa}												
1	0.0240						S_{va}												
1	0.0250						S_{bu}												
1	0.0268						S_{pro}												
1	0.0313						S_{ac}	**0.018**	3.35	0.10									
	1						S_{IC}	**0.021***		4.06									
		1					S_{IN}	**0.036***			6.89								
1	0.0301	0.0043	0.0002				S_I	**0.027**	5.21	0.15	0.02	0.001							
1	0.0313						X_{ch}	**8.020**	1.535.04	47.97									
1	0.0258	0.0071					X_{PT}	**8.481**	1.623.24	49.90	12.83								
1	0.0219		0.0003				X_{li}	**11.416**	2.185.17	47.91		0.75							
1	0.0301	0.0043	0.0002				X_I	**11.946**	2.286.50	65.57	10.22	0.46							
			1.0000				S_{IP}	**0.006***				1.20							
1	0.0301						X_{PHA}	**0.025**	4.72	0.12									
			1	0.3333	0.3333		X_{PP}	**0.015***				2.78	0.93	0.93					
1	0.0305	0.0062	0.0007				X_{PAO}	**3.862**	739.25	22.55	4.55	0.51							
						1	S_{SO_4}												
						1	S_{Na}	**0.003***							0.58				
				1			S_K	**0.001***					0.10						
						1	S_{Cl}	**0.029***								5.58			
						1	S_{Ca}	**0.007***									1.44		
					1		S_{Mg}	**0.008***						1.49					
-1.7143		1					S_{N_2}	**0.0004*****	-1.67		0.07								

total loading (kmol.day^{-1})		**241.88**	**34.21**	**5.73**	**1.02**	**2.42**	**0.58**	**5.58**	**1.44**	
total loading (kg.day^{-1})	**8,385.87**	**2,902.08**	**478.92**	**177.66**	**40.07**	**58.90**	**13.40**	**198.11**	**57.42**	

*units are kmol.m^{-3}

**not used as state variable in ADM1 but necessary to close the COD and N mass balances

Table 1.4 Mass balance for a subset of the ADM1 state variables before the interface (model A_1)

COD	β_C	β_N	β_P	β_K	β_{Mg}	β_X	symbol	kg COD.m^{-3}	COD	C	N	P	K	Mg	Na	Cl	Ca	S	Fe
	kmol C. kg stoich^{-1}	kmol N. kg stoich^{-1}	kmol P. kg stoich^{-1}	kmol K. kg stoich^{-1}.	kmol Mg. kg stoich^{-1}	kmol X. kg stoich^{-1}			kg COD.day^{-1}	kmol C. day^{-1}	kmol N. day^{-1}	kmol P. day^{-1}	kmol K. day^{-1}	kmol Mg. day^{-1}	kmol Na. day^{-1}	kmol Cl. day^{-1}	kmol Ca. day^{-1}	kmol S. day^{-1}	kmol Fe. day^{-1}
1	0.0313						S_{su}	**0.013**	2.51	0.08									
1	0.0307						S_{aa}	**0.006**	1.12	0.03	0.01								
1	0.0214						S_{fa}	**0.116**	22.11	0.47									
1	0.0240						S_{va}	**0.012**	2.29	0.06									
1	0.0250						S_{bu}	**0.016**	2.99	0.07									
1	0.0268						S_{pro}	**0.019**	3.60	0.10									
1	0.0313						S_{ac}	**0.055**	10.54	0.33									
1							S_{H_2}	**2.65E-07**	5.07E-05										
1	0.0156						S_{CH4}	**0.052**	10.03	0.16									
0	1						S_{IC}	**0.059***		11.38									
0		1					S_{IN}	**0.080***			15.25								
1	0.0301	0.0043	0.0002				S_I	**0.027**	5.21	0.15	0.02	0.001							
1	0.0313						X_{ch}	**1.441**	275.74	8.62									
1	0.0258	0.0071					X_{pr}	**1.513**	289.67	8.90	2.29								
1	0.0219		0.0001				X_{li}	**2.025**	387.51	8.50		0.13							
1	0.0301	0.0043	0.0002				X_I	**12.345**	2,362.90	71.24	10.13	0.49							
			1.0000				S_{IP}	**0.007***				1.53							
1	0.0301						X_{PHA}	**0.252**		48.31	1.21								
			1	0.3333	0.3333		X_{PP}	**8.05E-06**					1.54E-03	5.14E-04	5.14E-04				
1	0.0305	0.0062	0.0007				$X_{BIOMASS}$	**3.600**	688.99	21.02	4.24	0.48							
						1	S_{SO_4}												
						1	S_{Na}	**0.003***							0.58				
				1			S_K	**0.005***					1.02						
						1	S_{Cl}	**0.029***								5.58			
						1	S_{Ca}	**0.001***									0.10		
					1		S_{Mg}	**0.001***						0.22					
			2			3	$X_{Ca_3(PO_4)_2}$	**0.002***				0.89					1.34		
		1	1		1		$X_{MgNH_4PO_4}$	**0.011***			2.20	2.20		2.20					
1	0.0156						G_{H_2}	**0.004****	0.03										
							G_{CH_4}	**1.069.08****	4.276.30	66.82									
1							G_{CO_2}	**1.880.48****		42.30									
-1.7143		1					S_{N_2}	**0.0004*****	-1.67		0.07								
							total loading (kmol.day^{-1})			**241.88**	**34.21**	**5.73**	**1.02**	**2.42**	**0.58**	**5.58**	**1.44**		
							total loading (kg.day^{-1})		**8,385.87**	**2,902.08**	**478.92**	**177.66**	**40.07**	**58.90**	**13.40**	**198.11**	**57.42**		

*units are kmol.m^{-3}
**units are kg.day^{-1}
***not used as state variable in ADM1 but necessary to close the mass balances. Units are kmol.m^{-3}.

Table 1.5 Mass balance for a subset of the ASM2d state variables after the interface (model A_1)

COD	β_C	β_N	β_P	β_K	β_{Mg}	β_X	symbol	g.m^{-3}	COD	C	N	P	K	Mg	Na	Cl	Ca	S	Fe
	g C.gstoich^{-1}	g N.gstoich^{-1}	g P.gstoich^{-1}	g K.gstoich^{-1}	gMg.gstoich^{-1}	gX.gstoich^{-1}			kg COD. day^{-1}	kmol C. day^{-1}	kmol N. day^{-1}	kmol P. day^{-1}	kmol K. day^{-1}	kmol Mg. day^{-1}	kmol Na. day^{-1}	kmol Cl. day^{-1}	kmol Ca. day^{-1}	kmol S. day^{-1}	kmol Fe. day^{-1}
-1							S_{O_2}	**0,00**											
1	0.3661	0.0861	0.0215				S_F	**134.43**	25.73	8.19	0.86	0.14							
1	0.3750						S_A	**353.82**	67.72	25.40									
1	0.3618	0.0600	0.0065				S_I	**27.23**	5.21										
		1					S_{NH_X}	**1,291.68**			247.24								
-1.7143		1					S_{N_2}	**0.00**											
-4.5714		1					S_{NO_X}	**0.00**											
			1				S_{PO_4}	**298.09**				57.06							
	1						S_{IC}	**885.27**		169.45									
1	0.3618	0.0600	0.0065				X_I	**1,2704.93**	2431.81	879.78	145.97	15.78							
1	0.3184	0.0335	0.0056				X_S	**8218.94**	1573.16	500.94	52.73	8.79							
1	0.3661	0.0861	0.0215				X_H	**0.00**											
1	0.3661	0.0861	0.0215				X_{PAO}	**0.00**											
			1	0.42043	0.26140		X_{PP}	**0.00**											
1	0.3000						X_{PHA}	**0.00**											
1	0.3661	0.0861	0.0215				X_A	**0.00**											
				1			S_K	**208.84**					40.07						
					1		S_{Mg}	**28.29**						5.42					
						1	S_{Na}	**70.00**							13.40				
						1	S_{Cl}	**1,035.00**								198.11			
						1	S_{Ca}	**20.45**									3.92		
						1	S_{SO_4}	**0**											
							$X_{Ca_3(PO_4)_2}$	**722.17**				27.64					53.50		
							X_{MgNH_4PO}	**1,578.52**			30.81	68.22		53.48					
1							S_{H_2}	**2.67E-07*****	0.00										
1							S_{CH4}	**0.0524*****	10.12	1.90									
1							G_{H_2}	**0.004*****	0.03										
1							G_{CH_4}	**1.069.08*****	4.276.30	66.82									
	1						G_{CO_2}	**1.880.48*****		42.30									
		1					S_{N_2}	**5.07****	-1.67		0.97	-							

total loading (kg.day^{-1})	**8,385.87**	**2,902.08**	**478.92**	**177.66**	**40.07**	**58.90**	**13.40**	**198.11**	**57.42**	
total loading (kmol.day^{-1})		**241.88**	**34.21**	**5.73**	**1.02**	**2.42**	**0.58**	**5.58**	**1.44**	

*units are kg.day^{-1} or kg.m^{-3}

**not used as state variable but necessary to close the mass balances

EXTENSIONS/MODIFICATIONS TO THE ANAEROBIC DIGESTION MODEL NO. 1 (ADM1)

MODIFIED ADM1

Table 1.1a Biochemical rate coefficients ($\nu_{i,j}$) for soluble components (i=1-13, j=1-18)
Table 1.1b Biochemical rate coefficients ($\nu_{i,j}$) for particulate components (i=14-24, j=1-18)
Table 1.2 Process kinetic rate equations (ρ_j) for the biological reaction model
Table 1.3 Additional parameter values for the modified ADM1

P-EXTENSION

Table 2.1 Biochemical rate coefficients ($\nu_{i,j}$) for P model extension components
Table 2.2 Process kinetic rate equations (ρ_j) for the P extension to the biological reaction model
Table 2.3 Parameter values for P model extension

S-EXTENSION

Table 3.1 Biochemical rate coefficients ($\nu_{i,j}$) for S model extension components
Table 3.2 Process kinetic rate equations (ρ_j) for the S extension to the biological reaction model
Table 3.3 Parameter values for S model extension

Fe-EXTENSION

Table 4.1 Biochemical rate coefficients ($\nu_{i,j}$) and process kinetic rate equation (ρ_j) for the Fe model extension
Table 4.2 Parameter values for Fe model extension

LIQUID-GAS TRANSFER AND PRECIPITATION PROCESSES

Table 5.1 Stoichiometric matrix for liquid-gas transfer processes
Table 5.2 Stoichiometric matrix for precipitation processes

Table 1.1a Biochemical rate coefficients ($\nu_{i,j}$) for soluble components (i=1-13, j=1-18). In red modifications from the original implementation. Notice that X_c has been removed.

Component →	i	1	2	3	4	5	6	7	8	9	10	11	12	13
j	**Process ↓**	S_{su}	S_{aa}	S_{fa}	S_{va}	S_{bu}	S_{pro}	S_{ac}	S_{h2}	S_{ch4}	S_{IC}	S_{IN}	S_{IP}	S_I
1	Hydrolysis of Carbohydrates	1									$-\sum_{i=1\text{-}9,13\text{-}37} C_i \nu_{i,1}$	$-\sum_{i=1\text{-}9,13\text{-}37} N_i \nu_{i,1}$	$-\sum_{i=1\text{-}9,13\text{-}37} P_i \nu_{i,1}$	
2	Hydrolysis of Proteins		1								$-\sum_{i=1\text{-}9,13\text{-}37} C_i \nu_{i,2}$	$-\sum_{i=1\text{-}9,13\text{-}37} N_i \nu_{i,2}$	$-\sum_{i=1\text{-}9,13\text{-}37} P_i \nu_{i,2}$	
3	Hydrolysis of Lipids	$1-f_{fa,li}$		$f_{fa,li}$							$-\sum_{i=1\text{-}9,13\text{-}37} C_i \nu_{i,3}$	$-\sum_{i=1\text{-}9,13\text{-}37} N_i \nu_{i,3}$	$-\sum_{i=1\text{-}9,13\text{-}37} P_i \nu_{i,3}$	
4	Uptake of Sugars	-1				$(1-Y_{su})\,f_{bu,su}$	$(1-Y_{su})\,f_{pro,su}$	$(1-Y_{su})\,f_{ac,su}$	$(1-Y_{su})\,f_{h2,su}$		$-\sum_{i=1\text{-}9,13\text{-}37} C_i \nu_{i,4}$	$-\sum_{i=1\text{-}9,13\text{-}37} N_i \nu_{i,4}$	$-\sum_{i=1\text{-}9,13\text{-}37} P_i \nu_{i,4}$	
5	Uptake of Amino acids		-1		$(1-Y_{aa})\,f_{va,aa}$	$(1-Y_{aa})\,f_{bu,aa}$	$(1-Y_{aa})\,f_{pro,aa}$	$(1-Y_{aa})\,f_{ac,aa}$	$(1-Y_{aa})\,f_{h2,aa}$		$-\sum_{i=1\text{-}9,13\text{-}37} C_i \nu_{i,5}$	$-\sum_{i=1\text{-}9,13\text{-}37} N_i \nu_{i,5}$	$-\sum_{i=1\text{-}9,13\text{-}37} P_i \nu_{i,5}$	
6	Uptake of LCFA			-1				$(1-Y_{fa})\,0.70$	$(1-Y_{fa})\,0.30$		$-\sum_{i=1\text{-}9,13\text{-}37} C_i \nu_{i,6}$	$-\sum_{i=1\text{-}9,13\text{-}37} N_i \nu_{i,6}$	$-\sum_{i=1\text{-}9,13\text{-}37} P_i \nu_{i,6}$	
7	Uptake of Valerate				-1		$(1-Y_{c4})\,0.54$	$(1-Y_{c4})\,0.31$	$(1-Y_{c4})\,0.15$		$-\sum_{i=1\text{-}9,13\text{-}37} C_i \nu_{i,7}$	$-\sum_{i=1\text{-}9,13\text{-}37} N_i \nu_{i,7}$	$-\sum_{i=1\text{-}9,13\text{-}37} P_i \nu_{i,7}$	
8	Uptake of Butyrate					-1		$(1-Y_{c4})\,0.80$	$(1-Y_{c4})\,0.20$		$-\sum_{i=1\text{-}9,13\text{-}37} C_i \nu_{i,8}$	$-\sum_{i=1\text{-}9,13\text{-}37} N_i \nu_{i,8}$	$-\sum_{i=1\text{-}9,13\text{-}37} P_i \nu_{i,8}$	
9	Uptake of Propionate						-1	$(1-Y_{pro})\,0.57$	$(1-Y_{pro})\,0.43$		$-\sum_{i=1\text{-}9,13\text{-}37} C_i \nu_{i,9}$	$-\sum_{i=1\text{-}9,13\text{-}37} N_i \nu_{i,9}$	$-\sum_{i=1\text{-}9,13\text{-}37} P_i \nu_{i,9}$	
10	Uptake of Acetate							-1		$(1-Y_{ac})$	$-\sum_{i=1\text{-}9,13\text{-}37} C_i \nu_{i,10}$	$-\sum_{i=1\text{-}9,13\text{-}37} N_i \nu_{i,10}$	$-\sum_{i=1\text{-}9,13\text{-}37} P_i \nu_{i,10}$	
11	Uptake of Hydrogen								-1	$(1-Y_{h2})$	$-\sum_{i=1\text{-}9,13\text{-}37} C_i \nu_{i,11}$	$-\sum_{i=1\text{-}9,13\text{-}37} N_i \nu_{i,11}$	$-\sum_{i=1\text{-}9,13\text{-}37} P_i \nu_{i,11}$	
12	Decay of X_{su}										$-\sum_{i=1\text{-}9,13\text{-}37} C_i \nu_{i,12}$	$-\sum_{i=1\text{-}9,13\text{-}37} N_i \nu_{i,12}$	$-\sum_{i=1\text{-}9,13\text{-}37} P_i \nu_{i,12}$	$f_{sI,xb}$
13	Decay of X_{aa}										$-\sum_{i=1\text{-}9,13\text{-}37} C_i \nu_{i,13}$	$-\sum_{i=1\text{-}9,13\text{-}37} N_i \nu_{i,13}$	$-\sum_{i=1\text{-}9,13\text{-}37} P_i \nu_{i,13}$	$f_{sI,xb}$
14	Decay of X_{fa}										$-\sum_{i=1\text{-}9,13\text{-}37} C_i \nu_{i,14}$	$-\sum_{i=1\text{-}9,13\text{-}37} N_i \nu_{i,14}$	$-\sum_{i=1\text{-}9,13\text{-}37} P_i \nu_{i,14}$	$f_{sI,xb}$
15	Decay of X_{C4}										$-\sum_{i=1\text{-}9,13\text{-}37} C_i \nu_{i,15}$	$-\sum_{i=1\text{-}9,13\text{-}37} N_i \nu_{i,15}$	$-\sum_{i=1\text{-}9,13\text{-}37} P_i \nu_{i,15}$	$f_{sI,xb}$
16	Decay of X_{pro}										$-\sum_{i=1\text{-}9,13\text{-}37} C_i \nu_{i,16}$	$-\sum_{i=1\text{-}9,13\text{-}37} N_i \nu_{i,16}$	$-\sum_{i=1\text{-}9,13\text{-}37} P_i \nu_{i,16}$	$f_{sI,xb}$
17	Decay of X_{ac}										$-\sum_{i=1\text{-}9,13\text{-}37} C_i \nu_{i,17}$	$-\sum_{i=1\text{-}9,13\text{-}37} N_i \nu_{i,17}$	$-\sum_{i=1\text{-}9,13\text{-}37} P_i \nu_{i,17}$	$f_{sI,xb}$
18	Decay of X_{h2}										$-\sum_{i=1\text{-}9,13\text{-}37} C_i \nu_{i,18}$	$-\sum_{i=1\text{-}9,13\text{-}37} N_i \nu_{i,18}$	$-\sum_{i=1\text{-}9,13\text{-}37} P_i \nu_{i,18}$	$f_{sI,xb}$
		Monosaccharides (kg COD·m^{-3})	Amino acids (kg COD·m^{-3})	Long chain fatty acids (kg COD·m^{-3})	Total valerate (kg COD·m^{-3})	Total butyrate (kg COD·m^{-3})	Total propionate (kg COD·m^{-3})	Total acetate (kg COD·m^{-3})	Hydrogen (kg COD·m^{-3})	Methane (kg COD·m^{-3})	Inorganic carbon (kmol C·m^{-3})	Inorganic nitrogen (kmol N·m^{-3})	Inorganic phosphorus (kmol P·m^{-3})	Soluble inerts (kg COD·m^{-3})

In red are new/modified stoichiometric parameters.

Table 1.1b Biochemical rate coefficients ($\nu_{i,j}$) for particulate components (i=14-24, j=1-18). In red modifications from the original implementation. Notice that X_c has been removed.

Component →	i	14	15	16	17	18	19	20	21	22	23	24
j	**Process ↓**	X_{ch}	X_{pr}	X_{li}	X_{su}	X_{aa}	X_{fa}	X_{c4}	X_{pro}	X_{ac}	X_{h2}	X_I
1	Hydrolysis of Carbohydrates	-1										
2	Hydrolysis of Proteins		-1									
3	Hydrolysis of Lipids			-1								
4	Uptake of Sugars				Y_{su}							
5	Uptake of Amino acids					Y_{aa}						
6	Uptake of LCFA						Y_{fa}					
7	Uptake of Valerate							Y_{c4}				
8	Uptake of Butyrate							Y_{c4}				
9	Uptake of Propionate								Y_{pro}			
10	Uptake of Acetate									Y_{ac}		
11	Uptake of Hydrogen										Y_{h2}	
12	Decay of X_{su}	$f_{ch,xb}$	$f_{pr,xb}$	$f_{li,xb}$	-1							$f_{xI,xb}$
13	Decay of X_{aa}	$f_{ch,xb}$	$f_{pr,xb}$	$f_{li,xb}$		-1						$f_{xI,xb}$
14	Decay of X_{fa}	$f_{ch,xb}$	$f_{pr,xb}$	$f_{li,xb}$			-1					$f_{xI,xb}$
15	Decay of X_{C4}	$f_{ch,xb}$	$f_{pr,xb}$	$f_{li,xb}$				-1				$f_{xI,xb}$
16	Decay of X_{pro}	$f_{ch,xb}$	$f_{pr,xb}$	$f_{li,xb}$					-1			$f_{xI,xb}$
17	Decay of X_{ac}	$f_{ch,xb}$	$f_{pr,xb}$	$f_{li,xb}$						-1		$f_{xI,xb}$
18	Decay of X_{h2}	$f_{ch,xb}$	$f_{pr,xb}$	$f_{li,xb}$							-1	$f_{xI,xb}$
		Carbohydrates (kg COD·m^{-3})	Proteins (kg COD·m^{-3})	Lipids (kg COD·m^{-3})	Sugar degraders (kg COD·m^{-3})	Amino acid degraders (kg COD·m^{-3})	LCFA degraders k(g COD·m^{-3})	Valerate and butyrate degraders (kg COD·m^{-3})	Propionate degraders (kg COD·m^{-3})	Acetate degraders (kg COD·m^{-3})	Hydrogen degraders (kg COD·m^{-3})	Particulate inerts (kg COD·m^{-3})

In red are new/modified stoichiometric parameters.

Table 1.2 Process kinetic rate equations (ρ_j) for the biological reaction model. In red modifications from the original implementation

	Process	Kinetic rate expressions (ρ_j, kg COD m^{-3} d^{-1})
1	Hydrolysis of Carbohydrates	$k_{\mathrm{hyd,ch}} \cdot X_{\mathrm{ch}}$
2	Hydrolysis of Proteins	$k_{\mathrm{hyd,pr}} \cdot X_{\mathrm{pr}}$
3	Hydrolysis of Lipids	$k_{\mathrm{hyd,li}} \cdot X_{\mathrm{li}}$
4	Uptake of Sugars	$k_{\mathrm{m,su}} \cdot \frac{S_{\mathrm{su}}}{K_S + S_{\mathrm{su}}} \cdot X_{\mathrm{su}} \cdot I_1$
5	Uptake of Amino acids	$k_{\mathrm{m,aa}} \cdot \frac{S_{\mathrm{aa}}}{K_S + S_{\mathrm{aa}}} \cdot X_{\mathrm{aa}} \cdot I_1$
6	Uptake of LCFA	$k_{\mathrm{m,fa}} \cdot \frac{S_{\mathrm{fa}}}{K_S + S_{\mathrm{fa}}} \cdot X_{\mathrm{fa}} \cdot I_2$
7	Uptake of Valerate	$k_{\mathrm{m,c4}} \cdot \frac{S_{\mathrm{va}}}{K_S + S_{\mathrm{va}}} \cdot X_{\mathrm{c4}} \cdot \frac{1}{1 + \frac{S_{\mathrm{bu}}}{S_{\mathrm{va}}}} \cdot I_3 \cdot I_{\mathrm{h2s,c4}}$
8	Uptake of Butyrate	$k_{\mathrm{m,c4}} \cdot \frac{S_{\mathrm{bu}}}{K_S + S_{\mathrm{bu}}} \cdot \mathrm{X_{c4}} \cdot \frac{1}{1 + \frac{S_{\mathrm{va}}}{S_{\mathrm{bu}}}} \cdot I_3 \cdot I_{\mathrm{h2s,c4}}$
9	Uptake of Propionate	$k_{\mathrm{m,pr}} \cdot \frac{S_{\mathrm{pro}}}{K_S + S_{\mathrm{pro}}} \cdot X_{\mathrm{pro}} \cdot I_4 \cdot I_{\mathrm{h2s,pro}}$
10	Uptake of Acetate	$k_{\mathrm{m,ac}} \cdot \frac{S_{\mathrm{ac}}}{K_S + S_{\mathrm{ac}}} \cdot X_{\mathrm{ac}} \cdot I_5 \cdot I_{\mathrm{h2s,ac}}$
11	Uptake of Hydrogen	$k_{\mathrm{m,h2}} \cdot \frac{S_{h2}}{K_S + S_{\mathrm{h2}}} \cdot X_{\mathrm{h2}} \cdot I_6 \cdot I_{\mathrm{h2s,h2}}$
12	Decay of X_{su}	$k_{\mathrm{dec,X_{su}}} \cdot X_{\mathrm{su}}$
13	Decay of X_{aa}	$k_{\mathrm{dec,X_{aa}}} \cdot X_{\mathrm{aa}}$
14	Decay of X_{fa}	$k_{\mathrm{dec,X_{fa}}} \cdot X_{\mathrm{fa}}$
15	Decay of X_{C4}	$k_{\mathrm{dec,X_{c4}}} \cdot X_{\mathrm{c4}}$
16	Decay of X_{pro}	$k_{\mathrm{dec,X_{pro}}} \cdot X_{\mathrm{pro}}$
17	Decay of X_{ac}	$k_{\mathrm{dec,X_{ac}}} \cdot X_{\mathrm{ac}}$
18	Decay of X_{h2}	$k_{\mathrm{dec,X_{h2}}} \cdot X_{\mathrm{h2}}$

Inhibition factors:

$I_1 = I_{\mathrm{pH,aa}} \cdot I_{\mathrm{IN,lim}} \cdot I_{\mathrm{IP,lim}}$

$I_2 = I_{\mathrm{pH,aa}} \cdot I_{\mathrm{IN,lim}} \cdot I_{\mathrm{h2,fa}} \cdot I_{\mathrm{IP,lim}}$

$I_3 = I_{\mathrm{pH,aa}} \cdot I_{\mathrm{IN,lim}} \cdot I_{\mathrm{h2,c4}} \cdot I_{\mathrm{IP,lim}}$

$I_4 = I_{\mathrm{pH,aa}} \cdot I_{\mathrm{IN,lim}} \cdot I_{\mathrm{h2,pro}} \cdot I_{\mathrm{IP,lim}}$

$I_5 = I_{\mathrm{pH,ac}} \cdot I_{\mathrm{IN,lim}} \cdot I_{\mathrm{NH3,Xac}} \cdot I_{\mathrm{IP,lim}}$

$I_6 = I_{\mathrm{pH,h2}} \cdot I_{\mathrm{IN,lim}} \cdot I_{\mathrm{IP,lim}}$

where:

$$I_{h2s,ac} = \frac{1}{1 + \frac{Z_{h2s}}{K_{I,h2s,ac}}}$$

$$I_{h2s,c4} = \frac{1}{1 + \frac{Z_{h2s}}{K_{I,h2s,c4}}}$$

$$I_{h2s,h2} = \frac{1}{1 + \frac{Z_{h2s}}{K_{I,h2s,h2}}}$$

$$I_{h2s,pro} = \frac{1}{1 + \frac{Z_{h2s}}{K_{I,h2s,pro}}}$$

$$I_{IP,lim} = \frac{1}{1 + \frac{K_{S,IP}}{S_{IP}}}$$

Table 1.3 Additional parameter values for the modified ADM. The other parameters (values and definition) can be found in Batstone *et al.* (2002)

	Symbol	Description	Value	Units	Reference
1	$f_{ch,xb}$	fraction of carbohydrates from biomass	0.275	-	assumed in this study
2	$f_{li,xb}$	fraction of lipids from biomass	0.350	-	assumed in this study
3	$f_{pr,xb}$	fraction of proteins from biomass	0.275	-	assumed in this study
4	$f_{sI,xb}$	fraction of soluble inerts from biomass	0.0	-	assumed in this study
5	$f_{xI,xb}$	fraction of particulate inerts from biomass	0.1	-	assumed in this study
6	$K_{I,h2s,ac}$	50% inhibitory concentration of H_2S on acetogens	$460 \cdot 10^{-3}$	kg COD.m^{-3}	Fedorovich *et al.* (2003)
7	$K_{I,h2s,c4}$	50% inhibitory concentration of H_2S on c4 degraders	$481 \cdot 10^{-3}$	kg COD.m^{-3}	Fedorovich *et al.* (2003)
8	$K_{I,h2s,h2}$	50% inhibitory concentration of H_2S on hydrogenotrophic methanogens	$400 \cdot 10^{-3}$	kg COD.m^{-3}	Fedorovich *et al.* (2003)
9	$K_{I,h2s,pro}$	50% inhibitory concentration of propionate degraders	$481 \cdot 10^{-3}$	kg COD.m^{-3}	Fedorovich *et al.* (2003)
10	$K_{S,IP}$	P limitation for inorganic phosphorus	$2 \cdot 10^{-5}$	kmol P.m^{-3}	assumed in this study

Table 2.1 Biochemical rate coefficients ($\nu_{i,j}$) for the **new P model extension** components

Component →	**i**	**4**	**5**	**6**	**7**	**13**	**14**	**15**	**16**	**24**	**25**	**26**	**27**	**28**	**29**
j	**Process ↓**	S_{va}	S_{bu}	S_{pro}	S_{ac}	S_I	X_{ch}	X_{pr}	X_{li}	X_I	X_{PHA}	X_{PP}	X_{PAO}	S_K	S_{Mg}
19	Storage of S_{va} in X_{PHA}	-1									1	$-Y_{PO4}$		$Y_{PO4} \cdot K_{XPP}$	$Y_{PO4} \cdot Mg_{XPP}$
20	Storage of S_{bu} in X_{PHA}		-1								1	$-Y_{PO4}$		$Y_{PO4} \cdot K_{XPP}$	$Y_{PO4} \cdot Mg_{XPP}$
21	Storage of S_{pro} in X_{PHA}			-1							1	$-Y_{PO4}$		$Y_{PO4} \cdot K_{XPP}$	$Y_{PO4} \cdot Mg_{XPP}$
22	Storage of S_{ac} in X_{PHA}				-1						1	$-Y_{PO4}$		$Y_{PO4} \cdot K_{XPP}$	$Y_{PO4} \cdot Mg_{XPP}$
23	Lysis of X_{PAO}					$f_{sI,xb}$	$f_{ch,xb}$	$f_{pr,xb}$	$f_{li,xb}$	$f_{xI,xb}$			-1		
24	Lysis of X_{PP}											-1		K_{XPP}	Mg_{XPP}
25	Lysis of X_{PHA}	$f_{va,PHA}$	$f_{bu,PHA}$	$f_{pro,PHA}$	$f_{ac,PHA}$						-1				
		Total valerate (kg COD·m^{-3})	Total butyrate (kg COD·m^{-3})	Total propionate (kg COD·m^{-3})	Total acetate (kg COD·m^{-3})	Soluble inerts (kg COD·m^{-3})	Carbohydrates (kg COD·m^{-3})	Proteins (kg COD·m^{-3})	Lipids (kg COD·m^{-3})	Particulate inerts (kg COD·m^{-3})	Polyhydroxyalkanoates (kg COD·m^{-3})	Polyphosphates (kmol P·m^{-3})	Phosphorus accumulating organisms (kg COD·m^{-3})	Potassium (kmol K·m^{-3})	Magnesium (kmol Mg·m^{-3})

Table 2.2 Process kinetic rate equations (ρ_j) for the **new P extension** to the biological reaction model

	Process	Kinetic rate expressions (ρ_j, kg.m^{-3}.d^{-1} // kmol.m^{-3}.d^{-1})
19	Storage of S_{va} in X_{PHA}	$q_{PHA} \cdot \frac{S_{va}}{K_A + S_{va}} \cdot \frac{\frac{X_{PP}}{X_{PAO}}}{K_{PP} + \frac{X_{PP}}{X_{PAO}}} \cdot X_{PAO} \cdot \frac{S_{va}}{S_{va} + S_{bu} + S_{pro} + S_{ac}}$
20	Storage of S_{bu} in X_{PHA}	$q_{PHA} \cdot \frac{S_{bu}}{K_A + S_{bu}} \cdot \frac{\frac{X_{PP}}{X_{PAO}}}{K_{PP} + \frac{X_{PP}}{X_{PAO}}} \cdot X_{PAO} \cdot \frac{S_{bu}}{S_{va} + S_{bu} + S_{pro} + S_{ac}}$
21	Storage of S_{pro} in X_{PHA}	$q_{PHA} \cdot \frac{S_{pro}}{K_A + S_{pro}} \cdot \frac{\frac{X_{PP}}{X_{PAO}}}{K_{PP} + \frac{X_{PP}}{X_{PAO}}} \cdot X_{PAO} \cdot \frac{S_{pro}}{S_{va} + S_{bu} + S_{pro} + S_{ac}}$
22	Storage of S_{ac} in X_{PHA}	$q_{PHA} \cdot \frac{S_{ac}}{K_A + S_{ac}} \cdot \frac{\frac{X_{PP}}{X_{PAO}}}{K_{PP} + \frac{X_{PP}}{X_{PAO}}} \cdot X_{PAO} \cdot \frac{S_{ac}}{S_{va} + S_{bu} + S_{pro} + S_{ac}}$
23	Lysis of X_{PAO}	$b_{PAO} \cdot X_{PAO}$
24	Lysis of X_{PP}	$b_{PP} \cdot X_{PP}$
25	Lysis of X_{PHA}	$b_{PHA} \cdot X_{PHA}$

Table 2.3 Parameter values for the **new P model extension**

	Symbol	Description	Value	Units	Reference
1	b_{PAO}	lysis rate of PAOs	0.20	d^{-1}	Henze *et al.* (2000)
2	b_{PHA}	lysis rate of PHAs	0.20	d^{-1}	Henze *et al.* (2000)
3	b_{PP}	lysis rate of polyphosphates	0.20	d^{-1}	Henze *et al.* (2000)
4	$f_{ac,PHA}$	yield of acetate on PHA	0.40	kg COD.kg COD^{-1}	Henze *et al.* (2000)
5	$f_{bu,PHA}$	yield of butyrate on PHA	0.10	kg COD.kg COD^{-1}	assumed in this study
6	$f_{pro,PHA}$	yield of propionate on PHA	0.40	kg COD.kg COD^{-1}	assumed in this study
7	$f_{va,PHA}$	yield of valerate on PHA	0.10	kg COD.kg COD^{-1}	assumed in this study
8	K_A	saturation coefficient for acetate	$4 \cdot 10^{-3}$	kg COD^{-1}.m^{-3}	Henze *et al.* (2000)
9	K_{PP}	saturation coefficient for polyphosphate	$0.32 \cdot 10^{-3}$	kg COD^{-1}.m^{-3}	Henze *et al.* (2000)
10	q_{PHA}	rate constant for storage of PHA	3.0	kg COD.kg COD^{-1}.d^{-1}	Henze *et al.* (2000)
11	Y_{PO4}	yield of biomass on phosphate	$13 \cdot 10^{-3}$	kmol P.kg COD^{-1}	Henze *et al.* (2000)

Table 3.1 Biochemical rate coefficients ($\nu_{i,j}$) for the **new S model extension** components

Component → i		4	5	6	7	8	13	14	15	16	24	30	31	32	33	34	35
j	**Process ↓**	S_{va}	S_{bu}	S_{pro}	S_{ac}	S_{h2}	S_I	X_{ch}	X_{pr}	X_{li}	X_i	S_{SO4}	S_{IS}	X_{hSRB}	X_{aSRB}	X_{pSRB}	X_{c4SRB}
26	Growth of X_{hSRB} on S_{h2}					-1						$-\frac{(1-Y_{hSRB})}{64}$	$(1-Y_{hSRB})$	Y_{hSRB}			
27	Decay of X_{hSRB}						$f_{sI,xb}$	$f_{ch,xb}$	$f_{pr,xb}$	$f_{li,xb}$	$f_{xI,xb}$			-1			
28	Growth of X_{aSRB} on S_{ac}				-1							$-\frac{(1-Y_{aSRB})}{64}$	$(1-Y_{aSRB})$		Y_{aSRB}		
29	Decay of X_{aSRB}						$f_{sI,xb}$	$f_{ch,xb}$	$f_{pr,xb}$	$f_{li,xb}$	$f_{xI,xb}$				-1		
30	Growth of X_{pSRB} on S_{pro}			-1	$0.57\,(1-Y_{pSRB})$							$-\frac{0.43\,(1-Y_{pSRB})}{64}$	$0.43\,(1-Y_{pSRB})$			Y_{pSRB}	
31	Decay of X_{pSRB}						$f_{sI,xb}$	$f_{ch,xb}$	$f_{pr,xb}$	$f_{li,xb}$	$f_{xI,xb}$					-1	
32	Growth of X_{c4SRB} on S_{bu}		-1		$0.8\,(1-Y_{c4SRB})$							$-\frac{0.2\,(1-Y_{c4SRB})}{64}$	$0.2\,(1-Y_{c4SRB})$				Y_{c4SRB}
33	Growth of X_{c4SRB} on S_{va}	-1		$0.54\,(1-Y_{c4SRB})$	$0.31\,(1-Y_{c4SRB})$							$-\frac{0.15\,(1-Y_{c4SRB})}{64}$	$0.15\,(1-Y_{c4SRB})$				Y_{c4SRB}
34	Decay of X_{c4SRB}						$f_{sI,xb}$	$f_{ch,xb}$	$f_{pr,xb}$	$f_{li,xb}$	$f_{xI,xb}$						-1
		Total valerate (kg COD·m^{-3})	Total butyrate (kg COD·m^{-3})	Total propionate (kg COD·m^{-3})	Total acetate (kg COD·m^{-3})	Hydrogen (kg COD·m^{-3})	Soluble inerts (kg COD·m^{-3})	Carbohydrates (kg COD·m^{-3})	Proteins (kg COD·m^{-3})	Lipids (kg COD·m^{-3})	Particulate inerts (kg COD·m^{-3})	Sulfate (kmol S·m^{-3})	Hydrogen sulfide (kg COD·m^{-3})	H_2-degrading SRB (kg COD·m^{-3})	ac-degrading SRB (kg COD·m^{-3})	pro-degrading SRB (kg COD·m^{-3})	C4-degrading SRB (kg COD·m^{-3})

Table 3.2 Process kinetic rate equations (ρ_j) for **the new S extension** to the biological reaction model

Process		Kinetic rate expressions (ρ_j, kg COD.m^{-3}.d^{-1})
26	Growth of X_{hSRB} on S_{h2}	$k_{m,hSRB} \cdot \frac{S_{SO4}}{K_{S,SO4,hSRB} + S_{SO4}} \cdot \frac{S_{h2}}{K_{S,hSRB} + S_{h2}} \cdot X_{hSRB} \cdot I_{SRB6} \cdot I_{h2s,hSRB}$
27	Decay of X_{hSRB}	$k_{dec,X_{hSRB}} \cdot X_{hSRB}$
28	Growth of X_{aSRB} on S_{ac}	$k_{m,aSRB} \cdot \frac{S_{SO4}}{K_{S,SO4,aSRB} + S_{SO4}} \cdot \frac{S_{ac}}{K_{S,aSRB} + S_{ac}} \cdot X_{aSRB} \cdot I_{SRB5} \cdot I_{h2s,aSRB}$
29	Decay of X_{aSRB}	$k_{dec,X_{aSRB}} \cdot X_{aSRB}$
30	Growth of X_{pSRB} on S_{pro}	$k_{m,pSRB} \cdot \frac{S_{SO4}}{K_{S,SO4,pSRB} + S_{SO4}} \cdot \frac{S_{pr}}{K_{S,pSRB} + S_{pr}} \cdot X_{pSRB} \cdot I_{SRB4} \cdot I_{h2s,pSRB}$
31	Decay of X_{pSRB}	$k_{dec,X_{pSRB}} \cdot X_{pSRB}$
32	Growth of X_{c4SRB} on S_{bu}	$k_{m,c4SRB} \cdot \frac{S_{SO4}}{K_{S,SO4,c4SRB} + S_{SO4}} \cdot \frac{S_{va}}{K_{S,c4SRB} + S_{va}} \cdot \frac{S_{va}}{S_{bu} + S_{va}} \cdot X_{c4SRB} \cdot I_{SRB3} \cdot I_{h2s,c4SRB}$
33	Growth of X_{c4SRB} on S_{va}	$k_{m,c4SRB} \cdot \frac{S_{SO4}}{K_{S,SO4,c4SRB} + S_{SO4}} \cdot \frac{S_{bu}}{K_{S,c4SRB} + S_{bu}} \cdot \frac{S_{bu}}{S_{bu} + S_{va}} \cdot X_{c4SRB} \cdot I_{SRB3} \cdot I_{h2s,c4SRB}$
34	Decay of X_{c4SRB}	$k_{dec,X_{c4SRB}} \cdot X_{bSRB}$

Inhibition factors:

$I_{SRB3} = I_{pH,aa} \cdot I_{IN,lim} \cdot I_{IP,lim}$

$I_{SRB4} = I_{pH,aa} \cdot I_{IN,lim} \cdot I_{IP,lim}$

$I_{SRB5} = I_{pH,ac} \cdot I_{IN,lim} \cdot I_{IP,lim}$

$I_{SRB6} = I_{pH,h2} \cdot I_{IN,lim} \cdot I_{IP,lim}$

where:

$$I_{h2s,aSRB} = \frac{1}{1 + \frac{Z_{h2s}}{K_{I,h2s,aSRB}}}$$

$$I_{h2s,c4SRB} = \frac{1}{1 + \frac{Z_{h2s}}{K_{I,h2s,c4SRB}}}$$

$$I_{h2s,hSRB} = \frac{1}{1 + \frac{Z_{h2s}}{K_{I,h2s,hSRB}}}$$

$$I_{h2s,pSRB} = \frac{1}{1 + \frac{Z_{h2s}}{K_{I,h2s,pSRB}}}$$

$$I_{IP,lim} = \frac{1}{1 + \frac{K_{S,IP}}{S_{IP}}}$$

Table 3.3 Parameter values for **the new S model** extension. The other parameters (values and definition) can be found in Batstone *et al.* (2002)

	Symbol	Description	Value	Units	Reference
1	$k_{dec,X_{aSRB}}$	decay rate of aSRB	0.02	d^{-1}	Batstone *et al.* (2002)
2	$k_{dec,X_{c4SRB}}$	decay rate of c4SRB	0.02	d^{-1}	Batstone *et al.* (2002)
3	$k_{dec,X_{hSRB}}$	decay rate of hSRB	0.02	d^{-1}	Batstone *et al.* (2002)
4	$k_{dec,X_{pSRB}}$	decay rate of pSRB	0.02	d^{-1}	Batstone *et al.* (2002)
5	$K_{I,h2s,aSRB}$	50% inhibitory concentration of H_2S on aSRB	$499 \cdot 10^{-3}$	kg COD.m^{-3}	Fedorovich *et al.* (2003)
6	$K_{I,h2s,c4SRB}$	50% inhibitory concentration of H_2S on c4SRB	$520 \cdot 10^{-3}$	kg COD.m^{-3}	Fedorovich *et al.* (2003)
7	$K_{I,h2s,hSRB}$	50% inhibitory concentration of H_2S on hSRB	$499 \cdot 10^{-3}$	kg COD.m^{-3}	Fedorovich *et al.* (2003)
8	$K_{I,h2s,pSRB}$	50% inhibitory concentration of H_2S on pSRB	$520 \cdot 10^{-3}$	kg COD.m^{-3}	Fedorovich *et al.* (2003)
9	$k_{m,aSRB}$	maximum specific uptake rate of aSRB	10	kg COD.kg COD^{-1}.d^{-1}	assumed in this study
10	$k_{m,c4SRB}$	maximum specific uptake rate of c4SRB	23	kg COD.kg COD^{-1}.d^{-1}	assumed in this study
11	$k_{m,hSRB}$	maximum specific uptake rate of hSRB	41.125	kg COD.kg COD^{-1}.d^{-1}	assumed in this study
12	$k_{m,pSRB}$	maximum specific uptake rate of pSRB	16.25	kg COD.kg COD^{-1}.d^{-1}	assumed in this study
13	$K_{S,SO4,aSRB}$	half saturation constant for sulfate of aSRB	0.0002	kmol.m^{-3}	Fedorovich *et al.* (2003)
14	$K_{S,SO4,c4SRB}$	half saturation constant for sulfate of c4SRB	0.0002	kmol.m^{-3}	Fedorovich *et al.* (2003)
15	$K_{S,SO4,hSRB}$	half saturation constant for sulfate of hSRB	0.000104	kmol.m^{-3}	Fedorovich *et al.* (2003)
16	$K_{S,SO4,pSRB}$	half saturation constant for sulfate of pSRB	0.0002	kmol.m^{-3}	Fedorovich *et al.* (2003)
17	$K_{S,aSRB}$	half saturation constant of aSRB	0.176	kg COD.m^{-3}	assumed in this study
18	$K_{S,c4SRB}$	half saturation constant of c4SRB	0.1739	kg COD.m^{-3}	assumed in this study
19	$K_{S,hSRB}$	half saturation constant of hSRB	$5.96 \cdot 10^{-6}$	kg COD.m^{-3}	Batstone *et al.* (2006)
20	$K_{S,pSRB}$	half saturation constant of pSRB	0.088	kg COD.m^{-3}	assumed in this study
21	Y_{aSRB}	yield of aSRB	0.05	kg COD.kg COD^{-1}	Batstone *et al.* (2002)
22	Y_{c4SRB}	yield of c4SRB	0.06	kg COD.kg COD^{-1}	Batstone *et al.* (2002)
23	Y_{hSRB}	yield of hSRB	0.05	kg COD.kg COD^{-1}	Batstone *et al.* (2002)
24	Y_{pSRB}	yield of pSRB	0.04	kg COD.kg COD^{-1}	Batstone *et al.* (2002)

Table 4.1 Biochemical rate coefficients ($\nu_{i,j}$) and process kinetic rate equation (ρ_j) for the **new Fe model extension**

Component →	i	8	31	36	37	38	Kinetic rate expressions (ρ_j, kg m^{-3} d^{-1} // kmol m^{-3} d^{-1})
j	Process ↓	S_{h2}	S_{IS}	S_{Fe3}	S_{Fe2}	S^{o}	
35	Iron (II/III) Oxidation/Reduction (H_2)	-1		$-\frac{1}{i_{Fe2}}$	$\frac{1}{i_{Fe2}}$		$\frac{K_{Fe3,Fe2} * S_{Fe3} * S_{h2}}{16}$
36	Iron (II/III) Oxidation/Reduction (S_{IS})		-1	$-\frac{2 * i_{Fe2}}{i_{SiS}} \frac{1}{i_{Fe2}}$	$\frac{2 * i_{Fe2}}{i_{SiS}}$	$\frac{i_{i_{S^0}}}{i_{SiS}}$	$\frac{K_{Fe3,Fe2} * S_{Fe3} * S_{h2}}{64}$
		Hydrogen (kg COD·m^{-3})		Iron (III) (kmol·m^{-3})	Iron (II) (kg COD·m^{-3})	Iron (II) (kg COD·m^{-3})	

Table 4.2 Parameter values for the **new Fe model extension**

	Symbol	Description	Value	Units	Reference
1	i_{Fe2}	Conversion of Fe^{2+} into COD	8.0	kg COD.$kmol^{-1}$	assumed in this study
2	i_{S^0}	Conversion of S^0 into COD	48.0	kg COD.$kmol^{-1}$	assumed in this study
3	i_{SiS}	Conversion of S_{is} into COD	64.0	kg COD.$kmol^{-1}$	assumed in this study
3	$K_{Fe3,Fe2}$	Conversion rate of Fe^{3+} to Fe^{2+}	10^9	m^3.$kmol^{-1}$.day^{-1}	assumed in this study

Table 5.1 Stoichiometric matrix for liquid-gas transfer processes. In red modifications from the original implementation

Processes		Chemical states								Rate equations
		S_{h2}	S_{ch4}	S_{IC}	S_{IS}	G_{h2}	G_{ch4}	G_{co2}	G_{h2s}	
1	H_2 stripping	-1				1				$K_La\left(S_{h_2} - 16\,K_{H,h_2}\,P_{h_{2\,(g)}}\right)$
2	CH_4 stripping		-1				1			$K_La\left(S_{ch_4} - 64\,K_{H,ch_4}\,P_{ch_{4\,(g)}}\right)$
3	CO_2 stripping			-1				1		$K_La\left(Z_{co_2} - K_{H,co_2}\,P_{co_{2\,(g)}}\right)$
4	H_2S stripping				-1				1	$K_La\left(Z_{H2S} - 64\,K_{H,h_2S}\,P_{h_2s_{(g)}}\right)$

Table 5.2 Stoichiometric matrix for **the new precipitation processes**. $k_{cryst,i}$ (h^{-1}) represent the precipitation kinetics, a_i the activities and K_i the solubility products for each compound**.**

Processes		Chemical states											Rate equations	pKa	k_{cryst}
		S_{H^+}	S_{K^+}	S_{IN}	S_{IC}	S_{IS}	S_{Ca}	S_{Fe2}	S_{Mg}	S_{IP}	S_{Al}	S_{Fe3}			
1	CCM precipitation				1		1						$k_{cryst,CCM} X_{CCM} \left[\left(\frac{a_{Ca^{2+}}\, a_{CO_3{}^{2-}}}{K_{sp,CCM}}\right)^{1/2} - 1\right]^2$	8.480	0.35
2	ACC precipitation				1		1						$k_{cryst,ACC} X_{ACC} \left[\left(\frac{a_{Ca^{2+}}\, a_{CO_3{}^{2-}}}{K_{sp,ACC}}\right)^{1/2} - 1\right]^2$	8.3	0.001
3	ACP precipitation						3			2			$k_{cryst,ACP} X_{ACP} \left[\left(\frac{(a_{Ca^{2+}})^3 (a_{PO_4{}^{3-}})^2}{K_{sp,ACP}}\right)^{1/5} - 1\right]^2$	28.92	3
4	HAP precipitation	-1					5			3			$k_{cryst,HAP} X_{HAP} \left[\left(\frac{(a_{Ca^{2+}})^5 (a_{PO_4{}^{3-}})^3 a_{OH^-}}{K_{sp,HAP}}\right)^{1/9} - 1\right]^2$	44.333	0.001
5	DCPD precipitation	1					1			1			$k_{cryst,DCPD} X_{DCPD} \left[\left(\frac{a_{H^+} a_{Ca^{2+}}\, a_{PO_4{}^{3-}}}{K_{sp,DCPD}}\right)^{1/3} - 1\right]^2$	18.995	2
6	OCP precipitation	1					4			3			$k_{cryst,OCP} X_{OCP} \left[\left(\frac{a_{H^+} (a_{Ca^{2+}})^4 (a_{PO_4{}^{3-}})^3}{K_{sp,OCP}}\right)^{1/8} - 1\right]^2$	47.08	0.76
7	Struvite precipitation			1					1	1			$k_{cryst,Struv} X_{Struv} \left[\left(\frac{a_{NH_4{}^+} a_{Mg^{2+}} a_{PO_4{}^{3-}}}{K_{sp,Struv}}\right)^{1/3} - 1\right]^3$	13.6	5
8	Newberyite precipitation	1							1	1			$k_{cryst,Newb} X_{Newb} \left[\left(\frac{a_{H^+} a_{Mg^{2+}} a_{PO_4{}^{3-}}}{K_{sp,Newb}}\right)^{1/3} - 1\right]^2$	18.175	0.001
9	Magnesite precipitation				1		1						$k_{cryst,Mgs} X_{Mgs} \left[\left(\frac{a_{Ca^{2+}}\, a_{CO_3{}^{2-}}}{K_{sp,Mgs}}\right)^{1/2} - 1\right]^2$	7.46	0.001
10	k-Struvite precipitation		1						1	1			$k_{cryst,kStruv} X_{kStruv} \left[\left(\frac{a_{K^+} a_{Mg^{2+}} a_{PO_4{}^{3-}}}{K_{sp,kStruv}}\right)^{1/3} - 1\right]^2$	11.5508	0.001
11	FeS precipitation	-1				1		1					$k_{cryst,FeS} X_{FeS} \left[\left(\frac{a_{Fe^{2+}}\, a_{S^{2-}}}{K_{sp,FeS}}\right)^{1/2} - 1\right]^2$	2.95	100
12	AlPO4 precipitation									1	1		$k_{cryst,AlPO4} X_{AlPO4} \left[\left(\frac{a_{Al^{3+}}\, a_{PO_4{}^{3-}}}{K_{sp,AlPO4}}\right)^{1/2} - 1\right]^2$	18.2	0.001

13	$Fe_3(PO4)_2$ precipitation									2		3	$k_{cryst,Fe3(PO4)2} X_{Fe3(PO4)2} \left[\left(\frac{(a_{Fe^{2+}})^3 (a_{PO_4{}^{3-}})^2}{K_{sp,Fe3(PO4)2}} \right)^{1/2} - 1 \right]^2$		37.76	0.001

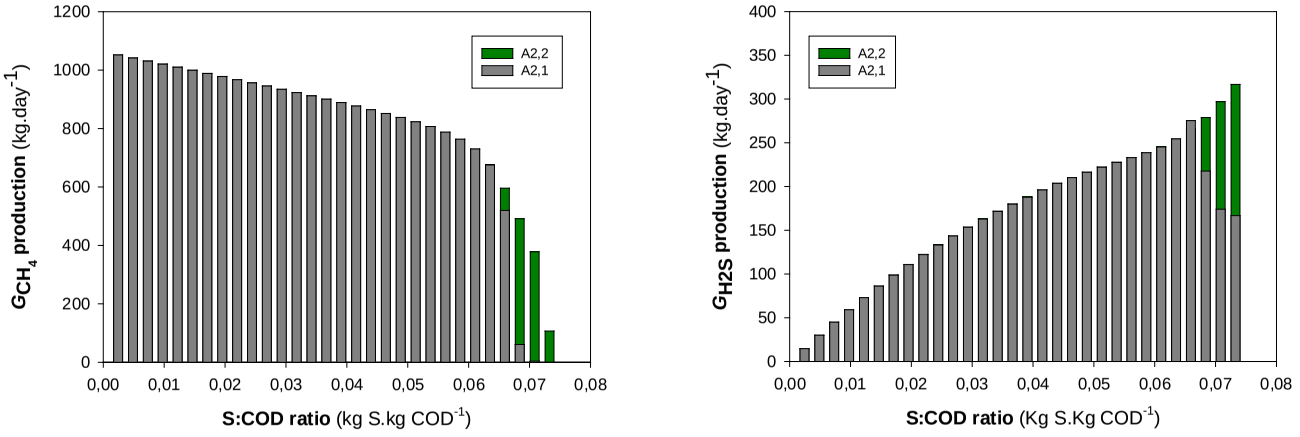

Figure 1. Effect of biochemical S transformations on biogas production: (a) methane (G_{CH_4}); and, (b) sulfide (G_{H_2S}). Discrepancies between model predictions starts at high S:COD values. Influent COD is 8,385 kg.day^{-1}.

Paper V

Water Research 113 (2017) 97–110

Contents lists available at ScienceDirect

Water Research

journal homepage: www.elsevier.com/locate/watres

Plant-wide modelling of phosphorus transformations in wastewater treatment systems: Impacts of control and operational strategies

K. Solon [a], X. Flores-Alsina [b], C. Kazadi Mbamba [c], D. Ikumi [d], E.I.P. Volcke [e], C. Vaneeckhaute [f], G. Ekama [d], P.A. Vanrolleghem [g], D.J. Batstone [c], K.V. Gernaey [b], U. Jeppsson [a, *]

[a] Division of Industrial Electrical Engineering and Automation, Department of Biomedical Engineering, Lund University, Box 118, SE-221 00, Lund, Sweden
[b] CAPEC-PROCESS Research Center, Department of Chemical and Biochemical Engineering, Technical University of Denmark, Building 229, DK-2800, Kgs. Lyngby, Denmark
[c] Advanced Water Management Centre, The University of Queensland, St Lucia, Brisbane, Queensland 4072, Australia
[d] Water Research Group, Department of Civil Engineering, University of Cape Town, Rondebosch, 7700, South Africa
[e] Department of Biosystems Engineering, Ghent University, Coupure Links 653, B-9000, Gent, Belgium
[f] BioEngine, Department of Chemical Engineering, Université Laval, Québec, QC, G1V 0A6, Canada
[g] modelEAU, Département de Génie Civil et de Génie des Eaux, Université Laval, Québec, QC, G1V 0A6, Canada

ARTICLE INFO

Article history:
Received 5 October 2016
Received in revised form
2 February 2017
Accepted 3 February 2017
Available online 6 February 2017

Keywords:
Benchmarking
Control strategies
Multiple mineral precipitation
Physico-chemical modelling
Nutrient removal
Struvite recovery

ABSTRACT

The objective of this paper is to report the effects that control/operational strategies may have on plant-wide phosphorus (P) transformations in wastewater treatment plants (WWTP). The development of a new set of biological (activated sludge, anaerobic digestion), physico-chemical (aqueous phase, precipitation, mass transfer) process models and model interfaces (between water and sludge line) were required to describe the required tri-phasic (gas, liquid, solid) compound transformations and the close interlinks between the P and the sulfur (S) and iron (Fe) cycles. A modified version of the Benchmark Simulation Model No. 2 (BSM2) (open loop) is used as test platform upon which three different operational alternatives (A_1, A_2, A_3) are evaluated. Rigorous sensor and actuator models are also included in order to reproduce realistic control actions. Model-based analysis shows that the combination of an ammonium (S_{NH_x}) and total suspended solids (X_{TSS}) control strategy (A_1) better adapts the system to influent dynamics, improves phosphate (S_{PO_4}) accumulation by phosphorus accumulating organisms (X_{PAO}) (41%), increases nitrification/denitrification efficiency (18%) and reduces aeration energy ($E_{aeration}$) (21%). The addition of iron (X_{FeCl_3}) for chemical P removal (A_2) promotes the formation of ferric oxides (X_{HFO-H}, X_{HFO-L}), phosphate adsorption ($X_{HFO-H,P}$, $X_{HFO-L,P}$), co-precipitation ($X_{HFO-H,P,old}$, $X_{HFO-L,P,old}$) and consequently reduces the P levels in the effluent (from 2.8 to 0.9 g P.m^{-3}). This also has an impact on the sludge line, with hydrogen sulfide production (G_{H_2S}) reduced (36%) due to iron sulfide (X_{FeS}) precipitation. As a consequence, there is also a slightly higher energy production ($E_{production}$) from biogas. Lastly, the inclusion of a stripping and crystallization unit (A_3) for P recovery reduces the quantity of P in the anaerobic digester supernatant returning to the water line and allows potential struvite ($X_{MgNH_4PO_4}$) recovery ranging from 69 to 227 kg.day^{-1} depending on: (1) airflow ($Q_{stripping}$); and, (2) magnesium ($Q_{Mg(OH)_2}$) addition. All the proposed alternatives are evaluated from an environmental and economical point of view using appropriate performance indices. Finally, some deficiencies and opportunities of the proposed approach when performing (plant-wide) wastewater treatment modelling/engineering projects are discussed.

© 2017 Elsevier Ltd. All rights reserved.

* Corresponding author.
E-mail address: ulf.jeppsson@iea.lth.se (U. Jeppsson).

http://dx.doi.org/10.1016/j.watres.2017.02.007
0043-1354/© 2017 Elsevier Ltd. All rights reserved.

Nomenclature

A	Alternative
AD	Anaerobic digestion
ADM1	Anaerobic Digestion Model No. 1
AER	Aerobic section
ANAER	Anaerobic section
ANOX	Anoxic section
ASM	Activated Sludge Model
ASM2d	Activated Sludge Model No. 2d
BOD	Biological oxygen demand
BSM2	Benchmark Simulation Model No. 2
CBIM	Continuity-based interfacing method
COD	Chemical oxygen demand
$CONV_{AD-AS}$	Conversion ADM1 – ASM2d interface
$CONV_{AS-AM}$	Conversion ASM2d – ADM1 interface
DO	Dissolved oxygen
EQI	Effluent quality index
Fe	Iron
GAO	Glycogen accumulating organisms
G_{CH_4}	Methane production rate (gas) (ADM1) ($kg.day^{-1}$)
G_{CO_2}	Carbon dioxide production rate (gas) (ADM1) ($kg.day^{-1}$)
G_{H2}	Hydrogen production rate (gas) (ADM1) ($kg.day^{-1}$)
G_{H_2S}	Hydrogen sulfide production rate (gas) (ADM1) ($kg.day^{-1}$)
MMP	Multiple mineral precipitation
OCI	Operational cost index
P	Phosphorus
PAO	Phosphorus accumulating organisms
PHA	Polyhydroxyalkanoates
PP	Polyphosphates
PRIM	Primary clarifier
$PROCESS_{AD-AS}$	Process ADM1– ASM2d interface
$PROCESS_{AS-AD}$	Process ASM2d – ADM1 interface
Q_{intr}	Internal recycle flow rate (between AER and ANOX) ($m^3.day^{-1}$)
S	Sulfur
SEC2	Secondary clarifier
SI	Saturation index
SRB	Sulfate-reducing bacteria
STRIP	Stripping unit
S_A	Acetate (ASM2d) (g COD.m^{-3})
S_{aa}	Amino acids (ADM1) (kg COD.m^{-3})
S_{ac}	Total acetic acid (ADM1) (kg COD.m^{-3})
S_{an}	Anions (ADM1) (kmol.m^{-3})
S_{bu}	Total butyric acid (ADM1) (kg COD.m^{-3})
S_{Ca}	Calcium (ASM2d, ADM1) (g.m^{-3}) (kmol.m^{-3})
S_{cat}	Soluble cations (ADM1) (kmol.m^{-3})
S_{Cl}	Chloride (ASM2d, ADM1) (g.m^{-3}) (kmol.m^{-3})
S_F	Fermentable substrate (ASM2d) (g COD.m^{-3})
S_{fa}	Fatty acids (ADM1) (kg COD.m^{-3})
$S_{Fe^{2+}}$	Iron (II) (ASM2d, ADM1) (g.m^{-3}) (kmol.m^{-3})
$S_{Fe^{3+}}$	Iron (III) (ASM2d, ADM1) (g.m^{-3}) (kmol.m^{-3})
S_{H_2}	Hydrogen (ADM1) (kg COD.m^{-3})
S_{IC}	Inorganic carbon (ADM1) (kmol.m^{-3})
S_{IN}	Inorganic nitrogen (ADM1) (kmol.m^{-3})
S_{IP}	Inorganic phosphorus (ADM1) (kmol.m^{-3})
S_{IS}	Inorganic total sulfides (ADM1) (kg COD.m^{-3})
S_K	Potassium (ASM2d, ADM1) (g.m^{-3}) (kmol.m^{-3})
S_{Mg}	Magnesium (ASM2d, ADM1) (g.m^{-3}) (kmol.m^{-3})
S_{Na}	Sodium (ASM2d, ADM1) (g.m^{-3}) (kmol.m^{-3})
S_{NH_x}	Ammonium plus ammonia nitrogen (ASM2d) (g.m^{-3})
S_{NO_x}	Nitrate plus nitrite (ASM2d) (g.m^{-3})
S_{pro}	Total propionic acid (ADM1) (kg COD.m^{-3})
S_{PO_4}	Phosphate (ASM2d) (g.m^{-3})
S_{su}	Sugars (ADM1) (kg COD.m^{-3})
S_{S_0}	Elemental sulfur (ADM1) (kmol.m^{-3})
S_{SO_4}	Sulfate (ASM2d, ADM1) (g.m^{-3}) (kmol.m^{-3})
S_{va}	Total valeric acid (ADM1) (kg COD.m^{-3})
THK/FLOT	Thickener/flotation
TIV	Time in violation
TKN	Total Kjeldahl nitrogen
TN	Total nitrogen
TP	Total phosphorus
TSS	Total suspended solids
VFA	Volatile fatty acids
WRRF	Water resource recovery facility
WWTP	Wastewater treatment plant
X_A	Autotrophic biomass (ASM2d) (g COD.m^{-3})
X_{ac}	Acetate degraders (ADM1) (kg COD.m^{-3})
X_{AlPO_4}	Aluminum phosphate (ASM2d, ADM1) (g.m^{-3}) (kmol.m^{-3})
X_B	Total biomass (ADM1) (kg COD.m^{-3})
X_c	Composite material (ADM1) (kg COD.m^{-3})
X_{C4}	Butyrate and valerate degraders (ADM1) (kg COD.m^{-3})
X_{CaCO_3}	Calcite (ASM2d, ADM1) (g.m^{-3}) (kmol.m^{-3})
$X_{CaCO_{3a}}$	Aragonite (ASM2d, ADM1) (g.m^{-3}) (kmol.m^{-3})
$X_{Ca_3(PO_4)_2}$	Amorphous calcium phosphate (ASM2d, ADM1) (g.m^{-3}) (kmol.m^{-3})
$X_{Ca_5(PO_4)_3(OH)}$	Hydroxylapatite (ASM2d, ADM1) (g.m^{-3}) (kmol.m^{-3})
$X_{Ca_8H_2(PO_4)_6}$	Octacalcium phosphate (ASM2d, ADM1) (g.m^{-3}) (kmol.m^{-3})
X_{ch}	Carbohydrates (ADM1) (kg COD.m^{-3})
X_{FeS}	Iron sulfide (ASM2d, ADM1) (mol.L^{-1}) (kmol.m^{-3})
X_H	Heterotrophic biomass (ASM2d) (g COD.m^{-3})
X_{HFO-H}	Hydrous ferric oxide with high number of active sites (ASM2d, ADM1) (g.m^{-3}) (kmol.m^{-3})
$X_{HFO-H,P}$	X_{HFO-H} with bounded adsorption sites (ASM2d, ADM1) (g.m^{-3}) (kmol.m^{-3})
$X_{HFO-H,P,old}$	Old $X_{HFO-H,P}$ with bounded adsorption sites (ASM2d, ADM1) (g.m^{-3}) (kmol.m^{-3})
X_{HFO-L}	Hydrous ferric oxide with low number of active sites (ASM2d, ADM1) (g.m^{-3}) (kmol.m^{-3})
$X_{HFO-L,P}$	X_{HFO-L} with bounded adsorption sites (ASM2d, ADM1) (g.m^{-3}) (kmol.m^{-3})
$X_{HFO-L,P,old}$	Old $X_{HFO-L,P}$ with bounded adsorption sites (ASM2d, ADM1) (g.m^{-3}) (kmol.m^{-3})
$X_{HFO-old}$	Inactive X_{HFO} (ASM2d, ADM1) (g.m^{-3}) (kmol.m^{-3})
X_i	Inert particulate organics (ASM2d, ADM1) (g COD.m^{-3}) (kg COD.m^{-3})
$X_{KNH_4PO_4}$	K-struvite (ASM2d, ADM1) (g.m^{-3}) (kmol.m^{-3})
X_{li}	Lipids (ADM1) (kg COD.m^{-3}) (g.m^{-3}) (kmol.m^{-3})
X_{MgCO_3}	Magnesite (ASM2d, ADM1) (g.m^{-3}) (kmol.m^{-3})
X_{MgHPO_4}	Newberyite (ASM2d, ADM1) (g.m^{-3}) (kmol.m^{-3})
$X_{MgNH_4PO_4}$	Struvite (ASM2d, ADM1) (g.m^{-3}) (kmol.m^{-3})
X_{PAO}	Phosphorus accumulating organisms (ASM2d, ADM1) (g COD.m^{-3}) (kg COD.m^{-3})
X_{PHA}	Polyhydroxyalkanoates (ASM2d, ADM1) (g COD.m^{-3}) (kg COD.m^{-3})
X_{PP}	Polyphosphates (ASM2, ADM1) (g.m^{-3}) (kmol.m^{-3})
X_{pr}	Proteins (ADM1) (kg COD.m^{-3})
X_{pro}	Propionate degraders (ADM1) (kg COD.m^{-3})
X_{SRB}	Sulfate-reducing bacteria (ADM1) (kg COD.m^{-3})
Z_i	Chemical species concentration of species i (algebraic variable of the physico-chemistry module) (kmol.m^{-3})

1. Introduction

The importance of plant-wide modelling has been emphasized by the chemical engineering community for a long time and the wastewater industry is also realizing the benefits of this approach (Skogestad, 2000; Gernaey et al., 2014). A wastewater treatment plant should be considered as an integrated process, where primary/secondary clarifiers, activated sludge reactors, anaerobic digesters, thickener/flotation units, dewatering systems, storage tanks, etc. are linked together and need to be operated and controlled not as individual unit operations, but taking into account all the interactions amongst the processes (Jeppsson et al., 2013). For this reason, during the last years wastewater engineering has promoted the development of integrated modelling tools handling these issues (Barker and Dold, 1997; Grau et al., 2007; Ekama, 2009; Nopens et al., 2010; Gernaey et al., 2014). Plant-wide models substantially increase the number of potential operational strategies that can be simulated, and thereby enable the study of a new dimension of control possibilities, such as studying the impact of activated sludge control strategies on the sludge line (Jeppsson et al., 2007), the effect of primary sedimentation on biogas production (Flores-Alsina et al., 2014a) and the handling of nitrogen-rich anaerobic digester supernatant (Volcke et al., 2006a; Ruano et al., 2011; Flores-Alsina et al., 2014a).

Although being valuable tools, the state of the art is that these plant-wide models are limited to the prediction of plant-wide organic carbon and nitrogen, and they are not properly taking into account the transformation of phosphorus (P) and its close interlinks with the sulfur (S) and iron cycles (Fe), particularly in a plant-wide context (Batstone et al., 2015). Phosphorus modelling is an essential requirement, particularly considering its role in eutrophication of many catchments and its potential re-use as a fertilizer (Verstraete et al., 2009). Therefore, this is an important issue for future model application and it will become of paramount importance during the transition of wastewater treatment plants (WWTP) to water resource recovery facilities (WRRFs), which will change the requirements for model-based analysis significantly for wastewater engineering studies (Vanrolleghem et al., 2014; Vanrolleghem and Vaneeckhaute, 2014).

The Activated Sludge Model No. 2d (ASM2d) specifically considers the role of phosphorus accumulating organisms (PAO) in the water line (Henze et al., 2000). Similar P-related processes should be included in the Anaerobic Digestion Model No. 1 (ADM1) (Batstone et al., 2002) as stated by Ikumi and co-workers (Ikumi et al., 2011, 2014). Potential uptake of organics by PAO to form polyhydroxyalkanoates (PHA) with the subsequent release of polyphosphates (PP) can also have an important effect on the anaerobic digestion (AD) products (biogas, precipitates) (Wang et al., 2016; Flores-Alsina et al., 2016). Nevertheless the ASM family (specifically the ASM2d for phosphorus) (Henze et al., 2000) and ADM1 (Batstone et al., 2002) are inadequate to describe plant-wide P transformations. Part of this is because the physico-chemical formulations in those models do not consider more complex phenomena in which P is involved. Indeed, P trivalence gives a strong non-ideal behaviour, which requires amongst other factors, continuous ionic strength tracking, extensive consideration of activities instead of molar concentrations and inclusion of complexation/ion pairing processes (Musvoto et al., 2000; Serralta et al., 2004; Solon et al., 2015; Flores-Alsina et al., 2015; Lizarralde et al., 2015). The latter is crucial to correctly describe chemical precipitation and predict the fate of phosphorus compounds, and to properly predict nutrient cycling through the entire plant (van Rensburg et al., 2003; Barat et al., 2011; Hauduc et al., 2015; Kazadi Mbamba et al., 2015a,b). There is also a general lack of consideration of biological and chemical transformation of Fe and S, throughout both aerobic and anaerobic stages. Specifically, the sulfur cycle regulates Fe availability (and Fe changes valency through oxidation/reduction) which then controls iron-phosphate complexing (Gutierrez *et al.*, 2010; Flores-Alsina et al., 2016). While biological and chemical complexation reactions of P have been described in the AD unit, these have not generally been considered in plant-wide interactions with the Fe/S cycles.

Model interfacing is also an important aspect to consider (Batstone et al., 2015) unless integrated plant-wide models with a single set of state variables are used (Barker and Dold, 1997; Grau et al., 2007; Ekama et al., 2006; Barat et al., 2013). Plant-wide modelling requires elemental mass balance verification (Hauduc et al., 2010) and continuity checking for all the components included in the model (Volcke et al., 2006b; Zaher et al., 2007; Nopens et al., 2009). Therefore, the quantities of C, N, P, Fe and S should be the same before and after an interface (Flores-Alsina et al., 2016). The main advantage of using an interface-based approach with respect to other integrated methodologies is that the original model structure can be used, and there is thus no need for state variable representation in all process units with the resulting increased use of computational power, model complexity and adverse model stability characteristics (Grau et al., 2009).

The main objective of this paper is to present (for the first time): (1) an approach for mechanistic description of all the main biological and physico-chemical processes required to predict organic P fluxes simultaneously in both water and sludge lines in the WWTP under different operational modes; (2) an analysis of the interactions between P, S and Fe on a plant-wide level; (3) a quantification of the compound fluxes and pH variations in each unit and through the entire plant; and, (4) an evaluation of the different operational/control strategies aimed at maximizing energy production, resource recovery and reduction of the environmental impact and operating expenses measured as effluent quality (*EQI*) and operational cost indices (*OCI*) (Copp, 2002; Nopens et al., 2010). The paper details the development of the new plant-wide model by presenting sequentially the different included sub-elements as well as the integration/interfacing aspects. The capabilities/potential of the proposed approach is illustrated with several case studies. Lastly, opportunities and limitations that arise from utilization of the new model are discussed as well.

2. Model description

2.1. Biological models

Sections 2.1.1 and 2.1.2 describe the additional processes and state variables included in the ADM1 and ASM2d, respectively, in order to take into account biologically mediated phosphorus transformations correctly. Additional modifications, with special emphasis to link the ADM and ASM with a physico-chemical model, are described in Section 3 (Model integration). Model details, mass balances and continuity verification can be found in the spreadsheet files provided within the Supplemental Information Section.

2.1.1. Anaerobic digestion model (ADM)

The ADM1 version, implemented in the plant-wide context provided by the Benchmark Simulation Model No. 2 (BSM2) (Batstone et al., 2002; Rosen et al., 2006) is extended with P, S and Fe interactions (Flores-Alsina et al., 2016). Phosphorus transformations account for kinetic decay of polyphosphates (X_{PP}) and potential uptake of volatile fatty acids (VFA) to produce polyhydroxyalkanoates (X_{PHA}) by phosphorus accumulating organisms (X_{PAO}) (Henze et al., 2000; Harding et al., 2011; Ikumi et al., 2011; Wang et al., 2016). Biological production of sulfides (S_{IS}) is

described by means of sulfate-reducing bacteria (X_{SRB}) utilising hydrogen (autolithotrophically) as electron source (Batstone, 2006). Potential hydrogen sulfide (Z_{H_2S}) inhibition and stripping to the gas phase (G_{H_2S}) are considered (Fedorovich et al., 2003; Pokorna-Krayzelova et al., 2017). Finally, chemical iron (III) ($S_{Fe^{3+}}$) reduction to iron (II) ($S_{Fe^{2+}}$) is accounted for by using hydrogen (S_{H_2}) and sulfides (S_{IS}) as electron donors (Stumm and Morgan, 1996).

2.1.2. Activated sludge model (ASM)

A modified version of the Activated Sludge Model No. 2d (ASM2d) is selected to describe organic carbon, nitrogen and phosphorus transformations in the biological reactor (Henze et al., 2000). In this implementation, biomass decay rates are electron-acceptor dependent (Siegrist et al., 1999; Gernaey and Jørgensen, 2004). Potassium (S_K) and magnesium (S_{Mg}) are accounted for as new state variables and are included in the stoichiometry of formation and release of polyphosphates (X_{PP}). Another modification with respect to the original ASM2d is that total suspended solids is calculated from its constituents ($X_{TSS} = X_{VSS} + X_{ISS}$ are described separately) (Ekama and Wentzel, 2004; Ekama et al., 2006) compared to the previous implementations wherein TSS is calculated as the sum of the assumed TSS content of each of the particulate state variables. This is mainly because the constituents of the inorganic suspended solids (X_{ISS}) are explicitly calculated as state variables with a contribution from polyphosphate (X_{PP}) in the activated sludge system. The model is also upgraded to describe the fate (oxidation/reduction reactions) of sulfur ($S_{SO_4^{2-}}$, S_{S_0}, S_{IS}) and iron ($S_{Fe^{3+}}$, $S_{Fe^{2+}}$) compounds in anaerobic, anoxic and aerobic conditions. Sulfate reduction is assumed to be biologically mediated by means of SRB (X_{SRB}) using two potential electron donors (S_A, S_F). Sulfide (S_{IS}) and ($S_{Fe^{2+}}$) oxidation is described as a purely chemical reaction using different electron acceptors (S_{O_2}, S_{NO_x}) (Batstone, 2006; Batstone et al., 2015; Gutierrez et al., 2010; Stumm and Morgan, 1996).

2.2. Physico-chemical models (PCM)

2.2.1. pH and ion speciation/pairing

In this study a general aqueous phase chemistry model describing pH variation and ion speciation/pairing in both ASM and ADM is used (Solon et al., 2015; Flores-Alsina et al., 2015). The model corrects for ionic strength via the Davies' approach to consider chemical activities instead of molar concentrations, performing all the calculations under non-ideal conditions. The general acid-base equilibria are formulated as a set of implicit algebraic equations (IAEs) and solved separately at each time step of the ordinary differential equation (ODE) solver using an extended multi-dimensional Newton-Raphson algorithm (Solon et al., 2015; Flores-Alsina et al., 2015). Acid-base parameters and activity coefficients are corrected for temperature effects. The species concentrations are expressed by a common nomenclature (Z_i) (Solon et al., 2015) and participate in physico-chemical processes such as gas exchange and mineral precipitation (see Sections 2.2.2 and 2.2.3).

2.2.2. Multiple mineral precipitation (MMP)

In this model, precipitation equations are described as a reversible process using the saturation index (*SI*) as the chemical driving force. The *SI* represents the logarithm of the ratio between the product of the respective activities of reactants that are each raised to the power of their respective stoichiometric coefficient, and the solubility product constant (K_{sp}) (temperature corrected). If $SI < 0$ the liquid phase is assumed to be undersaturated and a mineral might dissolve into the liquid phase, while if $SI > 0$ the liquid phase is assumed to be supersaturated and mineral precipitation might occur (Stumm and Morgan, 1996). The precipitation reaction rate depends on the kinetic rate coefficient, the concentration of the different species (Z_i), mineral solid phase (X_i) and the order of the reaction (n) (Kazadi Mbamba et al., 2015a,b). The proposed MMP model includes the minerals: calcite (X_{CaCO_3}), aragonite ($X_{CaCO_{3a}}$), amorphous calcium phosphate ($X_{Ca_3(PO_4)_2}$), hydroxylapatite ($X_{Ca_5(PO_4)_3(OH)}$), octacalcium phosphate ($X_{Ca_8H_2(PO_4)_6}$), struvite ($X_{MgNH_4PO_4}$), newberyite (X_{MgHPO_4}), magnesite (X_{MgCO_3}), k-struvite ($X_{KNH_4PO_4}$) and iron sulfide (X_{FeS}). A special formulation is necessary to correctly describe precipitation of hydrous ferric oxides (X_{HFO-H}, X_{HFO-L}), phosphate adsorption ($X_{HFO-H,P}$, $X_{HFO-L,P}$) and co-precipitation ($X_{HFO-H,P,old}$, $X_{HFO-L,P,old}$) (Hauduc et al., 2015), since this is an adsorption rather than a precipitation reaction. Kinetic parameters were taken from Kazadi Mbamba et al. (2015a,b) and Hauduc et al. (2015).

2.2.3. Gas-liquid transfer

In open reactors, gas-liquid transfer is described as a function of the difference between the saturation concentration and the actual concentration of the gas dissolved in the liquid and the contact area between the gaseous and the aqueous phase (Truskey et al., 2009). The saturation concentration of the gas in the liquid is given by Henry's law of dissolution, which states that the saturation concentration is equal to the product of Henry's constant (K_H) multiplied by the partial pressure of the gas (P_i). The mass transfer rate constant ($K_L a_i$) is calculated for each gaseous component ($i = Z_{CO_2}$, Z_{H_2S}, Z_{NH_3} and S_{N_2}). This $K_L a_i$ is calculated with a proportionality factor relative to the reference compound oxygen ($K_L a_{O2}$). The proportionality factor depends on the relation between the diffusivity of the gas in the liquid (D_i) over the diffusivity of oxygen in the liquid (D_{O_2}) (Musvoto et al., 2000). This does not apply for $K_L a_{NH3}$ since NH_3 is a highly soluble gas and thus its mass transfer is controlled by the transfer rate in the gas phase (Lizarralde et al., 2015). In closed reactors, mass transfer between the liquid and the gas volume is described for selected gases ($i = Z_{CO_2}$, Z_{H_2S}, Z_{NH_3}, S_{CH_4} and S_{H_2}) as described in Rosen et al. (2006).

2.3. Model integration

2.3.1. ASM-PCM interface

The default implementation of the ASM was adjusted in order to include the PCM (additional details can be found in Flores-Alsina et al. (2015)). The main modifications are: (1) the use of inorganic carbon (S_{IC}) instead of alkalinity (S_{ALK}) as a state variable; (2) the inclusion of mass transfer equations for Z_{CO_2}, Z_{H_2S}, Z_{NH_3} and S_{N_2} (Batstone et al., 2015; Lizarralde et al., 2015); (3) additional (and explicit) consideration of multiple cations (S_{cat}: S_K, S_{Na}, S_{Ca}, S_{Mg}) and anions (S_{an}: S_{Cl}) which are tracked as soluble/reactive states; and, (4) chemical precipitation using metal hydroxides (X_{MeOH}) and metal phosphates (X_{MeP}) are omitted since the generalised kinetic precipitation model as described in Kazadi Mbamba et al. (2015a,b) and Hauduc et al. (2015) is used instead. Communication between the different models is straightforward. The outputs of the ASM at each integration step are used as inputs for the aqueous-phase module to estimate pH and ion speciation/pairing (works as a sub-routine) (see Section 2.2.1). The precipitation/stripping equations are formulated as ODEs and included in the overall mass balance.

2.3.2. ADM-PCM interface

The ADM is slightly modified to account for the updated physico-chemical model and new processes. The original pH solver proposed by Rosen et al. (2006) is substituted by the approach presented in Solon et al. (2015) and Flores-Alsina et al. (2015). C, N,

P, O and H fractions are taken from de Gracia et al. (2006). Finally, the original ADM1 pools of undefined cations (S_{cat}) and anions (S_{an}) are substituted for specific compounds (see Section 2.3.1). The existing gas-liquid transfer equations are extended to include Z_{H_2S} and Z_{NH_3} (Rosen et al., 2006). Similarly as for the ASM-PCM interface, the pH and ion speciation/pairing model works as a subroutine, while the multiple precipitation/stripping models are included within the system of ODEs in the ADM.

2.3.3. ASM-ADM-ASM interface

The interfaces between ASM-ADM-ASM are based on the continuity-based interfacing method (CBIM) described in Volcke et al. (2006b), Zaher et al. (2007) and Nopens et al. (2009) to ensure elemental mass and charge conservation. The ASM-ADM-ASM interfaces consider: (1) (instantaneous) processes ($PROCESS_{AS\text{-}AD}$/$PROCESS_{AD\text{-}AS}$); and, (2) (state variable) conversions ($CONV_{AS\text{-}AD}$/$CONV_{AD\text{-}AS}$). On the one hand, the ASM-ADM interface instantaneous processes ($PROCESS_{AS\text{-}AD}$) involve (amongst others) instantaneous removal of COD demanding compounds (i.e. S_{O_2} and S_{NO_3}) and immediate decay of (heterotrophic/autotrophic) biomass. Conversions ($CONV_{AS\text{-}AD}$) require the transformation of soluble fermentable organics (S_F), acetate (S_A) and biodegradable particulate organics (X_S) into amino acids (S_{aa})/sugars (S_{su})/fatty acids (S_{fa}) (soluble) and proteins (X_{pr})/lipids (X_{li})/carbohydrates (X_{ch}) (particulate), respectively. On the other hand, the ADM-ASM interface assumes ($PROCESS_{AD\text{-}AS}$) that all compounds that can be transferred into the gas phase (i.e. S_{H_2} and S_{CH_4}) are stripped, and also immediate decay of the AD biomass takes place. $CONV_{AD\text{-}AS}$ turns all the biodegradable organic particulates (X_{pr}, X_{li}, X_{ch}), organic solubles (S_{aa}, S_{fa}, S_{su}) and volatile fatty acids (S_{ac}, S_{pro}, S_{bu}, S_{va}) into X_S, S_F and S_A, respectively. There is no variation of Fe and S before and after the interface. A comprehensive description with detailed explanation of the involved processes, conversions and mass balance verification can be found in Flores-Alsina et al. (2016).

2.4. Additional elements

2.4.1. Influent generation/modelling principles

The model blocks for: (1) flow rate generation (FLOW); (2) chemical oxygen demand (COD), N and P generation (POLLUTANTS); (3) temperature profile generation (TEMPERATURE); and, (4) sewer network and first flush effect (TRANSPORT) defined in Gernaey et al. (2011) are used to generate the WWTP influent dynamics (12 months period of output data for the evaluation period with a 15 min sampling interval). The resulting daily average influent mass flow rates are 8386 kg COD.d^{-1}, 1014 kg N.d^{-1} and 197 kg P.d^{-1} for COD, N and P, respectively (see Fig. SS1 in Supplemental Information for the influent concentrations). The S:COD ratio is 0.003 kg S.kg COD^{-1} (note that the S influent load is set to a high value to have a noticeable effect in the AD). In addition, cation and anion profiles had to be added. The resulting pH is close to neutrality (pH ~ 7). More information about the flow rate pollution dynamics and how they are handled by the influent generator can be found in Flores-Alsina et al. (2014b), Martin and Vanrolleghem (2014) and Snip et al. (2016).

2.4.2. Ancillary processes and sensor/actuator models

Primary clarification is described according to Otterpohl and Freund (1992). The model is adjusted to reflect the experiments carried out by Wentzel et al. (2006) where biodegradable/unbiodegradable compounds show different settling velocities. The double exponential velocity function proposed by Takács et al. (1991) using a 10-layer reactive configuration (Flores-Alsina et al., 2012) is used as a fair representation of the secondary settling process and reactions occurring in the settler. Several correlations between sludge settleability parameters (such as stirred specific volume index, SSVI, and diluted sludge volume index, DSVI) and the Takács settling parameters (maximum Vesilind settling velocity, v_0, and hindered zone settling parameter, r_h) (Gernaey et al., 2014) have been used (Ekama et al., 1997). A reduction factor in the process kinetics is applied to the reactive secondary settler to obtain more realistic results (Guerrero et al., 2013). Flotation and dewatering units are described in Jeppsson et al. (2007). Biological reactions in both units are included using the simplified approach described in Gernaey et al. (2006). Stripping and crystallization units are described in Kazadi Mbamba et al. (2016). Response time, delay and white noise are included in sensor/actuator models in order to avoid creating unrealistic control applications (Rieger et al., 2003).

2.4.3. Plant layout

The presented set of models is implemented in a plant layout that consists of a primary clarifier (PRIM), an activated sludge unit (AS), a secondary settler (SEC2), a sludge thickener (THK/FLOT), an anaerobic digester (AD), a storage tank (ST) and a dewatering unit (DW). The main modification with respect to the original design (Nopens et al., 2010) relies on the activated sludge (AS) configuration. An anaerobic section (ANAER1, ANAER2) without oxygen (S_{O_2}) and nitrate (S_{NO_x}) is needed to promote anaerobic phosphorus release and to provide the phosphorus accumulating organisms (X_{PAO}) with a competitive advantage over other bacteria. Phosphorus release from the breakdown of polyphosphates (X_{PP}) provides the energy required for anaerobic uptake of polyhydroxyalkanoates (X_{PHA}). Next, PAO grow using intracellular storage products (i.e. X_{PHA}) as a substrate while taking up N and P as nutrients in the anoxic (ANOX1, ANOX2) and aerobic (AER1, AER2, AER3) reactors with oxygen (S_{O_2}) or nitrate (S_{NO_3}) (with less efficiency) as electron acceptors, respectively (see schematics in Fig. 1). It is important to highlight that this configuration does not represent an optimal design to remove P, because the biological P removal is dependent on the N removal via the nitrate concentration recycled to the anaerobic reactor via the underflow recycle (i.e. nitrates overflow may cause the anaerobic reactors to become anoxic). Nevertheless, it exemplifies the retrofit of many (C, N removal) plants adapting their plant layout to satisfy new and stricter effluent requirements (the authors do not presume that the given plant layout is the best configuration for retrofit situations; a Modified UCT or a Johannesburg configuration may be more appropriate). Additional details about the WWTP plant design and default operational conditions can be found in Gernaey et al. (2014) and in the software implementation (see Section 6).

2.4.4. Evaluation criteria

To assess the performance of combined N and P control strategies, an updated set of evaluation criteria are necessary (Jeppsson et al., 2013). The effluent quality index (*EQI*) (a weighted sum of effluent TSS, COD, BOD, TKN and nitrate) is updated to include the additional P load (organic and inorganic). Additional P upgrades have been necessary to include effluent violations (frequency and magnitude) and percentiles. The cost of additional recycles (anoxic, anaerobic), aerators (CO_2 stripping) and chemicals (in case the user wants to evaluate chemical P precipitation and recovery) are also added within the operational cost index (*OCI*). A detailed description of the additional evaluation criteria is given in the Supplemental Information Section.

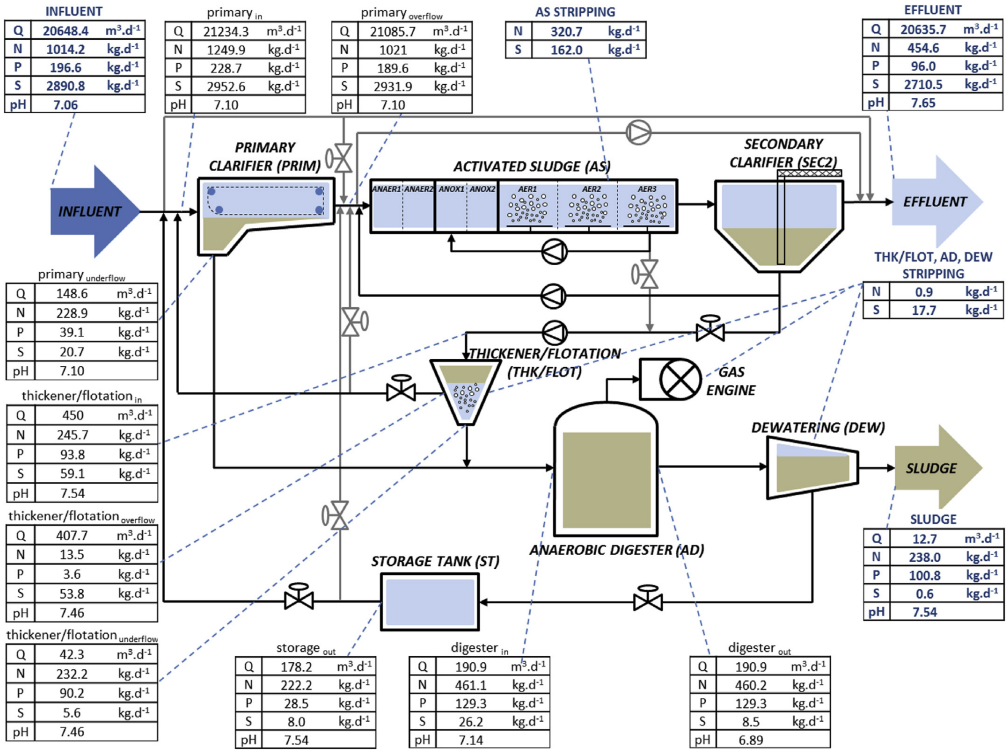

Fig. 1. Block flow diagram including overall and individual (N, P, S, pH) balances for the WWTP under study (scenario A_0).

3. Results and discussion

3.1. Steady-state simulations

The steady-state simulations for the open loop configuration are summarized in Fig. 1 in terms of the plant-wide overall mass balances and the individual ones for C, P, N, S, as well as for pH (plant-wide input and output mass flows in bold). Around 49% of the total incoming P load leaves the plant through the water line (mainly as soluble phosphate, S_{PO_4}). The remaining P (51%) goes to the sludge line (particulate). In the AD unit, soluble S_{PO_4} is substantially increased as a result of biomass (X_B, X_A, X_{PAO}) and polyphosphates (X_{PP}) decay. A fraction (78%) of the incoming P to the digester precipitates ($X_{Ca_3(PO_4)_2}$, $X_{MgNH_4PO_4}$) or becomes part of the organics (X_I, X_S). This will be disposed with the sludge. The remaining P is returned to the water line as soluble phosphate (S_{PO_4}) (22%). This increases the influent P load by almost 20% (see Fig. 1). As a consequence of this extra load the overall plant performance (in terms of phosphorus removal) for the open loop scenario is not good, giving effluent quality values (TP = 4.6 g P.m^{-3}) well above the standards (assumed TP_{limit} = 2.0 g P.m^{-3}).

Most of the nitrogen is depleted before reaching the sludge line (23% remaining) through nitrification-denitrification, assimilation with the biomass and gas stripping. More specifically, around 32% of the incoming N is converted to nitrogen gas (S_{N_2}) and 45% leaves the plant in form of S_{NH_x} or S_{NO_x}. Simulated (N) effluent values (TKN = 2.97 g N.m^{-3} and TN = 9.13 g N.m^{-3}) are well below the limits fixed by the BSM evaluation limit (TKN_{limit} = 4 g N.m^{-3} and TN_{limit} = 15 g N.m^{-3}). The N load going to the sludge line (23%) is basically associated with particulate organics (X_I, X_S) and biomass (X_B, X_A, X_{PAO}). Around 14 and 222 kg N.day^{-1} are returned to the water line after flotation/thickening and dewatering, respectively, adding 23% to the influent N load.

Sulfur arrives to the WWTP under study as sulfate (S_{SO_4}) and sulfides (S_{IS}) (S in the influent is set to a high value for demonstration purposes). In the anaerobic section of the activated sludge process there is a small reduction of S_{SO_4} to S_{IS} by SRB. In the anoxic/aerobic section most of the reduced S is re-oxidized to S_{SO_4} that becomes part of the effluent (93%), a part is stripped to the atmosphere (5%) and a small fraction of S_{SO_4} (2%) is transported to the AD unit where it is converted to hydrogen sulfide gas (G_{H_2S}) (65%) and dissolved sulfides (S_{IS}) (25%) with a concentration of 32 g S.m^{-3} (biogas composition by volume: G_{CH_4} = 62.00 %, G_{CO_2} = 37.46 %, G_{H_2S} = 0.54 %). A small fraction of sulfate remains unconverted (S_{SO_4}) (10%). The soluble S fractions are returned to the water line and are re-oxidized to sulfate in the activated sludge reactor. Compared to the N and P streams, the resulting increase in the influent S load is not very high (increase of 2%).

Table 1
Main characteristics of the implemented control/operational strategies.

Characteristics	DO controller	Ammonium controller	TSS controller	Phosphate controller	Airflow in STRIP	Magnesium controller
Measured variable(s)	S_{O_2} in AER2	S_{NH_x} in AER2	TSS in AER3	S_{PO_4} in AER3	-	-
Controlled Variable(s)	S_{O_2} in AER2	S_{O_2} in AER1, 2 & 3	TSS in AER3	S_{PO_4} in AER3	S_{CO_2} in STRIP	$X_{Mg(OH)_2}$ in STRIP
Set point/critical value	–	2 g N·m^{-3}	4000 g TSS·m^{-3} (if T < 15 °C) 3000 g TSS·m^{-3} (if T > 15 °C)	1 g P·m^{-3}	–	–
Manipulated variable	Q_{air} n AER1, 2 & 3	S_{O_2} set point in AER2	Q_w	Q_{FeCl_3}	$Q_{stripping}$	$Q_{Mg(OH)_2}$
Control algorithm	PI	Cascade PI	Cascade PI	PI	–	–
Applied in control strategies	A_1	A_1, A_2 & A_3	A_1, A_2 & A_3	A_2	A_3	A_3

Influent pH is close to neutrality (pH = 7.06). In this particular case, at the end of the water line pH is increased mainly due to carbon dioxide (Z_{CO_2}) stripping. Nevertheless, in other cases for systems with low buffer capacity, the loss of alkalinity via nitrification might decrease the pH far more strongly (Henze et al., 2008). The almost anaerobic conditions in the first units of the sludge line (secondary settler and thickener/flotation units) promote: (1) fermentation of organic soluble substrate (S_F) to acetate (S_A); and, (2) decay of X_{PP} and subsequent release of S_{IP}. As a consequence, there is a decrease of pH. In the AD, pH is slightly reduced again as a result of multiple mineral precipitation. In the dewatering unit, pH is raised again due to Z_{CO_2} stripping. There is no effect on the influent entering the primary clarifier. Similar observations about pH behaviour through the different plant units are reported in Lizarralde et al. (2015) and Kazadi Mbamba et al. (2016).

3.2. Dynamic simulations

All dynamic simulations (609 days) are preceded by steady-state simulations (300 days) but only the data generated during the final 364 days are used for plant performance evaluation. Default (open loop) operational conditions (Gernaey and Jørgensen, 2004) represent the baseline configuration (A_0) upon which the different operational/control/recovery strategies will be implemented, simulated and evaluated (see Table 1). Fig. 2 shows dynamic profiles for selected influent (Fig. 2a, b), effluent (Fig. 2d, e) and operational (Fig. 2c, f, g, h) variables.

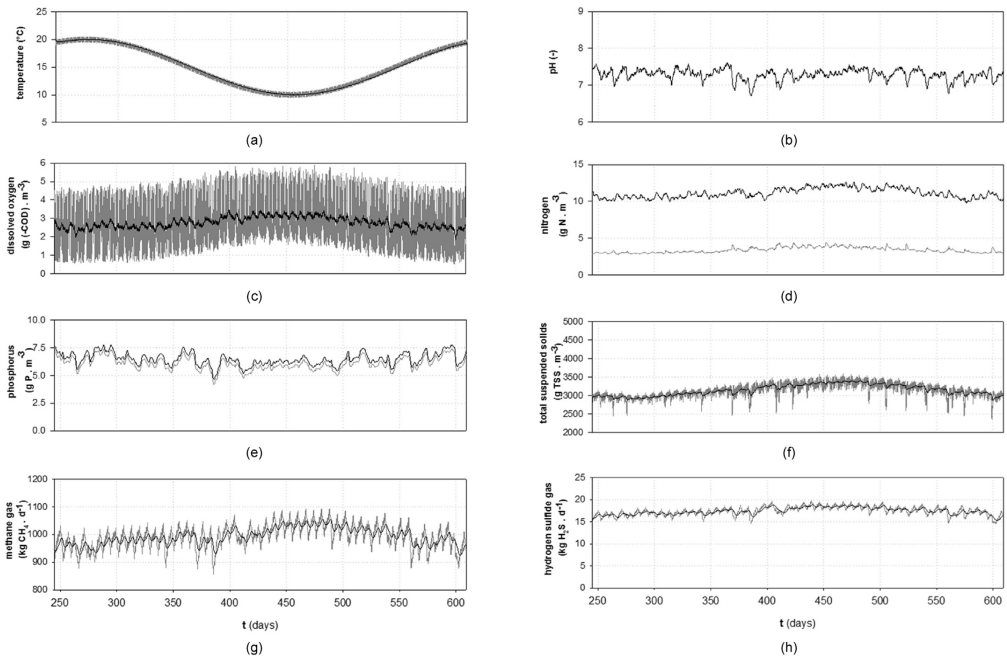

Fig. 2. Dynamic profiles (A_0 = open loop) for: (a) influent temperature; (b) influent pH; (c) dissolved oxygen in AER2; (d) effluent N (S_{NH_x} (grey) and TN (black)); (e) effluent P (S_{IP} (grey) and TP (black)); (f) TSS in AER3; (g) methane gas production; and, (h) hydrogen sulfide gas production. Simulation time is one year. A 3-day exponential filter is used to improve visualization of the results. Raw data is presented in grey (in (a), (b), (c), (f), (g) and (h)).

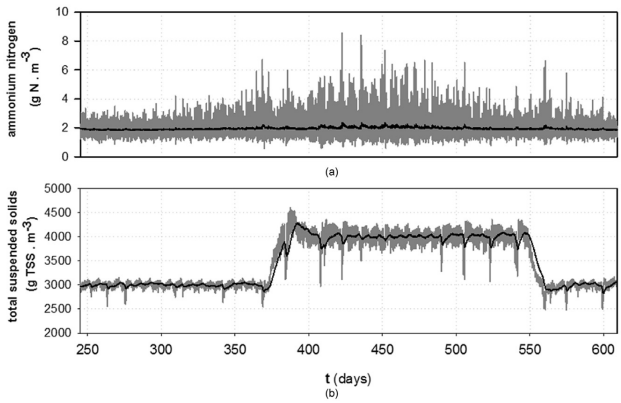

Fig. 3. Dynamic profiles (A_1) of: (a) S_{NH_x} in AER2; and, (b) X_{TSS} in AER3 after implementing alternative A_1. A 3-day exponential filter is used to improve visualization of the results. Raw data is presented in grey. (Note that T < 15 °C starts on day 357 and lasts until day 549).

3.2.1. Control strategy (A_1): cascade ammonium + wastage controller

The first alternative control strategy (A_1) is based on a cascade PI ammonium (S_{NH_x}) controller that manipulates the (S_{O_2}) set-point in AER2 (and also the airflow in AER1 and AER3 by a factor of 2.0 and 0.5, respectively) (Fig. 3a). The S_{O_2} concentration in AER2 is controlled by manipulating the air supply rate. The second controller regulates the total suspended solids (X_{TSS}) in AER3 by manipulating the wastage flow (Q_w) (Vanrolleghem et al., 2010). The set-point changes (set-point = 3000 gTSS.m^{-3} > 15 °C/4000 gTSS.m^{-3} < 15 °C) are made according to temperature (T) in order to set a longer SRT to maintain the nitrification capacity during the winter period (Fig. 3b). Additional details about the simulated control strategies can be found in Table 1. The S_{O_2} and T sensor are assumed to be close to ideal with a response time of 1 min in order to prevent unrealistic control applications. On the other hand, the S_{NH_x} sensor has a time delay of 10 min, with zero mean white noise (standard deviation of 0.5 g N.m^{-3}) (Rieger et al., 2003). The

Table 2
Evaluation criteria for the three evaluated control/operational strategies.

Operational alternatives →	Default	A_1	A_2	A_3	
$N_{Kjeldahl}$	3.5	3.6	3.6	3.7	g N.m^{-3}
N_{total}	11.2	9.2	9.1	8.5	g N.m^{-3}
P_{inorg}	5.95	2.9	0.9	0.6	g P.m^{-3}
P_{total}	6.4	3.7	1.7	1.5	g P.m^{-3}
EQI	**18 234**	**12 508**	**8237**	**7766**	kg pollution.d^{-1}
TIV S_{NH_x} (= 4 g N.m^{-3})	0.95	0.07	0.08	0.08	%
TIV N_{total} (= 14 g N.m^{-3})	0	0	0	0	%
TIV P_{total} (= 2 g P.m^{-3})	100	75	13.4	15.7	%
$E_{aeration}$	4000	3146	3218	3194	kWh.d^{-1}
$E_{production}$ [a]	5955	6054	6150	6038	kWh.d^{-1}
$SP_{disposal}$ [b]	3461	3538	3730	3487	kg TSS.d^{-1}
Q_{FeCl_3}	–	–	169	–	kg Fe.d^{-1}
$Q_{Mg(OH)_2}$	–	–	–	40	kg Mg.d^{-1}
$S_{recovered}$ [c]	–	–	–	206	kg struvite.d^{-1}
OCI [d]	**10 201**	**9495**	**13 770**	**8912**	–
G_{CH_4}	992	1009	1025	1006	kg CH_4.d^{-1}
G_{H_2S}	17.4	19.2	12.1	19.2	kg H_2S.d^{-1}
$\frac{N_{removed}}{OCI}$	0.079	0.089	0.062	0.097	kg N (removed).OCI^{-1}
$\frac{P_{removed}}{OCI}$	0.007	0.013	0.012	0.019	kg P (removed).OCI^{-1}

[a] The electricity generated by the turbine is calculated by using a factor for the energy content of the methane gas (50.014 MJ (kg CH_4)$^{-1}$) and assuming 43% efficiency for electricity generation.
[b] $SP_{disposal}$ refers to the amount of solids which accumulate in the plant over the time of evaluation combined with the amount of solids removed from the process (i.e. dewatered sludge). See Gernaey et al. (2014) for a more detailed description.
[c] $S_{recovered}$ refers to the amount of recovered struvite. See Supplemental Information for a more detailed description.
[d] Relative costs for chemicals are calculated assuming 2400 $/ton as Fe (ICIS, 2016), 600 $/ton as Mg (ICIS, 2016) and 200 $/ton as struvite (value) (Prasad and Shih, 2016; Jaffer et al., 2002; Münch and Barr, 2001).

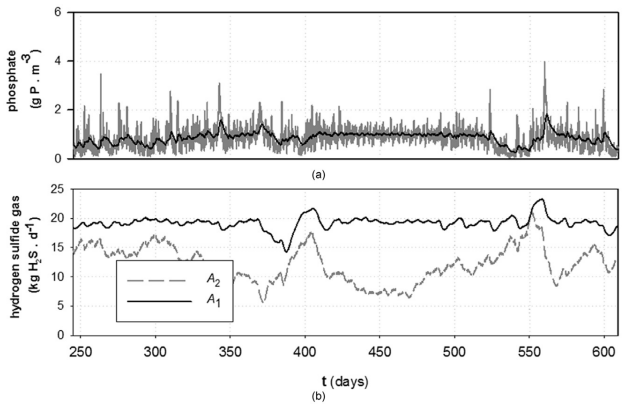

Fig. 4. Dynamic profiles (A_2) of: (a) S_{PO_4} in AER3; and, (b) G_{H_2S} in the AD after implementing alternative A_2. A 3-day exponential filter is used to improve visualization of the results. Raw data is presented in grey.

aeration system and the wastage pumping system are defined with significant dynamics assuming a response time of 4 min. Table 2 summarizes the values for the different evaluation criteria. The implementation of these controllers improves S_{PO_4} accumulation by X_{PAO} and increases nitrification/denitrification efficiency. This is mainly due to a better aeration strategy in the biological reactors. As a side effect, operational cost (*OCI*) is reduced and there is a substantial reduction of the energy consumed (see $E_{aeration}$ values in Table 2). As a further consequence, effluent quality values (N_{total}, P_{total}, *EQI*) are improved. Indeed, the open loop aeration system is highly inefficient (not sufficient during daytime and excessive at night) (see Fig. 2c). Summer/winter wasting schemes cause variations in the quantity of sludge arriving to the AD and therefore changes in the biogas production. This is translated into different potential energy recovery efficiencies (see $E_{production}$ values in Table 2).

3.2.2. Control strategy (A_2): Fe chemical precipitation in the AS section

The second alternative (A_2) involves the addition of iron (as X_{FeCl_3}, the model assumes a liquid solution of X_{FeCl_3}) in the AS section in addition to A_1 (see Table 1). The S_{PO_4} concentration in AER3 is controlled by manipulating the metal flow rate (Q_{FeCl_3}) (Fig. 4a). Additional details about the simulated control strategies can be found in Table 1. The S_{PO_4} and S_{NH_x} sensors have similar characteristics (10 min delay and zero mean white noise with a standard deviation of 0.5 g P or N.m^{-3}). Response time for Q_{FeCl_3} is also 10 min (avoiding unrealistic control actions).

Results reported in Table 2 show a reduction in P_{inorg}, time in violation (*TIV*) P_{total} as well as the *EQI* due to chemical P precipitation (see Figs. 2e and 4a, respectively). On the other hand, there is an increase in sludge production (SP_{total}) and the *OCI* as a trade-off. The aeration energy ($E_{aeration}$) also slightly increase from scenario A_1 to A_2 mainly due to reduced PAO activity brought about by chemical phosphorus removal; less organics are taken up by in the anaerobic part of the activated sludge unit in scenario A_2 and, as a consequence, more organics need to be oxidized in the aerobic part. It is important to highlight the additional beneficial effect of X_{FeCl_3} addition in the sludge line. Indeed, under anaerobic conditions hydrous ferric oxides (X_{HFO-H}, X_{HFO-L}) are chemically reduced to Fe (II) ($S_{Fe^{2+}}$) using hydrogen(S_{H_2}) and/or sulfides (S_{IS}) as electron donors. Also, iron phosphates ($X_{HFO-H,P}$, $X_{HFO-L,P}$) formed in the activated sludge process water line might re-dissolve under anaerobic conditions in the digesters to precipitate with sulfide (X_{FeS}). This is due to the much lower solubility of iron sulfide as compared to iron phosphate (Stumm and Morgan, 1996). The control strategy reduces undesirable inhibition/odour/corrosion problems, as well as risks for human health, as indicated by the higher G_{CH_4} and lower G_{H_2S} values compared to (A_1) (see Figs. 2h and 4b, respectively). Similar conclusions were reached by the experimental campaigns/measurements run by Mamais et al. (1994), Ge et al. (2013) and Zhang et al. (2013).

It is important to highlight that the addition of Fe substantially changes the whole P and S cycle through the entire plant while N fluxes are barely affected. The fraction of P sent to the sludge line is increased from 51 to 67% (94–127 kg P.day^{-1}) (mainly as $X_{HFO-H,P}$, $X_{HFO-L,P}$, $X_{HFO-H,P,old}$, $X_{HFO-L,P,old}$) (see Fig. SS2 in Supplemental Information). This Fe addition reduces the quantity of $X_{Ca_3(PO_4)_2}$ and $X_{MgNH_4PO_4}$ formed in the AD which, from a practical point of view, leads to less problems with their deposition in the pipes. Similar findings are also found in the following studies: Luedecke et al. (1989); Doyle and Parsons (2002) and Mamais et al. (1994). When it comes to S, there is a substantial reduction of the quantity of Z_{H_2S} in the AD due to the preferential binding with Fe (from 5100 to 4400 ppm). As a result, there is a lower quantity of H_2S in the gas phase and therefore the quantity of S leaving the plant via sludge disposal (as precipitate X_{FeS}) increases. There is a slight decrease of pH due to the increase of the contra-ion Cl^- added as part of the iron precipitation.

3.2.3. Control strategy (A_3): potential P recovery as struvite in the digester supernatant

The last alternative implies a modification of the original plant layout by adding a stripping unit (STRIP) for pH increase, a crystallizer (CRYST) to facilitate struvite recovery, a magnesium hydroxide dosage tank ($X_{Mg(OH)_2}$) and a dewatering unit (DEW2) for potential P recovery (Kazadi Mbamba et al., 2016). The assumed hydraulic retention times (HRT) of the STRIP and CRYST units are approximately 2 h and 18 h, respectively (Tchobanoglous et al., 2003). Fig. SS3 (in Supplemental Information) shows the effect of

the extra units on the total P fluxes. Simulation results indicate that the quantity of returning N and P from the AD supernatant is reduced from 221 to 201 kg N.day^{-1} and 30 to 1.3 kg P.day^{-1}, respectively (as a result of recovering P as $X_{MgNH_4PO_4}$). The latter leads to a reduction of the nutrient load to be treated in the biological reactor and decreases the quantity of P lost in the effluent (from 96 to 60 kg P.day^{-1}). When this is translated to evaluation indices (Table 2), a substantial reduction in the effluent related criteria (N_{total}, P_{total}, *EQI*) can be seen. The *OCI* is lower compared to A_2 due to: (1) the lower price of magnesium hydroxide ($X_{Mg(OH)_2}$) compared to iron chloride (X_{FeCl_3}); and, (2) the potential economic benefit resulting from selling struvite ($X_{MgNH_4PO_4}$).

Additional simulations show that these values can be modified by changing the airflow ($Q_{stripping}$) and the chemical dosage ($Q_{Mg(OH)_2}$) in the stripping unit. At high airflows ($Q_{stripping}$) the quantity of Z_{CO_2} stripped increases and consequently the pH (CO_2 has acidifying behaviour) (Fig. 5a, h). The latter favours struvite ($X_{MgNH_4PO_4}$) precipitation (Fig. 5b, g). A higher quantity of Mg ($Q_{Mg(OH)_2}$) also drives the pH higher (Fig. 5a, f). These results show that $X_{MgNH_4PO_4}$ precipitation is mainly limited by $Z_{Mg^{2+}}$ rather than $Z_{NH_4^+}$ and $Z_{PO_4^{3-}}$. This explains the substantial increase of $X_{MgNH_4PO_4}$ when the quantity of Mg is higher (note that an overdose of magnesium is also not beneficial due to possible precipitation of dolomite, etc.). The latter has an effect on P in the AD supernatant (Fig. 5e) and consequently the *EQI* (Fig. 5c). High $Q_{Mg(OH)_2}$ decreases the *OCI* since the struvite ($X_{MgNH_4PO_4}$) is accounted for as a potential benefit (Fig. 5d). Above the P/Mg stoichiometric ratios, additional Mg is just increasing the cost without further benefit, $Q_{Mg(OH)_2}$ > 40 kg Mg.day^{-1}. Fig. 5e, f, g and h show the dynamic profiles of pH at different $Q_{stripping}/Q_{Mg(OH)_2}$. One might notice the effect that the X_{TSS} controller has on the quantity of sludge leaving the AD as a result of changing the TSS set-point in AER3.

3.2.4. Environmental/economic evaluation summary

In all cases, the proposed alternatives (A_1, A_2, A_3) result in substantial improvements with respect to the open loop default configuration (A_0). The implementation of a better aeration strategy and time-varying sludge wasting scheme (A_1) results in a favourable alternative. Simulation results show that this option leads to larger N and P effluent reductions, but also a more cost-effective way to operate the plant. Both A_2 and A_3 substantially reduce the quantity of effluent P. The main difference between the two relies on that A_3 implies a major modification of the plant layout. Capital expenditures of the CRYST, STRIP, blowers, civil, electrical and piping works should be included in order to make a more complete assessment. In contrast, alternative A_2 can be arranged easily with an extra dosing tank. Even though the potential benefit that comes from struvite ($S_{recovered}$) recovery is very uncertain and these results should be taken with care (Shu et al., 2006; Vaneeckhaute et al., 2017), the cost for each kg N and P removed is much higher for A_2 (see $N_{removed}/OCI$ and $P_{removed}/OCI$ values in Table 2). The latter means that the cost is dramatically lower for A_3 and payback time for the new installation should be short. It is important to highlight that a thorough economic study is

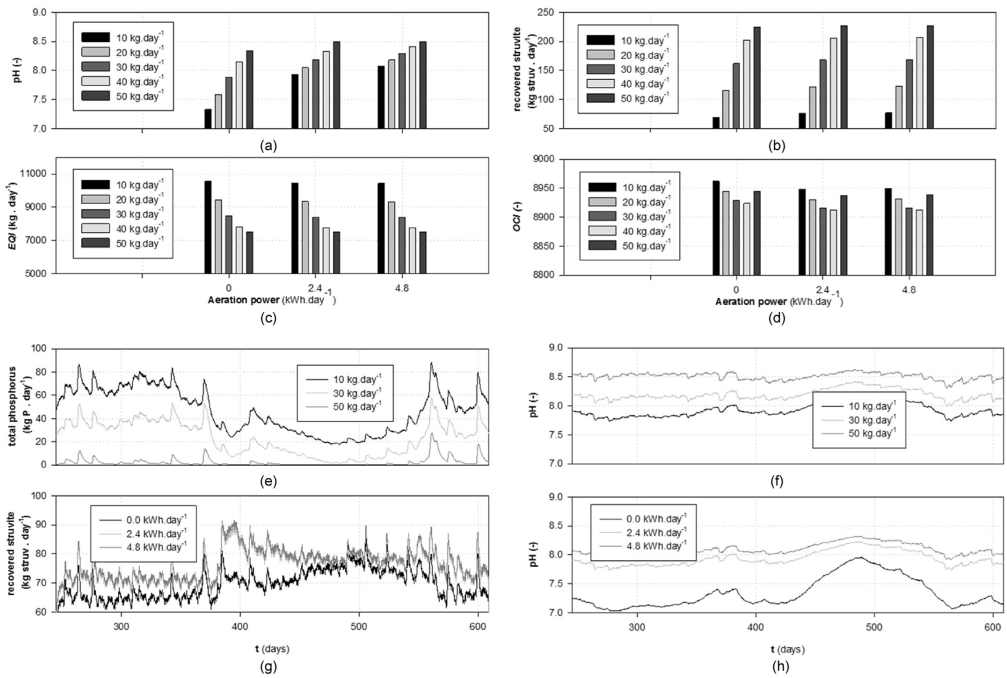

Fig. 5. Effect of aeration power $Q_{stripping}$ /dosage addition $Q_{Mg(OH)_2}$ on (a), (f), (h): pH in the stripping unit (STRIP); (b), (g): quantity of recovered struvite; (c) EQI; (d) OCI; and, (e) P content in the anaerobic digester supernatant. A 3-day exponential filter is used to improve visualization of the results in (e), (f), (g) and (h).

not carried out in this paper since it is not within the scope of the study.

4. Challenges and limitations of the proposed approach

The model results presented in this paper demonstrate the effects that different operational modes might have on the physico-chemical and biological transformations of P in a WRRF. The observations noted above also suggest the importance of linking the P with the S and Fe cycles since this paper identifies that potential control strategies not only address the primary goal, but have an effect that is cycled throughout the process (see Fig. 1, Fig. SS2). This is critical to enable the development, testing and evaluation of phosphorus control/recovery strategies in the context of water resource recovery facilities (Jeppsson et al., 2013). In the following section, we discuss the applicability of the model assumptions made to describe P, S and Fe interactions, the suitability of the number of considered processes and some practical implications for plant-wide modelling/development of resource recovery strategies.

4.1. Selection of the relevant process and interpretation of the results

The model presented in this paper accounts for some of the most important factors affecting the P, S and Fe cycles in a wastewater treatment facility (Batstone et al., 2015). Additional processes may be added to consider novel control strategies. For example, sulfide can be directly controlled in the digester through microaeration, which converts sulfide to elemental sulfur (Krayzelova et al., 2015). The approach taken in this paper in describing sulfide oxidation to elemental sulfur in the anaerobic zone of the activated sludge process is directly applicable to this problem.

When it comes to P recovery, important assumptions were made in order to run the third alternative (A_3). For example, calcium precipitation is not assumed in the crystallizer. This is due to the low amounts of calcium in this scenario, and because calcium generally complexes with carbonate (Kazadi Mbamba et al., 2015a). In high-calcium (hard) waters, it may become critical. Another important factor is that ideal solids separation in the crystallizer is assumed. This will depend on the specific implementation of the crystallizer and crystal recovery. Precipitate dissolution (and particularly Mg dissolution) is currently simplified. The latter may have an important effect on the overall process performance (Romero-Güiza et al., 2015). In the water line, competition between PAO and Glycogen Accumulating Organisms (GAO) (Lopez-Vazquez et al., 2007, 2009; Oehmen et al., 2010) is not accounted for. This may have a strong influence on the overall biological P removal. S and Fe oxidation processes have been modelled chemically, but there are numerous studies demonstrating that these processes are also biologically mediated (Xu et al., 2013). In any case, the oxidation processes goes to completion. This may have limited impact on the overall process, due to the ubiquitous capability of sulfur oxidation/reduction capability in heterotrophic organisms.

The alternating aerated/non-aerated periods might promote the formation of nitrous oxide gases (Ni et al., 2014; Ni and Yuan, 2015; Lindblom et al., 2016). When evaluating the suitability of different control/operational strategies, this factor is not included in the study, and if it was, it might partly change the overall discussion of the results (Flores-Alsina et al., 2014a; Sweetapple et al., 2014; Mannina et al., 2016). Closely related to that, it is important to point out that aeration energy could be better estimated with a more detailed piping/distribution model (Beltrán et al., 2011). In addition, the aeration model could be further improved using a detailed mass transfer model which might change the quantity of stripped gas (that might be overestimated with the current model) (Lizarralde et al., 2015). All these options, including evaluating the impact of influent flow equalization basins, are identified as promising research avenues that will be further studied in the near future (Jeppsson et al., 2013). The latter could be combined with proper electricity tariff models (Aymerich et al., 2015) and dramatically change the way how energy must be optimized. In this case study relative costs have been used (Jeppsson et al., 2007) due to the volatility of the prices (chemicals, electricity, sludge disposal, …). Proper cost estimates and variations (uncertainty ranges) will provide customized solutions for a particular case.

4.2. General applicability of the presented model

Even though the shown numeric results are case-specific, the presented tools are generally applicable, and an earlier version has been successfully applied to a real plant (Kazadi Mbamba et al., 2016). The influent characteristics (Gernaey et al., 2011) can be scaled to different situations (Flores-Alsina et al., 2014b; Snip et al., 2014; Snip et al., 2016; Kazadi Mbamba et al., 2016). The original BSM2 (only carbon and nitrogen) plant has been adapted to simulate the dynamics of some Swedish plants (Arnell et al., 2013). The ASM2d and ADM1 (separately) have been applied to multiple case studies successfully describing plant dynamics (Gernaey and Jørgensen, 2004; Batstone et al., 2015). The P principles upon which the new AD model is constructed are experimentally validated in different studies (Ikumi et al., 2011; Wang et al., 2016). The same applies to the S module in both AS (Gutierrez et al., 2010) and AD (Batstone, 2006; Barrera et al., 2015) models. As stated above, expansion to consider cases such as microaeration in anaerobic digesters can be done through direct adaptation of the approach taken in the activated sludge process.

The model may also be applied to integrated urban water systems, wherein, chemicals added/present in the sewer network or during drinking water production may have an impact on the downstream wastewater treatment processes (particularly for systems where there is no primary sedimentation) (Pikaar et al., 2014; Nielsen et al., 2005; Ge et al., 2013).

4.3. Optimization tool for resource recovery

The described approach has strong potential for optimizing resource recovery (i.e. biogas and phosphorus recovery) in a plant-wide context, and possibly also in the larger sewage catchment. For example, the potential energy/financial benefits of an improved biogas production can be balanced with the addition of selected chemicals (Flores-Alsina et al., 2016) or substrates for co-digestion (Arnell et al., 2016). Another potential option is P recovery (Vaneeckhaute, 2015). Results presented in Section 3.2.3 show that the total quantity of recovered P is rather small (31.8 kg $P.d^{-1}$/196.6 kg $P.d^{-1}$). This is mainly due to the different P losses/transformations through the different units in the plant. Different operational conditions (Marti et al., 2008, 2010; Latif et al., 2015) could reduce the quantity of P lost in the effluent, could minimize uncontrolled phosphorus precipitation in the anaerobic digester and enhance phosphorus recovery in the crystallizer. In a similar way, smarter dosing strategies (similarly to A_2) could be evaluated in order to reduce the use of chemicals and to adapt to changes in the P loads due to operational changes (summer/winter). Airflow in the stripping unit could be adjusted in order to reach a desired pH (feedback controller).

5. Conclusions

The main findings of this study are summarized in the following points:

1) A plant-wide model describing the main P transformations and the close interactions with the S and Fe cycles in wastewater treatment systems is presented;
2) Operational conditions have a strong effect on the fate of P compounds: accumulation by X_{PAO}, adsorption into Fe ($X_{HFO-H,P}$, $X_{HFO-L,P}$) and co-precipitation with different metals ($X_{HFO-H,P,old}$, $X_{HFO-L,P,old}$, $X_{Ca_3(PO_4)_2}$, $X_{MgNH_4PO_4}$);
3) Overall and individual mass balances quantify the distribution of P (as well as N, S and Fe) in both water and sludge line;
4) The set of models presented in this study makes up a useful engineering tool to aid decision makers/wastewater engineers when upgrading/improving the sustainability and efficiency of wastewater treatment systems (e.g. reduce consumption and increase recovery).

6. Software availability

The MATLAB/SIMULINK code of the models presented in this paper is available upon request, including the implementation of the physico-chemical and biological modelling framework in BSM2. Using this code, interested readers will be able to reproduce the results summarized in this study. To express interest, please contact Dr. Ulf Jeppsson (ulf.jeppsson@iea.lth.se) at Lund University (Sweden), Prof. Krist V. Gernaey (kvg@kt.dtu.dk) or Dr. Xavier Flores-Alsina (xfa@kt.dtu.dk) at the Technical University of Denmark (Denmark) or Prof. Damien Batstone (damienb@awmc.uq.edu.au) at The University of Queensland (Australia).

Acknowledgements

Ms Solon and Dr Flores-Alsina acknowledge the Marie Curie Program of the EU 7th Framework Programme FP7/2007–2013 under REA agreement 289193 (SANITAS) and 329349 (PROTEUS), respectively. Dr Flores-Alsina gratefully acknowledges the financial support of the collaborative international consortium WATER-JPI2015 WATINTECH (Reference ID 196) of the Water Challenges for a Changing World Joint Programming Initiative (Water JPI) 2015 call. Parts of this research were developed during the research stay of Dr Flores-Alsina at the Department of Civil Engineering at the University of Cape Town (South Africa) and at the Advanced Water Management Centre at The University of Queensland (Australia) and also developed during the short term scientific COST mission (STSM, COST Water2020) of Ms Solon at the Biosystems Control research unit at the Department of Biosystems Engineering at Ghent University (Belgium). The research was supported financially by The University of Queensland through the UQ International Scholarships (UQI). Peter Vanrolleghem holds the Canada Research Chair in Water Quality Modelling. Dr. Stephan Tait at the Advanced Water Management Centre at The University of Queensland (Australia) and Chris Brouckaert at the Pollution Research Group at the University of KwaZulu-Natal are acknowledged for their valuable contributions on the discussions during the model development. The International Water Association (IWA) is also acknowledged for their promotion of this collaboration through their sponsorship of the IWA Task Group on Generalized Physico-chemical Modelling Framework (PCM). A concise version of this paper was presented at Watermatex 2015 (Gold Coast, Australia, June 2015).

Appendix A. Supplementary data

Supplementary data related to this article can be found at http://dx.doi.org/10.1016/j.watres.2017.02.007.

References

Arnell, M., Astals, S., Åmand, L., Batstone, D.J., Jensen, P.D., Jeppsson, U., 2016. Modelling anaerobic co-digestion in Benchmark Simulation Model No. 2: parameter estimation, substrate characterisation and plant-wide integration. Water Res. 98, 138–146.
Arnell, M., Sehlen, R., Jeppsson, U., 2013. Practical use of wastewater treatment modelling and simulation as a decision support tool for plant operators—case study on aeration control at Linköping wastewater treatment plant. In: Proceedings of the 13th Nordic Wastewater Conference, Malmö, Sweden, 8–10 October 2013.
Aymerich, I., Rieger, L., Sobhani, R., Rosso, D., Corominas, L., 2015. The difference between energy consumption and energy cost: modelling energy tariff structures for water resource recovery facilities. Water Res. 81, 113–123.
Barat, R., Montoya, T., Seco, A., Ferrer, J., 2011. Modelling biological and chemically induced precipitation of calcium phosphate in enhanced biological phosphorus removal systems. Water Res. 45 (12), 3744–3752.
Barat, R., Serralta, J., Ruano, V., Jimenez, E., Ribes, J., Seco, A., Ferrer, J., 2013. Biological Nutrient Removal no 2 (BNRM2): a general model for wastewater treatment plants. Water Sci. Technol. 67 (7), 1481–1489.
Barker, P.S., Dold, P.L., 1997. General model for biological nutrient removal activated-sludge systems: model presentation. Water Environ. Res. 69 (5), 969–984.
Barrera, E.L., Spanjers, H., Solon, K., Amerlinck, Y., Nopens, I., Dewulf, J., 2015. Modeling the anaerobic digestion of cane-molasses vinasse: extension of the Anaerobic Digestion Model No. 1 (ADM1) with sulfate reduction for a very high strength and sulfate rich wastewater. Water Res. 71, 42–54.
Batstone, D.J., 2006. Mathematical modelling of anaerobic reactors treating domestic wastewater: rational criteria for model use. Rev. Environ. Sci. Biotechnol. 5, 57–71.
Batstone, D.J., Keller, J., Angelidaki, I., Kalyuzhnyi, S.V., Pavlostathis, S.G., Rozzi, A., Sanders, W.T.M., Siegrist, H., Vavilin, V.A., 2002. Anaerobic Digestion Model No. 1. IWA Scientific and Technical Report No. 13. IWA Publishing, London, UK.
Batstone, D.J., Puyol, D., Flores-Alsina, X., Rodriguez, J., 2015. Mathematical modelling of anaerobic digestion processes: applications and future needs. Rev. Environ. Sci. Biotechnol. 14 (4), 595–613.
Beltrán, S., Logrono, C., Maiza, M., Ayesa, E., 2011. Model based optimization of aeration system in WWTP. In: Proceedings of Watermatex2011, San Sebastian, Spain, 20–22 June 2011.
Copp, J.B. (Ed.), 2002. The COST Simulation Benchmark – Description and Simulator Manual. Office for Official Publications of the European Communities, Luxembourg, ISBN 92-894-1658-0.
de Gracia, M., Sancho, L., García-Heras, J.L., Vanrolleghem, P., Ayesa, E., 2006. Mass and charge conservation check in dynamic models: application to the new ADM1 model. Water Sci. Technol. 53 (1), 225–240.
Doyle, J.D., Parsons, S.A., 2002. Struvite formation, control and recovery. Water Res. 36 (16), 3925–3940.
Ekama, G.A., 2009. Using bioprocess stoichiometry to build a plant-wide mass balance based steady-state WWTP model. Water Res. 43 (8), 2101–2120.
Ekama, G.A., Barnard, J.L., Gunthert, F.W., Krebs, P., McCorquodale, J.A., Parker, D.S., Wahlberg, E.J., 1997. Secondary Settling Tanks: Theory, Modelling, Design and Operation. IWA Publishing, London, UK. IWA Scientific and Technical Report No. 6.
Ekama, G.A., Wentzel, M.C., 2004. A predictive model for the reactor inorganic suspended solids concentration in activated sludge systems. Water Res. 38 (8), 4093–4106.
Ekama, G.A., Wentzel, M.C., Sötemann, S.W., 2006. Tracking the inorganic suspended solids through biological treatment units of wastewater treatment plants. Water Res. 40 (19), 3587–3595.
Fedorovich, V., Lens, P., Kalyuzhnyi, S., 2003. Extension of anaerobic digestion model No. 1 with processes of sulfate reduction. Appl. Biochem. Biotechnol. 109, 33–45.
Flores-Alsina, X., Arnell, M., Amerlinck, Y., Corominas, L., Gernaey, K.V., Guo, L., Lindblom, E., Nopens, I., Porro, J., Shaw, A., Snip, L., Vanrolleghem, P.A., Jeppsson, U., 2014a. Balancing effluent quality, economical cost and greenhouse gas emissions during the evaluation of plant-wide wastewater treatment plant control strategies. Sci. Total Environ. 466–467, 616–624.
Flores-Alsina, X., Gernaey, K.V., Jeppsson, U., 2012. Benchmarking biological nutrient removal in wastewater treatment plants: influence of mathematical model assumptions. Water Sci. Technol. 65 (8), 1496–1505.
Flores-Alsina, X., Kazadi Mbama, C., Solon, K., Vrecko, D., Tait, S., Batstone, D., Jeppsson, U., Gernaey, K.V., 2015. A plant-wide aqueous phase chemistry module describing pH variations and ion speciation/pairing in wastewater treatment models. Water Res. 85, 255–265.
Flores-Alsina, X., Saagi, R., Lindblom, E., Thirsing, C., Thornberg, D., Gernaey, K.V., Jeppsson, U., 2014b. Calibration and validation of a phenomenological influent pollutant disturbance scenario generator using full-scale data. Water Res. 51, 172–185.
Flores-Alsina, X., Solon, K., Kazadi Mbamba, C., Tait, S., Jeppsson, U., Gernaey, K.V., Batstone, D.J., 2016. Modelling phosphorus, sulphur and iron interactions during the dynamic simulation of anaerobic digestion processes. Water Res. 95, 370–382.
Ge, H., Zhang, L., Batstone, D.J., Keller, J., Yuan, Z., 2013. Impact of iron salt dosage to sewers on downstream anaerobic sludge digesters: sulfide control and methane production. J. Environ. Eng. 139, 594–601.

Gernaey, K.V., Flores-Alsina, X., Rosen, C., Benedetti, L., Jeppsson, U., 2011. Dynamic influent pollutant disturbance scenario generation using a phenomenological modelling approach. Environ. Model. Softw. 26 (11), 1255–1267.
Gernaey, K.V., Jeppsson, U., Batstone, D.J., Ingildsen, P., 2006. Impact of reactive settler models on simulated WWTP performance. Water Sci. Technol. 53 (1), 159–167.
Gernaey, K.V., Jeppsson, U., Vanrolleghem, P.A., Copp, J.B., 2014. Benchmarking of Control Strategies for Wastewater Treatment Plants. IWA Publishing, London, UK. IWA Scientific and Technical Report No. 23.
Gernaey, K.V., Jørgensen, S.B., 2004. Benchmarking combined biological phosphorus and nitrogen removal wastewater treatment processes. Control Eng. Pract. 12 (3), 357–373.
Grau, P., Copp, J., Vanrolleghem, P.A., Takács, I., Ayesa, E., 2009. A comparative analysis of different approaches for integrated WWTP modelling. Water Sci. Technol. 59 (1), 141–147.
Grau, P., de Gracia, M., Vanrolleghem, P.A., Ayesa, E., 2007. A new plant-wide modelling methodology for WWTPs. Water Res. 41 (19), 4357–4372.
Gutierrez, O., Park, D., Sharma, K.R., Yuan, Z., 2010. Iron salts dosage for sulfide control in sewers induces chemical phosphorus removal during wastewater treatment. Water Res. 44 (11), 3467–3475.
Guerrero, J., Flores-Alsina, X., Guisasola, A., Baeza, J.A., Gernaey, K.V., 2013. Effect of nitrite, limited reactive settler and plant design configuration on the predicted performance of a simultaneous C/N/P removal WWTP. Bioresour. Technol. 136, 680–688.
Harding, T.H., Ikumi, D.S., Ekama, G.A., 2011. Incorporating phosphorus into plant wide wastewater treatment plant modelling anaerobic digestion. In: Proceedings of Watermatex2011, San Sebastian, Spain, 20–22 June 2011.
Hauduc, H., Rieger, L., Takács, I., Héduit, A., Vanrolleghem, P.A., Gillot, S., 2010. A systematic approach for model verification: application on seven published activated sludge models. Water Sci. Technol. 61 (4), 825–839.
Hauduc, H., Takács, I., Smith, S., Szabo, A., Murthy, S., Daigger, G.T., Spérandio, M., 2015. A dynamic physicochemical model for chemical phosphorus removal. Water Res. 73, 157–170.
Henze, M., Gujer, W., Mino, T., van Loosdrecht, M.C.M., 2000. Activated Sludge Models ASM1, ASM2, ASM2d, and ASM3. IWA Publishing, London, UK. IWA Scientific and Technical Report No. 9.
Henze, M., van Loosdrecht, M.C.M., Ekama, G.A., 2008. Biological Wastewater Treatment: Principles, Modeling, and Design. IWA Publishing, London, UK.
ICIS, 2016. Indicative Chemical Prices A-z. Retrieved from. http://www.icis.com/chemicals/channel-info-chemicals-a-z/ [Accessed 14 06 2016].
Ikumi, D.S., Brouckaert, C.J., Ekama, G.A., 2011. Modelling of struvite precipitation in anaerobic digestion. In: Proceedings of Watermatex2011, San Sebastian, Spain, 20–22 June 2011.
Ikumi, D.S., Harding, T.H., Ekama, G.A., 2014. Biodegradability of wastewater and activated sludge organics in anaerobic digestion. Water Res. 56 (1), 267–279.
Jaffer, Y., Clark, T.A., Pearce, P., Parsons, S.A., 2002. Potential phosphorus recovery by struvite formation. Water Res. 36 (7), 1834–1842.
Jeppsson, U., Alex, J., Batstone, D., Benedetti, L., Comas, J., Copp, J.B., Corominas, L., Flores-Alsina, X., Gernaey, K.V., Nopens, I., Pons, M.-N., Rodriguez-Roda, I., Rosen, C., Steyer, J.-P., Vanrolleghem, P.A., Volcke, E.I.P., Vrecko, D., 2013. Benchmark simulation models, quo vadis? Water Sci. Technol. 68 (1), 1–15.
Jeppsson, U., Pons, M.N., Nopens, I., Alex, J., Copp, J.B., Gernaey, K.V., Rosen, C., Steyer, J.P., Vanrolleghem, P.A., 2007. Benchmark Simulation Model No 2 – general protocol and exploratory case studies. Water Sci. Technol. 56 (8), 287–295.
Kazadi Mbamba, C., Flores-Alsina, X., Batstone, D.J., Tait, S., 2015a. A generalised chemical precipitation modelling approach in wastewater treatment applied to calcite. Water Res. 68, 342–353.
Kazadi Mbamba, C., Flores-Alsina, X., Batstone, D.J., Tait, S., 2015b. A systematic study of multiple minerals precipitation modelling in wastewater treatment. Water Res. 85, 359–370.
Kazadi Mbamba, C., Flores-Alsina, X., Batstone, D.J., Tait, S., 2016. Validation of a plant-wide modelling approach with minerals precipitation in a full-scale WWTP. Water Res. 100, 169–183.
Krayzelova, L., Bartacek, J., Díaz, I., Jeison, D., Volcke, E.I.P., Jenicek, P., 2015. Microaeration for hydrogen sulfide removal during anaerobic treatment: a review. Rev. Environ. Sci. Biotechnol. 14 (4), 703–725.
Latif, M.A., Mehta, C.M., Batstone, D.J., 2015. Low pH anaerobic digestion of waste activated sludge for enhanced phosphorous release. Water Res. 81, 288–293.
Lizarralde, I., Fernandez-Arevalo, T., Brouckaert, C., Vanrolleghem, P.A., Ikumi, D., Ekama, D., Ayesa, E., Grau, P., 2015. A new general methodology for incorporating physico-chemical transformations into multiphase wastewater treatment process models. Water Res. 74, 239–256.
Lindblom, E., Arnell, M., Flores-Alsina, X., Stenström, F., Gustavsson, D.J.I., Yang, J., Jeppsson, U., 2016. Dynamic modelling of nitrous oxide emissions from three Swedish sludge liquor treatment systems. Water Sci. Technol. 73 (4), 798–806.
Lopez-Vazquez, C.M., Hooijmans, C.M., Brdjanovic, D., Gijzen, H.J., van Loosdrecht, M.C.M., 2007. A practical method for quantification of phosphorus- and glycogen-accumulating organism populations in activated sludge systems. Water Environ. Res. 79 (13), 2487–2498.
Lopez-Vazquez, C.M., Oehmen, A., Hooijmans, C.M., Brdjanovic, D., Gijzen, H.J., Yuan, Z., van Loosdrecht, M.C.M., 2009. Modeling the PAO-GAO competition: effects of carbon source, pH and temperature. Water Res. 43 (2), 450–462.
Luedecke, C., Hermanowicz, S.W., Jenkins, D., 1989. Precipitation of ferric phosphate in activated sludge: a chemical model and its verification. Water Sci. Technol. 21 (4–5), 325–337.
Mamais, D., Pitt, P.A., Cheng, Y.W., Loiacono, J., Jenkins, D., 1994. Determination of ferric chloride dose to control struvite precipitation in anaerobic sludge digesters. Water Environ. Res. 66 (7), 912–918.
Mannina, G., Ekama, G., Caniani, D., Cosenza, A., Esposito, G., Gori, R., Garrido-Baserba, M., Rosso, D., Olsson, G., 2016. Greenhouse gases from wastewater treatment - a review of modelling tools. Sci. Total Environ. 551, 254–270.
Marti, N., Pastor, L., Bouzas, A., Ferrer, J., Seco, A., 2010. Phosphorus recovery by struvite crystallization in WWTPs: influence of the sludge treatment line operation. Water Res. 44 (7), 2371–2379.
Marti, N., Ferrer, J., Seco, A., Bouzas, A., 2008. Optimization of sludge line management to enhance phosphorus recovery in WWTP. Water Res. 42 (18), 4609–4618.
Martin, C., Vanrolleghem, P.A., 2014. Analysing, completing, and generating influent data for WWTP modelling: a critical review. Environ. Model. Softw. 60, 188–201.
Münch, E.V., Barr, K., 2001. Controlled struvite crystallisation for removing phosphorus from anaerobic digester sidestreams. Water Res. 35 (1), 151–159.
Musvoto, E.V., Wentzel, M.C., Ekama, G.A., 2000. Integrated chemical-physical processes modelling - II. Simulating aeration treatment of anaerobic digester supernatants. Water Res. 34 (6), 1868–1880.
Ni, B.J., Peng, L., Law, Y., Guo, J., Yuan, Z., 2014. Modeling of nitrous oxide production by autotrophic ammonia-oxidizing bacteria with multiple production pathways. Environ. Sci. Technol. 48 (7), 3916–3924.
Ni, B.J., Yuan, Z., 2015. Recent advances in mathematical modeling of nitrous oxides emissions from wastewater treatment processes. Water Res. 87, 336–346.
Nielsen, A.H., Lens, P., Vollertsen, J., Hvitved-Jacobsen, T., 2005. Sulfide–iron interactions in domestic wastewater from a gravity sewer. Water Res. 39 (12), 2747–2755.
Nopens, I., Batstone, D.J., Copp, J.B., Jeppsson, U., Volcke, E., Alex, J., Vanrolleghem, P.A., 2009. An ASM/ADM model interface for dynamic plant-wide simulation. Water Res. 43 (7), 1913–1923.
Nopens, I., Benedetti, L., Jeppsson, U., Pons, M.-N., Alex, J., Copp, J.B., Gernaey, K.V., Rosen, C., Steyer, J.-P., Vanrolleghem, P.A., 2010. Benchmark Simulation Model No 2 – finalisation of plant layout and default control strategy. Water Sci. Technol. 62 (9), 1967–1974.
Oehmen, A., Lopez-Vazquez, C.M., Carvalho, G., Reis, M.A.M., van Loosdrecht, M.C.M., 2010. Modelling the population dynamics and metabolic diversity of organisms relevant in anaerobic/anoxic/aerobic enhanced biological phosphorus removal processes. Water Res. 44 (15), 4473–4486.
Otterpohl, R., Freund, M., 1992. Dynamic models for clarifiers of activated sludge plants with dry and wet weather flows. Water Sci. Technol. 26 (5–6), 1391–1400.
Pikaar, I., Sharma, K.R., Hu, S., Gernjak, W., Keller, J., Yuan, Z., 2014. Reducing sewer corrosion through integrated urban water management. Science 345 (6198), 812–814.
Pokorna-Krayzelova, L., Mampaey, K.E., Vannecke, T.P.W., Bartacek, J., Jenicek, P., Volcke, E.I.P., 2017. Model-based Optimization of Microaeration for Biogas Desulfurization in UASB Reactors submitted for publication.
Prasad, M.N.V., Shih, K., 2016. Environmental Materials and Waste: Resource Recovery and Pollution Prevention. Elsevier Inc, London, UK.
Rieger, L., Alex, J., Winkler, S., Boehler, M., Thomann, M., Siegrist, H., 2003. Progress in sensor technology - progress in process control Part I: sensor property investigation and classification. Water Sci. Technol. 47 (2), 103–112.
Romero-Güiza, M.S., Tait, S., Astals, S., Del Valle-Zermeño, R., Martínez, M., Mata-Alvarez, J., Chimenos, J.M., 2015. Reagent use efficiency with removal of nitrogen from pig slurry via struvite: a study on magnesium oxide and related by-products. Water Res. 84, 286–294.
Rosen, C., Vrecko, D., Gernaey, K.V., Pons, M.-N., Jeppsson, U., 2006. Implementing ADM1 for plant-wide benchmark simulations in Matlab/Simulink. Water Sci. Technol. 54 (4), 11–19.
Ruano, M.V., Serralta, J., Ribes, J., Garcia-Usach, F., Bouzas, A., Barat, R., 2011. Application of the general model Biological Nutrient Removal Model No. 1 to upgrade two full-scale WWTPs. Environ. Technol. 33 (9), 1005–1012.
Serralta, J., Borras, L., Seco, A., 2004. An extension of ASM2d including pH calculation. Water Res. 38 (19), 4029–4038.
Shu, L., Schneider, P., Jegatheesan, V., Johnson, J., 2006. An economic evaluation of phosphorus recovery as struvite from digester supernatant. Bioresour. Technol. 97 (17), 2211–2216.
Siegrist, H., Brunner, I., Koch, G., Con Phan, L., Van Chieu, L., 1999. Reduction of biomass decay under anoxic and anaerobic conditions. Water Sci. Technol. 39 (1), 129–137.
Skogestad, S., 2000. Plantwide control: the search for the self-optimizing control structure. J. Process Control 10, 487–507.
Snip, L., Flores-Alsina, X., Plósz, B.G., Jeppsson, U., Gernaey, K.V., 2014. Modelling the occurrence, transport and fate of pharmaceuticals in wastewater systems. Environ. Model. Softw. 62, 112–127.
Snip, L.J.P., Flores-Alsina, X., Aymerich, I., Rodríguez-Mozaz, S., Barceló, D., Plósz, B.G., Corominas, L., Rodriguez-Roda, I., Jeppsson, U., Gernaey, K.V., 2016. Generation of synthetic data to perform (micro) pollutant wastewater treatment modelling studies. Sci. Total Environ. 569–570, 278–290.
Solon, K., Flores-Alsina, X., Kazadi Mbamba, C., Volcke, E.I.P., Tait, S., Batstone, D.J., Gernaey, K.V., Jeppsson, U., 2015. Effects of ionic strength and ion pairing on (plant-wide) modelling of anaerobic digestion processes. Water Res. 70, 235–245.

Stumm, W., Morgan, J.J., 1996. In: Schnoor, J.L., Zehnder, A. (Eds.), Aquatic Chemistry: Chemical Equilibria and Rates in Natural Waters. John Wiley and Sons, New York, NY, USA.
Sweetapple, C., Fu, G., Butler, D., 2014. Multi-objective optimisation of wastewater treatment plant control to reduce greenhouse gas emissions. Water Res. 55, 52–62.
Takács, I., Patry, G.G., Nolasco, D., 1991. A dynamic model of the clarification thickening process. Water Res. 25 (10), 1263–1271.
Tchobanoglous, G., Burton, F.L., Stensel, H.D., 2003. Wastewater Engineering: Treatment and Reuse, fourth ed. Massachusetts, USA: McGraw-Hill Education, Boston.
Truskey, G., Yuan, F., Katz, D.F., 2009. Transport Phenomena in Biological Systems (Upper Saddle River, New Jersey, USA: Prentice Hall).
Vaneeckhaute, C., 2015. Nutrient Recovery from Bio-digestion Waste: from Field Experimentation to Model-based Optimization. Université Laval, Québec, Canada. PhD thesis.
Vaneeckhaute, C., Lebuf, V., Michels, E., Belia, E., Vanrollegem, P.A., Tack, F.M.G., Meers, E., 2017. Nutrient recovery from digestate: systematic technology review and product classification. Waste Biomass Valorizat. 8 (1), 21–40.
van Rensburg, P., Musvoto, E.V., Wentzel, M.C., Ekama, G.A., 2003. Modelling multiple mineral precipitation in anaerobic digester liquor. Water Res. 37 (13), 3087–3097.
Vanrolleghem, P.A., Corominas, L., Flores-Alsina, X., 2010. Real-time control and effluent ammonia violations induced by return liquor overloads. Proc. Water Environ. Fed. 2010 (9), 7101–7108.
Vanrolleghem, P.A., Flores-Alsina, X., Guo, L., Solon, K., Ikumi, D., Batstone, D.J., Brouckaert, C., Takács, I., Grau, P., Ekama, G.A., Jeppsson, U., Gernaey, K.V., 2014. Towards BSM2-GPS-X: a plant-wide benchmark simulation model not only for carbon and nitrogen, but also for greenhouse gases (G), phosphorus (P), sulphur (S) and micropollutants (X), all within the fence of WWTPs/WRRFs. In: Proceedings of the IWA/WEF Wastewater Treatment Modelling Seminar, Spa, Belgium, 30 March-2 April 2014.
Vanrolleghem, P.A., Vaneeckhaute, C., 2014. Resource recovery from wastewater and sludge: modelling and control challenges. In: Proceedings of the IWA Specialist Conference on Global Challenges for Sustainable Wastewater Treatment and Resource Recovery, Kathmandu, Nepal, 26–30 October 2014.
Verstraete, W., Van de Caveye, P., Diamantis, V., 2009. Maximum use of resources present in domestic "used water". Bioresour. Technol. 100 (23), 5537–5545.
Volcke, E.I.P., Gernaey, K.V., Vrecko, D., Jeppsson, U., van Loosdrecht, M.C.M., Vanrolleghem, P.A., 2006a. Plant-wide (BSM2) evaluation of reject water treatment with a SHARON-Anammox process. Water Sci. Technol. 54 (8), 93–100.
Volcke, E.I.P., van Loosdrecht, M.C.M., Vanrolleghem, P.A., 2006b. Continuity-based model interfacing for plant-wide simulation: a general approach. Water Res. 40 (15), 2817–2828.
Wang, R., Yongmei, L., Chen, W., Zou, J., Chen, Y., 2016. Phosphate release involving PAOs activity during anaerobic fermentation of EBPR sludge and the extension of ADM1. Chem. Eng. J. 297 (1), 436–447.
Wentzel, M., Ekama, G., Sotemann, S., 2006. Mass balance based plant wide treatment model – Part 1. Biodegradability of wastewater organics under anaerobic conditions. Water sa. 32 (3), 2675–2692.
Xu, X., Chen, C., Lee, D.J., Wang, A., Guo, W., Zhou, X., Guo, H., Yuan, Y., Ren, N., Chang, J.S., 2013. Sulfate-reduction, sulfide-oxidation and elemental sulfur bioreduction process: modeling and experimental validation. Bioresour. Technol. 147, 202–211.
Zaher, U., Grau, P., Benedetti, L., Ayesa, E., Vanrolleghem, P.A., 2007. Transformers for interfacing anaerobic digestion models to pre- and post-treatment processes in a plant-wide modelling context. Environ. Model. Softw. 22 (1), 40–58.
Zhang, J., Zhang, Y., Chang, J., Quan, X., Li, Q., 2013. Biological sulfate reduction in the acidogenic phase of anaerobic digestion under dissimilatory Fe (III)-reducing conditions. Water Res. 47 (6), 2033–2040.

Supplemental Information

Paper Title: Plant-wide modelling of phosphorus transformations in biological nutrient removal wastewater treatment systems: Impacts of control and operational strategies

Authors: Solon, K., Flores-Alsina, X., Kazadi Mbamba, C., Ikumi, D.S., Volcke, E.I.P., Vaneeckhaute, C., Ekama, G.A., Vanrolleghem, P.A., Batstone, D.J., Gernaey, K.V., Jeppsson, U.

The Effluent Quality Index (*EQI*, kg pollution units.d^{-1}) reflects the amount of pollution discharged onto surface waters averaged over the period of evaluation based on a weighting of the effluent loads of compounds that have a major influence on the quality of the receiving water. The *EQI* is updated to include the additional phosphorus load and is defined as:

$$EQI = \frac{1}{t_{\mathrm{obs}} \cdot 1000} \int_{t_{\mathrm{start}}}^{t_{\mathrm{end}}} \Big(\beta_{\mathrm{TSS}} \cdot \mathrm{TSS}_e(t) + \beta_{\mathrm{COD}} \cdot \mathrm{COD}_e(t) + \beta_{\mathrm{NKj}} \cdot S_{\mathrm{NKj}_e}(t) + \beta_{\mathrm{NO}} \cdot S_{\mathrm{NO}_e}(t) + \beta_{\mathrm{BOD}_5} \cdot \mathrm{BOD}_{5_e}(t) + \beta_{\mathrm{Porg}} \cdot S_{\mathrm{Porg}_e}(t) + \beta_{\mathrm{Pinorg}} \cdot S_{\mathrm{Pinorg}_e}(t) \Big) \cdot Q_e(t) \cdot dt$$

where:

$$\mathrm{COD}_e = S_{\mathrm{F}_e} + S_{\mathrm{A}_e} + S_{\mathrm{I}_e} + X_{\mathrm{I}_e} + X_{\mathrm{S}_e} + X_{\mathrm{B,H}_e} + X_{\mathrm{PAO}_e} + X_{\mathrm{PHA}_e} + X_{\mathrm{B,A}_e} + i_{\mathrm{COD}_{S_{\mathrm{Fe(II)}}}} \cdot S_{\mathrm{Fe(II)}_e} + i_{\mathrm{COD}_{S_{\mathrm{IS}}}} \cdot S_{\mathrm{IS}_e} + i_{\mathrm{COD}_{X_{\mathrm{S^0}}}} \cdot X_{\mathrm{S^0}_e} + X_{\mathrm{SRB}_e}$$

$$S_{\mathrm{NKj}_e} = S_{\mathrm{NH}_e} + i_{\mathrm{N}_{S_{\mathrm{F}}}} \cdot S_{\mathrm{F}_e} + i_{\mathrm{N}_{S_{\mathrm{I}}}} \cdot S_{\mathrm{I}_e} + i_{\mathrm{N}_{X_{\mathrm{I}}}} \cdot X_{\mathrm{I}_e} + i_{\mathrm{N}_{X_{\mathrm{S}}}} \cdot X_{\mathrm{S}_e} + i_{\mathrm{N_{BM}}} \cdot \Big(X_{\mathrm{B,H}_e} + X_{\mathrm{PAO}_e} + X_{\mathrm{B,A}_e} + X_{\mathrm{SRB}_e} \Big)$$

$$\mathrm{BOD}_{5_e} = 0.25 \cdot \Big(S_{\mathrm{F}_e} + S_{\mathrm{A}_e} + \big(1 - f_{S_{\mathrm{I}}}\big) \cdot X_{\mathrm{S}_e} + \big(1 - f_{X_{\mathrm{IH}}}\big) \cdot X_{\mathrm{B,H}_e} + \big(1 - f_{X_{\mathrm{IP}}}\big) \cdot \big(X_{\mathrm{PAO}_e} + X_{\mathrm{PHA}_e} \big) + \big(1 - f_{X_{\mathrm{IA}}}\big) \cdot \Big(X_{\mathrm{B,A}_e} + X_{\mathrm{SRB}_e} \Big) \Big)$$

$$S_{\mathrm{Porg}_e} = X_{\mathrm{PP}_e} + i_{\mathrm{P}_{S_{\mathrm{F}}}} \cdot S_{\mathrm{F}_e} + i_{\mathrm{P}_{S_{\mathrm{I}}}} \cdot S_{\mathrm{I}_e} + i_{\mathrm{P}_{X_{\mathrm{I}}}} \cdot X_{\mathrm{I}_e} + i_{\mathrm{P}_{X_{\mathrm{S}}}} \cdot X_{\mathrm{S}_e} + i_{\mathrm{P_{BM}}} \cdot \Big(X_{\mathrm{B,H}_e} + X_{\mathrm{PAO}_e} + X_{\mathrm{B,A}_e} + X_{\mathrm{SRB}_e} \Big)$$

$$S_{\mathrm{Pinorg}_e} = S_{\mathrm{PO4}_e}$$

The subscript e denotes the effluent. The individual calculations for each of the other components of the *EQI* are the same as presented in Gernaey et al. (2014). The β_i are weighting factors (see Table SS1) for the different types of pollutants to convert them into general pollution units, i_{COD_i} represents the COD content, i_{N_i} represents the nitrogen content, i_{P_i} represents the phosphorus content, t_{obs} is the total evaluation period and Q_e (m^3.d^{-1}) is the effluent flow rate. The concentrations are expressed in g.m^{-3}. The values for β_i have been deduced from Vanrolleghem et al. (1996) (Gernaey et al., 2014) (values for β_{Porg} and β_{Pinorg} are inferred from the eutrophication potential of phosphorus).

Table SS1. Values of the *EQI* weighting factors (β_i)

Weighting factors	β_{TSS}	β_{COD}	β_{NKj}	β_{NO}	β_{BOD_5}	β_{Porg}	β_{Pinorg}
Value (g pollution unit.g^{-1})	2	1	30	10	2	100	100

Another criterion is the Operational Cost Index (*OCI*). It is given as the weighted sum of costs related to sludge production, aeration, pumping, external carbon source, mixing, heating, and the potential benefit of methane production. Because of the modifications to the plant layout and operation, additional costs are now considered, such as those related to the additional recycles (anoxic, anaerobic), aerators (CO_2 stripping) and chemicals (for chemical phosphorus precipitation and/or recovery). The *OCI* is thus calculated as:

$$OCI = AE + PE + f_{SP} \cdot SP + f_{EC} \cdot EC + ME - f_{\mathrm{MP}} \cdot MP + \max(0, HE - 7MP) + f_{MA} \cdot MA + f_{Mg} \cdot Mg - f_{S_{\mathrm{recovered}}} \cdot S_{\mathrm{recovered}} + AE_{strip}$$

where *AE* (kWh.d^{-1}) is aeration energy, *PE* (kWH.d^{-1}) is pumping energy, *SP* (kg SS.d^{-1}) is sludge production for disposal, *EC* (kg COD.d^{-1}) is external carbon addition, *ME* (kWh.d^{-1}) is mixing energy, *MP* (kg CH_4.d^{-1}) is methane production and *HE* (kWh.d^{-1}) is the required heating energy for the anaerobic digester (if the heat generated by the gas motor (7*MP*) is higher than *HE* then no external energy is required). The individual calculations for these components are presented in Gernaey et al. (2014) as well as the weighting factors, f_i (see Table SS2) (values for f_{MA}, f_{Mg} and $f_{S_{\mathrm{recovered}}}$ are calculated based on the commercial prices of iron, magnesium and struvite, respectively). The additional costs considered are calculated as follows:

Metal addition (MA) (kg.d^{-1}) is calculated as:

$$MA = \frac{CONC_{\mathrm{METAL}}}{t_{\mathrm{obs}} \cdot 1000} \int_{t_{\mathrm{start}}}^{t_{\mathrm{end}}} \left(\sum_{k=1}^{7} Q_{\mathrm{METAL},k} \right) \cdot dt$$

where $Q_{\mathrm{METAL},k}$ (m^3.d^{-1}) is the flow rate of metal added to compartment k and $CONC_{\mathrm{METAL}}$ (g.m^{-3}) is the concentration of metal (in this case, iron) externally added in one of the activated sludge compartments.

Similarly, magnesium addition (Mg) (kg Mg.d^{-1}) is calculated as:

$$Mg = \frac{CONC_{\mathrm{Mg}}}{t_{\mathrm{obs}} \cdot 1000} \int_{t_{\mathrm{start}}}^{t_{\mathrm{end}}} Q_{\mathrm{Mg}} \cdot dt$$

where Q_{Mg} (m^3.d^{-1}) is the flow rate of Mg added to the stream just after the dewatering unit and $CONC_{\mathrm{Mg}}$ (g.m^{-3}) is the concentration of Mg added.

Recovered struvite ($S_{\mathrm{recovered}}$) (kg struvite.d^{-1}) is calculated as:

$$S_{\mathrm{recovered}} = \frac{CONC_{\mathrm{struv}}}{t_{\mathrm{obs}} \cdot 1000} \int_{t_{\mathrm{start}}}^{t_{\mathrm{end}}} Q_{\mathrm{struv}} \cdot dt$$

where Q_{struv} (m^3.d^{-1}) is the flow rate of struvite recovered and $CONC_{\mathrm{struv}}$ (g.m^{-3}) is the concentration of struvite.

Energy used in the stripping unit (AE_{strip}) (kWh.d^{-1}) is calculated as:

$$AE_{strip} = \frac{S_{\mathrm{O}}^{\mathrm{sat}}}{t_{\mathrm{obs}} \cdot 1.8 \cdot 1000} \cdot \mathrm{V}_{\mathrm{strip}} \int_{t_{\mathrm{start}}}^{t_{\mathrm{end}}} K_L a_{\mathrm{strip}}(t) \cdot dt$$

where $S_{\mathrm{O}}^{\mathrm{sat}}$ (g O_2.m^{-3}) is the saturated oxygen concentration at 15°C, 1.8 is the amount of O_2 (kg) that can be transferred per kWh, $\mathrm{V}_{\mathrm{strip}}$ (m^3) is the volume of the stripping unit and $K_L a_{\mathrm{strip}}$ (d^{-1}) is the mass transfer coefficient in the stripping unit.

Table SS2. Values of the *OCI* weighting factors (f_i)

Weighting factors	f_{SP}	f_{EC}	f_{MP}	f_{MA}	f_{Mg}	$f_{S_{\mathrm{recovered}}}$
Value	3	3	6	24	6	2

Gernaey, K.V., Jeppsson, U., Vanrolleghem, P.A. & Copp, J.B. (2014). *Benchmarking of Control Strategies for Wastewater Treatment Plants*. Scientific and Technical Report No. 23. London, UK: IWA Publishing.

Vanrolleghem, P.A., Jeppsson, U., Carstensen, J., Carlsson, B. & Olsson, G. (1996). Integration of wastewater treatment plant design and operation a systematic – approach using cost functions. *Water Science and Technology*, *34*(3-4), 159-171.

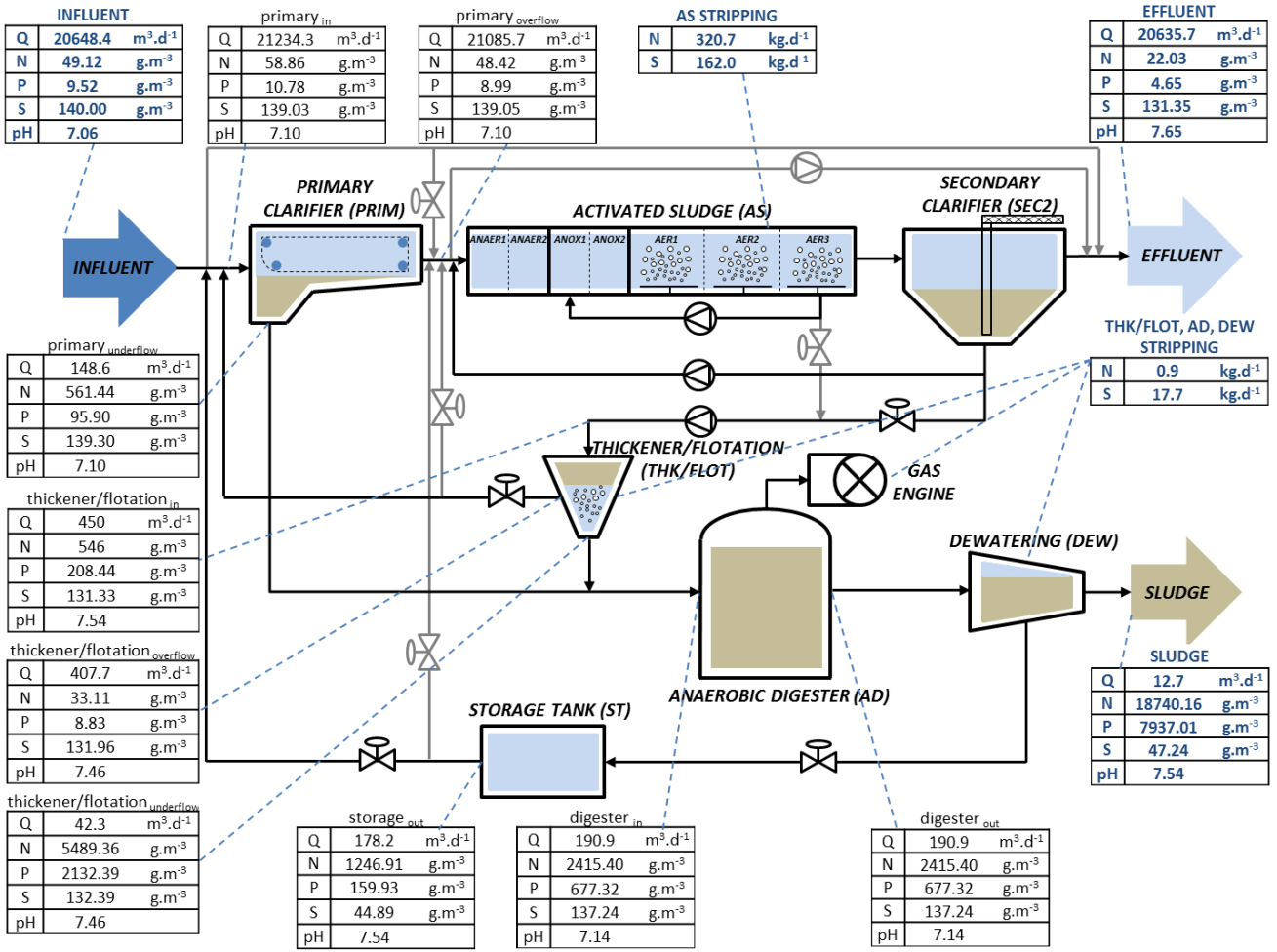

Figure SS1. Block flow diagram including overall and individual (N, P, S, pH) concentrations for the WWTP under study (scenario A_0).

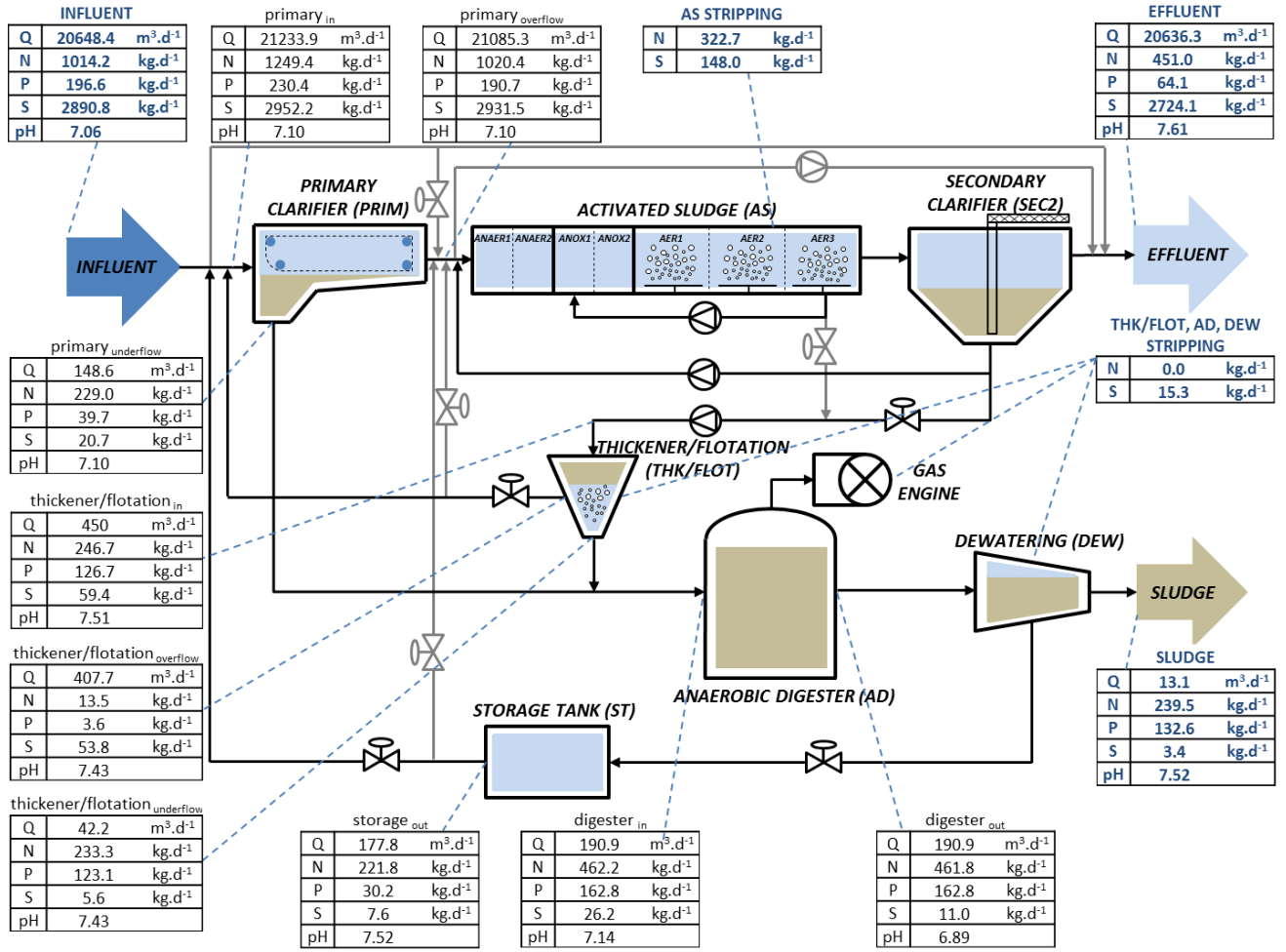

Figure SS2. Block flow diagram including overall and individual (N, P, S, pH) balances for the WWTP under study (scenario A_2).

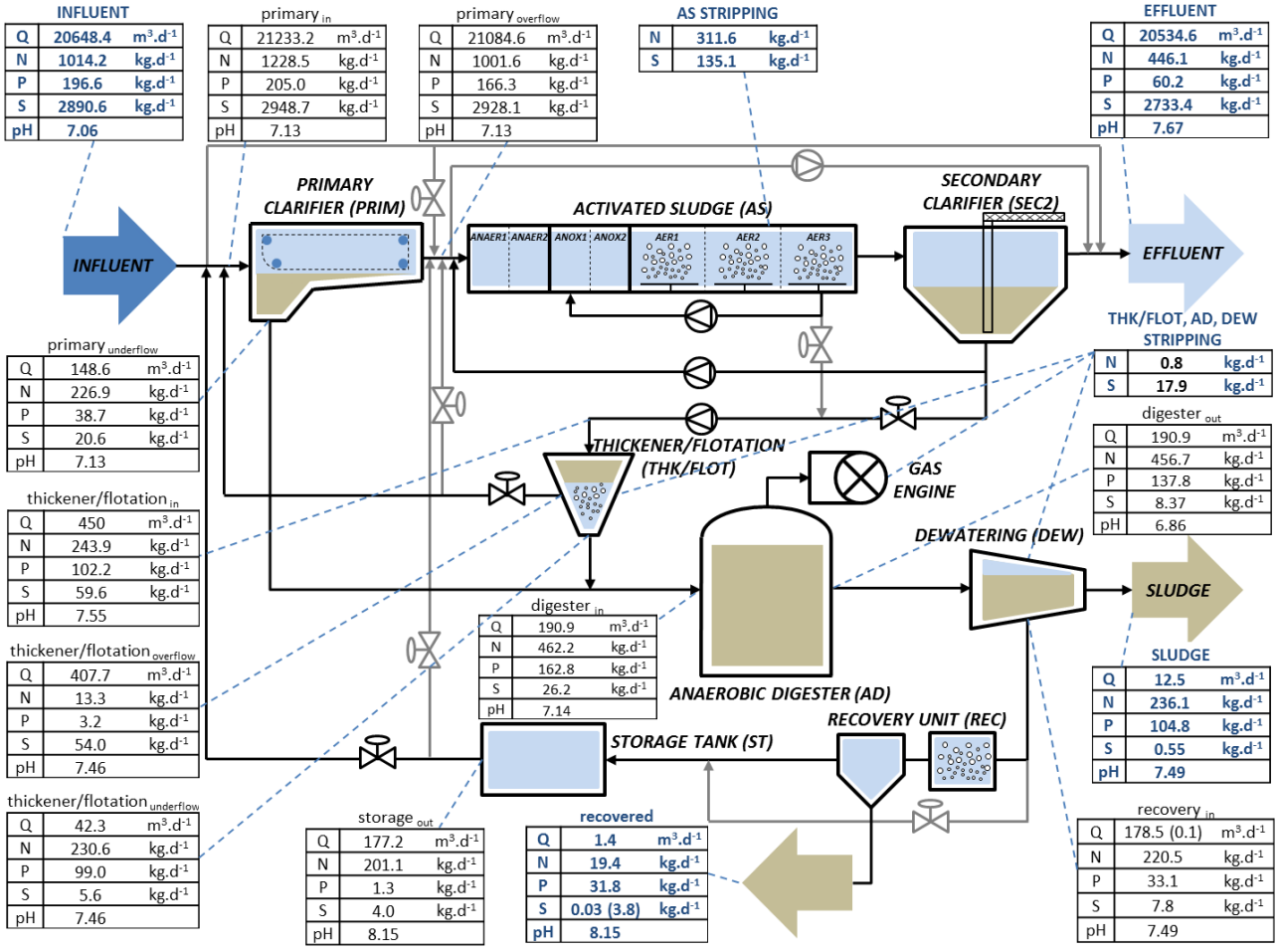

Figure SS3. Block flow diagram including overall and individual (N, P, S, pH) balances for the WWTP under study (scenario A_3).

Values in between parentheses represent: H_2S gas that is stripped (REC) and minor flow due to metal addition (DEW).

Kimberly Tumlos Solon has been a Marie Skłodowska-Curie ITN Ph.D. fellow at the Division of Industrial Electrical Engineering and Automation, Lund University. She has a background in Civil Engineering and Environmental Sanitation, obtaining her B.Sc. and M.Sc. degrees from the University of the Philippines and Ghent University in Belgium, respectively. Her current research interests focus on modelling of wastewater treatment processes and resource recovery. She is also an active Young Water Professional, contributing as an affiliated Management Committee member of the International Water Association's Modelling and Integrated Assessment Specialist Group.

Printed by Media-Tryck, Lund 2017 NORDIC ECOLABEL 3041 0903

LUND UNIVERSITY

Faculty of Engineering
Department of Biomedical Engineering
Division of Industrial Electrical Engineering and Automation

ISBN 978-91-88934-79-6
CODEN LUTEDX/(TEIE-1082/1-238/(2017)